

Advances

in Clinical and Experimental Medicine

MONTHLY ISSN 1899-5276 (PRINT) ISSN 2451-2680 (ONLINE)

advances.umw.edu.pl

2023, Vol. 32, No. 5 (May)

Impact Factor (IF) – 1.736
Ministry of Science and Higher Education – 70 pts
Index Copernicus (ICV) – 168.52 pts



WROCLAW
MEDICAL UNIVERSITY

Advances
in Clinical and Experimental
Medicine



Advances in Clinical and Experimental Medicine

ISSN 1899-5276 (PRINT)

ISSN 2451-2680 (ONLINE)

advances.umw.edu.pl

MONTHLY 2023
Vol. 32, No. 5
(May)

Advances in Clinical and Experimental Medicine (*Adv Clin Exp Med*) publishes high-quality original articles, research-in-progress, research letters and systematic reviews and meta-analyses of recognized scientists that deal with all clinical and experimental medicine.

Editorial Office

ul. Marcinkowskiego 2–6
50-368 Wrocław, Poland
Tel.: +48 71 784 12 05
E-mail: redakcja@umw.edu.pl

Publisher

Wrocław Medical University
Wybrzeże L. Pasteura 1
50-367 Wrocław, Poland

Online edition is the original version
of the journal

Editor-in-Chief

Prof. Donata Kurpas

Deputy Editor

Prof. Wojciech Kosmala

Managing Editor

Marek Misiak, MA

Statistical Editors

Wojciech Bombała, MSc
Anna Kopszak, MSc
Dr. Krzysztof Kujawa

Manuscript editing

Marek Misiak, MA, Jolanta Krzyżak, MA

Scientific Committee

Prof. Sabine Bährer-Kohler
Prof. Antonio Cano
Prof. Breno Diniz
Prof. Erwan Donal
Prof. Chris Fox
Prof. Naomi Hachiya
Prof. Carol Holland
Prof. Markku Kurkinen
Prof. Christos Lionis

Prof. Raimundo Mateos
Prof. Zbigniew W. Raś
Prof. Jerzy W. Rozenblit
Prof. Silvina Santana
Prof. James Sharman
Prof. Jamil Shibli
Prof. Michał Toborek
Prof. László Vécsei
Prof. Cristiana Vitale

Section Editors

Anesthesiology

Prof. Marzena Zielińska

Basic Sciences

Prof. Iwona Bil-Lula
Prof. Bartosz Kempisty
Dr. Wiesława Kranc
Dr. Anna Lebedeva
Dr. Maciej Sobczyński

Clinical Anatomy, Legal Medicine, Innovative Technologies

Prof. Rafael Boscolo-Berto

Dentistry

Prof. Marzena Dominiak
Prof. Tomasz Gedrange
Prof. Jamil Shibli

Laser Dentistry

Assoc. Prof. Kinga Grzech-Leśniak

Dermatology

Prof. Jacek Szepietowski

Emergency Medicine, Innovative Technologies

Prof. Jacek Smereka

Gynecology and Obstetrics

Prof. Olimpia Sipak-Szmigiel

Histology and Embryology

Dr. Mateusz Olbromski

Internal Medicine

Angiology

Dr. Angelika Chachaj

Cardiology

Prof. Wojciech Kosmala
Dr. Daniel Morris

Endocrinology

Prof. Marek Bolanowski

Gastroenterology

Assoc. Prof. Katarzyna Neubauer

Hematology

Prof. Andrzej Deptała

Prof. Dariusz Wołowicz

Nephrology and Transplantology

Assoc. Prof. Dorota Kamińska

Assoc. Prof. Krzysztof Letachowicz

Pulmonology

Prof. Anna Brzecka

Microbiology

Prof. Marzenna Bartoszewicz

Assoc. Prof. Adam Junka

Molecular Biology

Dr. Monika Bielecka

Prof. Jolanta Saczko

Neurology

Assoc. Prof. Magdalena Koszewicz

Assoc. Prof. Anna Pokryszko-Dragan

Dr. Masaru Tanaka

Neuroscience

Dr. Simone Battaglia

Oncology

Prof. Andrzej Deptała

Dr. Marcin Jędryka

Gynecological Oncology

Dr. Marcin Jędryka

Ophthalmology

Prof. Marta Misiuk-Hojła

Orthopedics

Prof. Paweł Reichert

Otolaryngology

Assoc. Prof. Tomasz Zatoński

Pediatrics

Pediatrics, Metabolic Pediatrics, Clinical Genetics, Neonatology, Rare Disorders

Prof. Robert Śmigiel

Pediatric Nephrology

Prof. Katarzyna Kiliś-Pstrusińska

Pediatric Oncology and Hematology

Assoc. Prof. Marek Ussowicz

Pharmaceutical Sciences

Assoc. Prof. Marta Kepińska

Prof. Adam Matkowski

Pharmacoeconomics, Rheumatology

Dr. Sylwia Szafranec-Buryło

Psychiatry

Prof. Jerzy Leszek

Assoc. Prof. Bartłomiej Stańczykiewicz

Public Health

Prof. Monika Sawhney

Prof. Izabella Uchmanowicz

Qualitative Studies, Quality of Care

Prof. Ludmiła Marcinowicz

Radiology

Prof. Marek Sząsiadek

Rehabilitation

Dr. Elżbieta Rajkowska-Labon

Surgery

Assoc. Prof. Mariusz Chabowski

Prof. Renata Taboła

Telemedicine, Geriatrics, Multimorbidity

Assoc. Prof. Maria Magdalena

Bujnowska-Fedak

Editorial Policy

Advances in Clinical and Experimental Medicine (Adv Clin Exp Med) is an independent multidisciplinary forum for exchange of scientific and clinical information, publishing original research and news encompassing all aspects of medicine, including molecular biology, biochemistry, genetics, biotechnology and other areas. During the review process, the Editorial Board conforms to the "Uniform Requirements for Manuscripts Submitted to Biomedical Journals: Writing and Editing for Biomedical Publication" approved by the International Committee of Medical Journal Editors (www.ICMJE.org). The journal publishes (in English only) original papers and reviews. Short works considered original, novel and significant are given priority. Experimental studies must include a statement that the experimental protocol and informed consent procedure were in compliance with the Helsinki Convention and were approved by an ethics committee.

For all subscription-related queries please contact our Editorial Office: redakcja@umw.edu.pl

For more information visit the journal's website: advances.umw.edu.pl

Pursuant to the ordinance of the Rector of Wrocław Medical University No. 12/XVI R/2023, from February 1, 2023, authors are required to pay a fee for each manuscript accepted for publication in the journal Advances in Clinical and Experimental Medicine. The fee amounts to 990 EUR for original papers and meta-analyses, 700 EUR for reviews, and 350 EUR for research-in-progress (RIP) papers and research letters.

Advances in Clinical and Experimental Medicine has received financial support from the resources of Ministry of Science and Higher Education within the "Social Responsibility of Science – Support for Academic Publishing" project based on agreement No. RCN/SP/0584/2021.



Ministry of Education and Science
Republic of Poland

Czasopismo Advances in Clinical and Experimental Medicine korzysta ze wsparcia finansowego ze środków Ministerstwa Edukacji i Nauki w ramach programu „Społeczna Odpowiedzialność Nauki – Rozwój Czasopism Naukowych” na podstawie umowy nr RCN/SP/0584/2021.



Ministerstwo
Edukacji i Nauki

Indexed in: MEDLINE, Science Citation Index Expanded, Journal Citation Reports/Science Edition, Scopus, EMBASE/Excerpta Medica, Ulrich's™ International Periodicals Directory, Index Copernicus

Typographic design: Piotr Gil, Monika Kołęda

DTP: Wydawnictwo UMW

Cover: Monika Kołęda

Printing and binding: Drukarnia I-BiS Bierońscy Sp.k.

Contents

Editorials

- 505 Masaru Tanaka, Ágnes Szabó, Laszlo Vécsei
Preclinical modeling in depression and anxiety: Current challenges and future research directions

Meta-analyses

- 511 Xiaojing Hu, Lili Pan, Wenjie Li
Meta-analysis on the efficacy of the norepinephrine reuptake inhibitors reboxetine and atomoxetine for the treatment of schizophrenia and attention deficit hyperactivity disorder
- 523 Yuanli Sun, Xiangchun Wu
Complications of implanted port catheters and peripherally inserted central catheters in chemotherapy-treated cancer patients: A meta-analysis

Original papers

- 533 Yongjun Hu, Yi Shen, Ding Chen, Weiye Zhong
Effects of arthroscopic anterior cruciate ligament reconstruction combined with sodium hyaluronate on knee function and inflammatory markers in anterior cruciate ligament injury patients with or without knee osteoarthritis
- 539 Piotr Łacina, Rachel E. Crossland, Joanna Wielińska, Anna Czyż, Agnieszka Szeremet, Marek Ussowicz, Tomasz Wróbel, Anne M. Dickinson, Katarzyna Bogunia-Kubik
Differential expression of miRNAs from extracellular vesicles in chronic graft-versus-host disease: A preliminary study
- 545 Ayse Gul Ferlengez, Cihad Tatar, Mahmut Said Degerli, Adil Koyuncu, Fatih Alper Ahlatci, Ali Emre Nayci, Aziz Ari, Ufuk Oguz Idiz
The role of serum nesfatin-1 in a rat model of acute pancreatitis
- 551 Hongxun Sang, Renli Zhao, Guohua Lai, Zhiwei Deng, Weida Zhuang, Mingjie Wu, Jiachang Wu
Bone marrow mesenchymal stem cell-derived exosomes attenuate the maturation of dendritic cells and reduce the rejection of allogeneic transplantation
- 563 Xiaoying Jiang, Xue Chen, RuoXi Dong, Jiawen Wang, Yibin Pan, Yongqing Cao
Establishment of a mouse model of inflammatory bowel disease using dextran sulfate sodium
- 575 Wenke Li, Yourang Jiang, Qi Pan, Guang Yang
miR-29a-5p regulates the malignant biological process of liver cancer cells through ARID2 regulation of EMT
- 583 Weiqiang Gan, Yanhong Kang, Yingjie Wu, Jianyun Zhu, Youming Chen, Jianyu Kuang, Jianguo Li, Lin Yang
Hepatitis B virus X protein induces p16 gene promoter methylation through upregulation of DNA methylation transferases DNMT1 and DNMT3A
- 593 Meihong Cai, Zhen Hu, Lin Liu, Jiangwei Su
hsa_circ_0038382 upregulates T-box transcription factor 5 to inhibit keloid formation by interacting with miR-940

Preclinical modeling in depression and anxiety: Current challenges and future research directions

Masaru Tanaka^{1,A–F}, Ágnes Szabó^{2,3,C,E,F}, Laszlo Vécsei^{2,1,C–F}

¹ Eötvös Loránd Research Network-Szegedi Tudományegyetem (ELKH-SZTE), Neuroscience Research Group, University of Szeged, Danube Neuroscience Research Laboratory, Hungary

² Department of Neurology, Albert Szent-Györgyi Medical School, University of Szeged, Hungary

³ Doctoral School of Clinical Medicine, University of Szeged, Hungary

A – research concept and design; B – collection and/or assembly of data; C – data analysis and interpretation; D – writing the article; E – critical revision of the article; F – final approval of the article

Advances in Clinical and Experimental Medicine, ISSN 1899–5276 (print), ISSN 2451–2680 (online)

Adv Clin Exp Med. 2023;32(5):505–509

Address for correspondence

Masaru Tanaka

E-mail: emtanaka2014@gmail.com

Funding sources

ELKH-SZTE Eötvös Loránd Research Network, and the University of Szeged, Hungary (grants No. OTKA-138125-K and No. TUDFO/47138-1/2019-ITM).

Conflict of interest

None declared

Received on April 12, 2023

Reviewed on April 18, 2023

Accepted on May 7, 2023

Published online on May 22, 2023

Abstract

This editorial highlights the limitations of preclinical models in accurately reflecting the complexity of anxiety and depression, which leads to a lack of effective treatments for these disorders. Inconsistencies in experimental designs and methodologies can entail conflicting or inconclusive findings, while an overreliance on medication can mask underlying problems. Researchers are exploring new approaches to preclinical modeling of negative emotional disorders, including using patient-derived cells, developing more complex animal models, and integrating genetic and environmental factors. Advanced technologies, such as optogenetics, chemogenetics and neuroimaging, are also being employed to improve the specificity and selectivity of preclinical models. Collaboration and innovation across different disciplines and sectors are needed to address complex societal challenges, which requires new models of funding and support that prioritize cooperation and multidisciplinary research. By harnessing the power of technology and new ways of working, researchers can collaborate more effectively to bring about transformative change.

Key words: depression, anxiety, PTSD, animal models, translational medicine

Cite as

Tanaka M, Szabó Á, Vécsei L. Preclinical modeling in depression and anxiety: Current challenges and future research directions. *Adv Clin Exp Med.* 2023;32(5):505–509. doi:10.17219/acem/165944

DOI

10.17219/acem/165944

Copyright

Copyright by Author(s)

This is an article distributed under the terms of the Creative Commons Attribution 3.0 Unported (CC BY 3.0) (<https://creativecommons.org/licenses/by/3.0/>)

Introduction

Depression and anxiety are prevalent symptoms of both systemic diseases and mental illnesses, affecting millions of people worldwide and significantly impacting their quality of life.^{1–6} The prevalence of these disorders remains high, yet effective treatments are still unavailable.⁷ The limited success in developing new therapies can be attributed, in part, to the absence of preclinical models that adequately replicate the intricate nature of negative emotional disorders in humans.⁸ Understanding the fundamental mechanisms of negative emotional disorders, identifying new therapeutic targets and evaluating novel treatments depend heavily on preclinical models, which are vital tools.^{9–12} Nonetheless, current preclinical models have limitations that impede their applicability to humans. For instance, the majority of animal models used for anxiety and depression rely on stress induction or genetic alterations that may not accurately reflect the pathophysiology of human conditions.¹³

This editorial gathers insights from various experts regarding the current challenges and future prospects of preclinical models in understanding negative emotional disorders. We aim to highlight the limitations of existing models and suggest new directions for research to improve the reliability and validity of preclinical models. Furthermore, we seek to promote the use of interdisciplinary approaches to explore the intricate mechanisms involved in the development and maintenance of negative emotional disorders. Ultimately, this editorial intends to stimulate new thinking and innovative ideas to help translate the insights gained from preclinical models into successful therapeutic interventions for these challenging disorders.

Current challenges in preclinical modeling

The use of animal models in scientific research has been a subject of controversy due to the ethical concerns associated with animal testing.^{14,15} Additionally, there is a lack of reliable and valid animal models that can accurately mimic human diseases and responses to drugs.¹⁶ Animal models may exhibit different physiological and genetic variations, which can lead to conflicting results that may not translate to humans. This can lead to misinterpretations of research findings and ineffective or even harmful treatments for human diseases.^{17–19} Therefore, it is important to continue the development of alternative testing methods that are more reliable, ethical, and accurate in predicting human responses.^{8,20}

Inconsistent experimental designs and methodologies present a significant challenge to scientific research. Variations in factors such as study size, duration, subject selection, measurement methods, and statistical analyses can generate conflicting or inconclusive findings.²¹ To address

this, researchers should aim to develop rigorous and standardized designs and methodologies that allow for valid and reliable comparisons across studies. This can help promote knowledge advancement and the development of effective interventions.

Identifying a novel target and ensuring safety and efficacy through extensive research studies in drug design and drug discovery are crucial prerequisites for a potential drug to proceed to clinical trials.^{22–28} Nevertheless, there has been an increasing trend towards overreliance on pharmacological interventions for the treatment of illnesses and conditions in recent years. While there is no denying that medication can be an effective way to manage symptoms and improve quality of life, relying too heavily on drugs comes with its own set of risks and downsides.²⁹ For one thing, overmedication can lead to unnecessary side effects, including fatigue, nausea and dizziness. Additionally, an overreliance on medication can sometimes mask underlying problems that may be better addressed through lifestyle changes, therapy or other non-pharmacological interventions.³⁰ To ensure that patients are receiving the best possible care, it is important to strike a balance between medication and other forms of treatment, and to always prioritize the least invasive approach whenever possible.³¹

Behavioral and physiological measures are useful indicators for analyzing human activities and responses to different (i.e., threatening) stimuli in the environment. However, there are several limitations to these measures that need to be considered.^{32–35} One limitation of behavioral measures is the possibility of social desirability bias, where participants may provide answers they believe will be accepted by others rather than their true opinions or behaviors.³⁶ Moreover, physiological measures can be prone to false readings due to the presence of environmental factors such as noise or electromagnetic interference. Additionally, physiological measures can only provide information about the immediate physiological response and not about long-term effects.^{37,38} Furthermore, these measures do not capture the cultural, social and emotional aspects that influence human behavior, which may lead to biases in the interpretation of results.³⁹ Therefore, it is essential to use multiple measures, including self-report data, to improve the accuracy and reliability of the findings.⁴⁰

Future research directions

To overcome these challenges, researchers are exploring new approaches to preclinical modeling that incorporate the complexity of human negative emotional disorders. One promising strategy is to use patient-derived cells, such as induced pluripotent stem cells (iPSCs), to create disease-specific models. The iPSCs can be reprogrammed from patient cells and differentiated into various types of brain cells, such as neurons and astrocytes, that are relevant to negative emotional disorders.⁴¹ These patient-specific

models have the potential to provide a more accurate representation of human disease and enable the testing of personalized therapies.⁴²

The development of novel and more complex animal models has been a major focus of research in recent years.^{8,43} These models allow researchers to study various diseases and conditions in animals that are more physiologically similar to humans, providing a beneficial tool for the production of innovative treatments and therapies, as well as aiding in the understanding of disease progression and mechanisms. However, it is important to keep ethical considerations in mind when utilizing animal models.⁴⁴ It is important to balance the potential benefits with ethical considerations to ensure that animal welfare is not compromised.

Integrating genetic and environmental factors is essential in developing strategies to prevent and treat diseases.⁴⁵ While genetics may play a significant role in an individual's susceptibility to certain diseases, environmental factors, such as lifestyle, diet and exposure to toxins, also play a crucial role in pathogenesis.⁴⁶ Understanding the complex interactions between these factors could lead to personalized healthcare interventions and more effective disease prevention and treatment.⁴⁷ For instance, researchers have found that certain genetic variants may increase an individual's susceptibility to certain cancers, but environmental factors such as exposure to cigarette smoke or an unhealthy diet may further increase this risk.⁴⁸ Conversely, lifestyle modifications such as a healthy diet and regular exercise can reduce the risk of disease development, even for individuals with genetic predispositions.⁴⁹

The incorporation of translational approaches refers to the process of moving scientific advances from laboratory settings to clinical applications.⁵⁰ This approach aims to improve the efficiency of drug development, minimize the time needed to invent new therapies, and increase the chances of successful clinical outcomes. It involves the integration of various scientific disciplines, advances in technology, and collaboration between academia, industry and regulatory bodies.²⁰ A successful translational approach can lead to the discovery of new biomarkers, identification of disease mechanisms, and advancement of targeted therapies.²⁰ Translational approaches have been instrumental in driving progress in modern medicine, and their ongoing utilization is vital to ensure the creation of safe and effective treatments for various ailments.²⁰

The fields of neuroscience and psychology have seen rapid progress in recent years, thanks to the application of new and innovative technologies. Another approach to improving preclinical models is to use advanced technologies, such as optogenetics and chemogenetics, or the application of noninvasive brain stimulation (NIBS), to manipulate specific brain circuits involved in negative emotional behaviors.^{51–54} These techniques allow researchers to precisely target brain regions and cell types, which

may improve the specificity and selectivity of preclinical models. Optogenetics has allowed researchers to gain unprecedented control over specific cells in the brain, providing a possibility to manipulate and monitor neural activity with precision.⁵⁵ Chemogenetics applies small molecules to modulate targeted neural circuits and study their functions *in vivo*.⁵⁶ These technologies have opened up new avenues for exploring the neural mechanisms underlying behavior, cognition and emotion, and have the potential to lead to new therapeutic interventions for a wide range of neurological and psychiatric disorders.

Similarly, neuroimaging techniques such as magnetic resonance imaging (MRI) and positron emission tomography (PET) have allowed researchers to visualize and quantify brain activity and structure in unprecedented detail, shedding new light on the neural basis of complex behaviors such as decision-making, creativity and social interaction.^{57–61} In addition to these technological advances, it is crucial to consider the heterogeneity of negative emotional disorders when designing preclinical models. Negative emotional disorders can manifest in different ways, and patients may respond to treatments differently.^{62–64} Therefore, preclinical models should account for this heterogeneity by incorporating the variability of the disease and the patient's characteristics. As these technologies continue to improve and evolve, they will undoubtedly play a crucial role in advancing our understanding of the human brain and improving our ability to diagnose and treat brain-related disorders.

Conclusion

Preclinical models play a critical role in improving our understanding as well as treatment of negative emotional disorders, including anxiety, depression and stress-related conditions. These disorders can have significant impact on both mental and physical health.⁶⁵ Preclinical models provide a controlled environment to study the underlying mechanisms of these disorders, identifying potential drug targets and treatment strategies. Animal models offer insight into the biological mechanisms of negative emotions and allow researchers to develop and test new therapeutic interventions.^{66,67} Researchers can study preclinical models to investigate neural circuits and molecules involved in emotional states, and identify changes associated with negative emotional disorders. However, a significant challenge in neuroscience research is creating preclinical models that accurately replicate the complexity of negative emotional disorders in humans. By incorporating patient-specific cells and advanced technologies and accounting for disease heterogeneity, researchers can improve the translational value of preclinical models and expedite the creation of novel treatments. To address the complex challenges the society is facing today, there is a growing call for greater collaboration and innovation in research efforts,

which are essential to tackle complex issues like climate change, healthcare, education, and inequality. Breaking down traditional silos and working across different disciplines and sectors can help identify new solutions and approaches. New models of funding and support are also needed to prioritize collaboration and multidisciplinary research, harnessing the power of technology to drive transformative change.

ORCID iDs

Masaru Tanaka  <https://orcid.org/0000-0003-4383-4024>

Ágnes Szabó  <https://orcid.org/0000-0002-3435-8866>

Laszlo Vécsei  <https://orcid.org/0000-0001-8037-3672>

References

- Hohls JK, König HH, Quirke E, Hajek A. Anxiety, depression and quality of life: A systematic review of evidence from longitudinal observational studies. *Int J Environ Res Public Health*. 2021;18(22):12022. doi:10.3390/ijerph182212022
- Gładka A, Zatoński T, Rymaszewska J. Association between the long-term exposure to air pollution and depression. *Adv Clin Exp Med*. 2022;31(10):1139–1152. doi:10.17219/acem/149988
- Carrera-González MDP, Cantón-Habas V, Rich-Ruiz M. Aging, depression and dementia: The inflammatory process. *Adv Clin Exp Med*. 2022;31(5):469–473. doi:10.17219/acem/149897
- Chen C. Recent advances in the study of the comorbidity of depressive and anxiety disorders. *Adv Clin Exp Med*. 2022;31(4):355–358. doi:10.17219/acem/147441
- Panov G. Higher depression scores in patients with drug-resistant schizophrenia. *J Integr Neurosci*. 2022;21(5):126. doi:10.31083/jjin2105126
- Panov G, Panova P. Obsessive-compulsive symptoms in patient with schizophrenia: The influence of disorganized symptoms, duration of schizophrenia, and drug resistance. *Front Psychiatry*. 2023;14:1120974. doi:10.3389/fpsy.2023.1120974
- Institute for Quality and Efficiency in Health Care (IQWiG). Depression: How effective are antidepressants? [last update: June 18, 2020]. In: *InformedHealth*. Cologne, Germany: Institute for Quality and Efficiency in Health Care (IQWiG); 2006. <https://www.ncbi.nlm.nih.gov/books/NBK361016/>.
- Tanaka M, Spekker E, Szabó Á, Polyák H, Vécsei L. Modelling the neurodevelopmental pathogenesis in neuropsychiatric disorders: Bioactive kynurenes and their analogues as neuroprotective agents. In celebration of 80th birthday of Professor Peter Riederer. *J Neural Transm*. 2022;129(5–6):627–642. doi:10.1007/s00702-022-02513-5
- Tanaka M, Schally AV, Telegdy G. Neurotransmission of the antidepressant-like effects of the growth hormone-releasing hormone antagonist MZ-4-71. *Behav Brain Res*. 2012;228(2):388–391. doi:10.1016/j.bbr.2011.12.022
- Tanaka M, Kádár K, Tóth G, Telegdy G. Antidepressant-like effects of urocortin 3 fragments. *Brain Res Bull*. 2011;84(6):414–418. doi:10.1016/j.brainresbull.2011.01.016
- Palotai M, Telegdy G, Tanaka M, Bagosi Z, Jászberényi M. Neuropeptide AF induces anxiety-like and antidepressant-like behavior in mice. *Behav Brain Res*. 2014;274:264–269. doi:10.1016/j.bbr.2014.08.007
- Polyák H, Galla Z, Nánási N, et al. The tryptophan–kynurenine metabolic system is suppressed in cuprizone-induced model of demyelination simulating progressive multiple sclerosis. *Biomedicines*. 2023;11(3):945. doi:10.3390/biomedicines11030945
- Tanaka M, Telegdy G. Involvement of adrenergic and serotonergic receptors in antidepressant-like effect of urocortin 3 in a modified forced swimming test in mice. *Brain Res Bull*. 2008;77(5):301–305. doi:10.1016/j.brainresbull.2008.08.012
- Becker M, Pinhasov A, Ornoy A. Animal models of depression: What can they teach us about the human disease? *Diagnostics (Basel)*. 2021;11(1):123. doi:10.3390/diagnostics11010123
- Ferdowsian HR, Beck N. Ethical and scientific considerations regarding animal testing and research. *PLoS One*. 2011;6(9):e24059. doi:10.1371/journal.pone.0024059
- Akhtar A. The flaws and human harms of animal experimentation. *Camb Q Healthc Ethics*. 2015;24(4):407–419. doi:10.1017/S0963180115000079
- Singh VP, Pratap K, Sinha J, Desiraju K, Bahal D, Kukreti R. Critical evaluation of challenges and future use of animals in experimentation for biomedical research. *Int J Immunopathol Pharmacol*. 2016;29(4):551–561. doi:10.1177/0394632016671728
- Nikolopoulou K. Reproducibility vs replicability: Difference & examples. Scribbr; 2022. <https://www.scribbr.com/methodology/reproducibility-repeatability-replicability/>. Accessed April 6, 2023.
- Barré-Sinoussi F, Montagutelli X. Animal models are essential to biological research: Issues and perspectives. *Future Science OA*. 2015;1(4):FSO63. doi:10.4155/fso.15.63
- Tanaka M, Szabó Á, Vécsei L. Integrating armchair, bench, and bedside research for behavioral neurology and neuropsychiatry: Editorial. *Biomedicines*. 2022;10(12):2999. doi:10.3390/biomedicines10122999
- Cohen DJ, Crabtree BF. Evaluative criteria for qualitative research in health care: Controversies and recommendations. *Ann Fam Med*. 2008;6(4):331–339. doi:10.1370/afm.818
- Zaremba M, Serafin P, Kleczkowska P. Antipsychotic drugs efficacy in dextromethorphan-induced psychosis. *Biomedicines*. 2023;11(1):123. doi:10.3390/biomedicines11010123
- Zyżyńska-Granica B, Mollica A, Stefanucci A, Granica S, Kleczkowska P. Comparative study of chemical stability of a PK20 opioid–neurotensin hybrid peptide and its analogue [Ile9]PK20: The effect of isomerism of a single amino acid. *Int J Mol Sci*. 2022;23(18):10839. doi:10.3390/ijms231810839
- Bukowska-Oško I, Sulejczak D, Kaczyńska K, et al. Lactoferrin as a human genome “guardian”: An overall point of view. *Int J Mol Sci*. 2022;23(9):5248. doi:10.3390/ijms23095248
- Kleczkowska P. Chimeric structures in mental illnesses: “Magic” molecules specified for complex disorders. *Int J Mol Sci*. 2022;23(7):3739. doi:10.3390/ijms23073739
- Kowalczyk P, Sulejczak D, Kleczkowska P, et al. Mitochondrial oxidative stress: A causative factor and therapeutic target in many diseases. *Int J Mol Sci*. 2021;22(24):13384. doi:10.3390/ijms222413384
- Sfera A, Hazan S, Kozlakidis Z, Klein C. Microbiota-derived psychedelics: Lessons from COVID-19. *Adv Clin Exp Med*. 2023;32(4):395–399. doi:10.17219/acem/159477
- Zhao X, Zhang H, Wu Y, Yu C. The efficacy and safety of St. John’s wort extract in depression therapy compared to SSRIs in adults: A meta-analysis of randomized clinical trials. *Adv Clin Exp Med*. 2022;32(2):151–161. doi:10.17219/acem/152942
- Kallivayalil R. Are we over-dependent on pharmacotherapy? *Indian J Psychiatry*. 2008;50(1):7. doi:10.4103/0019-5545.39750
- Jarbøl DE, Larsen PV, Gyrd-Hansen D, et al. Determinants of preferences for lifestyle changes versus medication and beliefs in ability to maintain lifestyle changes: A population-based survey. *Prev Med Rep*. 2017;6:66–73. doi:10.1016/j.pmedr.2017.02.010
- Nieuwlaet R, Wilczynski N, Navarro T, et al. Interventions for enhancing medication adherence. *Cochrane Database Syst Rev*. 2014;2014(11):CD000011. doi:10.1002/14651858.CD000011.pub4
- Battaglia S, Cardellicchio P, Di Fazio C, Nazzi C, Fracasso A, Borgomaneri S. Stopping in (e)motion: Reactive action inhibition when facing valence-independent emotional stimuli. *Front Behav Neurosci*. 2022;16:998714. doi:10.3389/fnbeh.2022.998714
- Battaglia S, Cardellicchio P, Di Fazio C, Nazzi C, Fracasso A, Borgomaneri S. The influence of vicarious fear-learning in “infecting” reactive action inhibition. *Front Behav Neurosci*. 2022;16:946263. doi:10.3389/fnbeh.2022.946263
- Battaglia S, Thayer JF. Functional interplay between central and autonomic nervous systems in human fear conditioning. *Trends Neurosci*. 2022;45(7):504–506. doi:10.1016/j.tins.2022.04.003
- Battaglia S, Orsolini S, Borgomaneri S, Barbieri R, Diciotti S, Di Pellegrino G. Characterizing cardiac autonomic dynamics of fear learning in humans. *Psychophysiology*. 2022;59(12):e14122. doi:10.1111/psyp.14122
- Nikolopoulou K. What is social desirability bias? Definition & examples. Scribbr; 2023. <https://www.scribbr.com/research-bias/social-desirability-bias/>. Accessed April 6, 2023.
- Munzel T, Gori T, Babisch W, Basner M. Cardiovascular effects of environmental noise exposure. *Eur Heart J*. 2014;35(13):829–836. doi:10.1093/eurheartj/ehu030

38. Mariappan PM, Raghavan DR, Abdel Aleem SHE, Zobia AF. Effects of electromagnetic interference on the functional usage of medical equipment by 2G/3G/4G cellular phones: A review. *J Adv Res.* 2016;7(5):727–738. doi:10.1016/j.jare.2016.04.004
39. Yetton BD, Revord J, Margolis S, Lyubomirsky S, Seitz AR. Cognitive and physiological measures in well-being science: Limitations and lessons. *Front Psychol.* 2019;10:1630. doi:10.3389/fpsyg.2019.01630
40. Balogh L, Tanaka M, Török N, Vécsei L, Taguchi S. Crosstalk between existential phenomenological psychotherapy and neurological sciences in mood and anxiety disorders. *Biomedicines.* 2021;9(4):340. doi:10.3390/biomedicines9040340
41. Vadodaria KC, Jones JR, Linker S, Gage FH. Modeling brain disorders using induced pluripotent stem cells. *Cold Spring Harb Perspect Biol.* 2020;12(6):a035659. doi:10.1101/cshperspect.a035659
42. Battaglia S, Di Fazio C, Vicario CM, Avenanti A. Neuropharmacological modulation of N-methyl-D-aspartate, noradrenaline and endocannabinoid receptors in fear extinction learning: Synaptic transmission and plasticity. *Int J Mol Sci.* 2023;24(6):5926. doi:10.3390/ijms24065926
43. Tanaka M, Török N, Vécsei L. Are 5-HT₁ receptor agonists effective anti-migraine drugs? *Exp Opin Pharmacother.* 2021;22(10):1221–1225. doi:10.1080/14656566.2021.1910235
44. Levy N. The use of animal as models: Ethical considerations. *Int J Stroke.* 2012;7(5):440–442. doi:10.1111/j.1747-4949.2012.00772.x
45. McAllister K, Mechanic LE, Amos C, et al. Current challenges and new opportunities for gene–environment interaction studies of complex diseases. *Am J Epidemiol.* 2017;186(7):753–761. doi:10.1093/aje/kwx227
46. Sears ME, Genus SJ. Environmental determinants of chronic disease and medical approaches: Recognition, avoidance, supportive therapy, and detoxification. *J Environ Publ Health.* 2012;2012:356798. doi:10.1155/2012/356798
47. Bookman EB, McAllister K, Gillanders E, et al. Gene–environment interplay in common complex diseases: Forging an integrative model. Recommendations from an NIH workshop. *Genet Epidemiol.* 2011;35(4):217–225. doi:10.1002/gepi.20571
48. Mbemi A, Khanna S, Njiki S, Yedjou CG, Tchounwou PB. Impact of gene–environment interactions on cancer development. *Int J Environ Res Public Health.* 2020;17(21):8089. doi:10.3390/ijerph17218089
49. Franzago M, Santurbano D, Vitacolonna E, Stuppia L. Genes and diet in the prevention of chronic diseases in future generations. *Int J Mol Sci.* 2020;21(7):2633. doi:10.3390/ijms21072633
50. Abernethy AP, Wheeler JL. True translational research: Bridging the three phases of translation through data and behavior. *Behav Med Pract Policy Res.* 2011;1(1):26–30. doi:10.1007/s13142-010-0013-z
51. Battaglia S, Nazzi C, Thayer JF. Fear-induced bradycardia in mental disorders: Foundations, current advances, future perspectives. *Neurosci Biobehav Rev.* 2023;149:105163. doi:10.1016/j.neubiorev.2023.105163
52. Battaglia S, Garofalo S, Di Pellegrino G, Starita F. Revaluing the role of vmPFC in the acquisition of Pavlovian threat conditioning in humans. *J Neurosci.* 2020;40(44):8491–8500. doi:10.1523/JNEUROSCI.0304-20.2020
53. Battaglia S, Harrison BJ, Fullana MA. Does the human ventromedial prefrontal cortex support fear learning, fear extinction or both? A commentary on subregional contributions. *Mol Psychiatry.* 2022;27(2):784–786. doi:10.1038/s41380-021-01326-4
54. Borgomaneri S, Battaglia S, Garofalo S, Tortora F, Avenanti A, Di Pellegrino G. State-dependent TMS over prefrontal cortex disrupts fear-memory reconsolidation and prevents the return of fear. *Curr Biol.* 2020;30(18):3672–3679.e4. doi:10.1016/j.cub.2020.06.091
55. Yao JP, Hou WS, Yin ZQ. Optogenetics: A novel optical manipulation tool for medical investigation. *Int J Ophthalmol.* 2012;5(4):517–522. doi:10.3980/j.issn.2222-3959.2012.04.22
56. Campbell EJ, Marchant NJ. The use of chemogenetics in behavioural neuroscience: Receptor variants, targeting approaches and caveats. *Br J Pharmacol.* 2018;175(7):994–1003. doi:10.1111/bph.14146
57. Adamu MJ, Qiang L, Zakariyya RS, Nyatega CO, Kawuwa HB, Younis A. An efficient turbo decoding and frequency domain turbo equalization for LTE based narrowband Internet of things (NB-IoT) systems. *Sensors.* 2021;21(16):5351. doi:10.3390/s21165351
58. Nyatega C, Qiang L, Jajere M, Kawuwa HB. Atypical functional connectivity of limbic network in attention deficit/hyperactivity disorder. *Clin Schizophr Relat Psychoses.* 2022;16(2). doi:10.3371/CSRP.NCLQ.053122
59. Nyatega CO, Qiang L, Adamu MJ, Kawuwa HB. Gray matter, white matter and cerebrospinal fluid abnormalities in Parkinson's disease: A voxel-based morphometry study. *Front Psychiatry.* 2022;13:1027907. doi:10.3389/fpsy.2022.1027907
60. Nyatega CO, Qiang L, Adamu MJ, Younis A, Kawuwa HB. Altered dynamic functional connectivity of cuneus in schizophrenia patients: A resting-state fMRI study. *Appl Sci.* 2021;11(23):11392. doi:10.3390/app112311392
61. Okanda Nyatega C, Qiang L, Jajere Adamu M, Bello Kawuwa H. Altered striatal functional connectivity and structural dysconnectivity in individuals with bipolar disorder: A resting state magnetic resonance imaging study. *Front Psychiatry.* 2022;13:1054380. doi:10.3389/fpsy.2022.1054380
62. Borgomaneri S, Battaglia S, Avenanti A, Pellegrino GD. Don't Hurt Me No More: State-dependent transcranial magnetic stimulation for the treatment of specific phobia. *J Affect Disord.* 2021;286:78–79. doi:10.1016/j.jad.2021.02.076
63. Battaglia S. Neurobiological advances of learned fear in humans. *Adv Clin Exp Med.* 2022;31(3):217–221. doi:10.17219/acem/146756
64. Borgomaneri S, Battaglia S, Sciamanna G, Tortora F, Laricchiuta D. Memories are not written in stone: Re-writing fear memories by means of non-invasive brain stimulation and optogenetic manipulations. *Neurosci Biobehav Rev.* 2021;127:334–352. doi:10.1016/j.neubiorev.2021.04.036
65. Tanaka M, Vécsei L. Editorial of special issue 'Dissecting Neurological and Neuropsychiatric Diseases: Neurodegeneration and Neuroprotection'. *Int J Mol Sci.* 2022;23(13):6991. doi:10.3390/ijms23136991
66. Tanaka M, Török N, Tóth F, Szabó Á, Vécsei L. Co-players in chronic pain: Neuroinflammation and the tryptophan–kynurenine metabolic pathway. *Biomedicines.* 2021;9(8):897. doi:10.3390/biomedicines9080897
67. Tajti J, Szok D, Csáti A, Szabó Á, Tanaka M, Vécsei L. Exploring novel therapeutic targets in the common pathogenic factors in migraine and neuropathic pain. *Int J Mol Sci.* 2023;24(4):4114. doi:10.3390/ijms24044114

Meta-analysis on the efficacy of the norepinephrine reuptake inhibitors reboxetine and atomoxetine for the treatment of schizophrenia and attention deficit hyperactivity disorder

Xiaojing Hu^{1,A–C}, Lili Pan^{2,A–C}, Wenjie Li^{1,D–F}

¹ Department of Psychiatry, Shandong Mental Health Center, Shandong University, Jinan, China

² Department of Psychology, Taian Traditional Chinese Medicine Hospital, China

A – research concept and design; B – collection and/or assembly of data; C – data analysis and interpretation;

D – writing the article; E – critical revision of the article; F – final approval of the article

Advances in Clinical and Experimental Medicine, ISSN 1899–5276 (print), ISSN 2451–2680 (online)

Adv Clin Exp Med. 2023;32(5):511–522

Address for correspondence

Wenjie Li

E-mail: kudy2022@outlook.com

Funding sources

None declared

Conflict of interest

None declared

Received on February 28, 2022

Reviewed on August 2, 2022

Accepted on September 17, 2022

Published online on November 30, 2022

Cite as

Hu X, Pan L, Li W. Meta-analysis on the efficacy of the norepinephrine reuptake inhibitors reboxetine and atomoxetine for the treatment of schizophrenia and attention deficit hyperactivity disorder.

Adv Clin Exp Med. 2023;32(5):511–522.

doi:10.17219/acem/155802

DOI

10.17219/acem/155802

Copyright

Copyright by Author(s)

This is an article distributed under the terms of the Creative Commons Attribution 3.0 Unported (CC BY 3.0) (<https://creativecommons.org/licenses/by/3.0/>)

Abstract

Background. Norepinephrine transporter inhibitors that can alter the level of neurotransmitter in the brain are used to treat neurological disorders. However, a number of studies have reported their limited significance as a result of their slow onset of action and moderate efficacy.

Objectives. To determine the effects of norepinephrine reuptake inhibitors (NRIs), reboxetine and atomoxetine on schizophrenia and attention deficit hyperactivity disorder (ADHD).

Materials and methods. Relevant articles published between 2000 and 2022 were searched in the MEDLINE, CINAHL (via Ebsco), Web of Science and Scopus databases. Among the various NRIs, studies concerning the 2 potent drugs – reboxetine and atomoxetine – were selected for analysis. Odds ratios (ORs) with 95% confidence intervals (95% CIs) were estimated, along with the exploration of heterogeneity and publication bias, using RevMan software.

Results. A total of 14 eligible studies with a combined sample size of 970 patients were included. Using a random effects model, an OR of 0.55 (0.32–0.94), a Tau^2 value of 0.23, a χ^2 value of 12.31, 8 degrees of freedom (df), an I^2 of 35%, a Z value of 2.19, and a p-value of 0.03 were recorded for reboxetine. Atomoxetine had an OR of 0.35 (0.13–0.97), a Tau^2 value of 0.58, a χ^2 value of 7.31, 4 df, an I^2 of 45%, a Z value of 1.53, and a p-value of 0.04. All results were statistically significant with a low risk of publication bias, as was evident from the p-values >0.05 derived from the Egger's test and the Begg's test. These drugs provided comparable changes to control drugs in Hamilton Depression Rating Scale (HAM-D) scores, Positive and Negative Syndrome Scale (PANSS) scores and ADHD ratings. This confirms the efficacy of reboxetine for the treatment of schizophrenia and atomoxetine for the treatment of ADHD.

Conclusions. The present meta-analysis suggests that NRIs are efficacious and therefore they are potential candidate drugs for the treatment of schizophrenia and ADHD.

Key words: schizophrenia, neurological disorders, atomoxetine, attention deficit hyperactivity disorder, reboxetine

Introduction

Neurological disorders, including schizophrenia, attention deficit hyperactivity disorder (ADHD), depression, anxiety, and bipolar disorders, are very common medical ailments reported worldwide. These disorders are mainly associated with symptoms such as delusions, disorganized thinking, depression, abnormal social and motor behaviors, and hallucinations.¹ Treatment of these neurological disorders is achieved through cognitive therapy, rehabilitation, psychoeducation, family therapy, behavioral therapy, and the use of a variety of antipsychotic and anti-tremor medicines.² Among the various medications, drugs that can specifically alter the level of neurotransmitters in brain cells, such as dopamine reuptake inhibitors, gamma-aminobutyric acid reuptake inhibitors, and a variety of norepinephrine reuptake inhibitors (NRIs) are of much use.³ Norepinephrine reuptake inhibitors have the capacity to alter the activity of the norepinephrine transporter, which is a solute carrier protein that controls the movement of sodium and chloride ions. This mechanism of NRIs is dependent upon the reuptake of the neurotransmitters norepinephrine and dopamine, and therefore such drugs are potential candidates for the treatment of neurological disorders.^{4–6}

A variety of NRI drugs, including atomoxetine, reboxetine, viloxazine, and edivoxetine, are currently available for the treatment of neurological disorders (Fig. 1). Indeed, a number of randomized controlled trials have suggested the potential benefits of reboxetine for the treatment of schizophrenia patients.^{7–16} Similarly, the potential benefits of atomoxetine for the treatment of ADHD have been reported in randomized controlled trials.^{17–21} Salazar de Pablo et al. reported in their meta-analysis that these disorders are more prevalent in younger females.²² Meanwhile,

Tanaka et al. reported in their review article that such neurological disorders arise due to neurodevelopmental defects or the alteration of normal brain development during early embryonic life.²³ Such defects can be investigated using functional magnetic resonance imaging, as reported by Nyatega et al.²⁴ Furthermore, these developmental defects led to higher levels of dissociative schizophrenia symptoms, as shown by Panov.²⁵ Rog et al.²⁶ reported in their study that altered fatty acid metabolism was responsible for schizophrenia, while Gaebler et al.²⁷ demonstrated that vitamin D deficiency was responsible, and Correia et al.²⁸ suggested that alterations in serum lipid levels as a major cause of schizophrenia. Therefore, NRIs that can alter the level of neurotransmitters are potential candidate drugs for these neurological disorders.^{29,30} Additionally, De Crescenzo et al. contended that pharmacotherapy using noradrenergic agents was effective in the management of ADHD.³¹

Objectives

In this study, a meta-analysis was conducted to assess the efficacy of 2 NRI medications, reboxetine and atomoxetine, in the treatment of schizophrenia and ADHD, respectively.

Materials and methods

Preferred Reporting Items for Systematic Reviews and Meta-analyses (PRISMA) normative recommendations were followed and the study protocol was registered at Shandong University, Jinan, China (registration No. SU#/IRB/2021/554).

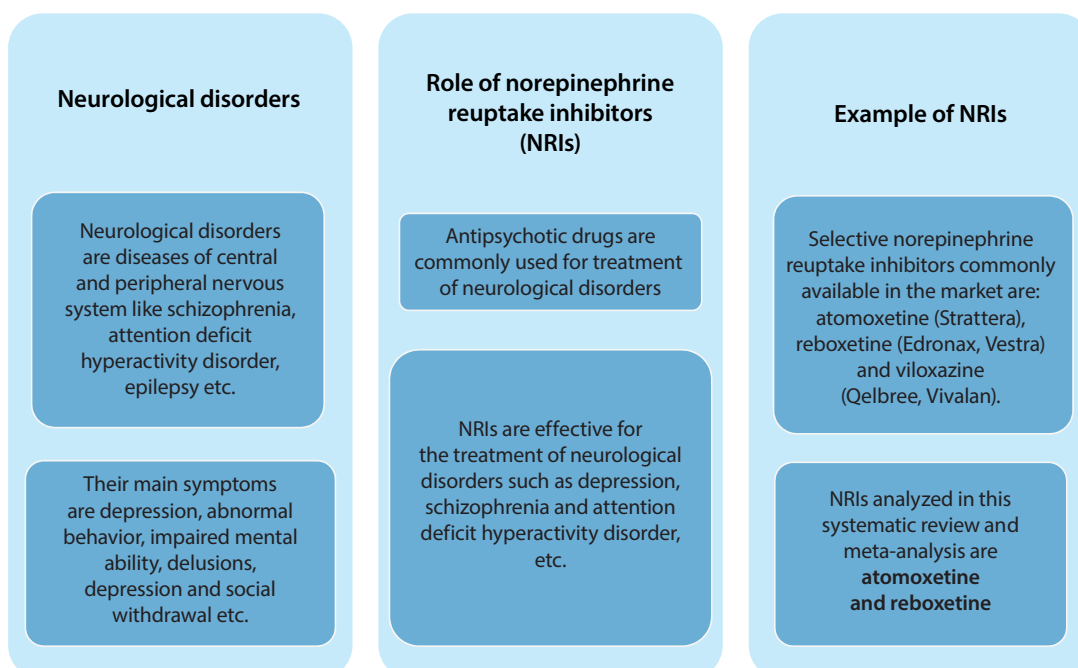


Fig. 1. Study details

Search strategy

This meta-analysis was based on an extensive literature search of MEDLINE (via PubMed), CINAHL (via Ebsco), Scopus, and Web of Science databases. Studies published between the years 2000 and 2022 were searched using the following keywords: “neurological disorder”, “neurotransmitters”, “schizophrenia”, “systematic review”, “meta-analysis”, and “norepinephrine transporter inhibitors”. All of the included articles^{8–21} were assessed using the PRISMA guidelines, and studies were selected randomly irrespective of the language, publication status or the type of study (prospective, retrospective, clinical trial). A demographic summary of the patients was designed, with consideration to the variables included in the searched studies.

To assess the efficacy and safety of NRIs, as well as their genetic variants, reboxetine and atomoxetine were selected for analysis. Event data from the selected studies were extracted. In the selected studies, patients of different age groups were treated with either reboxetine, atomoxetine or control drugs, and their Hamilton Depression Rating Scale (HAM-D) score, Positive and Negative Syndrome Scale (PANSS) score and metabolic parameters were observed. Statistical parameters, including diagnostic

odds ratio (OR) with 95% confidence interval (95% CI) and heterogeneity of data of both drugs, were calculated with RevMan software v. 4.1 (<https://training.cochrane.org/online-learning/core-software/revman>). Data for both drugs were summarized using forest plots.

Two authors (XH and LP) scanned the relevant sources for related studies separately. Full-text articles of the studies were collected and abstracts were only used if they contained sufficient information for the review and meta-analysis. Obsolete references were excluded and useful studies were included as per the inclusion criteria. Event data with useful variables were collected by 2 researchers (XH and LP) independently.

Inclusion and exclusion criteria

Studies published between 2000 and 2022 that reported on the safety and efficacy of NRIs and their genetic variants for the treatment of schizophrenic patients were included. Mostly the full-text studies were included but some abstracts were also taken into account if had sufficient data, while studies with insufficient data, reporting the use of medicines other than NRIs, and those published before 2000, were excluded (Fig. 2).

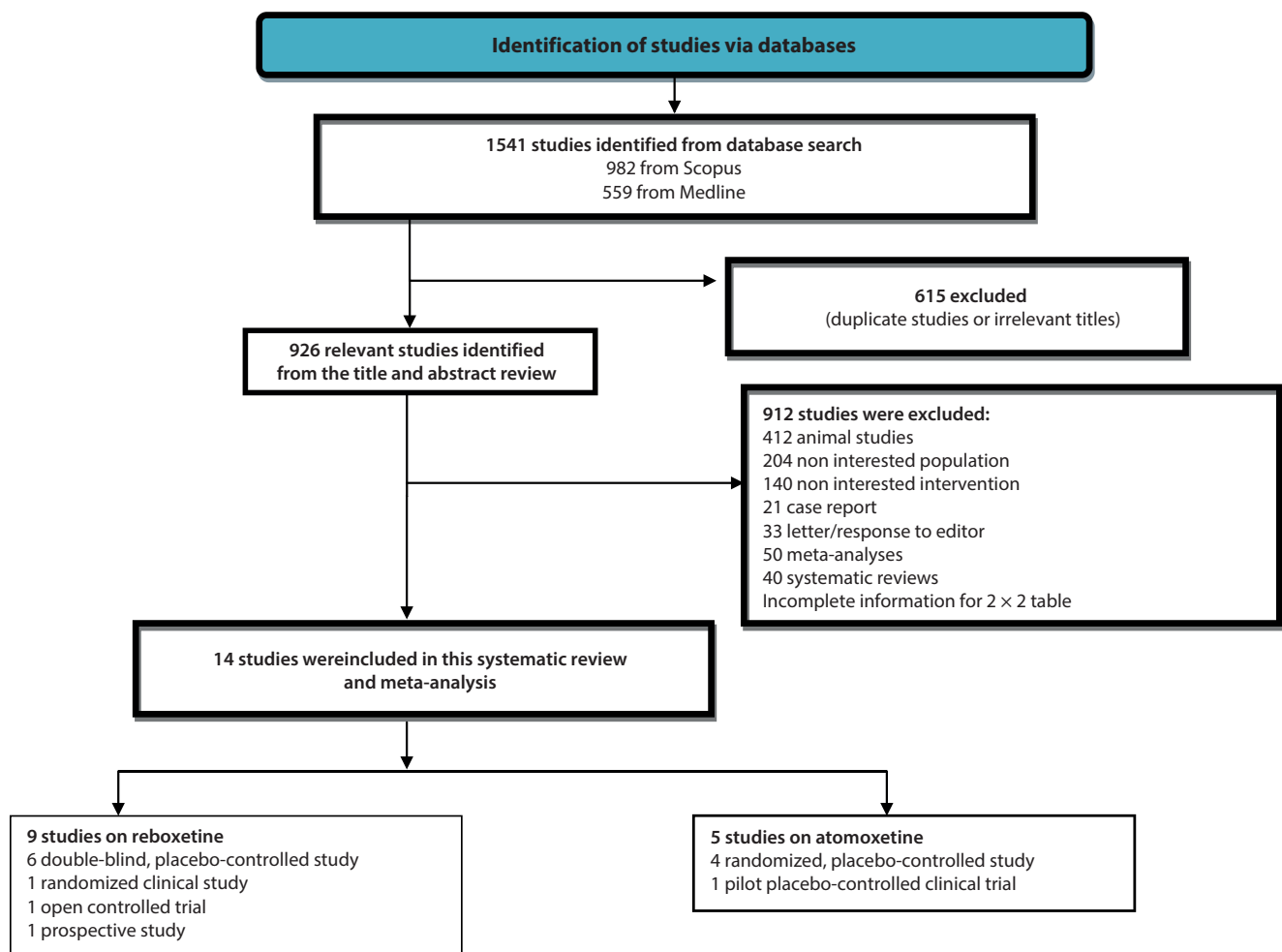


Fig. 2. Flow diagram for the selection of the studies based on the Preferred Reporting Items for Systematic Reviews and Meta-Analyses (PRISMA) guidelines

Evaluation of the analytical standard

Two reviewers (XH and LP) separately evaluated the methodological validity of the included studies and calculated the heterogeneity of the data. Author WL was responsible for resolving any disagreements between the authors XH and LP. The risk of bias of all the included studies was assessed and summarized using RevMan software.

Sources of heterogeneity

Investigated sources of heterogeneity included the use of full-text publication compared to abstracts, randomized controlled trials compared to retrospective studies, age group, number of patients, duration of treatment, scale of analysis, and comparison of St. John's wort with different selective serotonin reuptake inhibitor controls.

Statistical analyses

Diagnostic ORs for both reboxetine and atomoxetine were calculated using the DerSimonian and Laird technique. For this, a 2×2 table was constructed and a meta-analysis was performed. Pooled diagnostic ORs were then calculated with their 95% CIs, and their respective forest plots were designed. To investigate heterogeneity, Tau² value, χ^2 test, Z value, and I² index in random bivariate mode were calculated. To assess the risk of publication bias, the Deek's funnel plot for both types of studies, using either reboxetine or atomoxetine, was designed using MedCalc software v. 20.118 (MedCalc Software Ltd., Ostend, Belgium). The risk of publication bias was assessed using Egger's test and Begg's test.

Results

Literature search results

A total of 1541 studies were found in different databases. Among these studies, 615 were excluded after reading their titles and abstracts, and 926 records were further examined. Moreover, 912 studies were excluded as 412 were animal studies, 204 were of a population of non-interest, 140 studies were of non-interest interventions, 21 were case reports, 33 were letters/responses to the editor, 50 were meta-analyses, 40 were systematic reviews, and 12 were excluded due to incomplete information. Key reasons for omission were inadequate evidence and inappropriate comparison criteria required to create 2×2 tables for review. Only 14 studies were selected for final screening and meta-analysis (Fig. 2). Of the 14 studies included, 9 were related to the benefits of reboxetine and 5 were related to atomoxetine treatment.

Demographic details of the studies included in this meta-analysis are shown in Table 1. It describes authors of the study, year of publication, publishing journal, type of study, duration of study, total sample size, type and dosage of NRI used, control drug and its dosage, age and gender of patients, test scores analyzed, number of patients with positive outcomes, HAM-D scores, PANSS scores, metabolic parameters of patients, and p-values indicating statistical significance of the data. The risk of bias (Table 2) was assessed, summarized (Fig. 3) and shown as a bar graph (Fig. 4). Studies included in the analysis presented a low risk of bias, as is evident from the tables and graphs.

Fourteen clinical studies with a total of 970 schizophrenia patients were included, according to the inclusion criteria.

	Random sequence generation (selection bias)	Allocation concealment (selection bias)	Blinding of participants and personnel (performance bias)	Blinding of outcome assessment (detection bias)	Incomplete outcome data (attrition bias)	Selective reporting (reporting bias)	Other bias
Ball et al 2011 [20]	+	+	+		+		+
Brunnauer et al 2008 [11]	-	+	-	+	-	+	-
Freidman et al 2008 [18]	+	-	-	+	+		+
Michelson et al 2002 [17]	+	-	+	+		+	+
Muller et al 2006 [10]	+	-	+	+	-	-	+
Pourshams et al 2020 [21]	+	-	+	+		-	+
Poyurovsky et al 2009 [12]	+	-	+	+	+	+	
Schutz et al 2001 [8]	+	+	+	+	-	-	+
Shafiqi et al 2015 [16]	-	+	+	+	-	-	-
Takahashi et al 2009 [19]	+	+	-	+	+		
Usall et al 2014 [15]	+	-	+	+	-	-	+
Versiani et al 2002 [9]	+	-	+	+	-	+	+
Weizman et al 2013 [14]	+	-	+	+	-	+	+
Yavin et al 2009 [13]	+	-	+	+	+		+

Fig. 3. Risk of bias summary

Table 1. Demographic summary of included studies

Study ID and year	Journal title	Type of study	Norepinephrine transporter inhibitor studied	Total number of patients	Duration of study	Age of patient [years]	Evaluation of results	Gender	Drug dose	Evaluated HAM-D and PANSS scores	Positive outcome	p-value
Schutz and Berk ⁸ 2001	<i>International Clinical Psychopharmacology</i>	double-blind study	reboxetine	30	6 weeks	25–40	change in the baseline PANSS score	1 M/14 F	reboxetine (4–10 mg/day)	15.8 ± 7.29	12/15	0.7556
								1 M/14 F	placebo (10 mg/day)	14.1 ± 5.68	11/15	
Versiani et al. ⁹ 2002	<i>Journal of Clinical Psychiatry</i>	double-blind study	reboxetine	75	8 weeks	18–65	change in the baseline PANSS score	12 M/25 F	reboxetine (10 mg/day)	5.2	31/38	<0.05
								13 M/25 F	placebo (10 mg/day)	3.2	19/37	
Müller et al. ¹⁰ 2006	<i>Molecular Psychiatry</i>	prospective study	reboxetine	40	6 weeks	23–65	reduction in the HAM-D score	8 M/12 F	4–10 mg reboxetine plus placebo	12.1 ± 8.3	8/20	<0.0001
								12 M/8 F	10 mg reboxetine plus 400 mg celecoxib	7.9 ± 7.1	10/20	
Brunnauer et al. ¹¹ 2008	<i>Journal of Clinical Psychiatry</i>	randomized clinical study	reboxetine	40	2 years	40–60	reduction in the HAM-D score	11 M/9 F	reboxetine 4.5 mg/day	24.2 ± 6.7	16/20	<0.01
								11 M/9 F	mirtazapine 30 mg/day	22.6 ± 6.5	15/20	
Poyurovsky et al. ¹² 2009	<i>Israel Journal of Psychiatry and Related Science</i>	double-blind, placebo-controlled study	reboxetine	33	3 years	20–50	HAM-D score	10 M/6 F	reboxetine 4 mg/day	10.31 ± 3.34	11/17	0.92
								11 M/6 F	olanzapine 10 mg/day	10.18 ± 4.65	11/16	
Cohen-Yavin et al. ¹³ 2009	<i>Clinical Neuro-pharmacology</i>	open controlled trial	reboxetine	27	8 weeks	6–16	total DAS score	16 M	reboxetine 2–8 mg/day	15.6 ± 11.7	11/16	<0.005
								11 M	methylphenidate 10–20 mg/day	13.4 ± 13.1	11/11	
Amrami-Weizman et al. ¹⁴ 2013	<i>Psychopharmacology</i>	double-blind, placebo-controlled study	reboxetine	54	6 weeks	20–40	change in serum insulin level (microu/mL)	17 M/12 F	olanzapine/reboxetine 4 mg bid	2.76 ± 33.37	27/25	<0.05
								13 M/12 F	olanzapine/placebo (10 mg/day)	0.83 ± 13.79	19/29	

Table 1. Demographic summary of included studies – cont.

Study ID and year	Journal title	Type of study	Norepinephrine transporter inhibitor studied	Total number of patients	Duration of study	Age of patient [years]	Evaluation of results	Gender	Drug dose	Evaluated HAM-D and PANSS scores	Positive outcome	p-value
Usall et al. ¹⁵ 2014	<i>Journal of Clinical Psychiatry</i>	double-blind study	reboxetine	90	6 months	35–55	change in the baseline PANSS score	18 M/5 F 27 M/7 F 22 M/11 F	citalopram 4.5 mg/day reboxetine 6 mg/day placebo 6 mg/day	73.13 ± 10.31 72.06 ± 15.15 75.06 ± 18.62	17/23 24/33 23/34	0.6511
Shoja Shafiqi et al. ¹⁶ 2015	<i>Therapeutic Advances in Psychopharmacology</i>	double-blind study	reboxetine	50	12 weeks	2–43	reduction in the HAM-D score	25 M 25 M	25 patients received reboxetine 4 mg/day 25 patients received placebo 4 mg/day	5.36 ± 1.83 1.69 ± 6.02	19/25 6/25	<0.01
Michelson et al. ¹⁷ 2002	<i>American Journal of Psychiatry</i>	randomized, placebo-controlled study	atomoxetine	170	6 weeks	6–16	reduction in the ADHD rating scale	60 M/25 F 60 M/25 F	atomoxetine, 40 mg/day placebo 40 mg/day	12.8 ± 12.4 5.0 ± 10.4	68/85 66/85	<0.001
Friedman et al. ¹⁸ 2008	<i>Journal of Clinical Psychopharmacology</i>	pilot placebo-controlled clinical trial	atomoxetine	20	8 weeks	above 18	change in the baseline PANSS score	10 (6 M/4 F) 10 (5 M/5 F)	atomoxetine, 40 mg/day placebo 40 mg/day	4.7 ± 5.1 4.4 ± 8.9	8/10 6/10	0.15
Takahashi et al. ¹⁹ 2009	<i>Journal of Child and Adolescent Psychopharmacology</i>	randomized, double-blind, placebo-controlled study	atomoxetine	245	8 weeks	6–18	ADHD rating scale	52 M/10 F 52 M/10 F	atomoxetine 0.5 mg per day placebo (10 mg day)	38 ± 61.3 37 ± 59.7	61/62 60/62	0.01
Ball et al. ²⁰ 2011	<i>Clinical Schizophrenia & Related Psychoses</i>	double-blind controlled trial	atomoxetine	36	2 weeks	35–60 years	SAS total scores	13 M/6 F 12 M/5 F	atomoxetine 40 mg/day placebo 40 mg/day	1.2 ± 1.7 1.1 ± 1.1	13/17 5/18	0.02
Pourshams et al. ²¹ 2020	<i>Clinical Schizophrenia & Related Psychoses</i>	randomized controlled clinical study	atomoxetine	60	2 years	21–39 years	change in baseline PANSS score	16 M/14 F 17 M/13 F	atomoxetine, 40 mg/day placebo 40 mg/day	62.33 ± 9.37 52.16 ± 8.33	30/30 25/30	0.002

PANSS – Positive and Negative Syndrome Scale; HAM-D – Hamilton Depression Rating Scale; DAS – Depression, Anxiety and Stress score; ADHD – attention deficit hyperactivity disorder; SAS – Social Adjustment Score.

Table 2. Risk assessment for included studies

Study ID and year	Schutz and Berk ⁸ 2001	Versiani et al. ⁹ 2002	Müller et al. ¹⁰ 2006	Brunnauer et al. ¹¹ 2008	Poyurovsky et al. ¹² 2009	Cohen-Yavin et al. ¹³ 2009	Amrami-Weizman et al. ¹⁴ 2013	Usall et al. ¹⁵ 2014	Shoja Shafiqi et al. ¹⁶ 2015	Michelson et al. ¹⁷ 2002	Friedman et al. ¹⁸ 2008	Takahashi et al. ¹⁹ 2009	Ball et al. ²⁰ 2011	Pourshams et al. ²¹ 2020
Was a consecutive or random sample of patients enrolled?	Y	Y	Y	Y	Y	Y	Y	Y	Y	Y	Y	Y	Y	Y
Did the study avoid inappropriate exclusions?	Y	Y	Y	Y	Y	Y	Y	Y	Y	Y	Y	Y	Y	Y
Did all patients receive the same reference standard?	Y	Y	Y	Y	Y	Y	Y	Y	Y	Y	Y	Y	Y	Y
Were all patients included in the analysis?	N	N	N	N	N	N	N	N	N	N	N	N	N	N
Was the sample frame appropriate to address the target population?	Y	Y	Y	Y	Y	Y	Y	Y	Y	Y	Y	Y	Y	Y
Were study participants sampled in an appropriate way?	Y	Y	Y	Y	Y	Y	Y	Y	Y	Y	Y	Y	Y	Y
Were the study subjects and the setting described in detail?	Y	Y	Y	Y	Y	Y	Y	Y	Y	Y	Y	Y	Y	Y
Were valid methods used for the identification of the condition?	Y	Y	Y	Y	Y	Y	Y	Y	Y	Y	Y	Y	Y	Y
Was the condition measured in a standard, reliable way for all participants?	Y	Y	Y	Y	Y	Y	Y	Y	Y	Y	Y	Y	Y	Y
Was there appropriate statistical analysis?	Y	Y	Y	Y	Y	Y	Y	Y	Y	Y	Y	Y	Y	Y

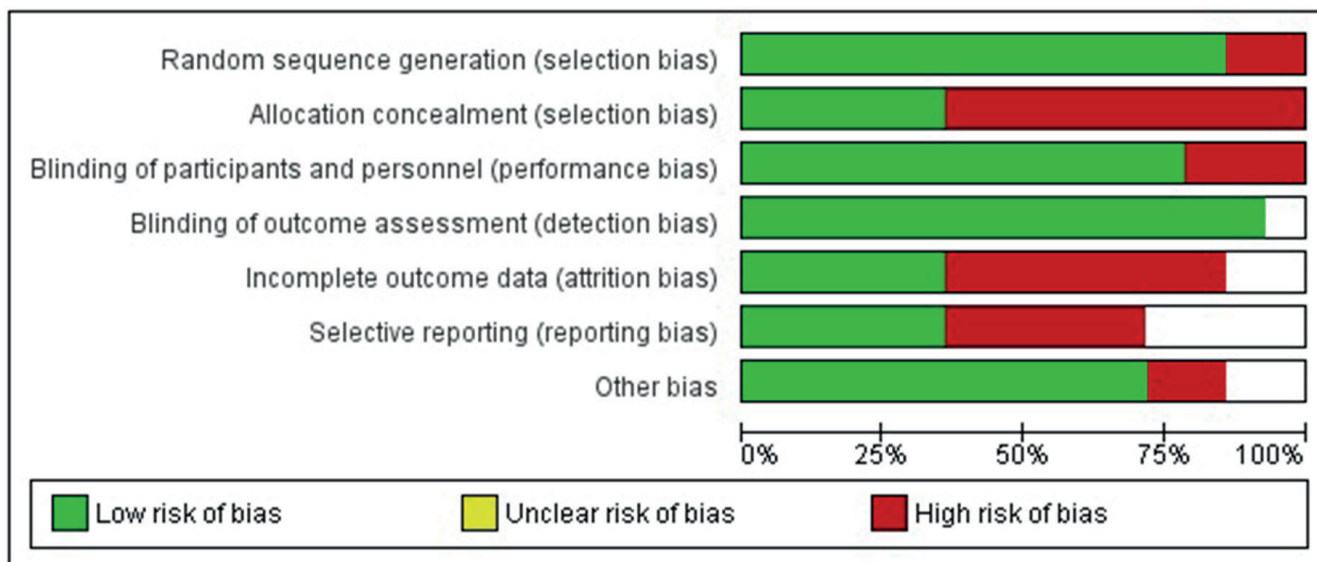


Fig. 4. Risk of bias graph

The included studies encompassed adult patients of different age groups who were chosen randomly and treated with either placebo or NRIs. In both cases, reductions in HAM-D score and PANSS score, as well as changes in metabolic parameters were observed.

Meta-analysis results

Meta-analysis of the included studies using a random effects model indicated that they had a low risk of publication bias since both the Egger’s test and the Begg’s test

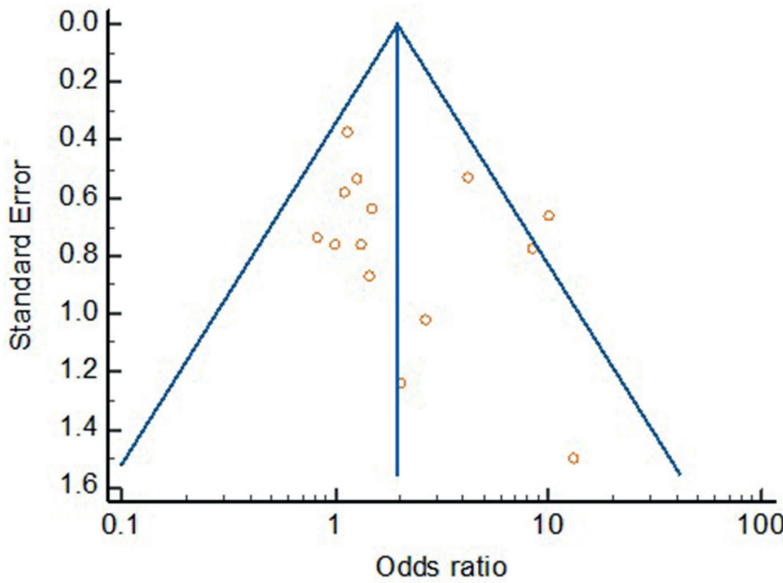


Fig. 5. Funnel plot for publication bias
95% CI – 95% confidence interval.

Publication bias	
Egger's test	
Intercept	1.2002
95% CI	-0.9821 to 3.3826
Significance level	P = 0.2539
Begg's test	
Kendall's Tau	0.3187
Significance level	P = 0.1124

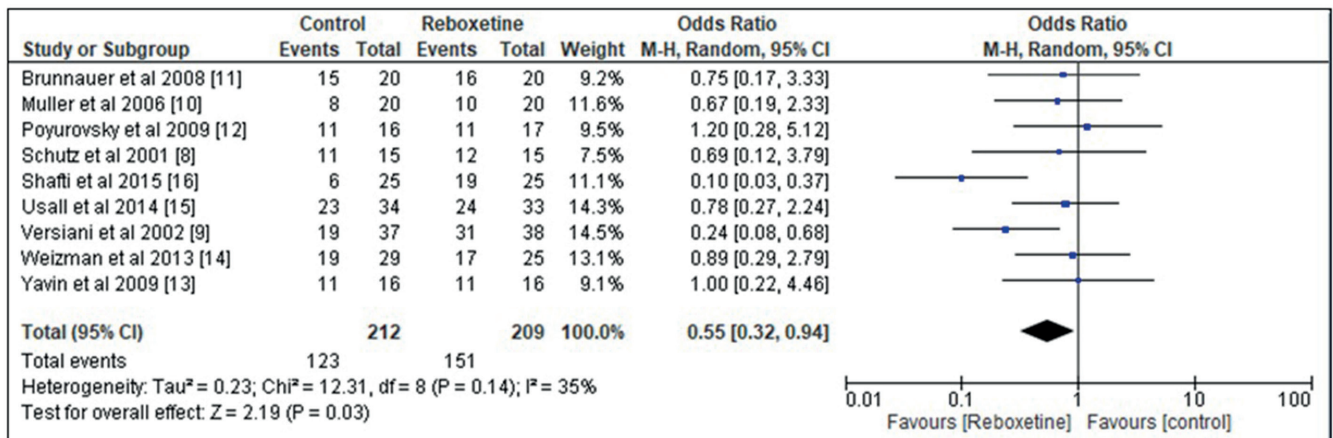


Fig. 6. Funnel plot for reboxetine
95% CI – 95% confidence interval; df – degrees of freedom; M-H – Mantel–Haenszel method.

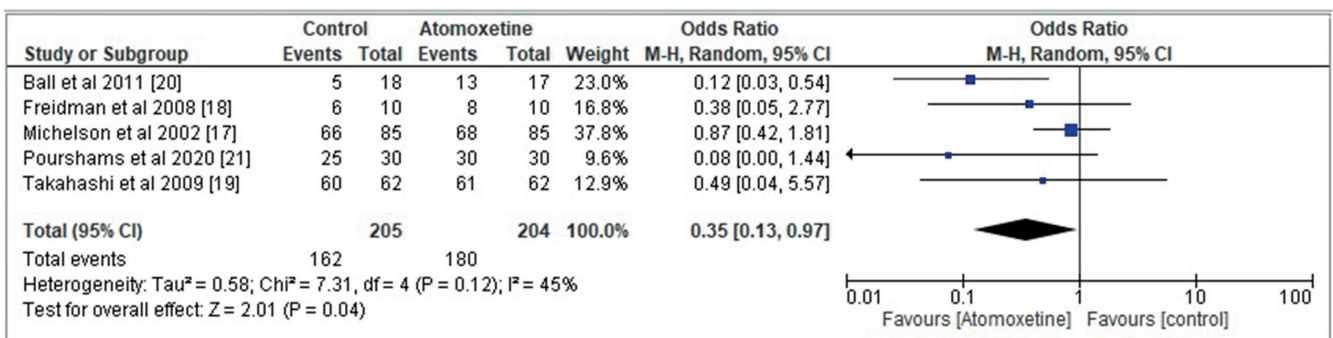


Fig. 7. Forest plot for the odds ratio of atomoxetine
95% CI – 95% confidence interval; df – degrees of freedom; M-H – Mantel–Haenszel method.

p-values were > 0.05. Specifically, the Egger's test gave a p-value of 0.25 and the Begg's test gave a p-value of 0.11 (Fig. 5). The analysis of reboxetine resulted in an OR value of 0.55 (0.32–0.94), a Tau² value of 0.23, a χ^2 value of 12.31, 8 degrees of freedom (df), I² value of 35%, a Z value of 2.19,

and a p-value of 0.03 (Fig. 6). Similarly, atomoxetine produced an OR of 0.35 (0.13–0.97), with Tau² value of 0.58, χ^2 value of 7.31, 4 df, an I² value of 45%, a Z value of 2.01, and a p-value of 0.04 (Fig. 7). All results were statistically significant and heterogeneous.

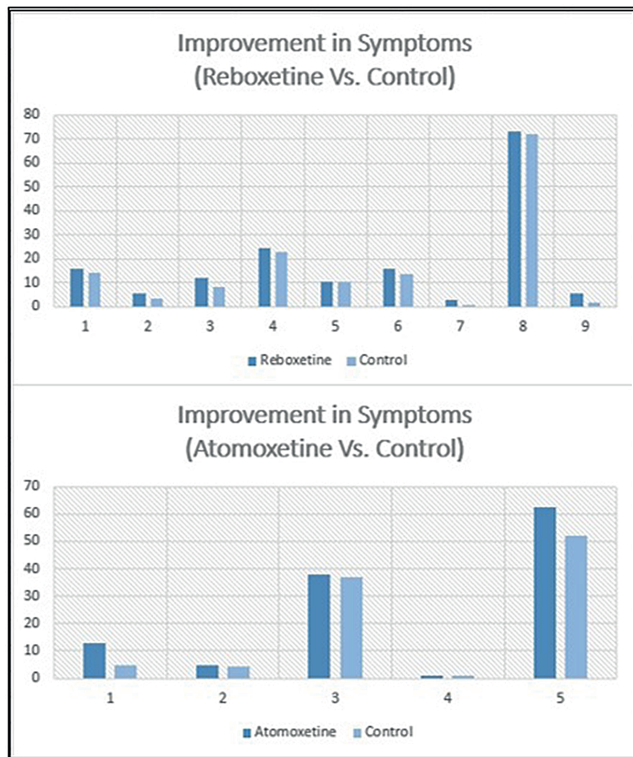


Fig. 8. Improvement in symptoms with norepinephrine reuptake inhibitors (NRIs) compared to controls

Greater efficacy and safety of the NRIs reboxetine and atomoxetine were demonstrated for the treatment of schizophrenia and ADHD patients. Indeed, both drugs led to a larger change in the evaluated test scores, including HAM-D and PANSS, in comparison to the control drugs (Table 3 and Fig. 8).

A statistical summary of the meta-analysis results is shown in Table 4. The pooled OR < 1 for both drugs suggests that they have comparable efficacy, and both have potential use in the treatment of schizophrenia and ADHD.

Combining all results of the meta-analysis, it is clear that reboxetine and atomoxetine are safe and as effective as comparable drugs. Indeed, these NRIs were effective in reducing HAM-D and PANSS scores, along with other clinical symptoms in schizophrenia patients. In fact, they have shown greater efficacy in comparison to control drugs and had fewer adverse side effects. Therefore, these drugs are a better alternative for the treatment of schizophrenia and ADHD.

Discussion

Neurological disorders such as schizophrenia and ADHD are serious health disorders that result in individuals becoming socially isolated, depressed, confused, unhappy, less organized, and sad. If left untreated, they can lead to more serious neurological issues such as borderline personality disorder, which can provoke suicide attempts.^{32–36} Studies suggest that fear conditioning, changes in the immune system and metabolic changes are also responsible for the development of these neurological disorders.^{37–40} Therefore, these disorders need to be detected in a timely manner using various neuroimaging modalities^{41–44} and should be treated using available strategies such as behavioral therapy, family therapy or with anti-psychotic medications.^{45,46} Indeed, NRIs are widely applied in the treatment of mental disorders.

Table 3. Comparison of norepinephrine transporter inhibitor drugs with control drugs

Study ID and year	Evaluation of results	Norepinephrine transporter inhibitors	Control
Reboxetine			
Schutz and Berk ⁸ 2001	change in the baseline PANSS score	15.8 ±7.29	14.1 ±5.68
Versiani et al. ⁹ 2002	change in the baseline PANSS score	5.2	3.2
Müller et al. ¹⁰ 2006	reduction in the HAM-D score	12.1 ±8.3	7.9 ±7.1
Brunnauer et al. ¹¹ 2008	reduction in the HAM-D score	24.2 ±6.7	22.6 ±6.5
Poyurovsky et al. ¹² 2009	HAM-D score	10.31 ±3.34	10.18 ±4.65
Cohen-Yavin et al. ¹³ 2009	total DAS score	15.6 ±11.7	13.4 ±13.1
Amrami-Weizman et al. ¹⁴ 2013	change in serum insulin level (microIU/mL)	2.76 ±33.37	0.83 ±13.79
Usall et al. ¹⁵ 2014	change in the baseline PANSS score	73.13 ±10.31	72.06 ±15.15
Shoja Shafiqi et al. ¹⁶ 2015	reduction in the HAM-D score	5.36 ±1.83	1.69 ±6.02
Atomoxetine			
Michelson et al. ¹⁷ 2002	reduction in the ADHD rating scale	12.8 ±12.4	5.0 ±10.4
Friedman et al. ¹⁸ 2008	change in the baseline PANSS score	4.7 ±5.1	4.4 ±8.9
Takahashi et al. ¹⁹ 2009	ADHD rating scale	38 ±61.3	37 ±59.7
Ball et al. ²⁰ 2011	SAS total scores	1.2 ±1.7	1.1 ±1.1
Pourshams et al. ²¹ 2020	change in the baseline PANSS score	62.33 ±9.37	52.16 ±8.33

PANSS – Positive and Negative Syndrome Scale; HAM-D – Hamilton Depression Rating Scale; DAS – Depression, Anxiety and Stress score; ADHD – attention deficit hyperactivity disorder; SAS – Social Adjustment Score.

Table 4. Statistical summary of included studies

Reboxetine: study ID and year	Odds ratio [#] (95% CI)	Atomoxetine: study ID and year	Odds ratio [#] (95% CI)
Brunnauer et al. ¹¹ 2008	0.75 (0.17–3.33)	Ball et al. ²⁰ 2011	0.12 (0.03–0.54)
Müller et al. ¹⁰ 2006	0.67 (0.19–2.33)	Friedman et al. ¹⁸ 2008	0.38 (0.05–2.77)
Poyurovsky et al. ¹² 2009	1.20 (0.28–5.12)	Michelson et al. ¹⁷ 2002	0.87 (0.42–1.81)
Schutz and Berk ⁸ 2001	0.69 (0.12–3.79)	Pourshams et al. ²¹ 2020	0.80 (0.00–1.44)
Shoja Shafiqi et al. ¹⁶ 2015	0.10 (0.03–0.37)	Takahashi et al. ¹⁹ 2009	0.49 (0.04–5.57)
Usall et al. ¹⁵ 2014	0.78 (0.27–2.24)		
Versiani et al. ⁹ 2002	0.24 (0.08–0.68)		
Amrami-Weizman et al. ¹⁴ 2013	0.89 (0.29–2.79)		
Cohen-Yavin et al. ¹³ 2009	1.00 (0.22–4.46)		
Total (95% CI)	0.55 (0.32–0.94)	Total (95% CI)	0.35 (0.13–0.97)

[#] Odds ratio is calculated using the Mantel–Haenszel (M–H) method with random effects; 95% CI – 95% confidence interval.

As Maletic et al. reported in their systematic review, alpha-adrenergic receptors play an important role in the aberrant regulation of arousal and cognition in schizophrenia.⁴⁷ Similarly, Mäki-Marttunen et al. noted the importance of the locus coeruleus-norepinephrine system in cognition and the pathophysiology of schizophrenia.⁴⁸ A study conducted by Navarra et al. reported on the potential benefits of atomoxetine for reducing clinical symptoms in an animal model of schizophrenia.⁴⁹ Furthermore, Locher et al. presented potential benefits of NRIs for the treatment of these psychiatric disorders in children.⁵⁰ Additionally, Outhred et al.,⁵¹ Ruhé et al.,⁵² Rubia et al.,⁵³ and Papakostas et al.⁵⁴ showed that NRIs are efficacious in the treatment of neurological disorders.

Similar to the available literature, current systematic review and meta-analysis also has low risk of bias and demonstrated that reboxetine and atomoxetine have significant ORs and favorable statistical parameters for the treatment of schizophrenia and ADHD. Indeed, comparable pooled OR values were 0.55 (0.32–0.94) for reboxetine and 0.35 (0.13–0.97) for atomoxetine. Both of these values are significant as they are less than 1. The results were heterogeneous and significant ($p < 0.05$) and there was a low risk of publication bias. These results are predictive of the potential benefits of atomoxetine and reboxetine for the treatment of neurological disorders and favor their use as beneficial drug candidates.

Limitations

Limitations of the present study include the variability of NRIs and control drugs used for the treatment of schizophrenia and ADHD patients. Also, the calculation of different scores including HAM-D scores, PANSS scores and metabolic parameters, using varying analytical tests performed by different persons, increased the risk of false-negative results. Furthermore, the data could be impacted to some extent by the fact that several analyzed studies did not report on the comparable efficacy of NRIs with conventional drugs. Data from other relevant studies

on the efficacy of NRIs for the treatment of schizophrenia and ADHD could have also included more results to guide the use of NRIs more precisely. Additionally, detailed data on patient's case history, physical examination, social well-being, and pathological tests would make the results of the studies more useful in planning the treatment.

Conclusions

For the treatment of neurological disorders such as schizophrenia and ADHD, various medications that can block the activity of selective neurotransmitters are currently in use. The current study was designed to conduct a meta-analysis on the efficacy of the NRIs reboxetine and atomoxetine for the treatment of schizophrenia and ADHD, respectively. On the basis of the statistically significant findings and alleviation clinical symptoms in patients with the use of these drugs, we recommend the use of these NRIs for the treatment of these medical disorders.

Data availability statement

The datasets generated during and/or analyzed during the current study are available from the corresponding author upon reasonable request.

ORCID iDs

Xiaojing Hu  <https://orcid.org/0000-0002-3659-6120>

Lili Pan  <https://orcid.org/0000-0001-5539-1692>

Wenjie Li  <https://orcid.org/0000-0002-3546-1224>

References

- Oud MJ, Meyboom-de Jong B. Somatic diseases in patients with schizophrenia in general practice: Their prevalence and health care. *BMC Fam Pract.* 2009;10(1):32. doi:10.1186/1471-2296-10-32
- Keith SJ, Kane JM. Partial compliance and patient consequences in schizophrenia: Our patients can do better. *J Clin Psychiatry.* 2003; 64(11):1308–1315. doi:10.4088/JCP.v64n1105
- Shuler K. Approaches to improve adherence to pharmacotherapy in patients with schizophrenia. *Patient Prefer Adherence.* 2014;8:701–714. doi:10.2147/PPA.S59371

4. Sinkeviciute I, Begemann M, Prikken M, et al. Efficacy of different types of cognitive enhancers for patients with schizophrenia: A meta-analysis. *NPJ Schizophr*. 2018;4(1):22. doi:10.1038/s41537-018-0064-6
5. Schlessinger A, Geier E, Fan H, et al. Structure-based discovery of prescription drugs that interact with the norepinephrine transporter, NET. *Proc Natl Acad Sci U S A*. 2011;108(38):15810–15815. doi:10.1073/pnas.1106030108
6. Zhou J. Norepinephrine transporter inhibitors and their therapeutic potential. *Drugs Fut*. 2004;29(12):1235. doi:10.1358/dof.2004.029.12.855246
7. Kishi T, Mukai T, Matsuda Y, Moriwaki M, Iwata N. Efficacy and safety of noradrenalin reuptake inhibitor augmentation therapy for schizophrenia: A meta-analysis of double-blind randomized placebo-controlled trials. *J Psychiatr Res*. 2013;47(11):1557–1563. doi:10.1016/j.jpsychires.2013.07.003
8. Schutz G, Berk M. Reboxetine add on therapy to haloperidol in the treatment of schizophrenia: A preliminary double-blind randomized placebo-controlled study. *Int Clin Psychopharmacol*. 2001;16(5):275–278. doi:10.1097/00004850-200109000-00004
9. Versiani M, Cassano G, Perugi G, et al. Reboxetine, a selective norepinephrine reuptake inhibitor, is an effective and well-tolerated treatment for panic disorder. *J Clin Psychiatry*. 2002;63(1):31–37. doi:10.4088/JCP.v63n0107
10. Müller N, Schwarz MJ, Dehning S, et al. The cyclooxygenase-2 inhibitor celecoxib has therapeutic effects in major depression: Results of a double-blind, randomized, placebo controlled, add-on pilot study to reboxetine. *Mol Psychiatry*. 2006;11(7):680–684. doi:10.1038/sj.mp.4001805
11. Brunnauer A, Laux G, David I, Fric M, Hermisson I, Moller HJ. The impact of reboxetine and mirtazapine on driving simulator performance and psychomotor function in depressed patients. *J Clin Psychiatry*. 2008;69(12):1880–1886. doi:10.4088/JCP.v69n1205
12. Poyurovsky M, Faragian S, Fuchs C, Pashinian A. Effect of the selective norepinephrine reuptake inhibitor reboxetine on cognitive dysfunction in schizophrenia patients: An add-on, double-blind placebo-controlled study. *Isr J Psychiatry Relat Sci*. 2009;46(3):213–220. PMID: 20039523
13. Cohen-Yavin I, Yoran-Hegesh R, Strous RD, Kotler M, Weizman A, Spivak B. Efficacy of reboxetine in the treatment of attention-deficit/hyperactivity disorder in boys with intolerance to methylphenidate: An open-label, 8-week, methylphenidate-controlled trial. *Clin Neuropharmacol*. 2009;32(4):179–182. doi:10.1097/WNF.0b013e318183796d
14. Amrami-Weizman A, Maayan R, Gil-Ad I, et al. The effect of reboxetine co-administration with olanzapine on metabolic and endocrine profile in schizophrenia patients. *Psychopharmacology (Berl)*. 2013;230(1):23–27. doi:10.1007/s00213-013-3199-1
15. Usall J, López-Carrilero R, Iniesta R, et al. Double-blind, placebo-controlled study of the efficacy of reboxetine and citalopram as adjuncts to atypical antipsychotics for negative symptoms of schizophrenia. *J Clin Psychiatry*. 2014;75(6):608–615. doi:10.4088/JCP.13m08551
16. Shoja Shafiti S, Jafarabad MS, Azizi R. Amelioration of deficit syndrome of schizophrenia by norepinephrine reuptake inhibitor. *Ther Adv Psychopharmacol*. 2015;5(5):263–270. doi:10.1177/2045125315591953
17. Michelson D, Allen AJ, Busner J, et al. Once-daily atomoxetine treatment for children and adolescents with attention deficit hyperactivity disorder: A randomized, placebo-controlled study. *Am J Psychiatry*. 2002;159(11):1896–1901. doi:10.1176/appi.ajp.159.11.1896
18. Friedman JI, Carpenter D, Lu J, et al. A pilot study of adjunctive atomoxetine treatment to second-generation antipsychotics for cognitive impairment in schizophrenia. *J Clin Psychopharmacol*. 2008;28(1):59–63. doi:10.1097/jcp.0b013e318161318f
19. Takahashi M, Takita Y, Yamazaki K, et al. A randomized, double-blind, placebo-controlled study of atomoxetine in Japanese children and adolescents with attention-deficit/hyperactivity disorder. *J Child Adolesc Psychopharmacol*. 2009;19(4):341–350. doi:10.1089/cap.2008.0154
20. Ball M, Warren K, Feldman S, McMahon R, Kelly D, Buchanan R. Placebo-controlled trial of atomoxetine for weight reduction in people with schizophrenia treated with clozapine or olanzapine. *Clin Schizophr Relat Psychoses*. 2011;5(1):17–25. doi:10.3371/CSRP.5.1.3
21. Pourshams M, Riahi F, Tashakori A, Erfanifar F. The evaluation of atypical antipsychotic augmentation with atomoxetine in the reduction of negative symptoms in patients with schizophrenia: A randomized, double-blind, placebo-controlled clinical trial. *Clin Schizophr Relat Psychoses*. 2020;14(2):54–57. <https://www.clinicalschizophrenia.net/articles/the-evaluation-of-atypical-antipsychotic-augmentation-with-atomoxetine-in-the-reduction-of-negative-symptoms-in-patients.pdf>. Accessed November 16, 2021.
22. Salazar de Pablo G, Woods SW, Drymonitou G, de Diego H, Fusar-Poli P. Prevalence of individuals at clinical high-risk of psychosis in the general population and clinical samples: Systematic review and meta-analysis. *Brain Sci*. 2021;11(11):1544. doi:10.3390/brainsci11111544
23. Tanaka M, Spekker E, Szabó Á, Polyák H, Vécsei L. Modelling the neurodevelopmental pathogenesis in neuropsychiatric disorders. Bioactive kynurenines and their analogues as neuroprotective agents: In celebration of 80th birthday of Professor Peter Riederer. *J Neural Transm*. 2022;129(5–6):627–642. doi:10.1007/s00702-022-02513-5
24. Nyatega CO, Qiang L, Adamu MJ, Younis A, Kawuwa HB. Altered dynamic functional connectivity of cuneus in schizophrenia patients: A resting-state fMRI study. *Appl Sci*. 2021;11(23):11392. doi:10.3390/app112311392
25. Panov G. Dissociative model in patients with resistant schizophrenia. *Front Psychiatry*. 2022;13:845493. doi:10.3389/fpsy.2022.845493
26. Rog J, Błażewicz A, Juchnowicz D, et al. The role of GPR120 receptor in essential fatty acids metabolism in schizophrenia. *Biomedicines*. 2020;8(8):243. doi:10.3390/biomedicines8080243
27. Gaebler AJ, Finner-Prével M, Sudar FP, et al. The interplay between vitamin D, exposure of anticholinergic antipsychotics and cognition in schizophrenia. *Biomedicines*. 2022;10(5):1096. doi:10.3390/biomedicines10051096
28. Correia BSB, Nani JV, Waladares Ricardo R, et al. Effects of psychostimulants and antipsychotics on serum lipids in an animal model for schizophrenia. *Biomedicines*. 2021;9(3):235. doi:10.3390/biomedicines9030235
29. Matthews PRL, Horder J, Pearce M. Selective noradrenaline reuptake inhibitors for schizophrenia. *Cochrane Database Syst Rev*. 2018;2018(1):CD010219. doi:10.1002/14651858.CD010219.pub2
30. Wilens TE, Spencer TJ. Understanding attention-deficit/hyperactivity disorder from childhood to adulthood. *Postgrad Med*. 2010;122(5):97–109. doi:10.3810/pgm.2010.09.2206
31. De Crescenzo F, Ziganshina LE, Yudina EV, et al. Noradrenaline reuptake inhibitors (NRIs) for attention deficit hyperactivity disorder (ADHD) in adults. *Cochrane Database Syst Rev*. 2018;2018(6):CD013044. doi:10.1002/14651858.CD013044
32. Hor K, Taylor M. Suicide and schizophrenia: A systematic review of rates and risk factors. *J Psychopharmacol*. 2010;24(4 Suppl):81–90. doi:10.1177/1359786810385490
33. Balhara YP, Verma R. Schizophrenia and suicide. *East Asian Arch Psychiatry*. 2012;22(3):126–133. PMID:23019287.
34. Siris SG. Suicide and schizophrenia. *J Psychopharmacol*. 2001;15(2):127–135. doi:10.1177/026988110101500209
35. James A, Lai FH, Dahl C. Attention deficit hyperactivity disorder and suicide: A review of possible associations. *Acta Psychiatr Scand*. 2004;110(6):408–415. doi:10.1111/j.1600-0447.2004.00384.x
36. Beauchaine TP, Ben-David I, Bos M. ADHD, financial distress, and suicide in adulthood: A population study. *Sci Adv*. 2020;6(40):eaba1551. doi:10.1126/sciadv.aba1551
37. Battaglia S, Orsolini S, Borgomaneri S, Barbieri R, Diciotti S, di Pellegrino G. Characterizing cardiac autonomic dynamics of fear learning in humans. *Psychophysiology*. 2022;2022:e14122. doi:10.1111/psyp.14122
38. Battaglia S, Thayer JF. Functional interplay between central and autonomic nervous systems in human fear conditioning. *Trends Neurosci*. 2022;45(7):504–506. doi:10.1016/j.tins.2022.04.003
39. Tanaka M, Tóth F, Polyák H, Szabó Á, Mándi Y, Vécsei L. Immune influencers in action: Metabolites and enzymes of the tryptophan-kynurenine metabolic pathway. *Biomedicines*. 2021;9(7):734. doi:10.3390/biomedicines9070734
40. Martin EI, Ressler KJ, Binder E, Nemeroff CB. The neurobiology of anxiety disorders: Brain imaging, genetics, and psychoneuroendocrinology. *Psychiatr Clin North Am*. 2009 Sep;32(3):549–75. doi:10.1016/j.psc.2009.05.004
41. Battaglia S, Fabius JH, Moravkova K, Fracasso A, Borgomaneri S. The neurobiological correlates of gaze perception in healthy individuals and neurologic patients. *Biomedicines*. 2022;10(3):627. doi:10.3390/biomedicines10030627

42. Trajkovic J, Di Gregorio F, Ferri F, Marzi C, Diciotti S, Romei V. Resting state alpha oscillatory activity is a valid and reliable marker of schizotypy. *Sci Rep.* 2021;11(1):10379. doi:10.1038/s41598-021-89690-7
43. Marsicano G, Cerpelloni F, Melcher D, Ronconi L. Lower multisensory temporal acuity in individuals with high schizotypal traits: A web-based study. *Sci Rep.* 2022;12(1):2782. doi:10.1038/s41598-022-06503-1
44. Borgomaneri S, Battaglia S, Avenanti A, di Pellegrino G. Don't Hurt Me No More: State-dependent transcranial magnetic stimulation for the treatment of specific phobia. *J Affect Disord.* 2021;286:78–79. doi:10.1016/j.jad.2021.02.076
45. Lacro JP, Dunn LB, Dolder CR, Leckband SG, Jeste DV. Prevalence of and risk factors for medication nonadherence in patients with schizophrenia: A comprehensive review of recent literature. *J Clin Psychiatry.* 2002;63(10):892–909. doi:10.4088/JCP.v63n1007
46. Finnerup NB, Attal N, Haroutounian S, et al. Pharmacotherapy for neuropathic pain in adults: A systematic review and meta-analysis. *Lancet Neurol.* 2015;14(2):162–173. doi:10.1016/S1474-4422(14)70251-0
47. Maletic V, Eramo A, Gwin K, Offord SJ, Duffy RA. The role of norepinephrine and its α -adrenergic receptors in the pathophysiology and treatment of major depressive disorder and schizophrenia: A systematic review. *Front Psychiatry.* 2017;8:42. doi:10.3389/fpsy.2017.00042
48. Mäki-Marttunen V, Andreassen OA, Espeseth T. The role of norepinephrine in the pathophysiology of schizophrenia. *Neurosci Behav Rev.* 2020;118:298–314. doi:10.1016/j.neubiorev.2020.07.038
49. Navarra R, Graf R, Huang Y, et al. Effects of atomoxetine and methylphenidate on attention and impulsivity in the 5-choice serial reaction time test. *Prog Neuropsychopharmacol Biol Psychiatry.* 2008;32(1):34–41. doi:10.1016/j.pnpbp.2007.06.017
50. Locher C, Koechlin H, Zion SR, et al. Efficacy and safety of selective serotonin reuptake inhibitors, serotonin-norepinephrine reuptake inhibitors, and placebo for common psychiatric disorders among children and adolescents: A systematic review and meta-analysis. *JAMA Psychiatry.* 2017;74(10):1011. doi:10.1001/jamapsychiatry.2017.2432
51. Outhred T, Hawkshead BE, Wager TD, Das P, Malhi GS, Kemp AH. Acute neural effects of selective serotonin reuptake inhibitors versus noradrenaline reuptake inhibitors on emotion processing: Implications for differential treatment efficacy. *Neurosci Biobehav Rev.* 2013;37(8):1786–1800. doi:10.1016/j.neubiorev.2013.07.010
52. Ruhé HG, Mason NS, Schene AH. Mood is indirectly related to serotonin, norepinephrine and dopamine levels in humans: A meta-analysis of monoamine depletion studies. *Mol Psychiatry.* 2007;12(4):331–359. doi:10.1038/sj.mp.4001949
53. Rubia K, Alegria AA, Cubillo AI, Smith AB, Brammer MJ, Radua J. Effects of stimulants on brain function in attention-deficit/hyperactivity disorder: A systematic review and meta-analysis. *Biol Psychiatry.* 2014;76(8):616–628. doi:10.1016/j.biopsych.2013.10.016
54. Papakostas GI, Nelson JC, Kasper S, Möller HJ. A meta-analysis of clinical trials comparing reboxetine, a norepinephrine reuptake inhibitor, with selective serotonin reuptake inhibitors for the treatment of major depressive disorder. *Eur Neuropsychopharmacol.* 2008;18(2):122–127. doi:10.1016/j.euroneuro.2007.07.005

Complications of implanted port catheters and peripherally inserted central catheters in chemotherapy-treated cancer patients: A meta-analysis

Yuanli Sun^{1,B,D}, Xiangchun Wu^{2,A,F}

¹ Department of Hematology, Huanggang Central Hospital, China

² Department of Medical Care Security, Huanggang Central Hospital, China

A – research concept and design; B – collection and/or assembly of data; C – data analysis and interpretation; D – writing the article; E – critical revision of the article; F – final approval of the article

Advances in Clinical and Experimental Medicine, ISSN 1899–5276 (print), ISSN 2451–2680 (online)

Adv Clin Exp Med. 2023;32(5):523–532

Address for correspondence

Xiangchun Wu

E-mail: wuxiangchun_sci@outlook.com

Funding sources

None declared

Conflict of interest

None declared

Received on June 26, 2022

Reviewed on July 29, 2022

Accepted on November 7, 2022

Published online on December 19, 2022

Cite as

Sun Y, Wu X. Complications of implanted port catheters and peripherally inserted central catheters in chemotherapy-treated cancer patients: A meta-analysis. *Adv Clin Exp Med.* 2023;32(5):523–532. doi:10.17219/acem/156346

DOI

10.17219/acem/156346

Copyright

Copyright by Author(s)

This is an article distributed under the terms of the Creative Commons Attribution 3.0 Unported (CC BY 3.0) (<https://creativecommons.org/licenses/by/3.0/>)

Abstract

Background. One of the most significant advancements in nursing technology for cancer patients has been the development of implantable port catheters and peripherally inserted central venous catheters. They create an essential, dependable route for subjects to receive chemotherapy, long-term infusions and nutritional care, and provide a site for regular blood draws.

Objectives. We performed a meta-analysis to evaluate the complications of implanted port catheters and peripherally inserted central catheters in chemotherapy-treated cancer patients.

Materials and methods. A systematic literature search up to April 2022 was performed and a total of 11,801 articles have been retrieved. Of these, 5017 concerned peripherally inserted central catheters and 6784 implanted port catheters to administer chemotherapy. Odds ratios (ORs) and mean differences (MDs) with 95% confidence intervals (95% CIs) were calculated to assess the complications of implanted port catheters and peripherally inserted central catheters in chemotherapy-treated cancer patients using dichotomous and contentious methods with random- or fixed-effects models.

Results. Peripherally inserted central catheters had significantly higher incidence of occlusion complications (OR: 5.43, 95% CI: 3.46–8.52, $p < 0.001$), longer durations of local infection (OR: 2.94, 95% CI: 2.17–4.00, $p < 0.001$), higher incidence of catheter-related infection (OR: 2.13, 95% CI: 1.19–3.83, $p = 0.01$), higher rate of malposition (OR: 6.46, 95% CI: 2.93–14.27, $p < 0.001$), higher rates of catheter-related thrombosis (OR: 2.71, 95% CI: 1.90–3.87, $p < 0.001$), higher incidence of phlebitis complications (OR: 6.67, 95% CI: 2.94–15.11, $p < 0.001$), higher incidence of accidental removal (OR: 3.38, 95% CI: 1.97–5.81, $p < 0.001$), and a shorter catheter lifespan (MD: –233.16, 95% CI: –449.52––16.80, $p = 0.03$) in subjects undergoing chemotherapy compared to those in whom implanted port catheters were used.

Conclusions. Implantable port catheter has advantages over peripherally inserted central catheter in decreasing cancer patients' complications. The outcomes provide evidence for practitioners to select which type of central venous catheters is better for cancer chemotherapy subject.

Key words: cancer treatment using chemotherapy, malposition complications, catheter-related thrombosis, peripherally inserted central catheters

Introduction

The 2nd most common cause of death worldwide is cancer. In China, more than 6 million new cancer cases are diagnosed each year. It is anticipated that the number of cancer patients is going to increase as the environmental and lifestyle factors change. Chemotherapy is frequently used in cancer treatment and can increase the survival times of patients suffering from metastatic cancers.¹ Many chemotherapy agents are administered intravenously and can cause harm to peripheral blood vessels. Central venous access is preferred over peripheral vascular access because recurrent venipunctures can cause discomfort for patients.² In cancer patients receiving chemotherapy, central venous access offers a higher level of security and comfort. The 2 most common infusion routes for chemotherapy are peripherally inserted central venous catheters and implanted port catheters.³ Peripherally inserted central venous catheters, which are central venous catheters placed in the brachial, basilic or cephalic veins, were first developed in the 1970s. In the 1980s, implanted port catheters were developed. These are inserted into the subclavian vein to serve as a port for intravenous access without the use of external catheter lines. One of the most significant developments in nursing technology for cancer patients has been the development of implanted port catheters and peripherally inserted central venous catheters. They create an essential, dependable path for patients to receive chemotherapy, long-term infusions and nutritional care, and provide a site for regular blood draws. As a result, nurses frequently ask about the comparative risks and benefits of these 2 options.² Patient safety and increasing cost awareness are major concerns in healthcare. Therefore, research is frequently centered on comparing the safety of these 2 popular infusion catheters.⁴ Medical decision-makers require more data to thoroughly assess the risks and financial advantages of these 2 types of medical equipment. However, the preference for central venous catheter in terms of safety is not supported by any solid or definitive research. The extent to which these 2 catheters are used differs by nation, with doctors more likely to advise subjects to have a peripherally inserted central venous catheter. The reason for their popularity may be their non-inferior complication rates as compared to the implanted port catheters, and the fact that they are less expensive to implant than the implanted port catheters.⁵ However, research has indicated that the long-term maintenance expenses of peripherally inserted central venous catheters may be even higher than those of implanted port catheters.⁶ According to one study, peripherally inserted central venous catheters have a higher incidence of complications than implanted port catheters (32.8%).⁷ However, in another observational study, complications during 106 intravenous catheterizations were equally common using both techniques.⁸ Occlusion, infection, malposition, catheter breakage, catheter-associated thrombosis, extravasation, phlebitis, pneumothorax, and inadvertent removal

rates are the most frequent catheter-related problems occurring in consequence of using peripherally implanted central venous catheters and implanted port catheters.⁹

Objectives

There is a dearth of information to help doctors and patients decide which catheters are the best choice in a given situation. To improve clinical decision-making, this meta-analysis compares the complications of implanted port catheters and peripherally inserted central catheters in chemotherapy-treated cancer patients.

Materials and methods

Information sources

The main goals of the current meta-analysis were to evaluate the effect of complications for implanted port catheters and peripherally inserted central catheters in chemotherapy-treated cancer patients. All included studies were conducted in humans. Study size or language had no bearing on inclusion. Review articles, comments and research that failed to provide a measure of the association were all excluded from the study. Figure 1 depicts a flowchart of our study. When the following inclusion criteria were satisfied, the publications were included in the meta-analysis. The meta-analysis encompassed studies:

1. Performed as either a prospective, observational, randomized controlled, or retrospective study;

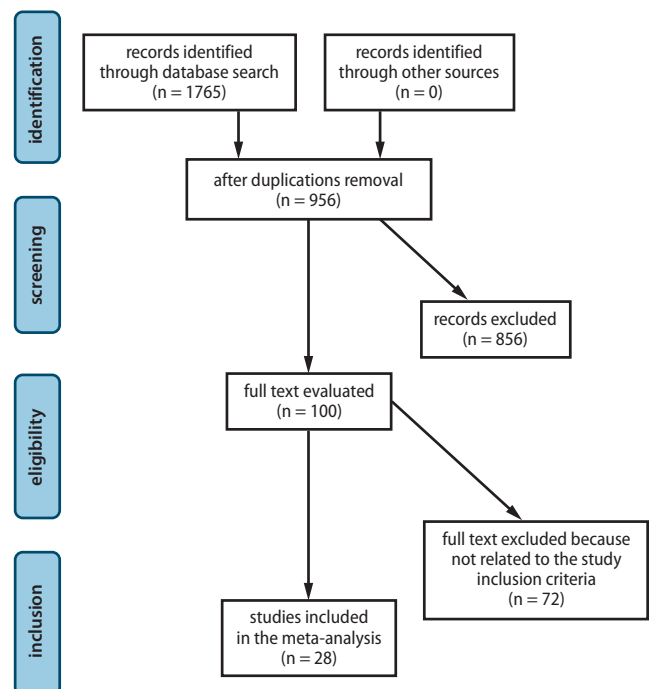


Fig. 1. Flowchart of the study process

Table 1. Search strategy for each database

Database	Search strategy
PubMed	#1 "cancer using chemotherapy" [MeSH terms] OR "peripherally placed central catheters" [all fields] OR "occlusion complications" [all fields] OR "catheter-related thrombosis" [all fields] #2 "implanted port catheters" [MeSH terms] OR "cancer using chemotherapy" [all fields] OR "catheter-related thrombosis" [all fields] OR "occlusion complications" [all fields] OR "malposition complications" [all fields] #3 #1 AND #2
Embase	#1 "cancer using chemotherapy"/exp OR "peripherally placed central catheters"/exp OR "occlusion complications"/exp OR "catheter-related thrombosis" #2 "implanted port catheters"/exp OR "occlusion complications"/exp OR "malposition complications"/exp OR "catheter-related thrombosis" #3 #1 AND #2
Cochrane Library	#1 "cancer using chemotherapy": ti, ab, kw [OR] "peripherally placed central catheters": ti, ab, kw OR "occlusion complications": ti, ab, kw (word variations have been searched) #2 "catheter-related thrombosis": ti, ab, kw OR "implanted port catheters": ti, ab, kw OR "occlusion complications": ti, ab, kw OR "malposition complications": ti, ab, kw OR "catheter-related thrombosis": ti, ab, kw (word variations have been searched) #3 #1 AND #2

MeSH – medical subject headings; ti, ab, kw – terms in the title, abstract or keyword field; exp – exploded indexing term.

2. Enrolling chemotherapy-treated cancer patients;
3. Relying on implanted port catheters and peripherally inserted central catheters for the intervention regimen;
4. Comparing implanted port catheters to peripherally inserted central catheters.

Studies that did not examine the effects of peripherally inserted central catheters and implanted port catheters in cancer patients receiving chemotherapy, research on patients treated without implanted port catheters or peripherally inserted central catheters, and studies where the significance of comparing the 2 outcomes was not emphasized were excluded.

Search strategy

According to the PICOS concept,^{10,11} a protocol of search techniques was created and defined as follows: P (population): chemotherapy-treated cancer patients; I (intervention/exposure): peripherally inserted central catheters and implanted port catheters; C (comparison): peripherally inserted central catheters compared to implanted port catheters; O (outcome): occlusion complications, duration of local infections at puncture sites, catheter-related infection, complications of malpositioning, catheter-related thrombosis, phlebitis complications, accidental removal, and catheter lifespan; S (study design): no restriction.¹²

First, we carried out a thorough search of Ovid, Embase, Cochrane Library, PubMed, and Google Scholar databases up until March 2022 using a combination of keywords and related terms for cancer such as: chemotherapy, peripherally inserted central catheters, implanted port catheters, malposition complications, catheter-related thrombosis, occlusion complications, length of local infection, phlebitis complications, accidental removal, and catheter lifespan, as shown in Table 1. To exclude studies that did not document a relationship between peripherally inserted central catheters and implanted port catheters, all recruited

studies were compiled into an EndNote (Clarivate, London, UK) file, duplicates were eliminated, and the titles and abstracts were checked and reviewed.

Data collection process

The data were condensed based on the following criteria: study- and subject-related characteristics in a standardized form, first author's last name, study period, publication year, country, region, population type, clinical and treatment characteristics, categories, qualitative and quantitative methods of evaluation, information source, outcome evaluation, and statistical analysis.¹³

Data items

When there were varying results from a single study on the impact of complications of peripherally inserted central catheters and implanted port catheters on chemotherapy-treated cancer patients, the data were collected separately.

Study risk of bias assessment

The 2 authors separately examined the methodological quality of the selected research to determine the likelihood of bias in the individual studies. The methodological quality was evaluated using the "risk of bias" instrument from the Cochrane Handbook for Systematic Reviews of Interventions v. 5.1.0.¹⁴ Each study was graded according to the evaluation criteria and classified based on one of the 3 risk levels of bias: low – all quality criteria were satisfied; moderate – one or more quality criteria were partially satisfied or unclear; or high – one or more of the criteria were not met or not included. Reevaluations of the original articles were performed to fix any inconsistencies.

Effect measures

Sensitivity studies were performed on studies that reported and examined the influence of peripherally inserted central catheters compared to implanted port catheters. The comparisons between peripherally inserted central catheters and implanted port catheters were used for sensitivity and subclass analyses.

Synthesis methods

The current meta-analysis used a random- or fixed-effect model with dichotomous techniques to compute the odds ratio (OR) and mean difference (MD), with a 95% confidence interval (95% CI). An I^2 index ranging from 0 to 100% was calculated. Values of around 0%, 25%, 50%, and 75% showed no, low, moderate, and high heterogeneity, respectively.¹⁵ A random effect was considered if the I^2 index was 50% or higher. If the I^2 index was less than 50%, the likelihood of employing fixed influences increased.¹⁵ However, additional characteristics that show a high degree of similarity between the included studies were analyzed to confirm the employment of the correct model. By stratifying the initial evaluation on the previously mentioned outcome categories, a subcategory analysis was completed. For the current analysis, the statistical significance for the differences between subcategories was defined as a p-value of 0.05.

Reporting bias assessment

The publication bias was assessed qualitatively and quantitatively using funnel plots of the logarithms of ORs compared to their standard errors (SEs) and the Egger's regression test (the publication bias was considered present if the p-value was 0.05).¹¹

Certainty assessment

Two-tailed tests were used to calculate all p-values. The Reviewer Manager v. 5.3 was used to provide the statistical analyses and graphs (The Nordic Cochrane Centre, The Cochrane Collaboration, Copenhagen, Denmark).

Results

Out of the 1765 relevant studies, a total of 28 articles published between 2010 and 2022 matched our inclusion criteria and were included in the meta-analysis.^{4,16–42} Table 2 displays the data from these research studies. The chosen studies encompassed 11,801 chemotherapy-treated cancer patients. Of these, 5017 were using peripherally inserted central catheters and 6784 were using implanted port catheters. At the commencement of this meta-analysis, there were 392,970 examined individuals

in total. Sixteen studies presented data grouped according to the occlusion complications, 11 presented data grouped according to the duration of local infections at the puncture sites, 18 according to the catheter-related infections, 7 according to malposition complications, 17 according to catheter-related thrombosis, 8 according to phlebitis complications, 9 according to accidental removal, and 5 according to catheter lifespan.

Peripherally inserted central catheters had a significantly higher risk of occlusion complications (OR: 5.43, 95% CI: 3.46–8.52, $p < 0.001$) with low heterogeneity ($I^2 = 31\%$), a longer duration of local infections at the puncture sites (OR: 2.94, 95% CI: 2.17–4.00, $p < 0.001$) with low heterogeneity ($I^2 = 49\%$), higher incidence of catheter-related infections (OR: 2.13, 95% CI: 1.19–3.83, $p = 0.01$) with moderate heterogeneity ($I^2 = 57\%$), higher incidence of malposition complications (OR: 6.46, 95% CI: 2.93–14.27, $p < 0.001$) with no heterogeneity ($I^2 = 4\%$), higher rates of catheter-related thrombosis (OR: 2.71, 95% CI: 1.90–3.87, $p < 0.001$) with moderate heterogeneity ($I^2 = 35\%$), higher incidence of phlebitis complications (OR: 6.67, 95% CI: 2.94–15.11, $p < 0.001$) with low heterogeneity ($I^2 = 25\%$), higher incidence of accidental removal (OR: 3.38, 95% CI: 1.97–5.81, $p < 0.001$) with no heterogeneity ($I^2 = 0\%$), and shorter catheter lifespans (MD: -233.16, 95% CI: -449.52 – -16.80, $p = 0.03$) with high heterogeneity ($I^2 = 100\%$) compared to implanted port catheters, as shown in Fig. 2–9.

Due to the limited data published for these variables, it was not possible to adjust for individual factors such as gender, age and ethnicity in stratified models to explore the impact of these factors on comparison outcomes. Visual inspection of funnel plots and quantitative measures using the Egger's regression test revealed no evidence of publication bias ($p = 0.89$). However, it was discovered that the majority of the included randomized controlled trials were of poor methodological quality, had no bias in selective reporting and included rather sparse outcome data.

Discussion

This meta-analysis included 11,801 chemotherapy-treated cancer patients. Of these, 5017 were using peripherally inserted central catheters and 6784 had implanted port catheters.^{4,16–42} Peripherally inserted central catheters had significantly higher incidence of occlusion complications, longer duration of local infections at puncture sites, higher incidence of catheter-related infections, higher incidence of malposition complications, higher incidence of catheter-related thrombosis, higher incidence of phlebitis complications, higher incidence of accidental removals, and shorter catheter lifespans compared to implanted port catheters.

A total of 28 cohort studies with more than 10,000 chemotherapy-treated cancer patients studied were included in this study. Practitioners should choose the appropriate type of catheter based on the subject's physical conditions,

Table 2. Characteristics of the studies selected for the meta-analysis

Study	Country	Total	Peripherally inserted central catheters	Implantable port catheters
Rotzinger et al. 2017 ⁴	Switzerland	2568	791	1777
Revel-Vilk et al. 2010 ¹⁶	Israel	314	188	126
Kim et al. 2010 ¹⁷	South Korea	96	24	72
Jain et al. 2013 ¹⁸	India	123	98	25
Patel et al. 2014 ¹⁹	Australia	70	36	34
Viard et al. 2015 ²⁰	France	123	98	25
Bratton et al. 2014 ²¹	USA	144	34	110
Liu 2017 ²²	China	298	120	178
Martella et al. 2015 ²³	Italy	102	45	57
Coady et al. 2015 ²⁴	UK	39	9	30
Wang 2016 ²⁵	China	110	60	50
Lefebvre et al. 2016 ²⁶	France	448	158	290
Verboom et al. 2017 ²⁷	Netherlands	112	10	102
Fang et al. 2017 ²⁸	China	105	60	45
Lu 2017 ²⁹	China	550	214	336
Tang 2014 ³⁰	China	2970	1509	1461
Vashi et al. 2017 ³¹	USA	202	191	11
Taxbro et al. 2019 ³²	Sweden	369	201	168
Clemons et al. 2020 ³³	Canada	48	25	23
Yin and Li 2020 ³⁴	China	763	65	698
Clatot et al. 2020 ³⁵	France	253	126	127
Wang et al. 2022 ³⁶	China	276	138	138
Burbridge et al. 2021 ³⁷	Canada	101	50	51
Yun and Yang 2021 ³⁸	South Korea	467	185	282
Comas et al. 2022 ³⁹	Spain	525	292	233
Zhang et al. 2022 ⁴⁰	China	96	48	48
Pénichoux et al. 2022 ⁴¹	France	479	213	266
McKeown et al. 2022 ⁴²	USA	50	29	21
Total		11,801	5017	6784

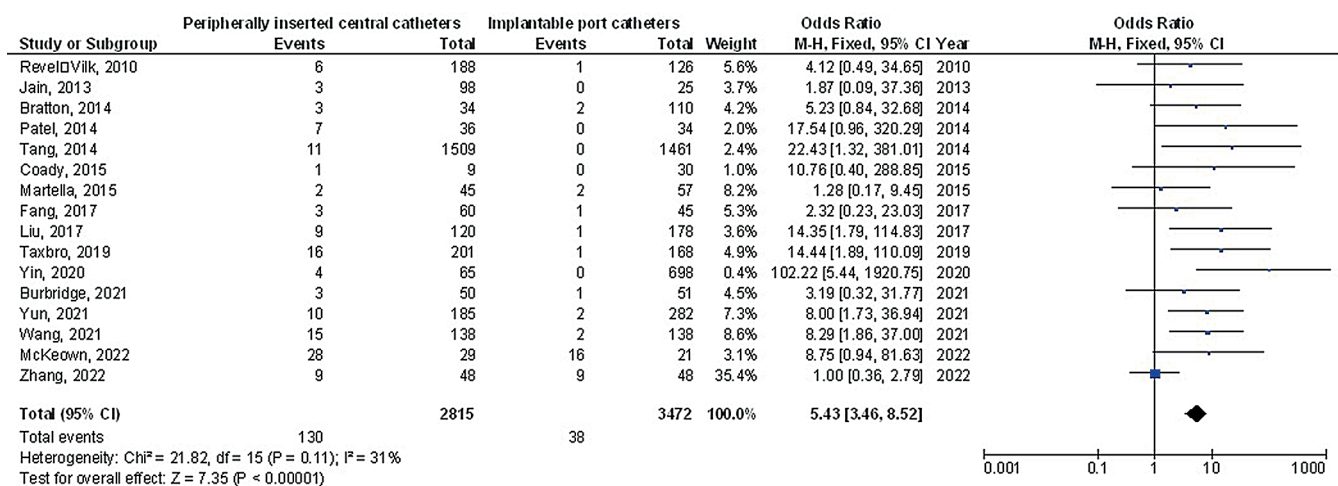


Fig. 2. Forest plot of peripherally inserted central catheters compared to implanted port catheters influence on occlusion complications
df – degrees of freedom; 95% CI – 95% confidence interval.

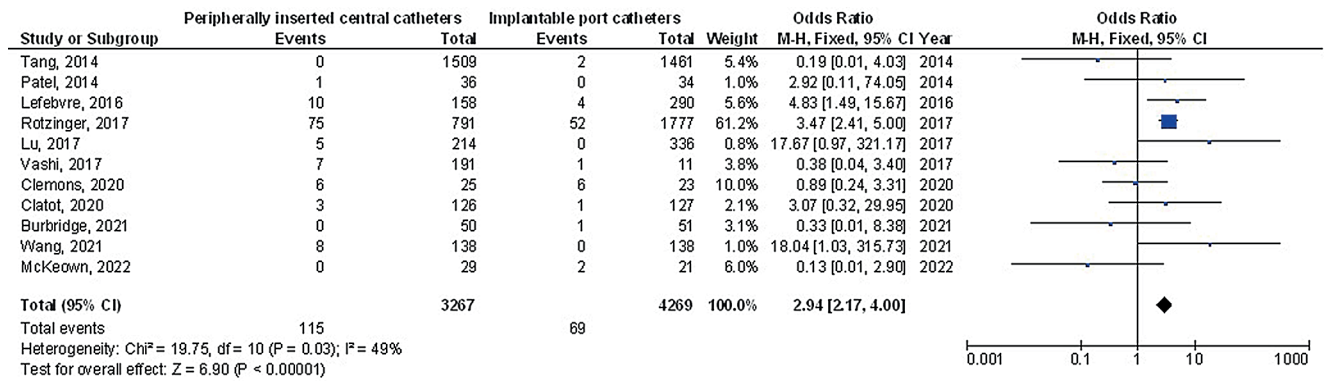


Fig. 3. Forest plot of peripherally inserted central catheters compared to implanted port catheters influence on the length of local infections at puncture sites
df – degrees of freedom; 95% CI – 95% confidence interval.

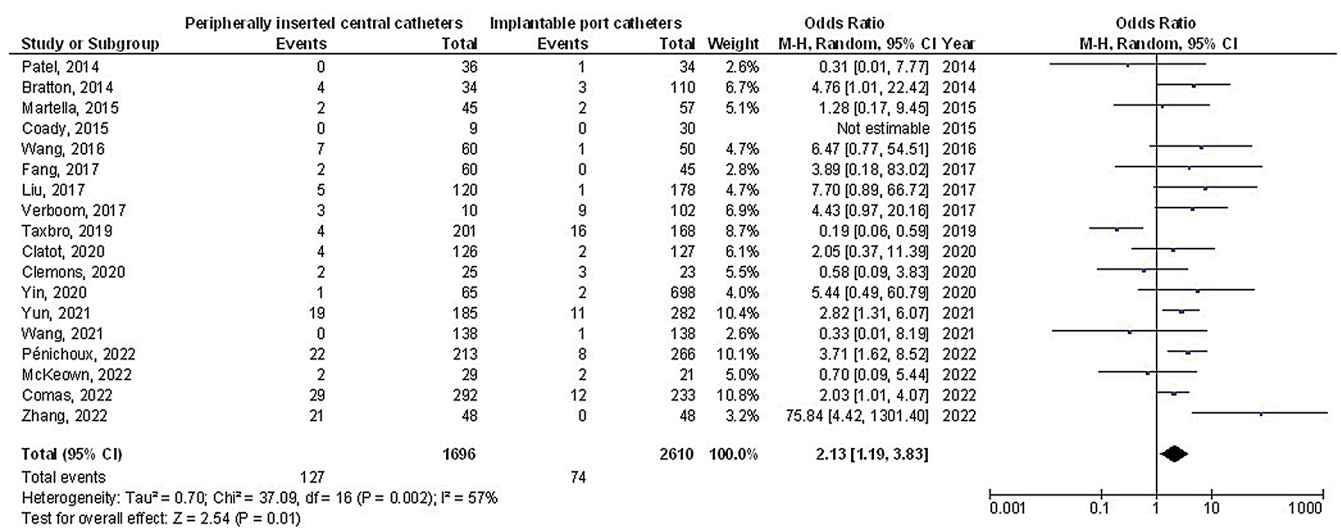


Fig. 4. Forest plot of peripherally inserted central catheters compared to implanted port catheters influence on catheter-related infections
df – degrees of freedom; 95% CI – 95% confidence interval.

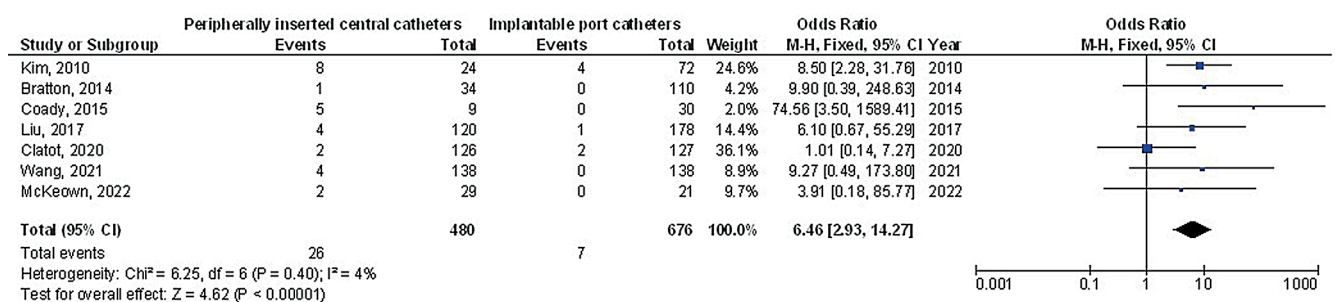


Fig. 5. Forest plot of peripherally inserted central catheters compared to implanted port catheters influence on malposition complications
df – degrees of freedom; 95% CI – 95% confidence interval.

the catheter lifespan, the incidence of complications, and other criteria.¹⁷ The shorter lifespan of the peripherally inserted central venous catheters compared to implantable port catheters may have been the result of higher complication rates associated with peripherally inserted central venous catheters and the higher unintentional removal rate.⁴³ A peripherally implanted central venous catheter can be left in place for several months (even

for a year), as stated in the Infusion Therapy Standards of Practice from 2021.⁴⁴ However, numerous studies have demonstrated that if nurses adhere to maintenance practices, an implanted port catheter can be utilized for several years.⁴⁵ Additionally, the use of an implanted port catheter spares subjects receiving treatment for longer than a year the discomfort brought on by frequent punctures. When comparing peripherally implanted central

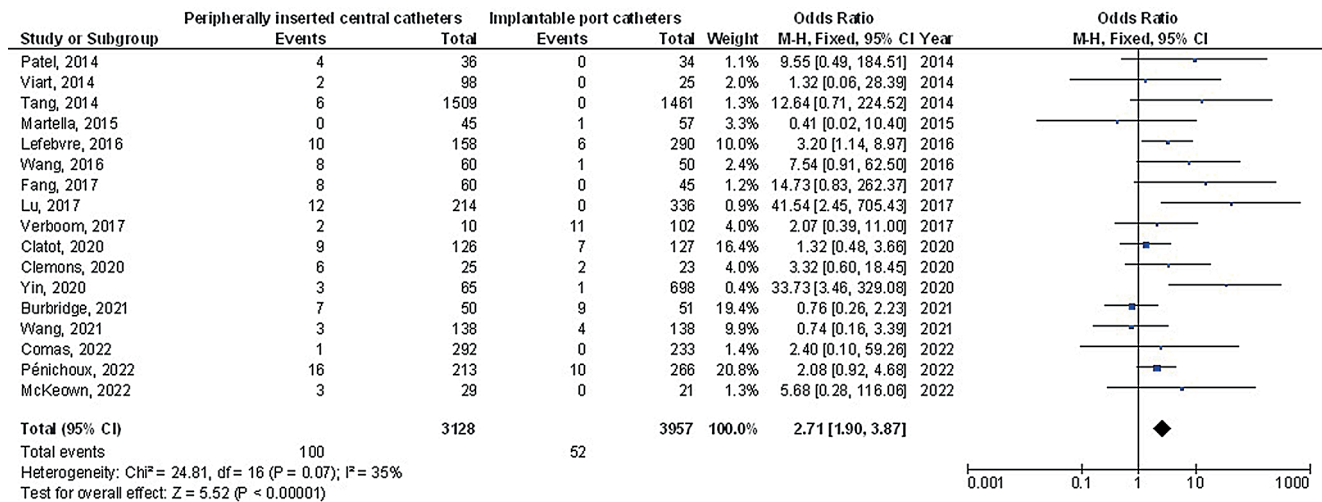


Fig. 6. Forest plot of peripherally inserted central catheters compared to implanted port catheters influence on rates of catheter-related thrombosis
df – degrees of freedom; 95% CI – 95% confidence interval.

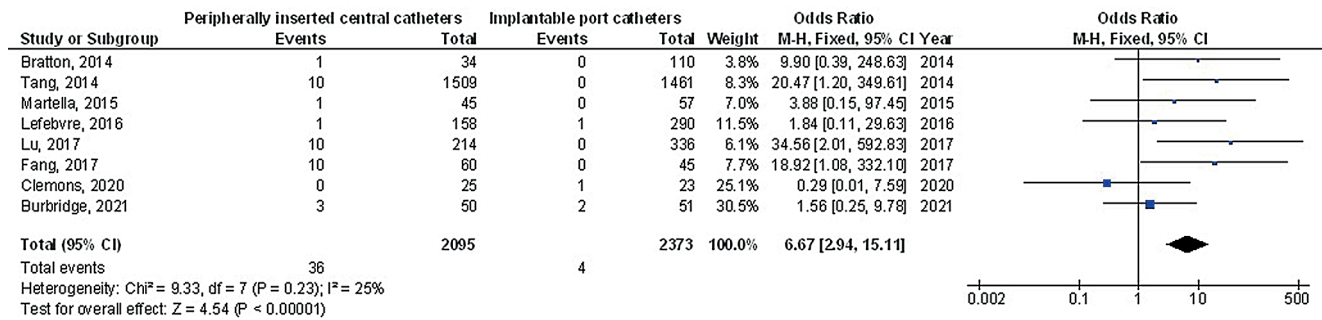


Fig. 7. Forest plot of peripherally inserted central catheters compared to implanted port catheters influence on phlebitis
df – degrees of freedom; 95% CI – 95% confidence interval.

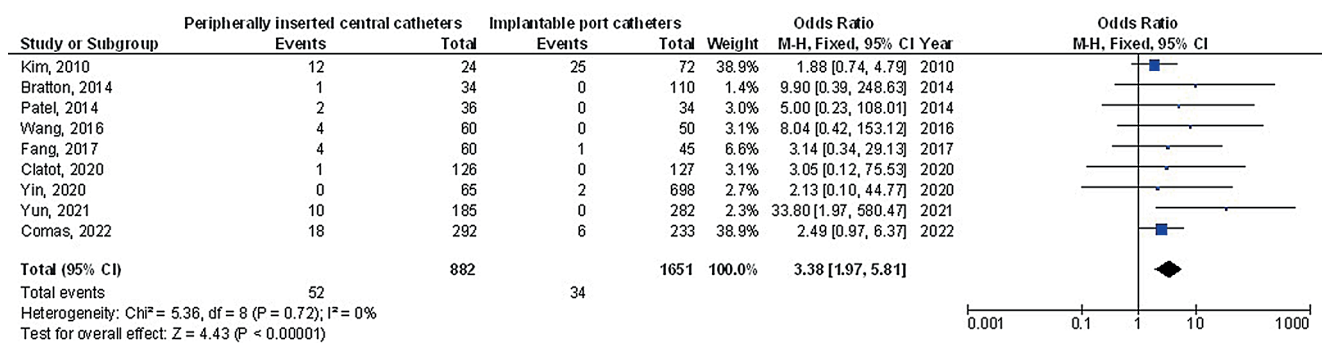


Fig. 8. Forest plot of peripherally inserted central catheters compared to implanted port catheters influence on accidental removal rates
df – degrees of freedom; 95% CI – 95% confidence interval.

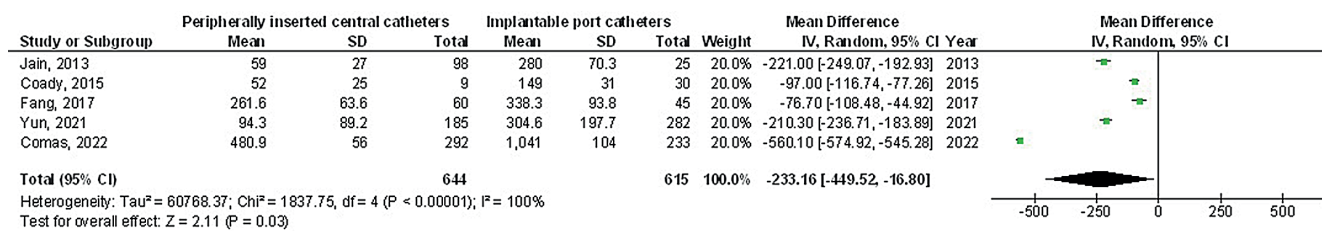


Fig. 9. Forest plot of peripherally inserted central catheters compared to implanted port catheters influence on a catheter's lifespan
df – degrees of freedom; 95% CI – 95% confidence interval; SD – standard deviation.

venous catheters to implantable port catheters, the overall incidence of all 7 problems considered in this study was higher. The risk of thrombosis and vessel or line obstruction was increased by the presence of cancer and the chemotherapy agents administered through the central venous catheters.⁴⁶ This meta-analysis showed that implanted port catheters had a lower incidence of central venous catheter thrombosis and occlusion compared to peripherally inserted catheters. Similar findings were reported in another systematic evaluation of risk variables for catheter-related thrombosis in cancer patients.⁴⁷ Possible explanations include the fact that peripherally inserted central venous catheter subjects require a longer length of catheter for vessel entry, whereas the shorter path of implantable port catheters causes comparatively minor stimulation to the vessel walls as it enters the blood vessels. The mechanical stimulus to the vascular endothelial cells of a foreign substance may encourage the activation of thrombotic factors, leading to vessel blockage. Moreover, this study demonstrated that compared to central venous catheters implanted peripherally, the incidence of implantable port catheter malposition, extravasation, phlebitis, and unintentional removal was decreased. The implantable port catheter base, which is anchored to the chest wall, might offer a more stable access point that is seldom influenced by upper limb movements. On the other hand, the insertion point for a peripherally implanted central venous catheter is frequently in the arm and is more likely to migrate with vigorous exercise, upper limb activity or even everyday mobility. According to our subgroup analysis findings, the incidence of peripherally inserted central venous catheter infections was higher compared to implantable port catheters. According to the research by Bouza et al., the skin (65%) and catheter or catheter joints (30%) are the most common entry points for infections (15%).⁴⁸ A peripherally inserted central venous catheter has an external section through which skin microbes may migrate into the blood, or more importantly, the subcutaneous areas, raising the possibility of infection. In contrast, the puncture seat and catheter of the implantable port catheters are implanted completely under the skin, without any portion of the device exposed. Additionally, difficulties with peripherally implanted central venous catheters seem to be more severe than those with implanted port catheters, which results in higher treatment expenditures. Therefore, it is easy to understand why implanted port catheters have lower long-term costs than those of peripherally inserted central venous catheters, which is consistent with the findings of a cost analysis conducted by Patel et al.¹⁹

This meta-analysis demonstrates how peripherally positioned central catheters and implanted port catheter problems can affect chemotherapy-treated cancer patients.^{49–54} Further research is still required to clarify these potential complications as well as to assess the impact of peripherally positioned central catheters compared to implanted

port catheters on the outcomes under investigation. Larger, more homogeneous samples are required for such research studies. These conclusions were also reported in a previous study, which used a similar meta-analysis method and revealed similarly encouraging results for peripherally inserted central catheters in terms of lowering puncture site infections and alleviating occlusion consequences.^{55–62} Since our meta-analysis was unable to determine whether differences in age and ethnicity are related to the results, well-conducted randomized controlled trials are required to evaluate these factors as well as the effect of different gender, age, ethnicity, and other variables.

Limitations


Since so many papers were not included in the meta-analysis, there might have been a selection bias. However, the excluded papers did not meet the requirements for inclusion in our meta-analysis. The sample size for 6 of the 28 chosen papers was less than 100. Additionally, we were unable to determine whether or not the outcomes were influenced by age and ethnicity. The study was undertaken to evaluate the impact of complications associated with peripherally inserted central catheters and implanted port catheters on chemotherapy-treated cancer patients. Data from the studies used may have introduced bias due to missing or incorrect information. The respondents' nutritional status, as well as the characteristics of age, sex and gender were all potential sources of bias.

Conclusions

Peripherally inserted central catheters had significantly higher incidence of occlusion complications, longer durations of local infections at puncture sites, higher incidence of catheter-related infection, higher malposition complications, higher rates of catheter-related thrombosis, higher incidence of phlebitis complications, higher accidental removals, and shorter catheter lifespans compared to implanted port catheters. The small sample size of 6 studies in the meta-analysis and the small number of studies evaluating many of the comparisons require care when analyzing the results.

ORCID iDs

Yuanli Sun  <https://orcid.org/0000-0003-3896-6292>

Xiangchun Wu  <https://orcid.org/0000-0001-7853-7543>

References

1. Ang P, Chia KH, Teoh MK, Wong KKY. Use of a peripherally implanted subcutaneous permanent central venous access device for chemotherapy: The Singapore General Hospital experience. *Aust NZ J Med*. 2000;30(4):470–474. doi:10.1111/j.1445-5994.2000.tb02054.x
2. Silvestri V, Nerini L, Missio G, et al. Levels of anxiety and pain during chemotherapy with peripheral versus central vascular access: An experimental evaluation. *J Vasc Access*. 2004;5(4):147–153. doi:10.1177/112972980400500403

3. Johansson E, Hammarskjöld F, Lundberg D, Arnlin M. Advantages and disadvantages of peripherally inserted central venous catheters (PICC) compared to other central venous lines: A systematic review of the literature. *Acta Oncol.* 2013;52(5):886–892. doi:10.3109/0284186X.2013.773072
4. Rotzinger R, Gebauer B, Schnapauff D, et al. Placement of central venous port catheters and peripherally inserted central catheters in the routine clinical setting of a radiology department: Analysis of costs and intervention duration learning curve. *Acta Radiol.* 2017;58(12):1468–1475. doi:10.1177/0284185117695664
5. Tan J, Liu L, Xie J, Hu L, Yang Q, Wang H. Cost-effectiveness analysis of ultrasound-guided Seldinger peripherally inserted central catheters (PICC). *Springerplus.* 2016;5(1):2051. doi:10.1186/s40064-016-3698-8
6. O'Brien J, Paquet F, Lindsay R, Valenti D. Insertion of PICCs with minimum number of lumens reduces complications and costs. *J Am Coll Radiol.* 2013;10(11):864–868. doi:10.1016/j.jacr.2013.06.003
7. Walshe LJ, Malak SF, Eagan J, Sepkowitz KA. Complication rates among cancer patients with peripherally inserted central catheters. *J Clin Oncol.* 2002;20(15):3276–3281. doi:10.1200/JCO.2002.11.135
8. Worth LJ, Seymour JF, Slavin MA. Infective and thrombotic complications of central venous catheters in patients with hematological malignancy: Prospective evaluation of nontunneled devices. *Support Care Cancer.* 2009;17(7):811–818. doi:10.1007/s00520-008-0561-7
9. Chan RJ, Northfield S, Larsen E, et al. Central venous Access device SeCurement And Dressing Effectiveness for peripherally inserted central catheters in adult acute hospital patients (CASCADE): A pilot randomised controlled trial. *Trials.* 2017;18(1):458. doi:10.1186/s13063-017-2207-x
10. Stroup DF. Meta-analysis of observational studies in epidemiology: A proposal for reporting. *JAMA.* 2000;283(15):2008. doi:10.1001/jama.283.15.2008
11. Higgins JPT. Measuring inconsistency in meta-analyses. *BMJ.* 2003;327(7414):557–560. doi:10.1136/bmj.327.7414.557
12. Liberati A, Altman DG, Tetzlaff J, et al. The PRISMA statement for reporting systematic reviews and meta-analyses of studies that evaluate health care interventions: Explanation and elaboration. *J Clin Epidemiol.* 2009;62(10):e1–e34. doi:10.1016/j.jclinepi.2009.06.006
13. Gupta A, Das A, Majumder K, et al. Obesity is independently associated with increased risk of hepatocellular cancer-related mortality: A systematic review and meta-analysis. *Am J Clin Oncol.* 2018;41(9):874–881. doi:10.1097/COC.0000000000000388
14. Higgins JPT, Altman DG, Gotzsche PC, et al. The Cochrane Collaboration's tool for assessing risk of bias in randomised trials. *BMJ.* 2011;343:d5928. doi:10.1136/bmj.d5928
15. Sheikhabahaei S, Trahan TJ, Xiao J, et al. FDG-PET/CT and MRI for evaluation of pathologic response to neoadjuvant chemotherapy in patients with breast cancer: A meta-analysis of diagnostic accuracy studies. *Oncologist.* 2016;21(8):931–939. doi:10.1634/theoncologist.2015-0353
16. Revel-Vilk S, Yacobovich J, Tamary H, et al. Risk factors for central venous catheter thrombotic complications in children and adolescents with cancer. *Cancer.* 2010;116(17):4197–4205. doi:10.1002/cncr.25199
17. Kim HJ, Yun J, Kim HJ, et al. Safety and effectiveness of central venous catheterization in patients with cancer: Prospective observational study. *J Korean Med Sci.* 2010;25(12):1748. doi:10.3346/jkms.2010.25.12.1748
18. Jain SA, Shukla SN, Talati SS, Parikh SK, Bhatt SJ, Maka V. A retrospective study of central venous catheters GCRI experience. *Indian J Med Peadiatr Oncol.* 2013;34(4):238–241. doi:10.4103/0971-5851.125234
19. Patel GS, Jain K, Kumar R, et al. Comparison of peripherally inserted central venous catheters (PICC) versus subcutaneously implanted port-chamber catheters by complication and cost for patients receiving chemotherapy for non-haematological malignancies. *Support Care Cancer.* 2014;22(1):121–128. doi:10.1007/s00520-013-1941-1
20. Viart H, Combe C, Martinelli T, Thomas J, Hida H. Comparison between implantation costs of peripherally inserted central catheter and implanted subcutaneous port [in French]. *Ann Pharm Fr.* 2015;73(3):239–244. doi:10.1016/j.pharma.2014.08.001
21. Bratton J, Johnstone PAS, McMullen KP. Outpatient management of vascular access devices in children receiving radiotherapy: Complications and morbidity. *Pediatr Blood Cancer.* 2014;61(3):499–501. doi:10.1002/pbc.24642
22. Liu Y. Comparison of implanted vascular access ports and PICC in breast cancer patients [in Chinese]. *Chin J Pract Nurs.* 2017;10(18):1413–1416. https://caod.oriprobe.com/articles/51201233/zhi_ru_shi_jing_mai_shu_ye_gang_yu_picc_zai_ru_xia.htm. Accessed June 20, 2022.
23. Martella F, Salutari V, Marchetti C, et al. A retrospective analysis of trabectedin infusion by peripherally inserted central venous catheters: A multicentric Italian experience. *Anticancer Drugs.* 2015;26(9):990–994. doi:10.1097/CAD.0000000000000275
24. Coady K, Ali M, Sidloff D, Kenningham RR, Ahmed S. A comparison of infections and complications in central venous catheters in adults with solid tumours. *J Vasc Access.* 2015;16(1):38–41. doi:10.5301/jva.5000300
25. Wang N, Dong Y, Zhang B, Gao Y, Fu H. Comparison of the application of IVPA and PICC in breast cancer patients [in Chinese]. *Med Philos B.* 2016;37(7):36–38. <http://www.chinadoi.cn/portal/mr.action?doi=10.12014/j.issn.1002-0772.2016.07b.09>. Accessed June 20, 2022.
26. Lefebvre L, Noyon E, Georgescu D, et al. Port catheter versus peripherally inserted central catheter for postoperative chemotherapy in early breast cancer: A retrospective analysis of 448 patients. *Support Care Cancer.* 2016;24(3):1397–1403. doi:10.1007/s00520-015-2901-8
27. Verboom MC, Ouwerkerk J, Steeghs N, et al. Central venous access related adverse events after trabectedin infusions in soft tissue sarcoma patients: Experience and management in a nationwide multicenter study. *Clin Sarcoma Res.* 2017;7(1):2. doi:10.1186/s13569-017-0066-6
28. Fang S, Yang J, Song L, Jiang Y, Liu Y. Comparison of three types of central venous catheters in patients with malignant tumor receiving chemotherapy. *Patient Prefer Adherence.* 2017;11:1197–1204. doi:10.2147/PPA.S142556
29. Lu X, Gao R, Zhang Y. Clinical use of ultrasound-guided implantable venous access port versus PICC in chemotherapy of breast cancer [in Chinese]. *Chin Remedies Clin.* 2017;17(1):13–16. http://en.cnki.com.cn/Article_en/CJFDTOTAL-YWLC201701005.htm. Accessed June 20, 2022.
30. Tang TT, Liu L, Li CX, et al. Which is better for patients with breast cancer: Totally implanted vascular access devices (TIVAD) or peripherally inserted central catheter (PICC)? *World J Surg.* 2019;43(9):2245–2249. doi:10.1007/s00268-019-05022-x
31. Vashi PG, Virginkar N, Popiel B, Edwin P, Gupta D. Incidence of and factors associated with catheter-related bloodstream infection in patients with advanced solid tumors on home parenteral nutrition managed using a standardized catheter care protocol. *BMC Infect Dis.* 2017;17(1):372. doi:10.1186/s12879-017-2469-7
32. Taxbro K, Hammarskjöld F, Thelin B, et al. Clinical impact of peripherally inserted central catheters vs implanted port catheters in patients with cancer: An open-label, randomised, two-centre trial. *Br J Anaesth.* 2019;122(6):734–741. doi:10.1016/j.bja.2019.01.038
33. Clemons M, Stober C, Kehoe A, et al. A randomized trial comparing vascular access strategies for patients receiving chemotherapy with trastuzumab for early-stage breast cancer. *Support Care Cancer.* 2020;28(10):4891–4899. doi:10.1007/s00520-020-05326-y
34. Yin L, Li J. Central venous catheter insertion in colorectal cancer patients, PICC or PC? *Cancer Manag Res.* 2020;12:5813–5818. doi:10.2147/CMAR.S250410
35. Clatot F, Fontanilles M, Lefebvre L, et al. Randomised phase II trial evaluating the safety of peripherally inserted catheters versus implanted port catheters during adjuvant chemotherapy in patients with early breast cancer. *Eur J Cancer.* 2020;126:116–124. doi:10.1016/j.ejca.2019.11.022
36. Wang K, Zhou Y, Huang N, Lu Z, Zhang X. Peripherally inserted central catheter versus totally implanted venous port for delivering medium- to long-term chemotherapy: A cost-effectiveness analysis based on propensity score matching. *J Vasc Access.* 2022;23(3):365–374. doi:10.1177/1129729821991360
37. Burbridge B, Lim H, Dwernychuk L, et al. Comparison of the quality of life of patients with breast or colon cancer with an arm vein port (TIVAD) versus a peripherally inserted central catheter (PICC). *Curr Oncol.* 2021;28(2):1495–1506. doi:10.3390/curroncol28020141
38. Yun WS, Yang SS. Comparison of peripherally inserted central catheters and totally implanted venous access devices as chemotherapy delivery routes in oncology patients: A retrospective cohort study. *Sci Prog.* 2021;104(2):003685042110118. doi:10.1177/00368504211011871

39. Comas M, Domingo L, Jansana A, et al. Cost-effectiveness analysis of peripherally inserted central catheters versus central venous catheters for in-hospital parenteral nutrition. *J Patient Saf.* 2022;18(7): e1109–e1115. doi:10.1097/PTS.0000000000001028
40. Zhang H, Li Y, Zhu N, Li Y, Fu J, Liu J. Comparison of peripherally inserted central catheters (PICCs) versus totally implantable venous-access ports in pediatric oncology patients: A single center study. *Sci Rep.* 2022;12(1):3510. doi:10.1038/s41598-022-07584-8
41. Pénichoux J, Rio J, Kammoun L, et al. Retrospective analysis of the safety of peripherally inserted catheters versus implanted port catheters during first-line treatment for patients with diffuse large B-cell lymphoma. *Eur J Haematol.* 2022;109(1):41–49. doi:10.1111/ejh.13767
42. McKeown C, Ricciuti A, Agha M, et al. A prospective study of the use of central venous catheters in patients newly diagnosed with acute myeloid leukemia treated with induction chemotherapy. *Support Care Cancer.* 2022;30(2):1673–1679. doi:10.1007/s00520-021-06339-x
43. Kabsy Y, Baudin G, Vinti H, et al. Peripherally inserted central catheters (PICC) in onco-hematology [in French]. *Bull Cancer.* 2010;97(9): 1067–1071. doi:10.1684/bdc.2010.1167
44. Gorski LA, Hadaway L, Hagle ME, et al. Infusion Therapy Standards of Practice, 8th Edition. *J Infus Nurs.* 2021;44(1S):S1–S224. doi:10.1097/NAN.0000000000000396
45. Kock HJ, Pietsch M, Krause U, Wilke H, Eigler FW. Implantable vascular access systems: Experience in 1500 patients with totally implanted central venous port systems. *World J Surg.* 1998;22(1):12–16. doi:10.1007/s002689900342
46. Singh G, Rathi A, Singh K, Sharma D. Venous thromboembolism in cancer patients: Magnitude of problem, approach, and management. *Indian J Cancer.* 2017;54(1):308. doi:10.4103/ijc.IJC_101_17
47. Saber W, Moua T, Williams EC, et al. Risk factors for catheter-related thrombosis (CRT) in cancer patients: A patient-level data (IPD) meta-analysis of clinical trials and prospective studies. *J Thromb Haemost.* 2011;9(2):312–319. doi:10.1111/j.1538-7836.2010.04126.x
48. Bouza E, Burillo A, Muñoz P. Catheter-related infections: Diagnosis and intravascular treatment. *Clin Microbiol Infect.* 2002;8(5):265–274. doi:10.1046/j.1469-0691.2002.00385.x
49. Abdelrahim ME, Assi KH, Chrystyn H. Relative bioavailability of terbutaline to the lung following inhalation, using urinary excretion: Relative bioavailability of terbutaline to the lung following inhalation, using urinary excretion. *Br J Clin Pharmacol.* 2011;71(4):608–610. doi:10.1111/j.1365-2125.2010.03873.x
50. Elgendy MO, Abdelrahim ME, Salah Eldin R. Potential benefit of repeated MDI inhalation technique counselling for patients with asthma. *Eur J Hosp Pharm.* 2015;22(6):318–322. doi:10.1136/ejpharm-2015-000648
51. ElHansy MHE, Boules ME, El Essawy AFM, et al. Inhaled salbutamol dose delivered by jet nebulizer, vibrating mesh nebulizer and metered dose inhaler with spacer during invasive mechanical ventilation. *Pulm Pharmacol Ther.* 2017;45:159–163. doi:10.1016/j.pupt.2017.06.004
52. Harb HS, Elberry AA, Rabea H, Fathy M, Abdelrahim MEA. Is Combi-haler usable for aerosol delivery in single limb non-invasive mechanical ventilation? *J Drug Deliv Sci Technol.* 2017;40:28–34. doi:10.1016/j.jddst.2017.05.022
53. Madney YM, Fathy M, Elberry AA, Rabea H, Abdelrahim MEA. Nebulizers and spacers for aerosol delivery through adult nasal cannula at low oxygen flow rate: An in-vitro study. *J Drug Deliv Sci Technol.* 2017;39:260–265. doi:10.1016/j.jddst.2017.04.014
54. Moustafa IOF, ElHansy MHE, Al Hallag M, et al. Clinical outcome associated with the use of different inhalation method with and without humidification in asthmatic mechanically ventilated patients. *Pulm Pharmacol Ther.* 2017;45:40–46. doi:10.1016/j.pupt.2017.04.007
55. Pu YL, Li ZS, Zhi XX, et al. Complications and costs of peripherally inserted central venous catheters compared with implantable port catheters for cancer patients: A meta-analysis. *Cancer Nurs.* 2020; 43(6):455–467. doi:10.1097/NCC.0000000000000742
56. Capozzi VA, Monfardini L, Sozzi G, et al. Peripherally inserted central venous catheters (PICC) versus totally implantable venous access device (PORT) for chemotherapy administration: A meta-analysis on gynecological cancer patients. *Acta Biomed.* 2021;92(5):e2021257. doi:10.23750/abm.v92i5.11844
57. Jiang M, Li CL, Pan CQ, Yu L. The risk of bloodstream infection associated with totally implantable venous access ports in cancer patient: A systematic review and meta-analysis. *Support Care Cancer.* 2020; 28(1):361–372. doi:10.1007/s00520-019-04809-x
58. Schears GJ, Ferko N, Syed I, Arpino JM, Alsbrooks K. Peripherally inserted central catheters inserted with current best practices have low deep vein thrombosis and central line-associated bloodstream infection risk compared with centrally inserted central catheters: A contemporary meta-analysis. *J Vasc Access.* 2021;22(1):9–25. doi:10.1177/1129729820916113
59. Wang P, Soh KL, Ying Y, Liu Y, Huang X, Huang J. Risk of VTE associated with PORTs and PICCs in cancer patients: A systematic review and meta-analysis. *Thromb Res.* 2022;213:34–42. doi:10.1016/j.thromres.2022.02.024
60. He E, Ye K, Zheng H. Clinical effect and safety of venous access ports and peripherally inserted central catheters in patients receiving tumor chemotherapy: A systematic review and meta-analysis. *Ann Palliat Med.* 2021;10(8):9105–9113. doi:10.21037/apm-21-1926
61. Balsorano P, Virgili G, Villa G, et al. Peripherally inserted central catheter-related thrombosis rate in modern vascular access era: When insertion technique matters. A systematic review and meta-analysis. *J Vasc Access.* 2020;21(1):45–54. doi:10.1177/1129729819852203
62. Liu B, Wu Z, Lin C, Li L, Kuang X. Applicability of TIVAP versus PICC in non-hematological malignancies patients: A meta-analysis and systematic review. *PLoS One.* 2021;16(8):e0255473. doi:10.1371/journal.pone.0255473

Effects of arthroscopic anterior cruciate ligament reconstruction combined with sodium hyaluronate on knee function and inflammatory markers in anterior cruciate ligament injury patients with or without knee osteoarthritis

Yongjun Hu^{1,2,A,D,F}, Yi Shen^{1,C,E}, Ding Chen^{1,B,C}, Weiye Zhong^{1,A,D–F}

¹ Department of Orthopedic Surgery, The Second Xiangya Hospital and Central South University, Changsha, China

² Department of General Surgery, The Second Xiangya Hospital and Central South University, Changsha, China

A – research concept and design; B – collection and/or assembly of data; C – data analysis and interpretation;

D – writing the article; E – critical revision of the article; F – final approval of the article

Advances in Clinical and Experimental Medicine, ISSN 1899–5276 (print), ISSN 2451–2680 (online)

Adv Clin Exp Med. 2023;32(5):533–538

Address for correspondence

Weiye Zhong

E-mail: zhongweiye@csu.edu.cn

Funding sources

None declared

Conflict of interest

None declared

Received on July 6, 2022

Reviewed on August 5, 2022

Accepted on November 17, 2022

Published online on December 29, 2022

Cite as

Hu Y, Shen Y, Chen D, Zhong W. Effects of arthroscopic anterior cruciate ligament reconstruction combined with sodium hyaluronate on knee function and inflammatory markers in anterior cruciate ligament injury patients with or without knee osteoarthritis. *Adv Clin Exp Med.* 2023;32(5):533–538. doi:10.17219/acem/156659

DOI

10.17219/acem/156659

Copyright

Copyright by Author(s)

This is an article distributed under the terms of the Creative Commons Attribution 3.0 Unported (CC BY 3.0) (<https://creativecommons.org/licenses/by/3.0/>)

Abstract

Background. Anterior cruciate ligament injury (ACLI) is a common sports injury of the knee joint, and ACLI patients often develop early knee osteoarthritis (KOA) after surgery. This may be due to the activation of a post-surgical inflammatory response.

Objectives. To investigate the treatment efficacy of arthroscopic anterior cruciate ligament reconstruction (AACL) combined with sodium hyaluronate (SH) in ACLI patients with and without KOA.

Materials and methods. This prospective cohort study included 226 ACLI patients with or without KOA who were admitted between July 2015 and December 2018 into The Second Xiangya Hospital, Changsha, China. All patients received AACL surgery combined with 50 mg SH. Serum levels of inflammatory markers were evaluated with enzyme-linked immunosorbent assay (ELISA), and knees were assessed using the Lysholm Knee Score and the International Knee Documentation Committee Knee Evaluation Form (IKDC). The range of motion of the knee joint was also measured.

Results. The mean disease course was 73.39 ± 30.90 months for ACLI patients with KOA, which was significantly longer than for those without KOA (3.74 ± 1.70 months). Also, surgery duration was remarkably longer for patients with KOA than it was for those without this disease. The Lysholm Knee Score and IKDC score, as well as the range of knee joint motion were significantly improved in all patients after treatment compared to baseline. However, no significant differences were found between the groups. One day, 3 days and 7 days after surgery, significantly higher inflammatory marker levels were found in the patients with KOA than in those without KOA.

Conclusions. The AACL combined with SH was efficacious as it improved knee function and inflammation in all patients, while patients without KOA exhibited a more rapid recovery from the post-surgical inflammatory response.

Key words: inflammatory markers, knee osteoarthritis, sodium hyaluronate, anterior cruciate ligament injury, arthroscopic anterior cruciate ligament reconstruction

Background

Anterior cruciate ligament injury (ACLI) is a common sports injury of the knee joint, and is also a frequent result of falls, traffic accidents and excessive knee flexion.^{1,2} Incidence of ACLI in the USA is reported to be more than 120,000 cases per year.³ Reconstruction surgery is currently the preferred treatment method for ACLI,^{4,5} with arthroscopic anterior cruciate ligament reconstruction (AACLR) widely used in this regard.⁶ Furthermore, the number of patients receiving AACLR gradually increased between 2004 and 2009.⁷ Despite the methods available for the treatment of ACLI, patients often develop early knee osteoarthritis (KOA) after surgery, which may be due to the activation of an inflammatory response.^{8,9} Nonetheless, ACLI patients may still develop KOA if they do not receive treatment for their injury promptly.¹⁰

Besides AACLR, the use of sodium hyaluronate (SH) is a clinical option for many injuries, including spinal cord injury¹¹ and partial-thickness rotator cuff tears.¹² However, the application of SH to ACLI is not fully understood. Moreover, studies on the use of AACLR and SH in ACLI patients with KOA, as well as their effects on inflammatory mediators are inadequate.

Objectives

The current study aimed to investigate the effects of AACLR combined with SH in the treatment of ACLI patients with or without KOA, with a particular focus on dynamic changes of inflammatory markers. This research may provide more clinical evidence for the application of AACLR and SH in ACLI patients with KOA.

Materials and methods

Patients

This prospective cohort study included 226 patients with ACLI who were admitted between July 2015 and December 2018 into The Second Xiangya Hospital, Changsha, China. All enrolled patients were divided into ACLI combined with KOA (ACLI/KOA) group and ACLI without KOA (ACLI) group, according to each patient's diagnosis. A diagnosis of ACLI was confirmed using X-ray and magnetic resonance imaging (MRI), in addition to arthroscopic assessment during surgery. The KOA was diagnosed according to the 2019 guidelines for the diagnosis and treatment of osteoarthritis (OA) published by the Chinese Medical Association of Orthopedic Surgeons.¹³ Inclusion criteria included: 1) meeting the diagnosis criteria for ACLI and KOA; 2) a complete rupture of the anterior cruciate ligament; 3) no treatment, painkillers or anti-inflammatory drugs in the 3 months before the study; and 4) unilateral

ACLI. The following exclusion criteria were applied: 1) central or ipsilateral lower extremity nerve injury, varus or valgus deformity of the knee joint, or fracture and/or open injury of the lower extremities; 2) bilateral ACLI; 3) inflammatory diseases such as ankylosing spondylitis or system inflammation such as severe pneumonia. For ACLI patients without KOA, the inclusion and exclusion criteria were the same as for those without ACLI/KOA, except for a diagnosis of KOA.

Written informed consent was obtained from all patients and the study was approved by the ethics committee of the Second Xiangya Hospital and Central South University, Changsha, China (approval No. CSU2015048). Institutional Review Board (IRB) approval was also obtained and the study adhered to the tenets of declaration of Helsinki.

Treatment strategy

Sample size calculation was performed using the following formula (Equation 1):

$$\frac{[(t\alpha + t\beta)s]^2}{\delta}$$

where α – significant level, β – error probability, δ – effective difference, and s – overall standard deviation.

Lysholm Knee Score after 1 week was used as the main study outcome, with an increase of at least 6 considered to be effective. From previous experience of the authors, the mean Lysholm Knee Score is approx. 30–50 ± 8 in such patients before surgery. It was estimated based on our clinical experience that 1 week after surgery the score would be approx. 40–60 ± 8. Thus, the following values were used to calculate the sample size: $\delta = 6$, $s = 8$, $\alpha = 0.05$, and $\beta = 0.10$. As a result of these calculations, the minimum sample size for the study was 113 patients per group.

All patients were consecutively enrolled in the study and underwent the Lachman test and routine pre-operation examination. This included whole blood tests, routine stool and urine tests, coagulation function tests, liver and kidney function tests, etc. All surgeries were conducted by the same team of surgeons.

All patients received AACLR in combination with SH. For the AACLR surgery, ACLI/KOA patients received combined spinal epidural anesthesia using 5% levobupivacaine (3 mL). A pneumatic tourniquet was prepared and the pressure was maintained at 60 kPa. The arthroscope (Smith & Nephew, Inc. Endoscopy Division, London, UK) was inserted from an infrapatellar medial to lateral approach, and the anatomical structures of the meniscus, cartilage and anterior and posterior cruciate ligament of the knee joint were assessed. The joint cavity was cleaned and the injured meniscus was repaired. If there was hyperplasia and stenosis of the intercondylar fossa, it was expanded and the hyperplastic synovium was excised. Autologous ipsilateral semitendinosus and gracilis tendon were used for transplantation. Briefly, a 3 cm incision was made 2 cm from

the medial tibial tubercle, and the semitendinosus and gracilis tendons were partly resected. The muscle tissues attached to tendons at both ends were removed and both ends of the tendon were knitted and sutured with antibacterial microthread. Then, the broken end of the anterior cruciate ligament was excised and a plasma knife was used to cauterize the center of the anterior cruciate ligament between the tibia and femur. After bending the knee to 90°, a tibial canal locator was introduced under arthroscopic guidance, and a guide needle was inserted into the joint through the medial incision of the tibial tubercle. The locator was removed and a tibial canal was created using a tibial hollow drill. A femoral canal was then created using the same method. The tendon bundle was inserted into the loop of an endobutton plate and the grafts were pulled into the tibia and femur canals, using the traction line. After the endobutton plate was turned over and fixed to the surface of the bone cortex through the canal, the fixed traction line was tightened. The knee joint was repeatedly flexed and extended 30 times under the tension of the tendon bundle to ensure that the tendon bundle had no entrapment or impact. The tibial end of the tendon bundle was fixed with screws at the outer opening of the tibial canal under the guidance of the guide needle. After satisfactory fixation, the articular cavity was washed thoroughly and the skin was sutured layer by layer. The affected limb was then dressed and bandaged.

All ACLI patients without KOA (ACLI group) underwent the surgery using the same method except for the expansion of the intercondylar fossa and excision of the hyperplastic synovium. All patients had 50 mg SH (2.5 mL/25 mg; Shandong Boshilun Furida Pharmaceutical Company Ltd., Shangdong, China) injected into the knee joint cavity immediately after the wound was sutured.

After surgery, the affected limbs of all patients were raised and bandaged with an elastic bandage. All patients received an ice compress to the affected area for 30 min every 2 h for the 1st day. Celecoxib (0.4 g each time) (Pfizer Pharmaceuticals LLC, New York, USA) was used if pain affected sleeping.

During the first 3 days following surgery, patients were asked to perform static contraction of the quadriceps femoris muscle. After the first 3 days post surgery, patients were asked to do quadriceps training. From 3 weeks following surgery, patients could attempt to walk on crutches, and after 2 months, they could attempt to walk normally and perform knee hyperextension and squat training. Athletic sports could be undertaken approx. 6–8 months after surgery.

Evaluation of inflammatory mediators

Blood samples were collected from all patients before surgery, as well as 1 day, 3 days, 7 days, 1 month, 2 months, and 3 months post surgery. Serum levels of the inflammatory markers – C-reactive protein (CRP), interleukin

(IL)-1 β , IL-6, IL-10, and tumor necrosis factor alpha (TNF- α) – were measured with enzyme-linked immunosorbent assay (ELISA) using commercially available kits (all from Abcam, Cambridge, UK).

Data collection and measurement

Patients' demographic data including age, gender and body mass index (BMI) were recorded. Clinical characteristics including disease course, injury side, intraoperative indices of surgery duration, and postoperative complications, were collected. The Lysholm Knee Score and the International Knee Documentation Committee Knee Evaluation Form (IKDC) were examined before surgery and 1 month, 3 months and 6 months following surgery. The range of motion of the knee joint (the angle between the new position of the distal bone and the proximal end when the distal end of the joint moved towards or away from the proximal end) was evaluated before and 6 months after surgery.

Statistical analyses

All continuous data were normally distributed, which was confirmed using Kolmogorov–Smirnov analysis (results shown in Supplementary Table 1: <https://doi.org/10.5281/zenodo.7120784>). Continuous data were expressed as mean \pm standard deviation (M \pm SD). Comparisons between the 2 groups were conducted using an unpaired t-test. For comparison of data before and after treatment, a paired t-test was used. Rates were compared using χ^2 test. All analyses were performed using GraphPad Prism v. 6.0 (GraphPad Software, San Diego, USA) and SPSS v. 18.0. (SPSS Inc., Chicago, USA), with a statistical difference considered as $p < 0.05$.

Results

Basic characteristics and intraoperative indices of all patients

The basic characteristics of all patients are shown in Table 1. The mean disease course was 73.39 \pm 30.90 months for the ACLI/KOA group, which was significantly longer than the 3.74 \pm 1.70 months for the ACLI group ($p < 0.05$). Furthermore, surgery duration was remarkably longer for the ACLI/KOA group than it was for the ACLI group ($p < 0.05$). No significant differences were found for other indices.

Comparison of Lysholm Knee Score, IKDC score and the range of knee joint motion between groups

The Lysholm Knee Score, IKDC score and the range of knee joint motion were compared between the 2 groups.

Table 1. Basic characteristics and intraoperative indices of all patients

Variables	ACLI/KOA (n = 113)	ACLI (n = 113)	t or χ^2	p-value
Age [years]	35.23 ±10.97	36.76 ±10.40	-1.083	0.280
Sex, female (%)	41 (36.28)	39 (34.51)	0.069	0.793
BMI [kg/m ²]	24.20 ±2.94	24.19 ±3.01	0.022	0.982
Disease course (ACLI) [months]	73.39 ±30.90	3.74 ±1.70	23.921	<0.001
Injury side, n (%)			0.142	0.707
left	53 (46.90)	56 (49.56)	-	-
right	60 (53.10)	57 (50.44)	-	-
Surgery duration [min]	129.28 ±11.78	121.55 ±11.06	5.088	<0.001

Comparison was made with unpaired t-test between ACLI/KOA and ACLI group for continuous data on age, body mass index (BMI), disease course and surgery duration. Rates (sex and injury side) were analyzed using χ^2 test. ACLI – anterior cruciate ligament injury; KOA – knee osteoarthritis; SH – sodium hyaluronate; ACLR – arthroscopic anterior cruciate ligament reconstruction.

Table 2. Comparison of Lysholm Knee Score, International Knee Documentation Committee Knee Evaluation Form (IKDC) score and the range of motion of knee joint among different groups

Variables		ACLI/KOA (n = 113)	ACLI (n = 113)	t	p-value
Lysholm Knee Score	before	42.74 ±6.68	41.47 ±6.35	1.467	0.143
	1 month	55.30 ±5.80*	55.57 ±5.62*	-0.359	0.720
	3 months	64.16 ±6.09*	64.55 ±5.67*	-0.508	0.611
	6 months	88.82 ±3.54*	89.13 ±3.55*	-0.657	0.511
IKDC score	before	43.01 ±7.02	42.44 ±7.24	0.603	0.547
	1 months	52.48 ±7.37*	53.19 ±7.32*	-0.731	0.465
	3 months	62.07 ±6.68*	62.04 ±7.20*	0.028	0.977
	6 months	89.57 ±4.12*	89.53 ±3.94*	0.070	0.944
Knee joint motion [°]	before	65.27 ±5.86	65.53 ±6.00	-0.325	0.745
	6 months	115.40 ±8.55*	115.24 ±8.63*	0.136	0.892

Comparison was made with unpaired t-test between ACLI/KOA and ACLI group. *p < 0.05 compared with the baseline using paired t-test. ACLI – anterior cruciate ligament injury; KOA – knee osteoarthritis; SH – sodium hyaluronate; ACLR – arthroscopic anterior cruciate ligament reconstruction.

No significant differences were found between the groups before the study, while all 3 scores significantly improved after 6 months in both groups compared to baseline scores (p < 0.05, Table 2). However, no significant differences were found between the ACLI/KOA and ACLI groups after surgery.

Dynamic changes of inflammatory markers in different groups

To further investigate the effects of different surgery methods, dynamic changes in inflammatory markers were evaluated. As shown in Fig. 1, before surgery, the levels of pro-inflammatory markers (CRP, IL-1 β , IL-6, and TNF- α), as well as levels of anti-inflammatory IL-10, were higher in ACLI/KOA patients compared to the ACLI patients (p < 0.05). After treatment, significant differences were found 1 day, 3 days and 7 days after surgery, with markedly higher inflammatory markers found in ACLI/KOA patients compared to those without KOA (p < 0.05).

Postoperative complications

Postoperative complications were compared between the 2 groups. There was 1 case of incision infection in the ACLI/KOA group and no complications were found in the ACLI group (Table 3).

Table 3. Postoperative complications in different groups

Variables, n (%)	ACLI/KOA (n = 113)	ACLI (n = 113)
Incision infection	0 (0)	0 (0)
Intra-articular infection	0 (0)	1 (0.88)

ACLI – anterior cruciate ligament injury; KOA – knee osteoarthritis; SH – sodium hyaluronate; ACLR – arthroscopic anterior cruciate ligament reconstruction.

Discussion

Despite several studies on the application of ACLR in the treatment of ACLI, few have focused on the effects of ACLR on ACLI patients with KOA. In the present

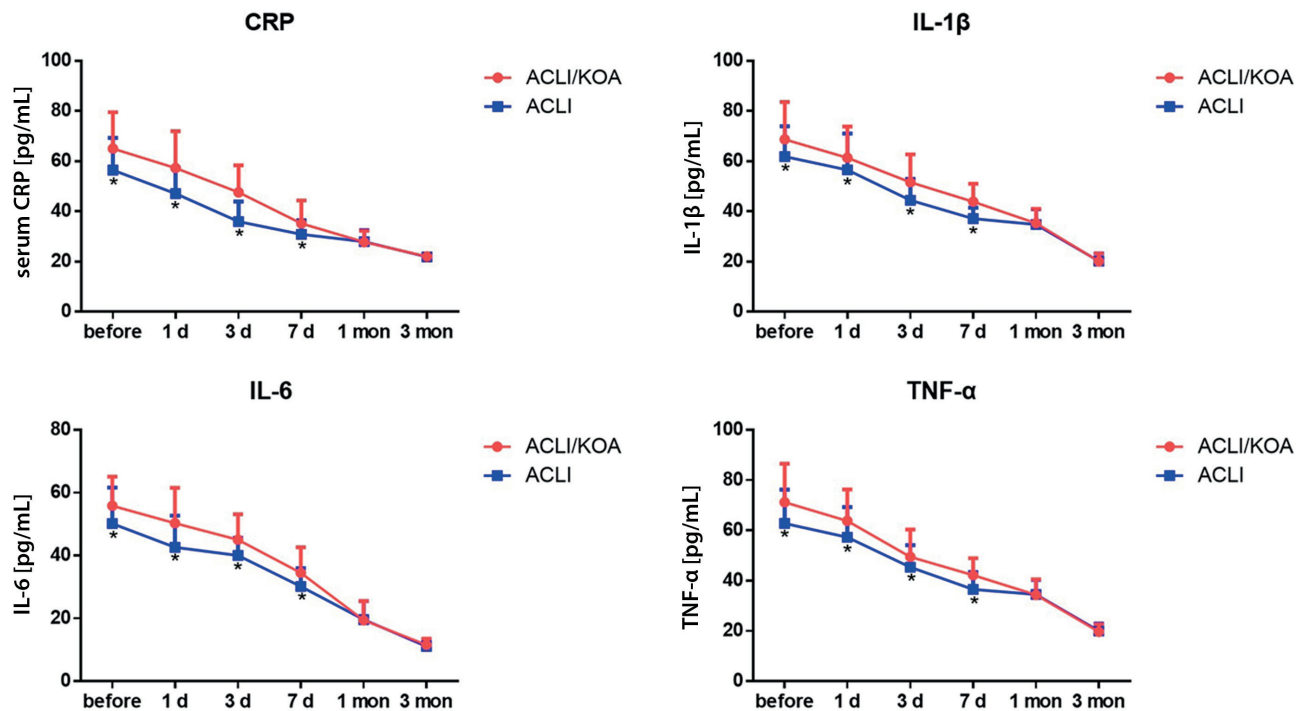


Fig. 1. Dynamic changes in the inflammatory markers C-reactive protein (CRP), interleukin (IL)-1 β , IL-6, and tumor necrosis factor alpha (TNF- α) in both groups. A comparison between the 2 groups was conducted using an unpaired t-test. Data are expressed as mean \pm standard deviation (M \pm SD)

* $p < 0.05$ compared to anterior cruciate ligament injury/knee osteoarthritis (ACLI/KOA) group.

study, it was demonstrated that AACL combined with SH was efficacious in ACLI/KOA patients. Indeed, there were improvements in the recovery of knee function and inflammatory markers. Meanwhile, ACLI patients without KOA experienced a more rapid recovery from the inflammatory response than ACLI/KOA patients.

Some studies have demonstrated a relationship between chronic ACLI and KOA. Generally, ACLI patients have a higher risk of developing KOA, even after reconstruction surgery. In a meta-analysis, Lie et al. demonstrated that 10 years after ACLI, patients may develop KOA, and that meniscectomy might be a risk factor.¹⁴ In another study, it was found that adults developed OA earlier than adolescents 5 and 10 years after ACLI reconstruction surgery.¹⁵ The activation of inflammation is one of the key factors in KOA development, and inflammatory markers were found to be elevated in KOA patients. In ACLI patients, it was found that levels of matrix metalloproteinase-13 (MMP-13), IL-6, IL-1 β , and caspase-3 were all significantly upregulated in chondrocytes, especially in patients who had not undergone reconstruction surgery.¹⁶ A systematic review showed that ACL patients without reconstruction had elevated collagen turnover, and the overall inflammatory cytokine response in synovial fluid increased in ACL patients who had reconstruction surgery.¹⁷ However, recent research demonstrated that 5 years after the injury, inflammatory biomarkers could not predict the incidence of KOA, which indicated that the correlation between inflammatory biomarkers and KOA was weak in the long term

following reconstruction surgery in ACLI patients.¹⁸ Despite the findings of these studies, the dynamic changes in inflammatory markers in ACLI patients with KOA are not clear, especially in the short term. In the current study, ACLI/KOA patients had higher levels of inflammatory markers than ACLI patients without KOA, which may be due to the influence of KOA. It was also found that AACL combined with SH was efficacious, as it reduced the inflammatory response in ACLI patients regardless of a diagnosis of KOA.

The application of AACL to ACLI has been reported in several investigations. Trung et al. demonstrated that ACL reconstruction using the anterior half of the peroneus longus muscle improved knee function in ACLI patients.¹⁹ Another study found that simultaneous AACL and posterior cruciate ligament reconstruction with hamstring tendon autograft significantly enhanced knee function, with a 90% satisfaction rate found in patients.²⁰

The SH has been reported to improve the formation of nascent neural networks in spinal cord injury,⁸ while another study demonstrated that both SH and MD-Knee were effective in the treatment of KOA.²¹ Furthermore, intra-articular injection of SH into the ankle was reported to provide pain relief and to delay the need for surgery in patients with OA of the ankle.²² However, very little research has investigated the application of SH in the treatment of ACLI. In the current study, it was found that AACL combined with SH was efficacious in both ACLI/KOA and ACLI, which is consistent with the results of previous studies.

Limitations

Limitations include the small sample size, the limited number of tested inflammatory factors and short follow-up period. Further studies that address these limitations will provide deeper insight into the use of ACLR combined with SH in patients who have ACLI with or without KOA.

Conclusions


This prospective cohort study demonstrated the efficacy of ACLR in combination with SH in patients with ACLI with or without KOA. Results showed that the described approach enhanced the recovery of knee function and reduced the inflammatory response in both groups. Furthermore, ACLI patients without KOA recovered more rapidly from the inflammatory response.

ORCID iDs

Yongjun Hu  <https://orcid.org/0000-0002-2377-2420>

Yi Shen  <https://orcid.org/0000-0002-1383-9871>

Ding Chen  <https://orcid.org/0000-0001-7926-5148>

Weiyue Zhong  <https://orcid.org/0000-0003-1469-7024>

References

1. Padua DA, DiStefano LJ, Hewett TE, et al. National Athletic Trainers' Association position statement: Prevention of anterior cruciate ligament injury. *J Athl Train*. 2018;53(1):5–19. doi:10.4085/1062-6050-99-16
2. Montalvo AM, Schneider DK, Webster KE, et al. Anterior cruciate ligament injury risk in sport: A systematic review and meta-analysis of injury incidence by sex and sport classification. *J Athl Train*. 2019;54(5):472–482. doi:10.4085/1062-6050-407-16
3. Kaeding CC, Léger-St-Jean B, Magnussen RA. Epidemiology and diagnosis of anterior cruciate ligament injuries. *Clin Sports Med*. 2017;36(1):1–8. doi:10.1016/j.csm.2016.08.001
4. Shea KG, Carey JL, Richmond J, et al. The American Academy of Orthopaedic Surgeons evidence-based guideline on management of anterior cruciate ligament injuries. *J Bone Joint Surg*. 2015;97(8):672–674. doi:10.2106/JBJS.N.01257
5. Cole BJ, Cotter EJ, Wang KC, Davey A. Patient understanding, expectations, outcomes, and satisfaction regarding anterior cruciate ligament injuries and surgical management. *Arthroscopy*. 2017;33(5):1092–1096. doi:10.1016/j.arthro.2017.01.049
6. Herzog MM, Marshall SW, Lund JL, Pate V, Spang JT. Cost of outpatient arthroscopic anterior cruciate ligament reconstruction among commercially insured patients in the United States, 2005–2013. *Orthop J Sports Med*. 2017;5(1):232596711668477. doi:10.1177/2325967116684776
7. Leathers M, Merz A, Wong J, Scott T, Wang J, Hame S. Trends and demographics in anterior cruciate ligament reconstruction in the United States. *J Knee Surg*. 2015;28(5):390–394. doi:10.1055/s-0035-1544193
8. Paschos NK. Anterior cruciate ligament reconstruction and knee osteoarthritis. *World J Orthop*. 2017;8(3):212–217. doi:10.5312/wjo.v8.i3.212
9. Wellsandt E, Gardinier ES, Manal K, Axe MJ, Buchanan TS, Snyder-Mackler L. Decreased knee joint loading associated with early knee osteoarthritis after anterior cruciate ligament injury. *Am J Sports Med*. 2016;44(1):143–151. doi:10.1177/0363546515608475
10. Simon D, Mascarenhas R, Saltzman BM, Rollins M, Bach BR, MacDonald P. The relationship between anterior cruciate ligament injury and osteoarthritis of the knee. *Adv Orthop*. 2015;356:928301. doi:10.1155/2015/928301
11. Shang J, Qiao H, Hao P, et al. bFGF-sodium hyaluronate collagen scaffolds enable the formation of nascent neural networks after adult spinal cord injury. *J Biomed Nanotechnol*. 2019;15(4):703–716. doi:10.1166/jbn.2019.2732
12. Cai Y, Sun Z, Liao B, Song Z, Xiao T, Zhu P. Sodium hyaluronate and platelet-rich plasma for partial-thickness rotator cuff tears. *Med Sci Sports Exerc*. 2019;51(2):227–233. doi:10.1249/MSS.0000000000001781
13. Zhang Z, Huang C, Jiang Q, et al. Guidelines for the diagnosis and treatment of osteoarthritis in China (2019 edition). *Ann Transl Med*. 2020;8(19):1213–1213. doi:10.21037/atm-20-4665
14. Lie MM, Risberg MA, Storheim K, Engebretsen L, Øiestad BE. What's the rate of knee osteoarthritis 10 years after anterior cruciate ligament injury? An updated systematic review. *Br J Sports Med*. 2019;53(18):1162–1167. doi:10.1136/bjsports-2018-099751
15. Johnson VL, Roe JP, Salmon LJ, Pinczewski LA, Hunter DJ. Does age influence the risk of incident knee osteoarthritis after a traumatic anterior cruciate ligament injury? *Am J Sports Med*. 2016;44(9):2399–2405. doi:10.1177/0363546516648318
16. Papathanasiou I, Michalitsis S, Hantes ME, et al. Molecular changes indicative of cartilage degeneration and osteoarthritis development in patients with anterior cruciate ligament injury. *BMC Musculoskelet Disord*. 2016;17(1):21. doi:10.1186/s12891-016-0871-8
17. Harkey MS, Luc BA, Golightly YM, et al. Osteoarthritis-related biomarkers following anterior cruciate ligament injury and reconstruction: A systematic review. *Osteoarthritis Cartilage*. 2015;23(1):1–12. doi:10.1016/j.joca.2014.09.004
18. Roemer FW, Englund M, Turkiewicz A, et al. Molecular and structural biomarkers of inflammation at two years after acute anterior cruciate ligament injury do not predict structural knee osteoarthritis at five years. *Arthritis Rheumatol*. 2019;71(2):238–243. doi:10.1002/art.40687
19. Trung DT, Manh SL, Nguyen Thanh L, Chu Dinh T, Chu Dinh T. Preliminary result of arthroscopic anterior cruciate ligament reconstruction using anterior half of peroneus longus tendon autograft. *Open Access Maced J Med Sci*. 2019;7(24):4351–4356. doi:10.3889/oamjms.2019.390
20. Panigrahi R, Kumari Mahapatra A, Priyadarshi A, Singha Das D, Palo N, Ranjan Biswal M. Outcome of simultaneous arthroscopic anterior cruciate ligament and posterior cruciate ligament reconstruction with hamstring tendon autograft: A multicenter prospective study. *Asian J Sports Med*. 2016;7(1):e29287. doi:10.5812/asjms.29287
21. Martin Martin LS, Massafra U, Bizzi E, Migliore A. A double blind randomized active-controlled clinical trial on the intra-articular use of Md-Knee versus sodium hyaluronate in patients with knee osteoarthritis ("Joint"). *BMC Musculoskelet Disord*. 2016;17(1):94. doi:10.1186/s12891-016-0948-4
22. Murphy EP, Curtin M, McGoldrick NP, Thong G, Kearns SR. Prospective evaluation of intra-articular sodium hyaluronate injection in the ankle. *J Foot Ankle Surg*. 2017;56(2):327–331. doi:10.1053/j.jfas.2016.09.017

Differential expression of miRNAs from extracellular vesicles in chronic graft-versus-host disease: A preliminary study

Piotr Łacina^{1,B–F}, Rachel E. Crossland^{2,B,C,E,F}, Joanna Wielińska^{1,B,C,E,F}, Anna Czyż^{3,B,E,F}, Agnieszka Szeremet^{3,B,E,F}, Marek Ussowicz^{4,B,E,F}, Tomasz Wróbel^{3,B,E,F}, Anne M. Dickinson^{2,A,E,F}, Katarzyna Bogunia-Kubik^{1,A,D–F}

¹ Laboratory of Clinical Immunogenetics and Pharmacogenetics, Hirsfeld Institute of Immunology and Experimental Therapy, Polish Academy of Sciences, Wrocław, Poland

² Translational and Clinical Research Institute, Faculty of Medical Sciences, Newcastle University, United Kingdom

³ Department of Haematology, Blood Neoplasms and Bone Marrow Transplantation, Wrocław Medical University, Poland

⁴ Department of Paediatric Bone Marrow Transplantation, Oncology and Haematology, Wrocław Medical University, Poland

A – research concept and design; B – collection and/or assembly of data; C – data analysis and interpretation;

D – writing the article; E – critical revision of the article; F – final approval of the article

Advances in Clinical and Experimental Medicine, ISSN 1899–5276 (print), ISSN 2451–2680 (online)

Adv Clin Exp Med. 2023;32(5):539–544

Address for correspondence

Piotr Łacina

E-mail: piotr.lacina@hirsfeld.pl

Funding sources

This work was supported by the National Science Centre (Kraków, Poland) (grant No. 2018/31/B/NZ2/03065) and European Cooperation in Science & Technology under the COST Action CA17138 (Integrated European Network on Chronic Graft Versus Host Disease: EUROGRAFT) (<https://www.gvhd.eu>).

Conflict of interest

None declared

Received on July 15, 2022

Reviewed on August 17, 2022

Accepted on September 13, 2022

Published online on November 18, 2022

Abstract

Background. Chronic graft-versus-host disease (cGvHD) is a complex disorder that typically manifests after allogeneic hematopoietic stem cell transplantation (HSCT). It is a major cause of non-relapse mortality, which makes finding biomarkers associated with its occurrence a priority. Recent studies increasingly indicate that microRNAs (miRNAs, short regulatory RNA molecules) can be used as biomarkers of various disorders. They can circulate in patients' bodies encapsulated within extracellular vesicles (EVs).

Objectives. To identify miRNAs associated with the occurrence of cGvHD in EVs isolated from the plasma of patients after allogeneic HSCT.

Materials and methods. We performed global miRNA expression profiling in a pilot cohort of 3 cGvHD cases and 4 non-cGvHD patients without disease symptoms 90 days after the transplantation (control group).

Results. The 2 groups were naturally clustered according to their miRNA profiles using unsupervised hierarchical clustering analysis. We identified 3 miRNAs that were differentially expressed in the cGvHD patients compared to the non-cGvHD patients. The levels of hsa-miR-630 and hsa-miR-374b-5p were lower in the cGvHD patients: 4.1-fold ($p = 0.002$) and 2.7-fold ($p = 0.044$), respectively. In contrast, the levels of hsa-miR-29c-3p were 5.8-fold higher ($p = 0.004$).

Conclusions. Our results suggest that miRNA profiles from plasma EVs may act as markers of cGvHD onset.

Key words: allogeneic HSCT, extracellular vesicles, miRNA profiling, chronic GvHD

Cite as

Łacina P, Crossland RE, Wielińska J, et al. Differential expression of miRNAs from extracellular vesicles in chronic graft-versus-host disease: A preliminary study. *Adv Clin Exp Med.* 2023;32(5):539–544. doi:10.17219/acem/155373

DOI

10.17219/acem/155373

Copyright

Copyright by Author(s)

This is an article distributed under the terms of the Creative Commons Attribution 3.0 Unported (CC BY 3.0) (<https://creativecommons.org/licenses/by/3.0/>)

Background

Graft-versus-host disease (GvHD) is a common complication after allogeneic hematopoietic stem cell transplantation (HSCT), which is the main therapeutic procedure for patients with hematologic malignancies, such as leukemias, lymphomas and multiple myeloma. Graft-versus-host disease is driven by the presence of donor-derived T cells and manifests itself in one of the two forms: acute (aGvHD) or chronic (cGvHD). Chronic graft-versus-host disease is one of the most significant long-term complications in patients after HSCT, being the leading cause of non-relapse mortality.¹ The disease significantly reduces the quality of life for post-transplant patients and is associated with various other comorbidities.² Since up to 50% of patients develop cGvHD following HSCT,² it is important to identify suitable prognostic markers for the earlier detection of the disease, particularly biomarkers that are easily detectable in biological fluids.

Short-circulating RNA molecules, known as microRNAs (miRNAs), have been increasingly studied during the last decade as potential biomarkers of various diseases. They are small (22–25 nucleotides) non-coding molecules that downregulate genes by binding to the 3'UTR region of their mRNA.³ The miRNAs are present in many biological fluids, including plasma and serum.^{4,5} They are known to be very stable and resistant to RNases and detrimental storage conditions. Specific changes in miRNA expression patterns can be associated with different diseases.⁶ Their stability, robustness and presence in easily collected fluids, such as plasma, have made them promising candidates for biomarkers of disease.⁷ The miRNAs are mostly found either bound to protective proteins or inside extracellular vesicles (EVs), which shield them from the environment.⁸

Extracellular vesicles are lipid bilayer structures of varying sizes that can transport various molecules, such as proteins, lipids, carbohydrates, and nucleic acids, including miRNAs.⁹ They are released by cells to mediate intercellular communication and can release their contents into another cell by fusing with its cell membrane. Extracellular vesicle content can differ markedly between different body fluids. Blood EVs show slightly different contents depending on the fluid they are harvested from (serum or plasma).¹⁰ The impact of EVs differs depending on the content of their cargo. However, they have been shown to be implicated in many processes, and they may be involved in the development of various pathological disorders.¹¹ Extracellular vesicles may also be involved in the modulation of the immune response and complications arising after HSCT.¹²

While many biomarkers, mostly proteins, have been described in aGvHD, there is a need for cGvHD markers.¹³ Earlier studies have shown that the miRNA signature in both serum and plasma can be a marker for aGvHD.^{3,14} Previous studies have also revealed that EVs can affect the development and symptoms of cGvHD in a mouse

model.¹⁵ Current multiplex methods, such as NanoString nCounter[®] technology, facilitate the analysis of the full spectrum of differentially expressed miRNAs. While sets of miRNAs differentially expressed in aGvHD are already established,¹⁶ to date, there have been no studies focusing on miRNAs in cGvHD.

Objectives

In this study, we aimed to profile 798 highly conserved human miRNAs in EVs isolated from the plasma of a group of post-HSCT patients to establish a panel of miRNAs from EVs differentially expressed in cGvHD patients.

Materials and methods

A total of 7 patients were investigated, including 4 patients without cGvHD 90 days after the transplantation (the control group) and 3 cGvHD patients who presented with extensive symptomatology. Their characteristics are presented in Table 1. All patients were transplanted either at the Department of Haematology, Blood Neoplasms and Bone Marrow Transplantation, or the Department of Paediatric Bone Marrow Transplantation, Oncology and Haematology (Wroclaw Medical University, Poland). The study was approved by Bioethics Committee of Wroclaw Medical University, Poland on July 1, 2019 (approval No. 561/2019). Written informed consent was obtained from the participants, and the study was performed in compliance with the Declaration of Helsinki.

Plasma was separated from whole blood samples through centrifugation and stored at -80°C . Extracellular vesicles were precipitated from 2 mL of plasma samples using the Total Exosome Isolation Kit (Thermo Fisher Scientific, Waltham, USA), following the supplier's instructions. Total RNA was isolated from the resuspended EVs using the Total Exosome RNA and Protein Isolation Kit (Thermo Fisher Scientific), following the manufacturer's recommendations. For further analysis, the isolated RNA samples were concentrated to 25 μL using Amicon Ultra-0.5 Centrifugal Filter Units (Merck Group, Darmstadt, Germany). The RNA was quantified using a Bioanalyzer and RNA 6000 pico kit (Agilent Technologies, Santa Clara, USA). Any variation in RNA recovery between the samples was compensated for by the use of NanoString endogenous controls.

The miRNA profile was analyzed in 3 μL of concentrated total RNA samples using the nCounter[®] Human v3 miRNA Expression Assay Kit (NanoString Technologies, Inc., Seattle, USA), following the supplier's protocols. The code set included 798 microRNAs, 5 mRNA housekeeping controls (*ACTB*, *B2M*, *GAPDH*, *RPL19*, and *RPLP0*), 6 ligation controls, 8 negative controls, and 6 positive controls.

The output raw data obtained from nCounter[®] miRNA profiling were normalized using nSolver Analysis Software

Table 1. Characteristics of patients

Patient No.	Diagnosis	Age	Sex	Donor (SIB/HAP/MUD)	Transplant material	Conditioning regimen	aGvHD grade	Viral infections EBV/CMV/other	cGvHD	Fig. 1 [#]
1	AML	22	F	HAP	BM	RIC	I (skin)	no/yes/no	no	non-cGvHD I
2	AML	58	F	MUD	PBPC	RIC	I (skin)	no/yes/no	no	non-cGvHD II
3	MDS	63	M	MUD	PBPC	RIC	no	no/yes/no	no	non-cGvHD III
4	PMF	56	M	MUD	PBPC	MAC	no	no/yes/no	no	non-cGvHD IV
5	AML	61	F	MUD	PBPC	RIC	I (skin)	yes/yes/no	extensive lung, liver	cGvHD I
6	MDS/AML	14	F	MUD	PBPC	RIC	I (skin), IV (gut)	no/no/no	extensive skin	cGvHD II
7	AML	18	F	SIB	BM	MAC	III (liver)	no/no/BKV cystitis	extensive liver	cGvHD III

AML – acute myeloid leukemia; PMF – primary myelofibrosis; MDS – myelodysplastic syndrome; F – female recipient; M – male recipient; SIB – HLA-matched sibling donor; HAP – haploidentical family member; MUD – matched unrelated donor; BM – bone marrow; PBPC – peripheral blood progenitor cells; RIC – reduced intensity conditioning; MAC – myeloablative conditioning; aGvHD – acute graft-versus-host disease; cGvHD – chronic graft-versus-host disease; EBV – Epstein-Barr virus; CMV – cytomegalovirus; BKV – BK virus; # reflects sample description in Fig. 1.

v. 2.5 (NanoString Technologies, Inc.) with code set content normalization based on the top 100 miRNAs with geometric mean and standard flagging limits. Additionally, fold change expression differences between the groups of patients compared in the study were calculated based on normalized count data.

Statistical analysis was performed according to the procedures designed at the Haematological Sciences Department of Newcastle University (UK), as described by Crossland et al. in 2017.³ In short, various R statistical packages were used within RStudio software (RStudio, Boston, USA) in order to generate volcano plots (“ggplots”) and heatmaps (“glops” and “RColorBrewer”) based on an unsupervised clustering approach of the normalized expression counts with a Euclidean (L2 norm) distance measure and “Complete” as the agglomeration method.

Gene analysis and pathway prediction for the identified miRNAs were performed based on the method described by Lou et al.¹⁷ The miRNet database (<http://www.mirnet.ca/>), which uses data from 11 different databases, was used to identify potential gene targets of miRNAs obtained from NanoString.¹⁸ Subsequently, the target genes were used to construct protein–protein interaction networks in the STRING database (<http://string-db.org/>),¹⁹ separately for miRNAs upregulated and downregulated in cGvHD. Hub genes were then identified using Cytoscape software (v. 3.7.2; <https://cytoscape.org/>)²⁰ and used in KEGG pathway enrichment analysis performed in the Database for Annotation, Visualization and Integrated Discovery (DAVID) (<https://david.ncifcrf.gov/>).²¹

Results

Out of the 798 miRNAs tested, 73 had sufficiently high levels above background after normalization in at least 2 samples and were subsequently included in a further analysis. The unsupervised hierarchical clustering analysis

was able to separate samples according to their disease status (cGvHD compared to non-cGvHD). Three miRNAs were significantly differentially expressed in cGvHD compared to non-cGvHD; miR-374b-5p and miR-630 were downregulated, while miR-29c-3p was upregulated (Table 2 and Fig. 1).

Potential target genes for the 3 miRNAs were identified using miRNet. A total of 254 potential target genes were found for upregulated hsa-miR-29c-3p, while 76 and

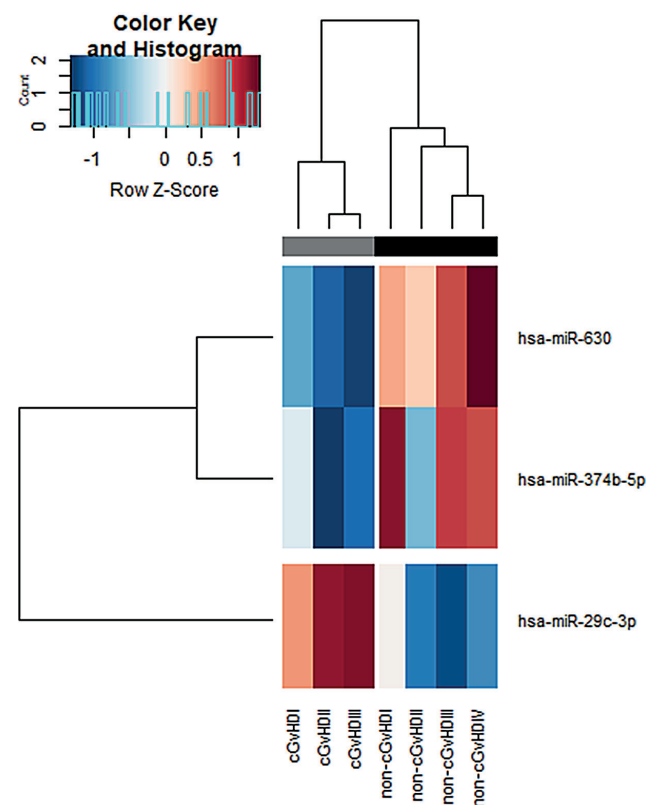


Fig. 1. Fold change in plasma levels of microRNAs (miRNAs) between chronic graft-versus-host disease (cGvHD) and non-cGvHD patients. Hierarchical clustering of differentially expressed miRNAs is shown based on normalized digital expression counts

Table 2. MicroRNAs (miRNAs) found to be differentially expressed between patients with chronic graft-versus-host disease (cGVHD) and non-cGVHD controls

miRNA	fold change	p-value
hsa-miR-29c-3p	5.83	0.004
hsa-miR-374b-5p	-2.71	0.045
hsa-miR-630	-4.13	0.002

234 were found for downregulated hsa-miR-630 and hsa-miR-374b-5p, respectively (3 genes, *APOL6*, *LRIG3* and *ATXN1*, were shared between the up- and downregulated miRNAs). The genes obtained from miRNet were then used to construct protein–protein interaction networks and identify their hub genes based on the degree of connectivity. The 10 hub genes linked to the upregulated hsa-miR-29c-3p were: *VEGFA*, *GAPDH*, *PTEN*, *JUN*, *MMP2*, *SIRT1*, *ITGB1*, *CDC42*, *COL1A2*, and *COL1A1*. The 10 hub genes linked to the downregulated miRNAs were: *AKT1*, *CCND1*, *VEGFA*, *PPP2CA*, *GSK3B*, *SPI1*, *SMURF2*, *YY1*, *SNAI2*, and *YAP1* (Fig. 2). Subsequent KEGG pathway enrichment analysis revealed that the targets of the upregulated hsa-miR-29c-3p were enriched in many pathways, including those associated with focal adhesion ($p < 0.001$) and leukocyte transendothelial migration ($p = 0.009$). On the other hand, the targets of the downregulated miRNAs were enriched in pathways associated with transforming growth factor beta (TGF- β) signaling ($p = 0.004$) and various cancers ($p < 0.05$).

Discussion

In this study, we identified a set of miRNAs from plasma EVs (hsa-miR-29c-3p, hsa-miR-374b-5p and hsa-miR-630) that could potentially serve as diagnostic markers of cGVHD. Due to the importance of early diagnosis, various studies have been conducted to identify suitable biological markers of cGVHD, with most of them focusing on serum/plasma proteins. Much less is known about potential non-protein markers. Regarding miRNAs, it has been shown that miR-21 and the miR-17-92 cluster may be of importance in cGVHD.^{22,23}

This study is the first to date to profile a wide spectrum of miRNAs differentially expressed in cGVHD EVs. Earlier studies have revealed that EVs can have a major influence on cGVHD.^{15,24} The miRNA profiling studies have been conducted on aGVHD patients, although they did not focus on EV-derived miRNAs.¹⁴ While they used different sample material, there was 1 miRNA (hsa-miR-374b-5p) that was differentially expressed in these aGVHD studies and also differentially expressed in our cGVHD EV samples;¹⁴ both were downregulated. Earlier studies demonstrated that miR-374b-5p is associated mainly with nonhematological cancers,

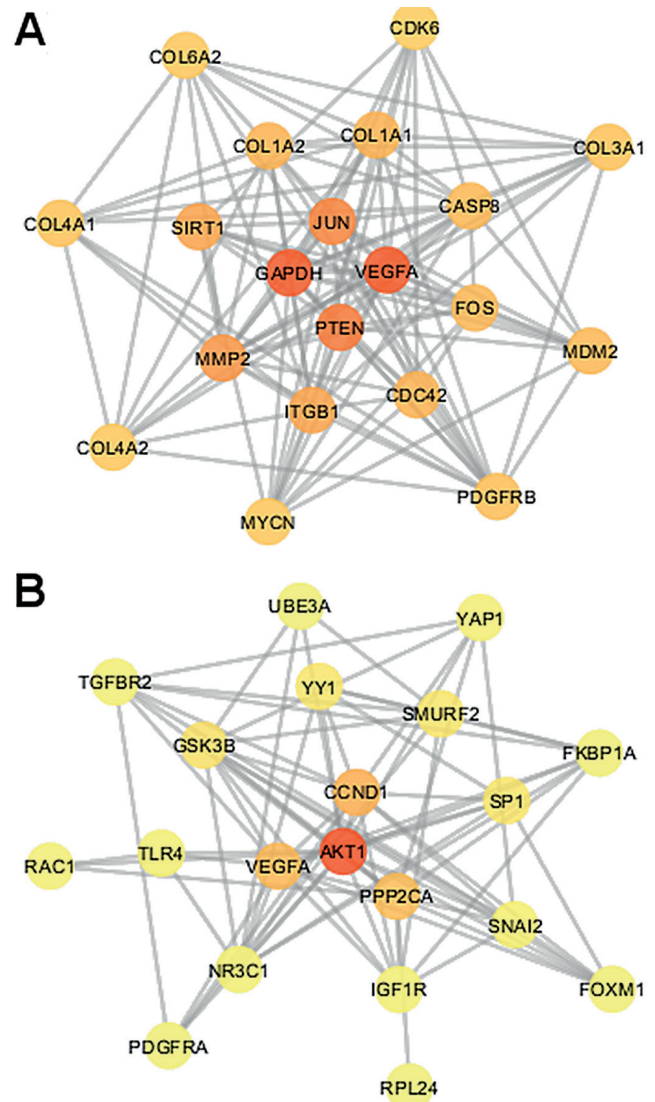


Fig. 2. Hub genes in the protein–protein interaction network. Twenty hub genes with the highest degree of connectivity in the protein–protein interaction networks of (A) upregulated microRNA (miRNA) target genes and (B) downregulated miRNA target genes. Data were analyzed using the method described by Lou et al.¹⁷

being upregulated in some and downregulated in others.^{25,26} The miRNA hsa-miR-374b-5p was also shown to modulate the type-I interferon response.²⁷ The other miRNA we found to be upregulated in cGVHD, miR-630, was likewise reported to be overexpressed in some cancers,²⁸ while it suppressed the proliferation in others, including the interaction with the TGF- β signaling pathway.²⁹ Incidentally, TGF- β was found to have a major role in the development of cGVHD.^{30,31} This seems to be consistent with our results, which suggest that the miRNAs found to be possibly downregulated in cGVHD may be implicated in TGF- β signaling and cancer pathways. It is, however, not known specifically how the downregulation of the aforementioned miRNAs could influence the onset of cGVHD.

The miRNA identified by our study as potentially up-regulated in cGvHD, miR-29c-3p, has also been extensively studied in various other diseases. It was found to be down-regulated in acute lymphoblastic leukemia.³² Furthermore, many studies determined that miR-29c-3p suppresses proliferation, migration and cancer cell migration.^{33–36} Likewise, earlier studies established migration-related CD146 expression on T cells to be elevated in patients with cGvHD.^{37,38} This seems to be in accordance with the results of our analysis, which indicate that miR-29c-3p may be implicated in leukocyte transendothelial migration.

All the patients in the current study had prior hematological disorders of myeloid lineage, although the group was not entirely homogeneous; most patients had either acute myeloid leukemia or myelodysplastic syndrome, except for 1 non-cGvHD patient who had primary myelofibrosis. Reduced intensity conditioning was used in most patients before transplantation, although 2 patients (1 in each studied group) were administered myeloablative conditioning. For most patients, the transplantation was from a matched unrelated donor. The potential impact of these differences on miRNA profile is difficult to establish. This study compared a group of 3 patients who developed cGvHD with a group of 4 patients without cGvHD, with samples collected 3 months after the transplantation. The number of patients studied was quite low; therefore, the results presented here should be treated with caution and are subject to validation in larger cohorts of patients. Additionally, it should be noted that all 3 of the cGvHD patients and 2 non-cGvHD patients developed prior aGvHD symptoms. These symptoms indicated mild cGvHD (grade I) involving skin in the non-cGvHD group. In the cGvHD group, 1 patient developed grade IV aGvHD in the gut, and another patient developed grade III aGvHD in the liver. This aGvHD occurrence could have influenced our results, although only miR-374b-5p was expressed similarly in our study and in earlier non-EV aGvHD studies. The miRNAs reported earlier as aGvHD serum EV biomarkers did not coincide with the miRNAs detected by us as differentially expressed in cGvHD samples.⁷ All patients except 1 were also affected by viral infections (cytomegalovirus (CMV) and BK virus (BKV)). Viruses are known to express their own miRNAs,³⁹ but little is known about the impact CMV/BKV infections have on host miRNA profiles. Cytomegalovirus infection is known to affect human miRNA expression in its early stage, although a study on infants with congenital CMV did not find any of the 3 miRNAs described in our study to be affected.^{40,41}










Limitations

This study has many shortcomings. The most important is the low number of patients analyzed in both groups. Additionally, there are slight differences in the characteristics of the patients (as described in the Discussion section) that could have had an effect on the results.

Conclusions

This study suggests that hsa-miR-29c-3p, hsa-miR-374b-5p and hsa-miR-630 are differentially expressed in plasma EVs from cGvHD patients and may be considered diagnostic markers of this disease. However, due to the very small cohort of patients included and the presence of other potentially confounding factors, this should be regarded as a preliminary study, and its results should be confirmed on a larger group of patients.

ORCID iDs

Piotr Łacina  <https://orcid.org/0000-0002-9659-9403>
 Rachel E. Crossland  <https://orcid.org/0000-0001-6138-160X>
 Joanna Wielńska  <https://orcid.org/0000-0002-1048-5254>
 Anna Czyż  <https://orcid.org/0000-0001-6641-0182>
 Agnieszka Szeremet  <https://orcid.org/0000-0002-1897-3180>
 Marek Ussowicz  <https://orcid.org/0000-0001-5725-4835>
 Tomasz Wróbel  <https://orcid.org/0000-0002-6612-3535>
 Anne M. Dickinson  <https://orcid.org/0000-0002-7356-7636>
 Katarzyna Bogunia-Kubik  <https://orcid.org/0000-0001-9744-0376>

References

- Lee SJ, Vogelsang G, Flowers MED. Chronic graft-versus-host disease. *Biol Blood Marrow Transplant.* 2003;9(4):215–233. doi:10.1053/bbmt.2003.50026
- Juric MK, Shevtsov M, Mozes P, et al. B-cell-based and soluble biomarkers in body liquids for predicting acute/chronic graft-versus-host disease after allogeneic hematopoietic stem cell transplantation. *Front Immunol.* 2017;7:660. doi:10.3389/fimmu.2016.00660
- Crossland RE, Norden J, Juric MK, et al. Expression of serum microRNAs is altered during acute graft-versus-host disease. *Front Immunol.* 2017;8:308. doi:10.3389/fimmu.2017.00308
- Chen X, Ba Y, Ma L, et al. Characterization of microRNAs in serum: A novel class of biomarkers for diagnosis of cancer and other diseases. *Cell Res.* 2008;18(10):997–1006. doi:10.1038/cr.2008.282
- Mitchell PS, Parkin RK, Kroh EM, et al. Circulating microRNAs as stable blood-based markers for cancer detection. *Proc Natl Acad Sci U S A.* 2008;105(30):10513–10518. doi:10.1073/pnas.0804549105
- Weber JA, Baxter DH, Zhang S, et al. The microRNA spectrum in 12 body fluids. *Clin Chem.* 2010;56(11):1733–1741. doi:10.1373/clinchem.2010.147405
- Wang K, Yuan Y, Cho JH, McClarty S, Baxter D, Galas DJ. Comparing the microRNA spectrum between serum and plasma. *PLoS One.* 2012;7(7):e41561. doi:10.1371/journal.pone.0041561
- Cortez MA, Bueso-Ramos C, Ferdin J, Lopez-Berestein G, Sood AK, Calin GA. MicroRNAs in body fluids: The mix of hormones and biomarkers. *Nat Rev Clin Oncol.* 2011;8(8):467–477. doi:10.1038/nrclinonc.2011.76
- Maas SLN, Breakefield XO, Weaver AM. Extracellular vesicles: Unique intercellular delivery vehicles. *Trends Cell Biol.* 2017;27(3):172–188. doi:10.1016/j.tcb.2016.11.003
- Zhang X, Takeuchi T, Takeda A, Mochizuki H, Nagai Y. Comparison of serum and plasma as a source of blood extracellular vesicles: Increased levels of platelet-derived particles in serum extracellular vesicle fractions alter content profiles from plasma extracellular vesicle fractions. *PLoS One.* 2022;17(6):e0270634. doi:10.1371/journal.pone.0270634
- Shah R, Patel T, Freedman JE. Circulating extracellular vesicles in human disease. *N Engl J Med.* 2018;379(10):958–966. doi:10.1056/NEJMra1704286
- Lia G, Di Vito C, Cerrano M, et al. Extracellular vesicles after allogeneic hematopoietic cell transplantation: Emerging role in post-transplant complications. *Front Immunol.* 2020;11:422. doi:10.3389/fimmu.2020.00422
- Paczesny S. Discovery and validation of graft-versus-host disease biomarkers. *Blood.* 2013;121(4):585–594. doi:10.1182/blood-2012-08-355990

14. Xiao B, Wang Y, Li W, et al. Plasma microRNA signature as a noninvasive biomarker for acute graft-versus-host disease. *Blood*. 2013;122(19):3365–3375. doi:10.1182/blood-2013-06-510586
15. Guo L, Lai P, Wang Y, et al. Extracellular vesicles derived from mesenchymal stem cells prevent skin fibrosis in the cGVHD mouse model by suppressing the activation of macrophages and B cells immune response. *Int Immunopharmacol*. 2020;84:106541. doi:10.1016/j.intimp.2020.106541
16. Crossland RE, Norden J, Kralj Juric M, et al. Serum and extracellular vesicle microRNAs miR-423, miR-199, and miR-93 as biomarkers for acute graft-versus-host disease. *Front Immunol*. 2017;8:1446. doi:10.3389/fimmu.2017.01446
17. Lou W, Liu J, Ding B, et al. Identification of potential miRNA–mRNA regulatory network contributing to pathogenesis of HBV-related HCC. *J Transl Med*. 2019;17(1):7. doi:10.1186/s12967-018-1761-7
18. Fan Y, Siklenka K, Arora SK, Ribeiro P, Kimmins S, Xia J. miRNet: Dissecting miRNA–target interactions and functional associations through network-based visual analysis. *Nucleic Acids Res*. 2016;44(W1):W135–W141. doi:10.1093/nar/gkw288
19. Szklarczyk D, Franceschini A, Wyder S, et al. STRING v10: Protein–protein interaction networks, integrated over the tree of life. *Nucleic Acids Res*. 2015;43(D1):D447–D452. doi:10.1093/nar/gku1003
20. Shannon P, Markiel A, Ozier O, et al. Cytoscape: A software environment for integrated models of biomolecular interaction networks. *Genome Res*. 2003;13(11):2498–2504. doi:10.1101/gr.1239303
21. Huang DW, Sherman BT, Lempicki RA. Systematic and integrative analysis of large gene lists using DAVID bioinformatics resources. *Nat Protoc*. 2009;4(1):44–57. doi:10.1038/nprot.2008.211
22. Garchow B, Kiriakidou M. MicroRNA-21 deficiency protects from lupus-like autoimmunity in the chronic graft-versus-host disease model of systemic lupus erythematosus. *Clin Immunol*. 2016;162:100–106. doi:10.1016/j.clim.2015.11.010
23. Wu Y, Schutt S, Paz K, et al. MicroRNA-17-92 is required for T-cell and B-cell pathogenicity in chronic graft-versus-host disease in mice. *Blood*. 2018;131(17):1974–1986. doi:10.1182/blood-2017-06-789321
24. Lai P, Chen X, Guo L, et al. A potent immunomodulatory role of exosomes derived from mesenchymal stromal cells in preventing cGVHD. *J Hematol Oncol*. 2018;11(1):135. doi:10.1186/s13045-018-0680-7
25. Zhang K, Wang YW, Wang YY, et al. Identification of microRNA biomarkers in the blood of breast cancer patients based on microRNA profiling. *Gene*. 2017;619:10–20. doi:10.1016/j.gene.2017.03.038
26. Li H, Liang J, Qin F, Zhai Y. MiR-374b-5p-FOXP1 feedback loop regulates cell migration, epithelial–mesenchymal transition and chemosensitivity in ovarian cancer. *Biochem Biophys Res Commun*. 2018;505(2):554–560. doi:10.1016/j.bbrc.2018.09.161
27. Rastogi M, Singh SK. Modulation of type-I interferon response by hsa-miR-374b-5p during Japanese encephalitis virus infection in human microglial cells. *Front Cell Infect Microbiol*. 2019;9:291. doi:10.3389/fcimb.2019.00291
28. Jiang N. miR-630 overexpression in hepatocellular carcinoma tissues is positively correlated with alpha-fetoprotein. *Med Sci Monit*. 2015;21:667–673. doi:10.12659/MSM.892515
29. Chen WX, Zhang ZG, Ding ZY, et al. MicroRNA-630 suppresses tumor metastasis through the TGF- β - miR-630-Slug signaling pathway and correlates inversely with poor prognosis in hepatocellular carcinoma. *Oncotarget*. 2016;7(16):22674–22686. doi:10.18632/oncotarget.8047
30. Liem LM, Fibbe WE, van Houwelingen HC, Goulmy E. Serum transforming growth factor-beta1 levels in bone marrow transplant recipients correlate with blood cell counts and chronic graft-versus-host disease. *Transplantation*. 1999;67(1):59–65. doi:10.1097/00007890-199901150-00009
31. Marinelli Busilacchi E, Costantini A, Mancini G, et al. Nilotinib treatment of patients affected by chronic graft-versus-host disease reduces collagen production and skin fibrosis by downmodulating the TGF- β and p-SMAD pathway. *Biol Blood Marrow Transplant*. 2020;26(5):823–834. doi:10.1016/j.bbmt.2020.01.014
32. He Z, Liao Z, Chen S, et al. Downregulated miR-17, miR-29c, miR-92a and miR-214 may be related to *BCL11B* overexpression in T cell acute lymphoblastic leukemia. *Asia Pac J Clin Oncol*. 2018;14(5):e259–e265. doi:10.1111/ajco.12979
33. Lu K, Feng F, Yang Y, et al. High-throughput screening identified miR-7-2-3p and miR-29c-3p as metastasis suppressors in gallbladder carcinoma. *J Gastroenterol*. 2020;55(1):51–66. doi:10.1007/s00535-019-01627-0
34. Chen G, Zhou T, Li Y, Yu Z, Sun L. p53 target miR-29c-3p suppresses colon cancer cell invasion and migration through inhibition of PHLDB2. *Biochem Biophys Res Commun*. 2017;487(1):90–95. doi:10.1016/j.bbrc.2017.04.023
35. Zhang S, Jin J, Tian X, Wu L. hsa-miR-29c-3p regulates biological function of colorectal cancer by targeting SPARC. *Oncotarget*. 2017;8(61):104508–104524. doi:10.18632/oncotarget.22356
36. Wang H, Fu L, Wei D, et al. MiR-29c-3p suppresses the migration, invasion and cell cycle in esophageal carcinoma via CCNA2/p53 axis. *Front Bioeng Biotechnol*. 2020;8:75. doi:10.3389/fbioe.2020.00075
37. Li W, Liu L, Gomez A, et al. Proteomics analysis reveals a Th17-prone cell population in presymptomatic graft-versus-host disease. *JCI Insight*. 2016;1(6):e86660. doi:10.1172/jci.insight.86660
38. Forcade E, Paz K, Flynn R, et al. An activated Th17-prone T cell subset involved in chronic graft-versus-host disease sensitive to pharmacological inhibition. *JCI Insight*. 2017;2(12):e92111. doi:10.1172/jci.insight.92111
39. Sorel O, Dewals BG. MicroRNAs in large herpesvirus DNA genomes: Recent advances. *Biomol Concepts*. 2016;7(4):229–239. doi:10.1515/bmc-2016-0017
40. Buzdin AA, Artcibasova AV, Fedorova NF, et al. Early stage of cytomegalovirus infection suppresses host microRNA expression regulation in human fibroblasts. *Cell Cycle*. 2016;15(24):3378–3389. doi:10.1080/15384101.2016.1241928
41. Kawano Y, Kawada J, Kamiya Y, et al. Analysis of circulating human and viral microRNAs in patients with congenital cytomegalovirus infection. *J Perinatol*. 2016;36(12):1101–1105. doi:10.1038/jp.2016.157

The role of serum nesfatin-1 in a rat model of acute pancreatitis

Ayşe Gul Ferlengez^{1,A,D,F}, Cihad Tatar^{2,A,F}, Mahmut Said Degerli^{3,D–F}, Adil Koyuncu^{4,B,C},
Fatih Alper Ahlatcı^{5,C}, Ali Emre Naycı^{2,B,C}, Aziz Ari^{2,C,D}, Ufuk Oguz Idiz^{2,D,E}

¹ Department of Anesthesiology and Reanimation, University of Health Sciences Istanbul Training and Research Hospital, Türkiye

² Department of General Surgery, University of Health Sciences Istanbul Training and Research Hospital, Türkiye

³ Department of General Surgery, Esenler Maternity and Children's Hospital, Istanbul, Türkiye

⁴ Department of General Surgery, University of Health Sciences Haseki Training and Research Hospital, Istanbul, Türkiye

⁵ Department of Pathology, Corlu State Hospital, Tekirdag, Türkiye

A – research concept and design; B – collection and/or assembly of data; C – data analysis and interpretation;

D – writing the article; E – critical revision of the article; F – final approval of the article

Advances in Clinical and Experimental Medicine, ISSN 1899–5276 (print), ISSN 2451–2680 (online)

Adv Clin Exp Med. 2023;32(5):545–549

Address for correspondence

Mahmut Said Degerli

E-mail: drmsdegerli@gmail.com

Funding sources

None declared

Conflict of interest

None declared

Received on August 27, 2022

Reviewed on September 2, 2022

Accepted on September 28, 2022

Published online on November 25, 2022

Abstract

Background. Acute pancreatitis (AP) is a disease that can still be fatal despite rapid advances in medicine. The relationship between serum nesfatin-1 levels and AP is still to be fully resolved.

Objectives. To investigate the utility of serum nesfatin-1 levels in the diagnosis of AP.

Materials and methods. Twenty-four male Sprague Dawley rats were divided into control, mild pancreatitis and severe pancreatitis groups (n = 8/group). Acute pancreatitis was induced by cerulein injection and the control group received saline injections. Then, the serum nesfatin-1, amylase, lipase, aspartate aminotransferase (AST), and alanine aminotransferase (ALT) levels were determined. A pathologist blinded to the study scored the severity of pancreatitis.

Results. There was a considerable decrease in serum nesfatin-1 levels in parallel to the severity of pancreatitis, though there was no statistically significant relationship observed between pancreatitis and nesfatin-1. In addition, there was no significant difference in AST or ALT levels among the groups. However, a strong positive correlation between amylase and lipase levels was observed (p < 0.05). The severe pancreatitis group (group 3) had a higher lipase level and pathology score than mild pancreatitis group (group 2), and this difference was statistically significant.

Conclusions. Serum nesfatin-1 may be used as a diagnostic and severity marker in pancreatitis in the future.

Key words: rat, acute pancreatitis, nesfatin-1

Cite as

Ferlengez AG, Tatar C, Degerli MS, et al. The role of serum nesfatin-1 in a rat model of acute pancreatitis.

Adv Clin Exp Med. 2023;32(5):545–549.

doi:10.17219/acem/156141

DOI

10.17219/acem/156141

Copyright

Copyright by Author(s)

This is an article distributed under the terms of the Creative Commons Attribution 3.0 Unported (CC BY 3.0)

(<https://creativecommons.org/licenses/by/3.0/>)

Background

Acute pancreatitis (AP) has high mortality and morbidity rates despite technological advancements in medicine. It is caused by nonbacterial acute inflammation that can exhibit clinical and histological remission and develops due to activated pancreatic enzymes leaking into the parenchyma and digesting the gland.^{1,2} Pathological tests for AP can return a wide spectrum of findings, ranging from mild interstitial edema to severe hemorrhagic gangrene and necrosis. The clinical signs of AP manifest to various degrees and can include indefinite abdominal pain, hypotension, fluid sequestration, metabolic disorders, and sepsis. The mortality rate is related to the severity of pancreatitis and could be as high as 30–39% in patients with necrotizing pancreatitis.³ Currently, there is no marker available with high sensitivity and specificity that could predict patient progress to severe pancreatitis. Nonetheless, biomarker studies are still ongoing, as it is thought that being able to predict the onset of severe pancreatitis could reduce mortality and morbidity rates.

Adipose tissue releases cytokines such as tumor necrosis factor- α and interleukin-1, and is an essential mediator of inflammation and metabolism. In addition, adipose tissue releases a range of adipokines such as resistin, leptin, visfatin, adiponectin, and the recently discovered nesfatin-1.^{4,5} Oh-I et al. identified nesfatin-1 in 2006 as a satiety peptide comprising 82 amino acids found in many hypothalamic nuclei, including the paraventricular nucleus.⁴ This adipokine has been shown to be associated with metabolic syndrome and obesity, and several studies have demonstrated its various functions. Indeed, studies have shown the effects of nesfatin-1 on feeding behavior, autonomic control of visceral functions, neuroendocrine regulation, development and differentiation of adipose tissue, inflammation, thermoregulation, pancreatic insulin secretion, and glucose homeostasis in the liver, sleep, attention, anxiety, and stress. Moreover, nesfatin-1 was reported to regulate gastric emptying, gastric acid secretion, gastric motility, and reproductive functions.^{6–9} In addition, a previous study determined that serum nesfatin-1 levels may have diagnostic value in acute mesenteric ischemia.¹⁰

Objectives

This study aimed to investigate the utility of serum nesfatin-1 levels in the diagnosis of AP and in predicting severe pancreatitis, using a cerulein-induced model of pancreatitis in rats.

Materials and methods

Animals

Male Sprague Dawley rats ($n = 24$) aged 4 months and weighing between 300–350 g were acquired from Experimental Animals Laboratory of Bezmialem Vakif University (Istanbul, Türkiye) and maintained on a standard pellet diet. All in vivo experiments were conducted at the Experimental Animal Laboratory of Bezmialem Vakif University Hospital after obtaining the approval of the Ethics Committee of Bezmialem Vakif University (approval No. 2018/107).

Experimental design

Rats were divided into 3 groups ($n = 8$ /group), including a control group and 2 treatment groups. Surgical procedures were performed under anesthesia induced using 10 mg/kg xylazine and 50 mg/kg ketamine hydrochloride, which were injected intramuscularly. Animals in group 1 were subcutaneously administered 5 physiological saline injections at 1-hour intervals to achieve a total dose of 50 μ g/kg. Rats in group 2 were subcutaneously administered 5 cerulein injections at 1-hour intervals to achieve a total dose of 50 μ g/kg. Group 3 received a total dose of 100 μ g/kg of cerulein, which was also administered through a series of 5 subcutaneous injections at 1-hour intervals. Rats were decapitated 7 h after the first injection of cerulein or saline, and approx. 7–8 cm^3 of blood were drawn from each tail vein. Blood was then stored for 40 min at room temperature before further processing.

Biochemical analyses

Blood samples were centrifuged (3500 rpm, 4°C for 10 min) to facilitate serum separation. The extracted serum was transferred to 0.5 cm^3 Eppendorf tubes and delivered to the biochemistry laboratory for detection of nesfatin-1, amylase, lipase, aspartate aminotransferase (AST), and alanine aminotransferase (ALT).

Histopathological examination

Laparotomy was performed by midline incision following decapitation, and pancreatic tissue was excised for histopathological assessment. Specimens were placed in 10% formaldehyde and delivered to the pathology laboratory. Tissue sections were stained using hematoxylin and eosin (H&E) and then investigated (Fig. 1,2). Edema, inflammation, localization, and necrosis were scored between 0 and 4 using the Schonberg index.¹¹

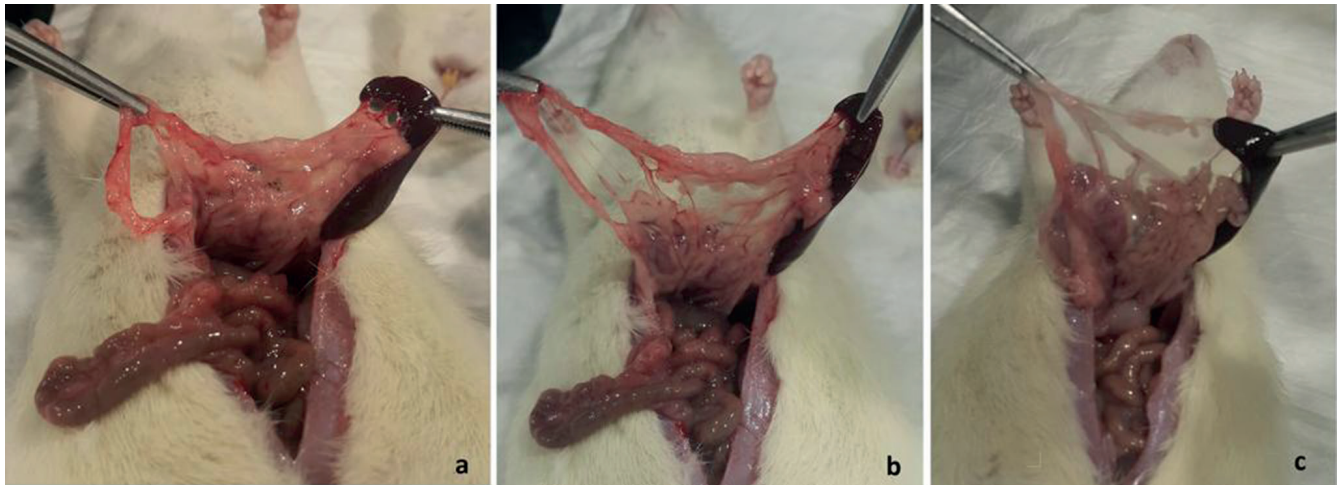


Fig. 1. Macroscopic findings. a – group 1; b – group 2; c – group 3.

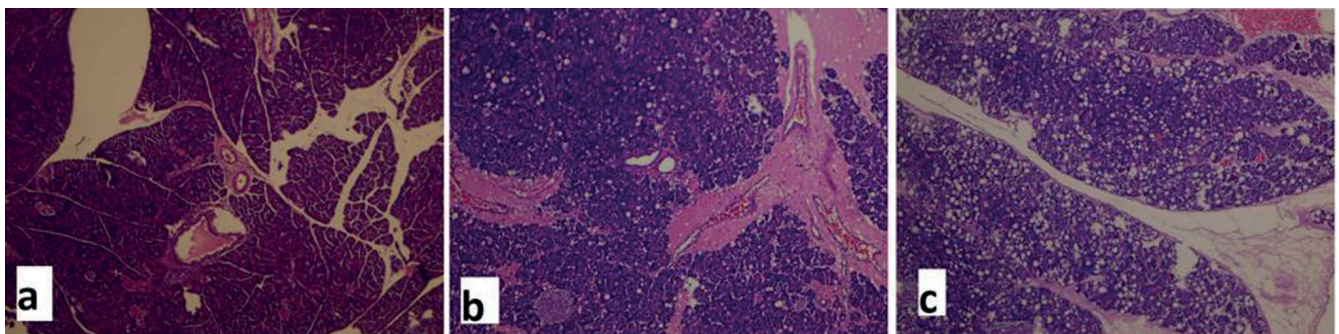


Fig. 2. Histopathological examination (hematoxylin and eosin (H&E) staining, x100 magnification). a – group 1; b – group 2; c – group 3.

Statistical analyses

Descriptive statistics were summarized with mean, median, standard deviation, frequency, minimum, maximum, and ratio values. The distribution of variables was assessed using the Kolmogorov–Smirnov test, and the Kruskal–Wallis test was used to analyze independent quantitative data. Pairwise comparisons were undertaken using the Bonferroni-corrected Mann–Whitney U test. The IBM SPSS v. 22.0 software (IBM Corp., Armonk, USA) was used for all statistical analyses. A value of $p < 0.05$ was considered statistically significant.

Results

No rats were excluded from the study. Table 1 summarizes serum nesfatin-1, amylase, lipase, AST, and ALT levels, as well as pathology scores for all groups. The pathology scores revealed that none of the rats in the control group appeared to develop pancreatitis. However, group 2 had a mean pathology score of 6 and all rats in this group developed mild pancreatitis, whilst group 3 had a mean pathology score of 9 and all rats in this group developed severe pancreatitis.

Biochemical analyses indicated no significant differences in AST, ALT or serum nesfatin-1 levels between

Table 1. Biochemical and pathological results

Variables	Group 1 (n = 8)			Group 2 (n = 8)			Group 3 (n = 8)			p-value	H value
	Q1	Q3	median	Q1	Q3	median	Q1	Q3	median		
AST [U/L]	105.5	154.3	129.5	120.5	198.0	151.0	137.5	179.3	162.0	0.165 ^K	3.599
ALT [U/L]	60.8	87.8	72.5	67.5	90.5	77.5	69.5	87.3	80.0	0.715 ^K	0.672
Amylase [U/L]	1466	1580	1545 ^{**}	2307	3366	2928	2623	3515	3096.5	0.003^K	11.661
Lipase [U/L]	144.5	271.0	204 ^{**}	2506	3872	3087 [*]	2011	3905	3264.5	0.003^K	11.415
Pathology score	0.0	1.0	1.0 ^{**}	4.0	7.3	6.5 [*]	7.5	9.0	9.0	0.001^K	14.023
Serum nesfatin-1	18.5	60.2	33.3	19.4	32.1	25.6	13.1	24.8	17.8	0.106 ^K	4.487

^KKruskal–Wallis (pairwise comparison was made using the Mann–Whitney U test); ^{*}statistically significant difference with group 3; [#]statistically significant difference with group 2; Q1 – 1st quartile; Q3 – 3rd quartile; AST – aspartate aminotransferase; ALT – alanine aminotransferase. Values in bold are statistically significant.

the groups. However, groups 2 and 3 had increased amylase ($p = 0.003$) and lipase levels ($p = 0.003$), and higher pathology scores ($p = 0.001$) in comparison to controls. There was no difference between groups 2 and 3 in terms of amylase levels ($p = 0.423$), although group 3 did have a higher lipase level and pathology score than group 2.

Discussion

Acute pancreatitis leads to the autodigestion of the pancreas, which is initiated by the activation of pancreatic enzymes within the gland.^{12,13} It can also lead to systemic inflammatory conditions during its progression, in addition to localized events. Oxygen free radicals have been shown to have a substantial role in the development of AP,¹⁴ and are known to react with various molecules. In particular, oxygen free radicals cause the peroxidation of membrane phospholipids, which disturbs the integrity of the cell membrane and leads to cell death.

Data from extensive experimental studies have shown that oxygen free radicals are produced as essential mediators in the pathogenesis of several types of tissue damage, including AP. Indeed, oxygen free radicals are known to be involved in the pathophysiology of AP in both the early phase and during its progression.^{11,13,14}

Kolgazi et al. showed that intraperitoneal injection of nesfatin-1 had anti-inflammatory effects in an acetic acid-induced model of gastritis.¹⁶ Nesfatin-1 achieved this effect by ensuring a balance between oxidant and antioxidant systems, in addition to inhibiting key pro-inflammatory mediators. Moreover, Ozturk et al. reported that nesfatin-1 had an anti-inflammatory effect in a model of ischemic colitis through the inhibition of neutrophil infiltration into tissues and the suppression of free radical formation.⁵ Furthermore, nesfatin-1 exhibited an antioxidant effect in colitis via oxytocin and ghrelin receptors.

Ayada et al. investigated the consequence of chronic systemic nesfatin-1 administration on the effectors of microcirculation and oxidant-antioxidant status in a rat model of intestinal ischemia/reperfusion injury.¹⁷ They concluded that nesfatin-1 could balance the oxidative status by decreasing the level of endothelial nitric oxide synthesis and by inhibiting its production.

Gonzalez et al. reported that insulin-producing beta cells of rats and mice co-express pronesfatin immunoreactivity.¹⁸ Furthermore, prohormone convertases, the same enzymes that convert proinsulin to mature insulin, cleave pronesfatin to nesfatin-1, -2 and -3.

Considering the various roles of nesfatin-1 in various models of AP, we analyzed the relationship between serum nesfatin-1 levels and AP. It was found that rats with AP had decreased serum nesfatin-1 levels, and this decrease was even greater in rats with severe pancreatitis. However, there was no statistical significance in the difference between the levels of AP and severe pancreatitis. This finding

of decreased nesfatin-1 can be interpreted in 2 different ways. The 1st possibility is that nesfatin is produced by pancreatic tissues and has proven anti-inflammatory effects, meaning that it may have been consumed at a higher rate to balance the oxidative status in AP. The 2nd possible interpretation is that the decrease in nesfatin production may have been lower in mild pancreatitis than in severe pancreatitis because the latter involves greater deterioration of the pancreas.

To the best of our knowledge, only 2 studies have examined the relationship between AP and nesfatin levels. In a study by Ulger et al., serum nesfatin-1 levels were measured on the days of admission and discharge in patients diagnosed with AP.¹⁹ However, a comparison of the 2 time points did not reveal any difference in nesfatin-1 levels. In another study comprising 97 patients, Türkoğlu et al. compared nesfatin-1 levels between mild and severe pancreatitis, and found no significant intergroup difference.²⁰ However, the study was limited by the lack of a control group.

As far as we know, this is the first study to compare serum nesfatin-1 levels among control, mild and severe pancreatitis groups.

Limitations

The most important limitation of the study is that it was an animal-based study, and clinical studies are required.

Conclusions

Although there was a considerable decrease in serum nesfatin-1 levels that paralleled the severity of pancreatitis, no statistically significant relationship was observed between pancreatitis and nesfatin-1. Therefore, serum nesfatin-1 may be used as a diagnostic and/or severity marker of pancreatitis in the future.

ORCID iDs

Ayse Gul Ferlengez  <https://orcid.org/0000-0002-0440-2467>
 Cihad Tatar  <https://orcid.org/0000-0002-0407-9655>
 Mahmut Said Degerli  <https://orcid.org/0000-0002-8313-7904>
 Adil Koyuncu  <https://orcid.org/0000-0002-5354-2036>
 Fatih Alper Ahlatci  <https://orcid.org/0000-0002-2287-7749>
 Ali Emre Nayci  <https://orcid.org/0000-0001-8029-443X>
 Aziz Ari  <https://orcid.org/0000-0002-7806-2354>
 Ufuk Oguz Idiz  <https://orcid.org/0000-0002-8462-7809>

References

- Lee PJ, Papachristou GI. New insights into acute pancreatitis. *Nat Rev Gastroenterol Hepatol*. 2019;16(8):479–496. doi:10.1038/s41575-019-0158-2
- Mederos MA, Reber HA, Girgis MD. Acute pancreatitis: A review. *JAMA*. 2021;325(4):382. doi:10.1001/jama.2020.20317
- Bugiantella W, Rondelli F, Boni M, et al. Necrotizing pancreatitis: A review of the interventions. *Int J Surg*. 2016;28:S163–S171. doi:10.1016/j.ijsu.2015.12.038
- Oh-I S, Shimizu H, Satoh T, et al. Identification of nesfatin-1 as a satiety molecule in the hypothalamus. *Nature*. 2006;443(7112):709–712. doi:10.1038/nature05162

5. Ozturk CC, Oktay S, Yuksel M, Akakin D, Yarat A, Kasimay Cakir O. Anti-inflammatory effects of nesfatin-1 in rats with acetic acid-induced colitis and underlying mechanisms. *J Physiol Pharmacol*. 2015;66(5): 741–750. PMID:26579580.
6. Stengel A, Taché Y. Nesfatin-1: Role as possible new potent regulator of food intake. *Regul Pept*. 2010;163(1–3):18–23. doi:10.1016/j.regpep.2010.05.002
7. Stengel A, Goebel M, Yakubov I, et al. Identification and characterization of nesfatin-1 immunoreactivity in endocrine cell types of the rat gastric oxyntic mucosa. *Endocrinology*. 2009;150(1):232–238. doi:10.1210/en.2008-0747
8. Ramanjaneya M, Chen J, Brown JE, et al. Identification of nesfatin-1 in human and murine adipose tissue: A novel depot-specific adipokine with increased levels in obesity. *Endocrinology*. 2010;151(7): 3169–3180. doi:10.1210/en.2009-1358
9. Aydin S. Multi-functional peptide hormone NUCB2/nesfatin-1. *Endocrine*. 2013;44(2):312–325. doi:10.1007/s12020-013-9923-0
10. Tatar C, Ahlatci F, Idiz U, et al. May nesfatin-1 be a biomarker in acute mesenteric ischemia? *J Coll Physicians Surg Pak*. 2019;29(10):928–931. doi:10.29271/jcpcsp.2019.10.928
11. Schoenberg MH, Buchler M, Gaspar M, et al. Oxygen free radicals in acute pancreatitis of the rat. *Gut*. 1990;31(10):1138–1143. doi:10.1136/gut.31.10.1138
12. Devenyi ZJ, Orchard JL, Powers RE. Xanthine oxidase activity in mouse pancreas: Effects of caerulein-induced acute pancreatitis. *Biochem Biophys Res Commun*. 1987;149(3):841–845. doi:10.1016/0006-291X(87)90484-0
13. Wisner J, Green D, Ferrell L, Renner I. Evidence for a role of oxygen derived free radicals in the pathogenesis of caerulein induced acute pancreatitis in rats. *Gut*. 1988;29(11):1516–1523. doi:10.1136/gut.29.11.1516
14. Dąbrowski A, Gabryelewicz A, Wereszczyńska-Sięmiątkowska U, Chyczewski L. Oxygen-derived free radicals in cerulein-induced acute pancreatitis. *Scand J Gastroenterol*. 1988;23(10):1245–1249. doi:10.3109/00365528809090199
15. Qi W, Tan D, Reiter R, et al. Melatonin reduces lipid peroxidation and tissue edema in cerulein induced acute pancreatitis in rats. *Dig Dis Sci*. 1999;44(11):2257–2262. doi:10.1023/A:1026656720868
16. Kolgazi M, Cantali-Ozturk C, Deniz R, et al. Nesfatin-1 alleviates gastric damage via direct antioxidant mechanisms. *J Surg Res*. 2015;193(1): 111–118. doi:10.1016/j.jss.2014.06.057
17. Ayada C, Toru Ü, Genç O, Akçılar R, Şahin S. Balanced oxidative status by nesfatin-1 in intestinal ischemia-reperfusion. *Int J Clin Exp Med*. 2015;8(3):3318–3324. PMID:26064221.
18. Gonzalez R, Tiwari A, Unniappan S. Pancreatic beta cells colocalize insulin and pro nesfatin immunoreactivity in rodents. *Biochem Biophys Res Commun*. 2009;381(4):643–648. doi:10.1016/j.bbrc.2009.02.104
19. Ulger BV, Gul M, Uslukaya O, et al. New hormones to predict the severity of gallstone-induced acute pancreatitis. *Turk J Gastroenterol*. 2015; 25(6):714–717. doi:10.5152/tjg.2014.6201
20. Türkoğlu A, Büyük A, Tanrıverdi MH, et al. The potential role of BMI, plasma leptin, nesfatin-1 and ghrelin levels in the early detection of pancreatic necrosis and severe acute pancreatitis: A prospective cohort study. *Int J Surg*. 2014;12(12):1310–1313. doi:10.1016/j.ijsu.2014.10.040

Bone marrow mesenchymal stem cell-derived exosomes attenuate the maturation of dendritic cells and reduce the rejection of allogeneic transplantation

Hongxun Sang^{1,A}, Renli Zhao^{2,B}, Guohua Lai^{2,3,B,C}, Zhiwei Deng^{4,B,C}, Weida Zhuang^{1,C,E}, Mingjie Wu^{3,C,E}, Jiachang Wu^{1,A,E}

¹ Department of Orthopedic Surgery, Shenzhen Hospital of Southern Medical University, China

² The Third School of Clinical Medicine, Southern Medical University, Guangzhou, China

³ Department of Orthopedic Surgery, Shenzhen Hospital of Southern Medical University, China

⁴ Division of Spine Surgery, Section II, Department of Orthopedics, The Third Affiliated Hospital of Southern Medical University, Guangdong Provincial Key Laboratory of Bone and Joint Degeneration Diseases, Southern Medical University, Academy of Orthopedics of Guangdong Province, Guangzhou, China

A – research concept and design; B – collection and/or assembly of data; C – data analysis and interpretation;

D – writing the article; E – critical revision of the article; F – final approval of the article

Advances in Clinical and Experimental Medicine, ISSN 1899–5276 (print), ISSN 2451–2680 (online)

Adv Clin Exp Med. 2023;32(5):551–561

Address for correspondence

Hongxun Sang

E-mail: hxsang@smu.edu.cn

Funding sources

This work was supported by National Natural Science Foundation of China (grant No. 81871767), Sanming Project of Medicine in Shenzhen (grant No. SZSM201612019), Shenzhen Key Laboratory of Digital Surgical Printing Project (grant No. ZDSYS201707311542415), Southern Medical University Clinical Project (grant No. LC2016ZD036), Shenzhen Fundamental Research Key Project (grant No. JCYJ20200109150641992), and the Key-Area Research and Development Program of Guangdong Province, China (grant No. 2020B010165004). The funder had the following involvement with the study: study design, collection, analysis, and interpretation of data, writing the paper and decision to submit it for publication.

Conflict of interest

None declared

Received on May 27, 2022

Reviewed on July 30, 2022

Accepted on November 17, 2022

Published online on March 7, 2023

DOI

10.17219/acem/156643

Copyright

Copyright by Author(s)

This is an article distributed under the terms of the Creative Commons Attribution 3.0 Unported (CC BY 3.0) (<https://creativecommons.org/licenses/by/3.0/>)

Abstract

Background. Bone mesenchymal stem cell (BMSC)-derived exosomes (B-exos) are attractive for applications in enabling alloantigen tolerance. An in-depth mechanistic understanding of the interaction between B-exos and dendritic cells (DCs) could lead to novel cell-based therapies for allogeneic transplantation.

Objectives. To examine whether B-exos exert immunomodulatory effects on DC function and maturation.

Materials and methods. After mixed culture of BMSCs and DCs for 48 h, DCs from the upper layer were collected to analyze the expression levels of surface markers and mRNAs of inflammation-related cytokines. Then, before being collected to detect the mRNA and protein expression levels of indoleamine 2,3-dioxygenase (IDO), the DCs were co-cultured with B-exos. Then, the treated DCs from different groups were co-cultured with naive CD4⁺ T cells from the mouse spleen. The proliferation of CD4⁺ T cells and the proportion of CD4⁺CD25⁺Foxp3⁺ T cells were analyzed. Finally, the skins of BALB/c mice were transplanted to the back of C57 mice in order to establish a mouse allogeneic skin transplantation model.

Results. The co-culture of DCs with BMSCs downregulated the expression of the major histocompatibility complex class II (MHC-II) and CD80/86 costimulatory molecules on DCs. Moreover, B-exos increased the expression of IDO in DCs treated with lipopolysaccharide (LPS). The proliferation of CD4⁺CD25⁺Foxp3⁺ T cells increased when cultured with B-exos-exposed DCs. Finally, mice recipients injected with B-exos-treated DCs had significantly prolonged survival after receiving the skin allograft.

Conclusions. Taken together, these data suggest that the B-exos suppress the maturation of DCs and increase the expression of IDO, which might shed light on the role of B-exos in inducing alloantigen tolerance.

Key words: exosomes, tolerance, bone marrow mesenchymal stem cell

Cite as

Sang H, Zhao R, Lai G, et al. Bone marrow mesenchymal stem cell-derived exosomes attenuate the maturation of dendritic cells and reduce the rejection of allogeneic transplantation. *Adv Clin Exp Med.* 2023;32(5):551–561. doi:10.17219/acem/156643

Background

Bone mesenchymal stem cells (BMSCs) have multipotent abilities – they can form bone, adipose and other mesenchymal tissues.¹ In addition to these differentiation capabilities, BMSCs possess immunomodulatory properties, including the ability to modulate immune cells, such as T cells, B cells, macrophages, and dendritic cells (DCs) in a non-major histocompatibility complex (MHC)-restricted manner.^{2–4} Several studies indicated that the immunosuppressive effect of MSCs occurs through paracrine or cell-to-cell contact mechanisms.⁵

Exosomes (exos) are small membrane vesicles, of 40–150 nm, released into the extracellular medium upon fusion of late multivesicular endosomes with the plasma cell membrane.⁶ Accumulating evidence has suggested that compared to BMSCs, exosomes have a stable biological activity and a low risk of immunological rejection.⁷

Dendritic cells are the most potent antigen-presenting cells (APCs) that play a prominent role in the development of T cell immune responses.^{8,9} In contrast to the ability of mature DCs (mDCs) to stimulate immunity, tolerogenic DCs (tolDCs) are involved in the maintenance of immunological tolerance via T cell unresponsiveness and generation of regulatory T (Treg) cells.¹⁰ Another study showed that MSC-exos induced immature DC (imDC) and mDC differentiation into tolDCs with low expression levels of costimulatory markers *in vitro*.¹¹ However, the mechanism underlying B-exos to induce tolDCs remains unknown. Additionally, whether B-exos from the recipient can drive DC differentiation into tolDCs and induce transplant immunotolerance is not yet clarified.

Therefore, we investigated whether B-exos exert immunomodulatory effects on DC maturation and function by examining the phenotypic and functional features of B-exos-exposed DCs in comparison to their untreated counterparts. We also established an allogeneic skin transplant mice model to elucidate the mechanism underlying B-exos-mediated immunomodulation.

Objectives

This study aimed to examine whether B-exos exert immunomodulatory effects on DC maturation and function.

Materials and methods

Animals

Five-week-old C57BL/6 and BALB/c mice (Animal Center of Southern Medical University, Guangzhou, China), weighing 25–30 g, were used as experimental animals. All animal experiments conducted in this study were approved by the Institutional Animal Use Committee

of Shenzhen Hospital, Southern Medical University, Guangzhou, China (approval No. 2021-0057), and performed according to the guidelines of the Care and Use of Laboratory Animals (Ministry of Health of the People's Republic of China, 1998).

Isolation and culture of BMSCs

The BMSCs were isolated from hind limb bones of 5-week-old C57 mice as described previously,¹² and cultured in minimum essential medium (MEM)-alpha growth medium containing 10% fetal bovine serum (FBS; Gibco, Thermo Fisher Scientific, Waltham, USA) and $\times 100$ penicillin and streptomycin solution (Gibco). The cells were passaged for 3–5 passages (P3–5) using 0.25% trypsin (Gibco) at 78–80% confluency, and used to collect exosomes.

Bovine extracellular vesicle (EV)-depleted medium was obtained by overnight ultracentrifugation of medium supplemented with 20% FBS at $100,000 \times g$ at 4°C for 8 h to eliminate the interference of exosomes from FBS.¹³ For exosome isolation, P3–5 BMSCs were washed twice with particle-free Dulbecco's phosphate-buffered saline (DPBS; Sigma-Aldrich, St. Louis, USA) and incubated with fresh medium for continuous culture for 48 h. Subsequently, the culture medium was collected for exosome isolation.

Characterization of BMSCs

Briefly, 10^6 BMSCs were seeded as a monolayer in 6-well plates. The OriCell™ C57 mouse BMSC adipogenic, osteogenic and chondrogenic differentiation kits (catalogs no. MUBMX-90031, MUBMX-90021 and MUBMX-9004, respectively) were used according to the manufacturer's instructions (Cyagen Biosciences Inc., Guangzhou, China). When the adipogenic, osteogenic and chondrogenic differentiation processes were completed, the cells were fixed with 4% paraformaldehyde for 30 min, stained with Oil Red O working solution, alizarin red and Alcian blue (Cyagen Biosciences), respectively, and rinsed with PBS.

Cultivation of BMDCs

Bone marrow-derived dendritic cells (BMDCs) were differentiated from bone marrow as described previously.¹⁴ Briefly, bone marrow cells were flushed from the femurs and tibias of 5-week-old C57 mice and cultured in complete RPMI 1640 medium containing 10% heat-inactivated FBS, 20 ng/mL recombinant mouse granulocyte-macrophage colony-stimulating factor (GM-CSF) (CK02; Novoprotein, Guangzhou, China) and 10 ng/mL recombinant mouse interleukin (IL)-4 (CK74; Novoprotein). The remaining clusters, loosely adherent to the Petri dish, were cultured at 37°C with 5% CO₂, and the medium was changed every other day. On day 7, the cells were collected and treated with different protocols, depending on the subsequent planned experiments.

Exosome isolation and analysis

Exosomes were obtained from the supernatant of BMSCs by differential ultracentrifugation, as described previously.¹³ Briefly, the pellet was obtained by centrifugation of the culture medium at $300 \times g$ at 4°C for 10 min. The supernatant was clarified as follows: $2000 \times g$ for 20 min, $10,000 \times g$ for 40 min, and finally $100,000 \times g$ at 4°C for 90 min before the resuspension in 50–100 μL of sterile DPBS.

The ultrastructure and size distribution of exosomes were analyzed with transmission electron microscopy (TEM; Hitachi Ltd., Tokyo, Japan) and Nanosight NS300 (Malvern Panalytical, Malvern, UK). Briefly, the exosome samples were fixed with 1% glutaraldehyde in PBS at room temperature for 5 min. The mixture was then spotted onto 300-mesh carbon/formvar-coated grids, dried at room temperature, washed with DPBS, and stained for contrast using uranyl acetate (50%) in water at room temperature for 10 min. Then, the exosome size and morphology were observed using a JEM-1011 electron microscope ($\times 25,000$ magnification; JEOL Ltd., Tokyo, Japan).

Cellular uptake of exosomes

The concentration of exosomes was determined using the FD™ BCA Protein Quantitative Kit (FDbio Science, Hangzhou, China). Exosomes were labeled with PKH26 using a membrane labeling kit (Sigma-Aldrich) according to the manufacturer's instruction. Briefly, PKH26 dye was diluted, added to the 10 μg of exosomes in 20- μL DPBS, and then incubated for 5 min after mixing by gentle pipetting. The excess dye was bound with 100 μL of 10% exosome-depleted FBS in RPMI 1640 medium. The exosomes were then diluted to 12 mL with DPBS and pelleted by ultracentrifugation at $100,000 \times g$ at 4°C for 1 h 10 min. The pellet was resuspended in 50 μL DPBS. The imDCs were incubated with 5 $\mu\text{g}/\text{mL}$ of PKH26-labeled exosomes for 12 h and stained with 3,3'-diiodoacetylcarboxyanine perchlorate (DiO; C1993S; Beyotime, Guangzhou, China) and 4',6-diamidino-2-phenylindole (DAPI, C1005; Beyotime) before being observed with a Benchtop High-Content Analysis System (CQ1; Yokogawa, Musashino, Japan).

Flow cytometry analysis

The P3 BMSCs were digested with 0.25% trypsin-EDTA and suspended to a concentration of 1×10^6 cells/mL in cell staining buffer (#156603; BioLegend, San Diego, USA). Next, the cell suspension was stained with antibodies from BioLegend against CD29-PE (#102207), CD44-PE (#103023), Sca-1-PE (#108107), CD11b-PE (#101207), CD45-PE (#157603), and CD19-PE (#152407) in the dark at 4°C for 45 min.

The imDCs were cultivated in six-well plates at 5×10^6 cells/well. Dendritic cells were left untreated (as a control)

or stimulated with 1 mg/mL lipopolysaccharide (LPS), 5 $\mu\text{g}/\text{mL}$ of BMSC-exos, or 1 mM 1-methyl-L-tryptophan (1MT; Sigma-Aldrich) for 48 h. Dendritic cells treated with LPS for 48 h and harvested at day 7 will represent mDC. Dendritic cells in different groups were then incubated with the following anti-mouse antibodies (BioLegend): fluorescein isothiocyanate (FITC)-conjugated anti-CD11c (#117305), phycoerythrin (PE)-conjugated anti-CD80 (#104707), -CD86 (#159203), and -MHC II (#116407). Subsequently, the cells were stained and observed using a Fortessa flow cytometer (BD Biosciences, Franklin Lakes, USA). Data were analyzed with FlowJo v. 10 software (FlowJo, LLC, Ashland, USA).

Intracellular staining was performed with a Foxp3/Transcription Factor Staining Buffer Set (KTR201-100; Liankebio, Hangzhou, China). Tregs were stained with FITC-conjugated anti-mouse CD4 (GK1.5), APC-conjugated anti-mouse CD25 (PC61.5), and PE-conjugated anti-mouse Foxp3 Ab (3G3) monoclonal antibodies (mAbs). The populations of Tregs in the co-cultured cell samples were defined as $\text{CD4}^+\text{CD25}^+\text{Foxp3}^+$.

Co-culture of BMSCs and DCs in a transwell system

Bone mesenchymal stem cells were cultured in complete medium in the lower well of transwell chambers (pore size: 0.4 μm ; Corning Costar; Corning, Corning, USA) to 80% confluency. Then, the medium was replaced with a complete RPMI 1640 medium containing 10% exosome-depleted FBS. For inhibition of exosome generation, BMSCs were incubated with 20 μM GW4869¹⁵ (Sigma-Aldrich) for 24 h, and the medium was replaced with RPMI 1640 containing 10% exosome-depleted FBS before co-culture. Subsequently, BMSCs were cultured in the lower compartment, while DCs were cultured in the upper compartment to avoid cell-to-cell contact. Dendritic cells were harvested for further experiments after co-culturing in the transwell system for 48 h.

Western blot

Proteins were extracted from the isolated exosomes or DCs from differentially treated groups using the Whole Cell Lysis Assay (KeyGen Biotech, Nanjing, China), and the concentration was determined using the BCA Protein Assay Kit (FD2001; Fude, Hangzhou, China). The lysates were resolved using 10% sodium dodecyl-sulfate polyacrylamide gel electrophoresis (SDS-PAGE), and the separated proteins were transferred to polyvinylidene fluoride (PVDF) membranes (EMD Millipore, Burlington, USA).

After blocking with 5% skimmed milk in Tris-buffered saline with Tween (TBST) buffer at room temperature for 1 h, the membranes were probed with the following primary antibodies at 4°C overnight (Abcam, Cambridge, UK): TSG101 (1:1000, ab125011), CD81 (1:1000, ab109201),

CD9 (1:2000, ab92726), CD63 (1:1000, ab217345), and indoleamine 2,3-dioxygenase (IDO) (1:1000, ab277522). Subsequently, the membranes were incubated with horseradish peroxidase (HRP)-coupled goat anti-rabbit IgG H&L (1:10,000, ab205718; Abcam) and developed using BeyoECL Star (Beyotime). The intensity of the immunoreactive bands was analyzed using the ChemiDoc Imaging System (Bio-Rad, Hercules, USA).

Co-culture of DCs and naïve CD4⁺ T cells for differentiation of Tregs

Naïve CD4⁺ T cells were purified from pooled single-cell suspensions of C57 spleen using a mouse naïve CD4⁺ T cell isolation kit (#480039; BioLegend). These purified naïve CD4⁺ T cells were co-cultured with DCs from differentially treated groups at an optimal ratio described previously.¹⁶ Then, 1MT, a selective IDO inhibitor, was added to the medium in the 1MT group before co-culture. The cells (T cell 10⁶ and DCs 2×10⁵) were cultured in 24-well plates with a total volume of 1 mL/well of culture medium. The medium was refreshed on days 3 and 5, and the cells were harvested for flow cytometry analysis on day 5.

Real-time quantitative polymerase chain reaction

Total RNA was isolated from DCs in different groups using TRIzol® (Thermo Fisher Scientific), following the manufacturer's protocols. The RNA quantity and quality were measured on a NanoDrop ND-1000 spectrophotometer (NanoDrop Technologies; Thermo Fisher Scientific). An equivalent of 1 µg RNA was reverse-transcribed using a reverse transcription kit (TransGen Biotech Co., Ltd., Beijing, China). Reverse transcription quantitative real-time polymerase chain reaction (RT-qPCR) was performed using a PerfectStart Green qPCR SuperMix kit (TransGen Biotech Co., Ltd.) on an ABI-7500 machine (Applied Biosystems; Thermo Fisher Scientific). The primer pairs are listed in Table 1. The data were analyzed using SDS relative quantification software (v. 2.2.2; Thermo Fisher Scientific). The relative fold change was calculated using the 2^{-ΔΔCt} method.¹⁷ All reactions were performed in triplicate and normalized to the expression of the internal control *Actin*.

Allogenic skin transplant

Full-thickness skin transplantation in mice was performed as described previously.¹⁸ Briefly, the donor mouse (BALB/c) was anesthetized, and the back skin from the hip to the neck was harvested and cut into 15-mm × 15-mm grafts. For the recipient (C57BL/6), 5×10⁶ DCs were given via the tail vein on postoperative day (POD) 0. The recipients in the positive group were given the same amount of PBS via the tail vein on POD0. Ten recipients were randomly assigned to each group. A 10-mm × 10-mm to 15-mm × 15-mm square of skin

Table 1. Primer pairs of genes

Gene	Sequence
<i>TGF-β</i> F	TGTCACAACCTCAGCCAACAGG
<i>TGF-β</i> R	CAACCAGCCTCCTAAACACCC
<i>IL-10</i> F	CAGAGCCACATGCTCCTAGA
<i>IL-10</i> R	TGTCCAGCTGGTCTTTGTT
<i>IL-12b</i> F	GACTCCAGGGGACAGGCTA
<i>IL-12b</i> R	CCAGGAGATGGTTAGCTTCTGA
<i>IL-6</i> F	GCTACCAAACCTGGATATAATCAGGA
<i>IL-6</i> R	CCAGGTAGCTATGGTACTCCAGAA
<i>IL-27</i> F	GCAGGGAATTCACAGTCAGC
<i>IL-27</i> R	GGACATAGCCCTGAACCTCA
<i>IDO1</i> F	GGGCTTTGCTCTACCACATC
<i>IDO1</i> R	AAGGACCCAGGGGCTGTAT
<i>Actin</i> F	GGCTGTATTCCCTCCATCG
<i>Actin</i> R	CCAGTTGGTAACAATGCCATG

was cut superficially after anesthesia. The graft from the donor was positioned on the graft bed, and 8 sutures were placed on the corners and the middle of each edge. Finally, the recipient mouse was wrapped in an adhesive bandage with a folded gauze over the graft. Signs of rejection were monitored daily. On POD12, skin and spleen samples were harvested for the analysis.

Histopathology

On POD12, skin samples were collected and animals were euthanized by CO₂ inhalation. The samples were fixed in 10% neutral-buffered formalin, processed in graded alcohols, sectioned into 5-µm-thick slices, and stained with hematoxylin and eosin (H&E). All slides were reviewed by an expert veterinary pathologist in a blinded manner.

Statistical analyses

The data are expressed as the means with 95% confidence interval (95% CI). Normal data distribution within the compared groups was verified with the use of the Shapiro–Wilk test, and the homogeneity of variance among the groups was evaluated with the use of the Levene's test. These results were provided in Supplementary Table 1 (<https://doi.org/10.5281/zenodo.7664412>) Three independent experiments were performed for validity, and at least 3 samples per test were taken for statistical analysis. Statistical analyses were performed using a one-way analysis of variance (ANOVA) combined with the least significant difference (LSD) test. Graft survival was compared through Kaplan–Meier analysis and the log-rank test. The value of *p* < 0.05 indicated statistical significance. Data were analyzed using GraphPad Prism v. 8 software (GraphPad Software Inc., San Diego, USA) and IBM SPSS v. 23.0 software (IBM Corp., Armonk, USA).

Results

Identification of BMSCs and B-exos

Bone mesenchymal stem cells from C57 mice could be induced towards osteogenic and lipogenic differentiation (Fig. 1A–C). The results of flow cytometry verified that the cells used in our experiment expressed identical BMSC markers in line with the definition of BMSCs (Fig. 1D).¹¹

Then, exosomes were isolated from the supernatant of P3–5 BMSCs according to the protocol presented in Fig. 2. The TEM, nanoparticle tracking analysis (NTA) and western blot analysis were used to analyze the ultrastructure, size distribution and specific protein, respectively. The results showed that the exosome size was about 89 nm (Fig. 3A), and the characteristic saucer shape was revealed with TEM (Fig. 3B). Additionally, the expression levels of CD63, CD9, CD81, and TSG101 were more abundant in the exosome protein lysate compared

to their parental cell protein lysate (Fig. 3C). These findings indicated the successful isolation of BMSCs and exosomes.

Exosome uptake and the effects on attenuation of DC maturation

To assess whether B-exos interact directly with DCs from C57 mice, imDCs differentiated from bone marrow were incubated with PKH26-labeled exosomes and monitored with fluorescence microscopy imaging for over 12 h. We observed that the cells endocytosed the exosomes and became fluorescent at 12 h (Fig. 4A). These findings implied that B-exos have the potential to communicate directly with allogenic imDCs.

Next, we investigated whether B-exos affect the phenotype and function of mDCs through an indirect contact with BMSCs in vitro in transwell chambers (Fig. 4B). The median fluorescence intensity (MFI) shift showed

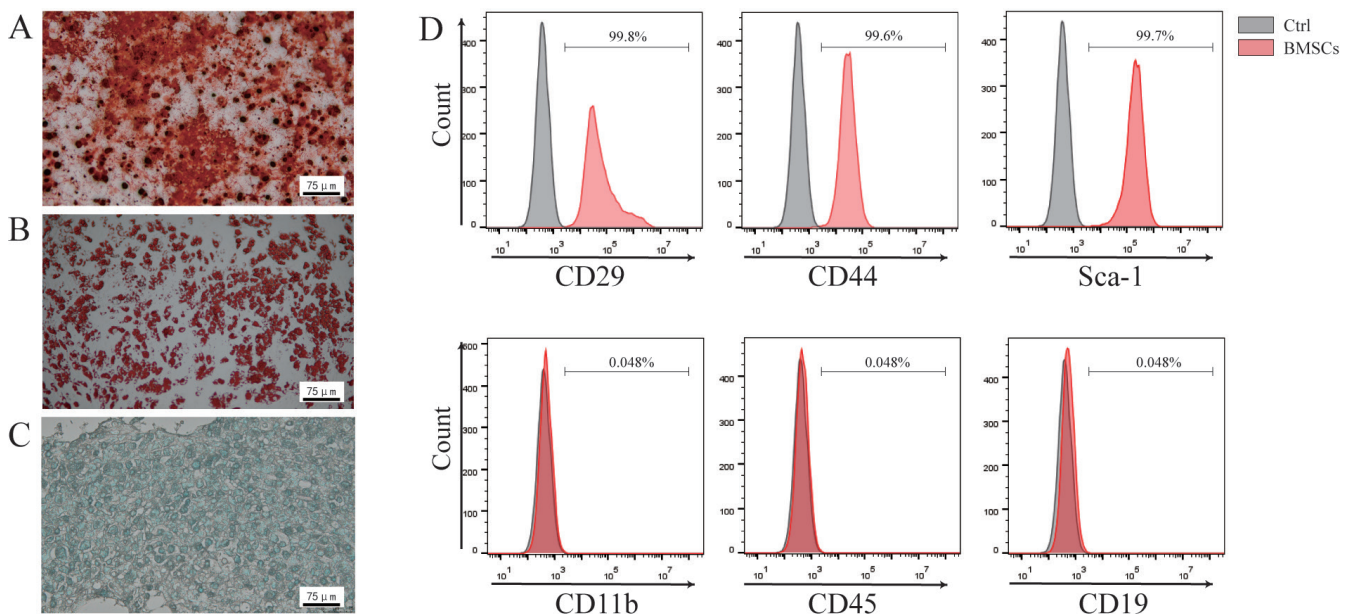


Fig. 1. Results of bone mesenchymal stem cell (BMSC) identification. A. After 28 days from osteogenic induction, calcium nodules could be seen under a microscope (×400 magnification); B. Red lipid droplets could be seen under a microscope (×400 magnification); C. Blue endoacidic mucopolysaccharides could be seen under a microscope (×400 magnification); D. Flow cytometry results showed that CD29, CD44 and Sca-1 were expressed on the surface of BMSCs, but CD11b, CD45 and CD19 were not

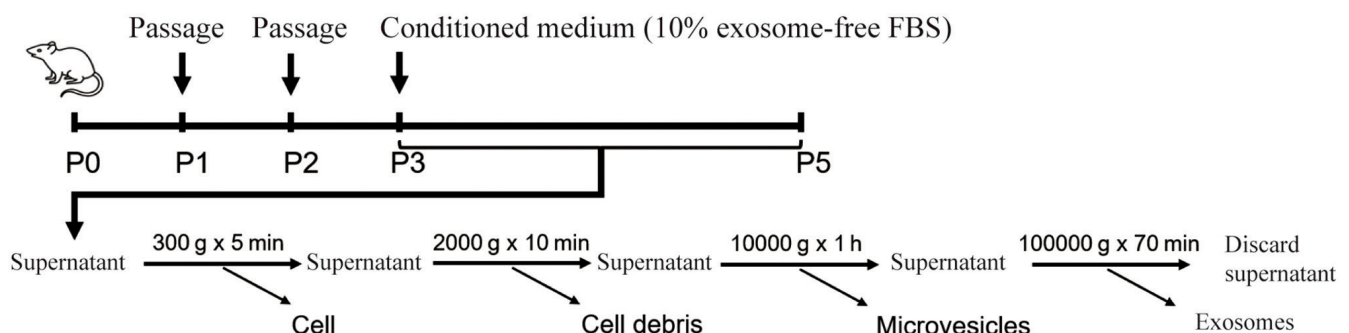


Fig. 2. Flow chart of bone mesenchymal stem cell (BMSC) culture and separation and purification of BMSC-derived exosomes (B-exos)

FBS – fetal bovine serum.

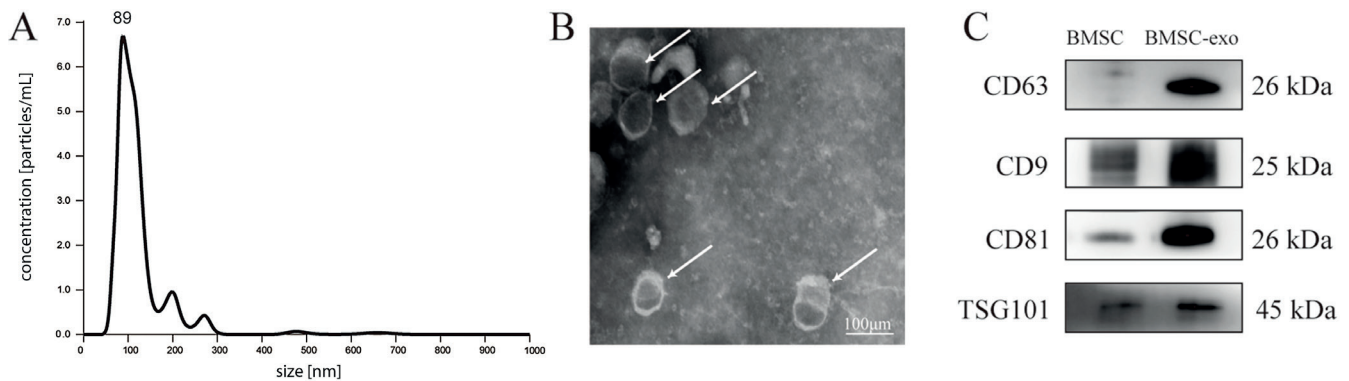


Fig. 3. Identification of bone mesenchymal stem cell (BMSC)-derived exosomes. A. Nanoparticle Tracking Analysis demonstrated that the BMSC-derived exosome (B-exo) had a mean particle diameter of 89 nm; B. Transmission electron microscopy (TEM) results revealed the characteristic saucer shape of exosomes (white arrows); C. CD9, CD63, CD81, and TSG101 were more abundant in the exosome protein lysis compared with BMSC protein lysis (a total of 5 μ g protein from BMSC lysis and 5 μ g protein from exosome lysis were tested)

a significant decrease in MHCII, CD86 and CD80 in DCs co-cultured with BMSCs compared to that of mDCs; however, these effects were attenuated when BMSCs were treated with GW4869, the exosome inhibitor (Fig. 4C,D).

Then, we performed RT-qPCR-based immune profiling of DCs from different groups. The BMSC-exposed DCs showed significantly increased transcripts of several immune-modulatory genes, including *IL-10*, *IL-12* and *TGF- β* , whereas transcripts of *IL-27* and *IL-6* were decreased compared to mDCs. However, these phenomena were attenuated after the treatment with GW4869 (Fig. 5).

IDO expression is increased during B-exos-induced differentiation of dendritic cells

Since BMSC-exposed mDCs increased the expression of IDO, we investigated the involvement of IDO in the induction of tolDCs by BMSC-exos. The exosomes were purified from BMSC supernatants and co-incubated with imDCs treated with or without LPS (5 μ g/mL) for 48 h. Then, we analyzed the effects of different doses (1, 2, 5, 8, or 10 μ g/mL) of BMSC-exos. Surprisingly, we found that the expression levels of IDO in mDCs were increased in 2- and 5- μ g/mL groups compared to the mDCs group, and the highest expression was obtained in the 5- μ g/mL group (Fig. 6A,B), considering it the optimal dosage for increasing IDO expression.

Effect of IDO on B-exos-exposed DCs

We also investigated if B-exos-treated DCs could induce Treg polarization. Naïve CD4⁺ T cells (1×10^6 /well) were isolated from the spleen and incubated with DCs (2.5×10^5 /well) in different groups for 5 days. As shown in Fig. 6C,D, the proportion of CD4⁺CD25⁺Foxp3⁺ T cells decreased in mDCs and 1MT-treated mDCs, but increased in B-exos-exposed DCs. These findings demonstrated that B-exos-exposed DCs induced Tregs by increasing the expression of IDO.

B-exos-exposed DCs enhanced allogeneic skin graft

Based on the enhancement of Treg polarization by B-exos-exposed DCs, we hypothesized that they could delay the allogeneic skin graft rejection with a concomitant increase in Tregs in the recipient mice. The back skins from BALB/c mice were grafted on BALB/c recipients and followed by caudal vein injections of 5×10^5 DCs per mouse on POD0 (Fig. 7A).

Recipient mice injected with DCs and DCs in the 1MT group rejected allograft skins (median survival time (MST): 14 days and 13 days, respectively; Fig. 7B), whereas those injected with B-exos-exposed DCs had significantly prolonged allograft survival (MST: 18 days). Therefore, the DCs in B-exos group significantly improved skin allograft survival.

Histological examination of skin allografts showed slight cell infiltration and preserved graft structure in transplant recipients injected with B-exos-exposed DCs on POD12. However, allografts from recipients injected with mDCs and DCs in the 1MT group showed severe myocyte damage and moderate inflammatory infiltration (Fig. 7C).

B-exos-exposed DCs induced the proliferation of recipient spleen CD4⁺CD25⁺Foxp3⁺ T cells

To determine if the delayed graft rejection was due to increased Treg polarization, the spleens of the mice from different groups were harvested on day 12 and assayed for Tregs. The level of CD4⁺CD25⁺Foxp3⁺ T cells was significantly higher in B-exos-exposed DC recipient animals compared to that of mDCs and DCs in the 1MT group (Fig. 8A,B).

Discussion

Due to their potential applications in enabling alloantigen tolerance, MSCs have been investigated thoroughly and found to exert an immunomodulatory effect that

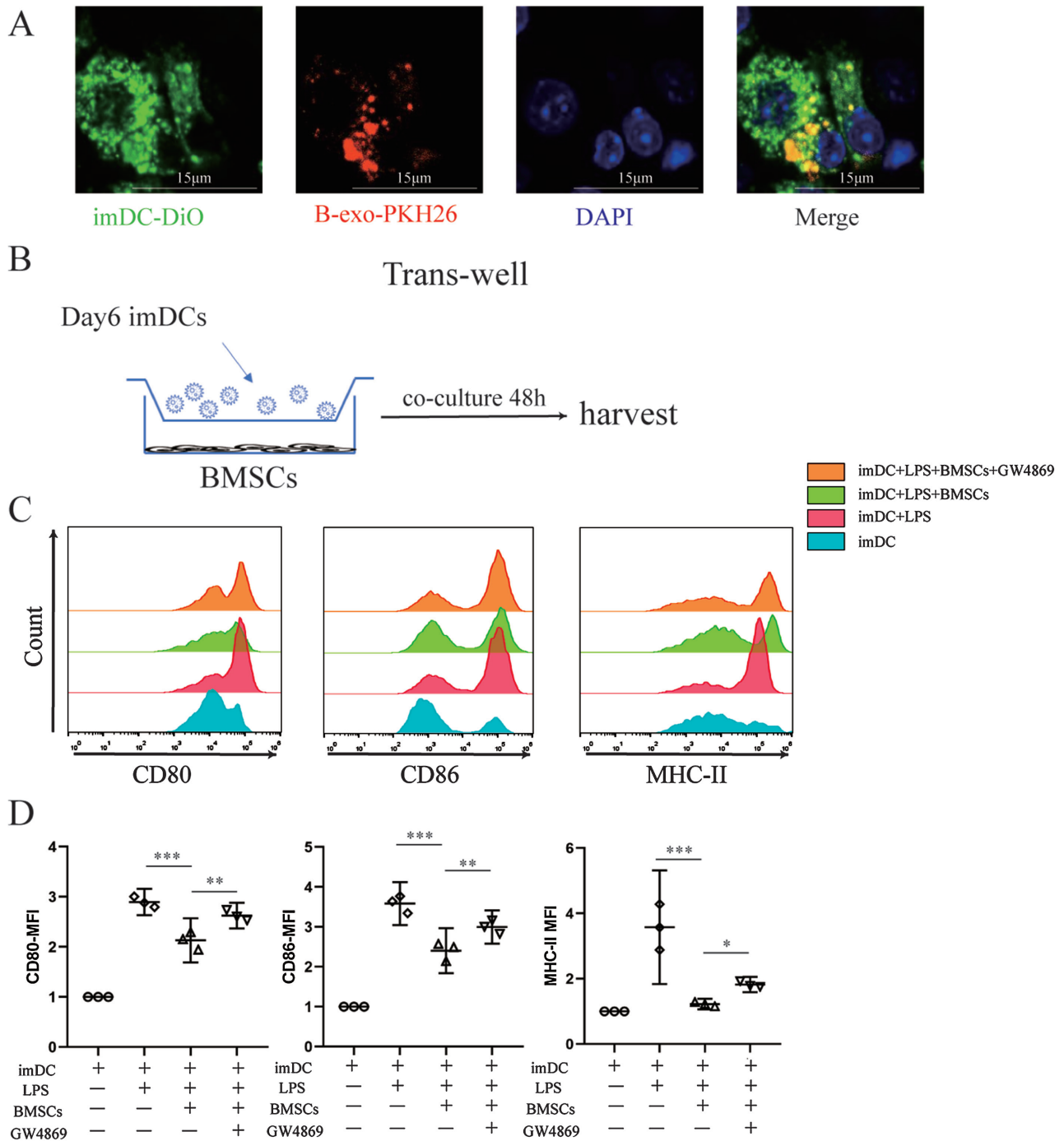


Fig. 4. Exosome uptake and effects on expression of surface markers of dendritic cells (DCs). **A.** Dendritic cell uptake assay observed with confocal microscopy demonstrated rapid uptake of bone mesenchymal stem cell (BMSC)-derived exosome (B-exo) (green: immature DC (imDC) membrane-DiO; red: exosome-PKH26; blue: cell nucleus-4',6-diamidino-2-phenylindole (DAPI)); **B.** Flow chart of transwell co-culture system; **C.** Representative histogram shows the expression of CD80, CD86 and major histocompatibility complex class II (MHC-II); **D.** Bar graphs represent the median fluorescence intensity (MFI) fold change of CD80, CD86 and MHC-II. The data are expressed as the means with 95% confidence interval (95% CI), n = 3

*p < 0.05; **p < 0.01; ***p < 0.001; LPS – lipopolysaccharide.

influences all cells involved in the immune response.¹⁹ Moreover, the paracrine effect is one of the critical mechanisms underlying immune tolerance.²⁰ As a tool of cell-to-cell communication, exosomes transfer biological material between the cells and regulate physiological and pathological conditions.¹⁹ Several studies have

shown that MSC-derived exosomes can affect the activity of immune cells. A recent study by Zhang et al.²¹ showed that MSC exosomes mediated cartilage repair enhancing proliferation, attenuating apoptosis and modulating immune reactivity by inducing M2 macrophages and reducing pro-inflammatory synovial cytokines. It indicated

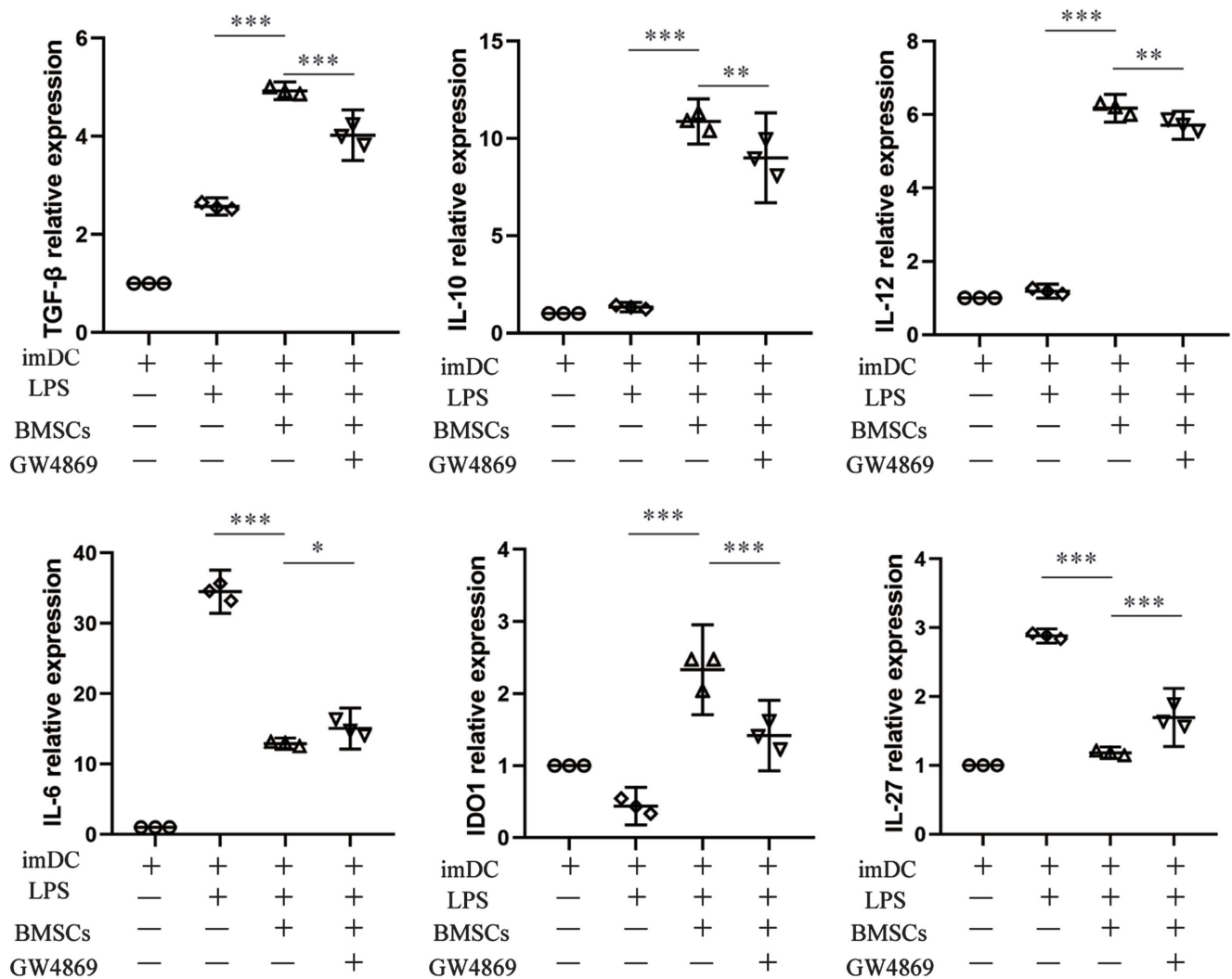


Fig. 5. Quantitative reverse transcription polymerase chain reaction (RT-qPCR) analysis conducted 48 h after co-culture showed the expression levels of cytokines associated with immune activity (immunoglobulin (IL)-6 and IL-27) and immune regulation (transforming growth factor beta (TGF- β), IL-10, IL-12, and of indoleamine 2,3-dioxygenase (IDO)). The data are expressed as the means with 95% confidence interval (95% CI), $n = 3$

imDC – immature dendritic cell; LPS – lipopolysaccharide; BMSCs – bone mesenchymal stem cells; * $p < 0.05$; ** $p < 0.01$; *** $p < 0.001$.

that the regenerative and immunomodulatory properties of MSCs were inherited by MSC-exos; which are convenient and recommended for alternative treatments.²² Taking together the results from rescue experiments, we concluded that BMSC-exos, as a form of remote secretion by BMSCs, attenuate the maturation and activation of DCs and induce mDCs into tolDCs.

Dendritic cells are essential in directing immune responses toward either immunity or tolerance.²³ Tolerogenic DCs are a subset of DCs that can induce tolerance through various mechanisms, including the induction of Tregs, and could be used in tolerizing immunotherapies.²⁴ Phase I and II clinical trials utilizing tolDCs have been conducted for kidney and liver transplant recipients.²⁵ A key mechanism involved in tolDC-mediated immunosuppression is the expression of IDO-1.²⁶ In addition to suppression of proliferation, IDO competence in human DCs is shown to support T cell regulatory function.^{27,28} The current data suggest that when exposed

to BMSC-exos, the proportion of CD4⁺CD25⁺Foxp3⁺ T cells was increased in the BMSC-exos-exposed DC group compared to those in the non-exposed DC group. Collectively, BMSC-exos enhanced the ability of DCs to induce Tregs via elevated expression of IDO. These results confirmed the findings of a previous study, wherein MSC exosomes required monocytes to mediate the differentiation of CD4⁺ T cells to Tregs.²⁹

Presently, the clinical application of MSCs to improve the prognosis of transplant recipients has broad prospects. Although MSC-derived exosomes have functions similar to MSCs, their direct application is not yet clear. Thus, in the present study, DCs were chosen as recipient cells to modulate allograft tolerance. The regulatory DCs promote liver transplant operational tolerance and are used in cell therapy for many autoimmune diseases.^{30,31} However, our cell injection strategy could not achieve long-term transplant survival. Notably, it is difficult to achieve tolerance or long-term survival without the use

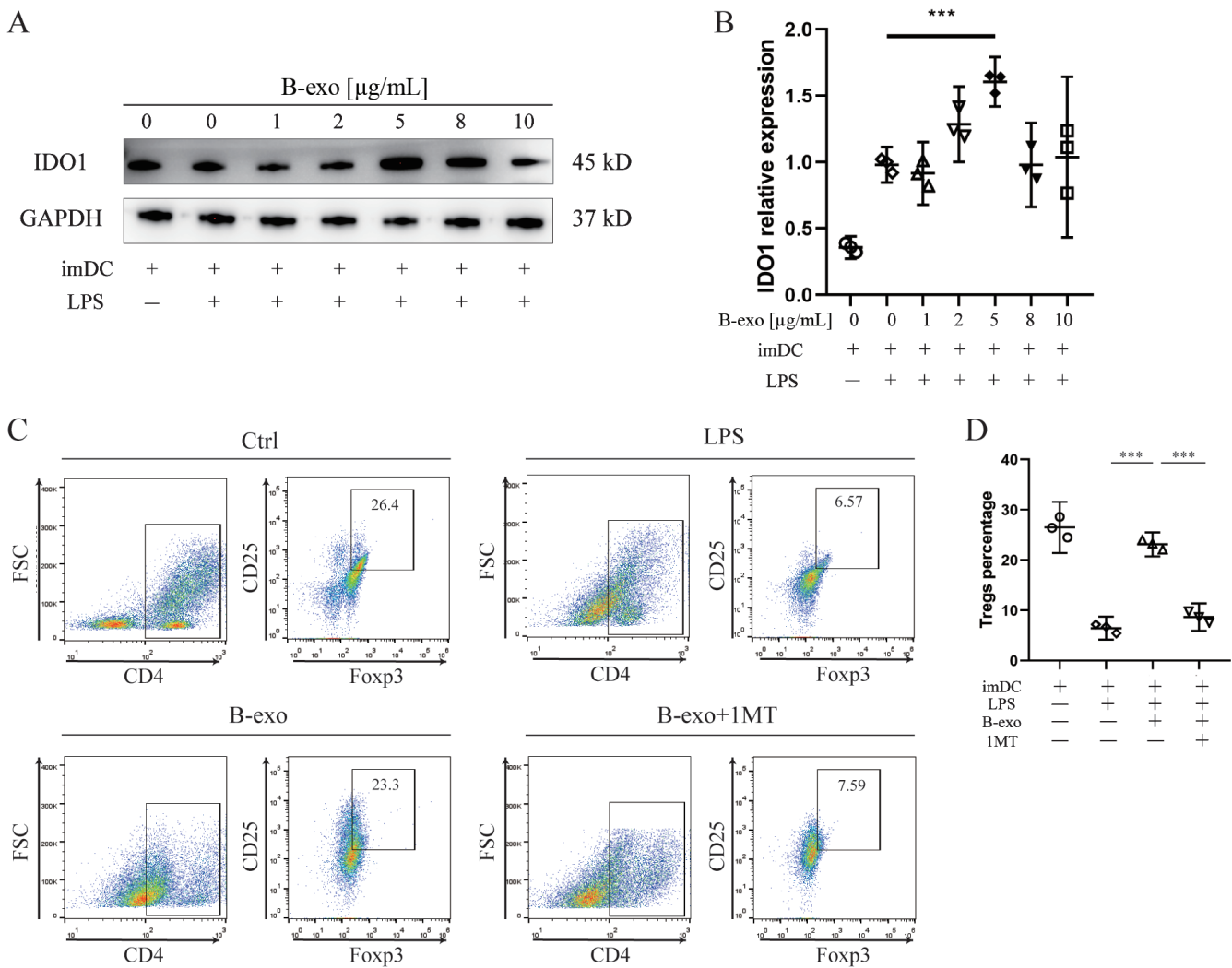


Fig. 6. Effect of of indoleamine 2,3-dioxygenase (IDO) on bone mesenchymal stem cell (BMSC)-derived exosome (B-exo)-exposed dendritic cells (DCs). A. The protein levels of IDO in DCs were changed by the exposure with B-exo in different concentrations; B. The gene expression levels of IDO in DCs were changed by the exposure with B-exo in different concentrations (n = 3); C. The percentage of CD4⁺Foxp3⁺ T cells was analyzed with flow cytometry after naïve CD4⁺ T was co-cultured with DCs; D. Cumulative data showed the percentage of CD4⁺Foxp3⁺ T cells. The data are expressed as the means with 95% confidence interval (95% CI), n = 3

GAPDH – glyceraldehyde 3-phosphate dehydrogenase; imDC – immature dendritic cell; LPS – lipopolysaccharide; 1MT – 1 mM 1-methyl-L-tryptophan. *p < 0.05; **p < 0.01; ***p < 0.001.

of immunosuppressants.¹⁹ Tolerogenic DCs combined with suboptimal doses of immunosuppressants may achieve specific allograft tolerance and long-term transplant survival.³²

Limitations

The present study showed that B-exos induce tolDCs and increase the expression of IDO, but the exact protein or non-coding RNA constituent that promotes this effect is yet to be identified. As a cargo for cell-to-cell communication, the bioactive molecules transferred by BMSC-exos to DCs are the key factors for future studies. The critical factors involved in the induction of tolDCs may be illustrated by RNA sequencing and proteomic analysis along with CRISPR/Cas9 deletion screening or antibody-blocking

studies. Besides, a small number of replications is a limitation of this study. In the following experiments, the sample size should be expanded to be able to verify reliably both the normal data distribution and homogeneity of variance. Multiple injection strategy of tolDCs combined with suboptimal doses of immunosuppressants might achieve specific allograft tolerance and long-term transplant survival.

Conclusions

The present study showed that B-exos induce mDCs into a tolDC population with low expression of costimulatory markers and higher IDO expression. In the in vivo study, allograft tolerance is induced by B-exos-exposed DCs with prolonged skin allograft survival.

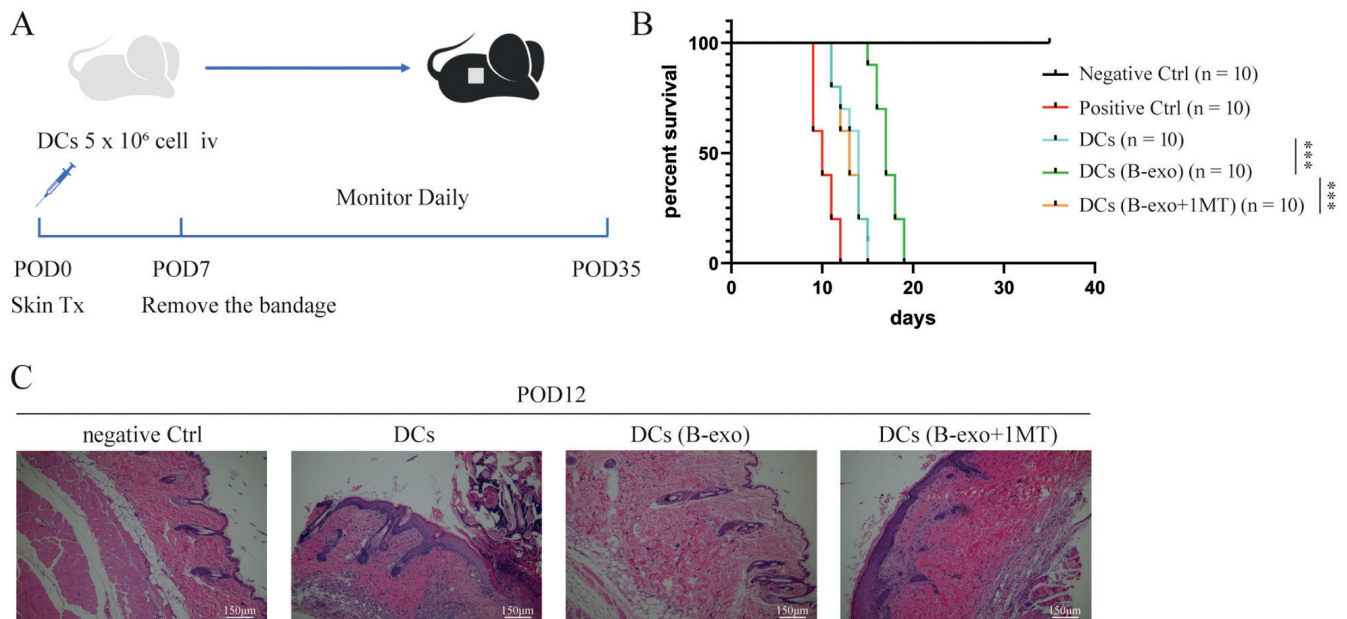


Fig. 7. Bone mesenchymal stem cell (BMSC)-derived exosome (B-exo)-exposed dendritic cells (DCs) enhanced allogeneic skin graft. A. Flowchart of mice skin transplantation surgery; B. Survival of skin grafts in different groups. Graft survival was compared using the Kaplan–Meier analysis and the log-rank test ($n = 10$); C. Hematoxylin and eosin (H&E) staining of skin grafts in different groups on postoperative day (POD) 12

1MT – 1 mM 1-methyl-L-tryptophan.

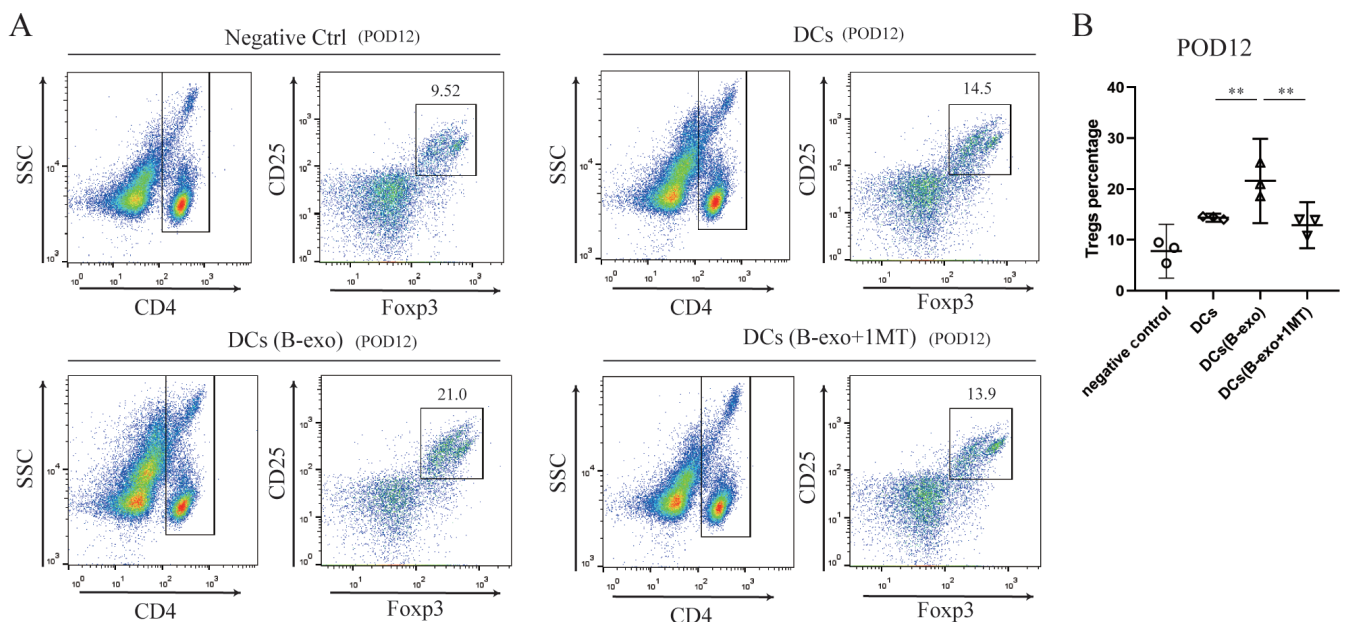


Fig. 8. Bone mesenchymal stem cell (BMSC)-derived exosome (B-exo)-exposed dendritic cells (DCs) induced CD4+Foxp3⁺ T in the spleen of the recipient. A. The percentage of CD4⁺Foxp3⁺ T cells in the spleen from recipients was analyzed using flow cytometry; B. Cumulative data showed the percentage of CD4⁺Foxp3⁺ T cells in spleen from recipients. The data are expressed as the means with 95% confidence interval (95% CI), $n = 3$

1MT – 1 mM 1-methyl-L-tryptophan; POD – postoperative day. * $p < 0.05$, ** $p < 0.01$, *** $p < 0.001$.

ORCID iDs

Hongxun Sang <https://orcid.org/0000-0001-6534-0231>
 Renli Zhao <https://orcid.org/0000-0002-6039-7447>
 Guohua Lai <https://orcid.org/0000-0003-4970-8459>
 Zhiwei Deng <https://orcid.org/0000-0002-6750-1892>
 Weida Zhuang <https://orcid.org/0000-0001-7394-7615>
 Mingjie Wu <https://orcid.org/0000-0001-7600-1323>
 Jiachang Wu <https://orcid.org/0000-0003-0262-0935>

References

- Pittenger MF, Mackay AM, Beck SC, et al. Multilineage potential of adult human mesenchymal stem cells. *Science*. 1999;284(5411):143–147. doi:10.1126/science.284.5411.143
- Le Blanc K. Immunomodulatory effects of fetal and adult mesenchymal stem cells. *Cytotherapy*. 2003;5(6):485–489. doi:10.1080/14653240310003611

3. Li X, Dong Y, Yin H, Qi Z, Wang D, Ren S. Mesenchymal stem cells induced regulatory dendritic cells from hemopoietic progenitor cells through Notch pathway and TGF- β synergistically. *Immunol Lett*. 2020;222:49–57. doi:10.1016/j.imlet.2020.03.005
4. Palomares Cabeza V, Hoogduijn MJ, Kraaijeveld R, et al. Pediatric mesenchymal stem cells exhibit immunomodulatory properties toward allogeneic T and B cells under inflammatory conditions. *Front Bioeng Biotechnol*. 2019;7:142. doi:10.3389/fbioe.2019.00142
5. Li YP, Paczesny S, Lauret E, et al. Human mesenchymal stem cells license adult CD34⁺ hemopoietic progenitor cells to differentiate into regulatory dendritic cells through activation of the Notch pathway. *J Immunol*. 2008;180(3):1598–1608. doi:10.4049/jimmunol.180.3.1598
6. Escola JM, Kleijmeer MJ, Stoorvogel W, Griffith JM, Yoshie O, Geuze HJ. Selective enrichment of tetraspan proteins on the internal vesicles of multivesicular endosomes and on exosomes secreted by human B-lymphocytes. *J Biol Chem*. 1998;273(32):20121–20127. doi:10.1074/jbc.273.32.20121
7. Raposo G, Stoorvogel W. Extracellular vesicles: Exosomes, microvesicles, and friends. *J Cell Biol*. 2013;200(4):373–383. doi:10.1083/jcb.201211138
8. Banchereau J, Steinman RM. Dendritic cells and the control of immunity. *Nature*. 1998;392(6673):245–252. doi:10.1038/32588
9. Lanzavecchia A, Sallusto F. Regulation of T cell immunity by dendritic cells. *Cell*. 2001;106(3):263–266. doi:10.1016/S0092-8674(01)00455-X
10. Yoo S, Ha SJ. Generation of tolerogenic dendritic cells and their therapeutic applications. *Immune Netw*. 2016;16(1):52–60. doi:10.4110/in.2016.16.1.52
11. Shahir M, Mahmoud Hashemi S, Asadirad A, et al. Effect of mesenchymal stem cell-derived exosomes on the induction of mouse tolerogenic dendritic cells. *J Cell Physiol*. 2020;235(10):7043–7055. doi:10.1002/jcp.29601
12. Soleimani M, Nadri S. A protocol for isolation and culture of mesenchymal stem cells from mouse bone marrow. *Nat Protoc*. 2009;4(1):102–106. doi:10.1038/nprot.2008.221
13. Kowal J, Arras G, Colombo M, et al. Proteomic comparison defines novel markers to characterize heterogeneous populations of extracellular vesicle subtypes. *Proc Natl Acad Sci USA*. 2016;113(8):E968–E977. doi:10.1073/pnas.1521230113
14. Wang W, Li J, Wu K, Azhati B, Rexiati M. Culture and identification of mouse bone marrow-derived dendritic cells and their capability to induce T lymphocyte proliferation. *Med Sci Monit*. 2016;22:244–250. doi:10.12659/MSM.896951
15. Xiao C, Wang K, Xu Y, et al. Transplanted mesenchymal stem cells reduce autophagic flux in infarcted hearts via the exosomal transfer of miR-125b. *Circ Res*. 2018;123(5):564–578. doi:10.1161/CIRCRESAHA.118.312758
16. Jain A, Irizarry-Caro RA, McDaniel MM, et al. T cells instruct myeloid cells to produce inflammasome-independent IL-1 β and cause autoimmunity. *Nat Immunol*. 2020;21(1):65–74. doi:10.1038/s41590-019-0559-y
17. Livak KJ, Schmittgen TD. Analysis of relative gene expression data using real-time quantitative PCR and the 2^{- $\Delta\Delta$ CT} method. *Methods*. 2001;25(4):402–408. doi:10.1006/meth.2001.1262
18. Cheng C, Lee C, Fryer M, et al. Murine full thickness skin transplantation. *J Vis Exp*. 2017;119:55105. doi:10.3791/55105
19. Zheng Q, Zhang S, Guo WZ, Li XK. The unique immunomodulatory properties of MSC-derived exosomes in organ transplantation. *Front Immunol*. 2021;12:659621. doi:10.3389/fimmu.2021.659621
20. Spees JL, Lee RH, Gregory CA. Mechanisms of mesenchymal stem/stromal cell function. *Stem Cell Res Ther*. 2016;7(1):125. doi:10.1186/s13287-016-0363-7
21. Zhang S, Chuah SJ, Lai RC, Hui JHP, Lim SK, Toh WS. MSC exosomes mediate cartilage repair by enhancing proliferation, attenuating apoptosis and modulating immune reactivity. *Biomaterials*. 2018;156:16–27. doi:10.1016/j.biomaterials.2017.11.028
22. Askenase PW. COVID-19 therapy with mesenchymal stromal cells (MSC) and convalescent plasma must consider exosome involvement: Do the exosomes in convalescent plasma antagonize the weak immune antibodies? *J Extracell Vesicles*. 2020;10(1):e12004. doi:10.1002/jev.2.12004
23. Castenmiller C, Keumatio-Doungtso BC, van Ree R, de Jong EC, van Kooyk Y. Tolerogenic immunotherapy: Targeting DC surface receptors to induce antigen-specific tolerance. *Front Immunol*. 2021;12:643240. doi:10.3389/fimmu.2021.643240
24. Obregon C, Kumar R, Pascual MA, Vassalli G, Golshayan D. Update on dendritic cell-induced immunological and clinical tolerance. *Front Immunol*. 2017;8:1514. doi:10.3389/fimmu.2017.01514
25. ten Brinke A, Martinez-Llordella M, Cools N, et al. Ways forward for tolerance-inducing cellular therapies: An AFACTT perspective. *Front Immunol*. 2019;10:181. doi:10.3389/fimmu.2019.00181
26. Mellor AL, Lemos H, Huang L. Indoleamine 2,3-dioxygenase and tolerance: Where are we now? *Front Immunol*. 2017;8:1360. doi:10.3389/fimmu.2017.01360
27. Chen W, Liang X, Peterson AJ, Munn DH, Blazar BR. The indoleamine 2,3-dioxygenase pathway is essential for human plasmacytoid dendritic cell-induced adaptive T regulatory cell generation. *J Immunol*. 2008;181(8):5396–5404. doi:10.4049/jimmunol.181.8.5396
28. Chung DJ, Rossi M, Romano E, et al. Indoleamine 2,3-dioxygenase-expressing mature human monocyte-derived dendritic cells expand potent autologous regulatory T cells. *Blood*. 2009;114(3):555–563. doi:10.1182/blood-2008-11-191197
29. Zhang B, Yin Y, Lai RC, Tan SS, Choo ABH, Lim SK. Mesenchymal stem cells secrete immunologically active exosomes. *Stem Cells Dev*. 2014;23(11):1233–1244. doi:10.1089/scd.2013.0479
30. Thomson AW, Humar A, Lakkis FG, Metes DM. Regulatory dendritic cells for promotion of liver transplant operational tolerance: Rationale for a clinical trial and accompanying mechanistic studies. *Hum Immunol*. 2018;79(5):314–321. doi:10.1016/j.humimm.2017.10.017
31. Li D, Zhao B, Luo Y, et al. Transplantation of Aire-overexpressing bone marrow-derived dendritic cells delays the onset of type 1 diabetes. *Int Immunopharmacol*. 2017;49:13–20. doi:10.1016/j.intimp.2017.05.023
32. Monguió-Tortajada, M, Lauzurica-Valdemoros R, Borràs FE. Tolerance in organ transplantation: From conventional immunosuppression to extracellular vesicles. *Front Immunol*. 2014;5:416. doi:10.3389/fimmu.2014.00416

Establishment of a mouse model of inflammatory bowel disease using dextran sulfate sodium

Xiaoying Jiang^{A–D}, Xue Chen^B, RuoXi Dong^B, Jiawen Wang^B, Yibin Pan^{D,E}, Yongqing Cao^{A,E,F}

Department of Anal-Rectal Surgery, Longhua Hospital, Shanghai University of Traditional Chinese Medicine, China

A – research concept and design; B – collection and/or assembly of data; C – data analysis and interpretation; D – writing the article; E – critical revision of the article; F – final approval of the article

Advances in Clinical and Experimental Medicine, ISSN 1899–5276 (print), ISSN 2451–2680 (online)

Adv Clin Exp Med. 2023;32(5):563–573

Address for correspondence

Yongqing Cao
E-mail: caoyq2133@163.com

Funding sources

National Natural Science Foundation of China (grant No. 81874469).

Conflict of interest

None declared

Acknowledgements

We would like to thank the employees of the laboratory at Shanghai University of Traditional Chinese Medicine for their contribution to this study. Additionally, we would like to thank thank Lab Ex China (Shanghai, China) for the service involving Meso Scale Discovery for inflammatory cytokines.

Received on June 30, 2022

Reviewed on July 12, 2022

Accepted on November 17, 2022

Published online on January 5, 2023

Abstract

Background. Dextran sulfate sodium (DSS)-induced murine colitis is the most commonly used model for the analysis of the pathogenesis of inflammatory bowel disease (IBD) and for the assessment of the efficacy of putative therapeutics. It has been suggested that mice should be given 2.5–10% DSS for 3–7 days to establish the model.

Objectives. To compare the IBD model in C57BL/6J mice given free access to water containing DSS at concentrations of 2.0%, 2.5% or 3.0% for 5, 7 or 10 days.

Materials and methods. Female mice (9 weeks old) were given access to drinking water containing DSS (2.0%, 2.5% or 3.0%) for 5–10 days. Body weight and colon length were then measured. Signs of edema, epithelial layer disruption, inflammatory cell infiltration, and cytokine induction, and severe colitis-related clinical signs were observed and analyzed.

Results. Weight of the mice decreased and disease activity index (DAI) score immediately increased in all 3 groups. The colon of mice in the 3.0% DSS group was shortened after 5 days, and the colon of mice in the 2.0% and 2.5% DSS groups was shortened after 7 days. A significantly increased intestinal injury score was observed on day 5 in the 3.0% DSS group, on day 7 in the 2.5% DSS group and on day 10 in the 2.0% DSS group. Cytokines were found to be elevated in all 3 groups after 5 days of DSS exposure, with higher DSS concentrations and longer administration times found to be associated with more serious inflammation of the intestinal tract. After 10 days of DSS administration, all mice in the 3.0% DSS group died.

Conclusions. It took 10 days for the 2.0% DSS group, 5 days for the 3.0% DSS group and 7 days for the 2.5% DSS group to develop obvious observable changes related to the induction of the IBD model. The individual differences within groups (within 10 days) could be reduced by prolonging the administration time. Excessive DSS concentration and longer DSS administration time (exceeding 7 days) may increase mortality of the mice.

Key words: concentration, inflammation, inflammatory bowel disease, dextran sulfate sodium, mouse model

Cite as

Jiang X, Chen X, Dong R, Wang J, Pan Y, Cao Y. Establishment of a mouse model of inflammatory bowel disease using dextran sulfate sodium. *Adv Clin Exp Med.* 2023;32(5):563–573. doi:10.17219/acem/156647

DOI

10.17219/acem/156647

Copyright

Copyright by Author(s)

This is an article distributed under the terms of the Creative Commons Attribution 3.0 Unported (CC BY 3.0) (<https://creativecommons.org/licenses/by/3.0/>)

Background

Inflammatory bowel disease (IBD) is a lifelong condition occurring in both adolescence and adulthood. It involves intestinal inflammation caused by impaired epithelium and can lead to aberrant gut microbiota and immune cell infiltration.^{1,2} The clinical symptoms of IBD encompass abdominal pain, diarrhea, mucus, pus, bloody stool, and weight loss. In the long term, the development of IBD increases the risk of disability and cancer. Although the etiology of IBD is still elusive, research has shown that genetic, environmental and gut microbial factors are potential contributors to its development.^{3–5}

Over the past decades, a variety of IBD models, such as spontaneous colitis models, adoptive transfer models, genetically modified models, and inducible colitis models, have been successfully developed.⁶ Animals, including mice, rats, dogs, and rabbits, have been used to establish these models.⁷ The C57BL/6J inbred mouse strain is commonly employed in dextran sulfate sodium (DSS)-induced IBD models and is found to be more suitable for chronic colitis induction than the BALB/c mouse strain.⁸

Among various animals and methods used for modeling IBD, establishing a C57BL/6J mouse model using DSS is relatively simple and therefore widely used. Perse and Cerar reported that adding 2.0% or 5.0% DSS to drinking water for 4–9 days was sufficient to induce acute colitis.⁶ However, reports on model differences after DSS administration within this concentration range are scarce. Hence, DSS was used in this study at 3 different concentrations (2.0%, 2.5% and 3.0%) to establish a C57BL/6J mouse model of IBD and to observe changes in symptoms and cytokine levels.

Objectives

This study aimed to compare models of IBD in C57BL/6J mice given free access to drinking water containing DSS at concentrations of 2.0%, 2.5% or 3.0% for 5, 7 or 10 days.

Materials and methods

Ethics statement

All experimental procedures involving animals were approved by the Laboratory Animal Care (approval No. SCXK-2018-0003) and Institutional Animal Care Use Committee (IACUC) at Shanghai University of Traditional Chinese Medicine (approval No. PZSHUTCM210416003).

Animals

The 9-week-old C57BL/6J wide-type (WT) female mice (weight >20 g) were purchased (Shanghai Lingchang Biology Science and Technology Co. Ltd., Shanghai,

China) and housed in the animal facility of Longhua Hospital, Shanghai University of Traditional Chinese Medicine (Shanghai, China). All experiments were performed according to the local, institutional and federal regulations for vertebrate animal research. Mice were reared in a normal environment (temperature 22 ± 2°C, humidity 40–60%), with a 12-hour light/dark cycle, and fed ad libitum for 1 week. The animals (n = 75) were divided into a 2.0% DSS group, 2.5% DSS group, 3.0% DSS group, and a control group (n = 21 mice in each DSS group and n = 12 in the control group). To induce colitis, 10-week-old female mice were administered DSS of different concentrations via drinking water, and their body weight, activities and condition (such as diarrhea and bloody stools) were observed and recorded. After 5 days of induction, 3 mice from each IBD group and 4 mice from the control group were euthanized. After 7 and 10 days of induction, 6 mice from each IBD group and 4 mice from the control group were euthanized. Decisions on the experimental protocol were reached through simple random sampling.

Dextran sulfate sodium administration

The molecular weight of DSS (MP Biomedicals Inc., Santa Ana, USA) ranged from 36 kDa to 50 kDa.² Dextran sulfate sodium solutions (2.0%, 2.5% and 3%) were prepared using sterile drinking water and 100 mL of DSS was given to 5–6 mice per cage for 2 days. Before replenishing the DSS solutions, the remaining liquid was discarded.

Experimental design

After 1 week of acclimation, the 10-week-old mice were randomized into 4 groups and given access to distilled water containing 2.0%, 2.5% or 3.0% DSS, or distilled water for 10 days. Their body weight, excrement and fecal bleeding were monitored daily. Three or 6 mice from different groups were euthanized using pentobarbital sodium (0.1–0.2 mL, 0.1%) via intraperitoneal injection on the 5th, 7th and 10th day. Serum samples were collected for subsequent testing, the entire large intestine was harvested and the colon length was measured (Fig. 1).

Weight and disease activity index

Body weight was recorded and a small fecal sample was collected from each mouse every day. Three major physical endpoints, including weight loss, diarrhea and rectal bleeding, were assessed using the disease activity index (DAI) scoring system⁹ (Table 1). Fecal samples were examined for consistency and tested for blood using the Fecal Occult Blood Complete test kit (BASO Diagnostics Inc., Zhuhai, China).

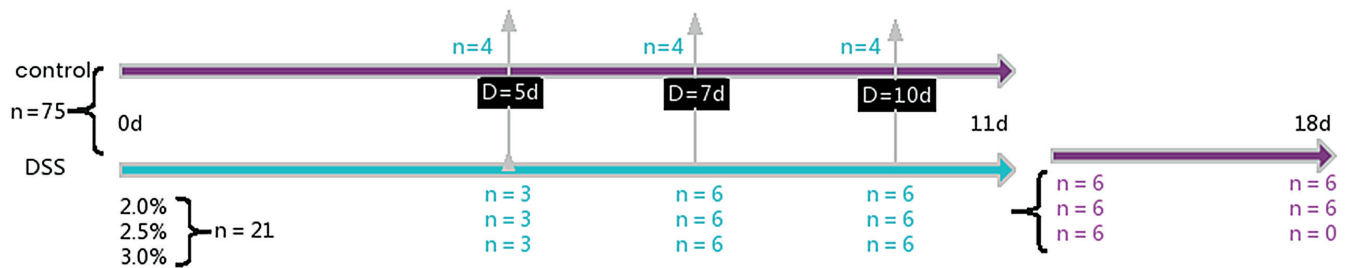


Fig. 1. Experimental design
DSS – dextran sulfate sodium.

Table 1. Assessment of 3 major endpoints by means of disease activity index (DAI)

Score	Stool consistency	Rectal bleeding	Weight loss
0	normal	stool with normal color	no weight loss
1	mildly soft	brown stool	5–10% weight loss
2	very soft	reddish stool	11–15% weight loss
3	watery	bloody stool	16–20% weight loss
4	–	–	>20% weight loss

DAI score = sum of all items divided by 3.

Histopathological evaluation of colitis

Mid and distal colon samples were fixed in 4% buffered formalin, dehydrated through a gradient of ethanol, clarified with xylene, embedded in paraffin, then cut into 4-µm-thick sections and stained with hematoxylin and eosin (H&E). Colonic histopathological evaluation was performed and recorded by 2 blinded investigators. The tissue sections were assessed using grading standards described by Morris et al. (Table 2) and Scheiffele et al. (Table 3).^{10,11}

Meso scale discovery

Meso Scale Discovery (MSD) was carried out using commercially available kits (K15048D and K0081254; Lab Ex., Shanghai, China). Mouse serum samples were thawed on ice, diluted twice, centrifuged (3000 g at 4°C for 5 min), and left at room temperature for 20 min. Then, 1000 µL diluent was added and samples were left to sit for 20 min before being mixed thoroughly. Next, the antibody diluent (3 mL with 60 µL of each test antibody), a washing solution (0.05% phosphate-buffered saline (PBS) and Tween-20)

Table 2. Pathological score

Morphological manifestations of colonic mucosa	Score
Basically normal	0
Local congestion without ulcer	1
Ulcer, but no congestion	2
Only 1 ulcer and inflammation	3
More than 2 ulcers and inflammation	4
Ulcer length greater than 2 cm	5
The ulcer length greater than 2 cm and adding 1 point to the total score for each additional 1 cm	6–10

Table 3. Histological score

Pathological manifestations	Score
No significant inflammation	0
Mild lymphocyte infiltration (high visual field: ≤10%) and no structural change of intestinal wall	1
Moderate lymphocyte infiltration (observed using high visual field: 10–25%), thickened intestinal wall, and longer intestinal crypt, but no ulcer penetrating mucous membrane	2
Significant lymphocyte infiltration (observed using high visual field: 25–50%), thickened intestinal wall and increased blood vessel density	3
A large number of lymphocytes in the intestinal wall (high visual field: ≥50%), lengthened and twisted intestinal crypt, ulcers, thickened intestinal wall, and increased blood vessel density	4

and a plate reading solution were prepared. The washing solution (150 μL /well) was used to wash each well 3 times. Then, 50 μL of sample and detection antibody were added to each well, and the plate was sealed with sealing film and shaken at room temperature for 2 h. The washing process was repeated 3 times. Next, detection antibody (25 μL) was added to each well, the plate was sealed with sealing film and shaken at room temperature for 2 h. Once again, the washing process was repeated 3 times. Finally, 150 μL of plate reading solution was added to each well, and plates were read using the Meso QuickPlex SQ 120 (Meso Scale Discovery, Rockville, USA).

Statistical analyses

The IBM SPSS v. 22.0 (IBM Corp., Armonk, USA) and GraphPad Prism 9 (GraphPad Software, San Diego, USA) software were used for all analyses. The normality of data was initially assessed using the Shapiro–Wilk method. Normally distributed data are presented as mean and standard deviation ($M \pm \text{SD}$), and non-normal data are presented as median (Me) and quartiles (Q_{25} , Q_{75}). The Kruskal–Wallis H test was used to analyze data that was not normally distributed, as well as normally distributed data without homogeneity of variance. For data that had normal distribution and homogeneity of variance, the comparisons between the 2 groups were made using the Student's unpaired t-test. The multi-group comparisons and trends were analyzed with repeated measures analysis of variance (rm-ANOVA). The value of $p < 0.05$ represented a statistically significant difference.

Results

Body weight

Weight loss is a sufficient, objective and economical indicator of DSS-induced colitis in mice.¹² Loss of $>20\%$ of initial body weight is a physiological indicator of animal stress and imminent demise.¹³ After 3 days of ad libitum access to DSS-spiked water, the weight of the 3 treatment groups decreased. Weight loss in the 2.0% and 2.5% groups did not differ; however, significantly different weight loss was found between the DSS groups and the control group. Furthermore, weight loss decreased at a faster rate in the 3.0% DSS group. After 10 days, the DSS-spiked water was removed and replaced with distilled water. However, mice in the 3.0% DSS group continued to lose weight and eventually died. On the 7th day after DSS removal, body weight in the 2.0% and 2.5% groups had gradually increased and returned to pre-DSS weight (Fig. 2).

Disease activity index scores

Disease activity index scores between DSS groups were not significantly different, although significant differences were

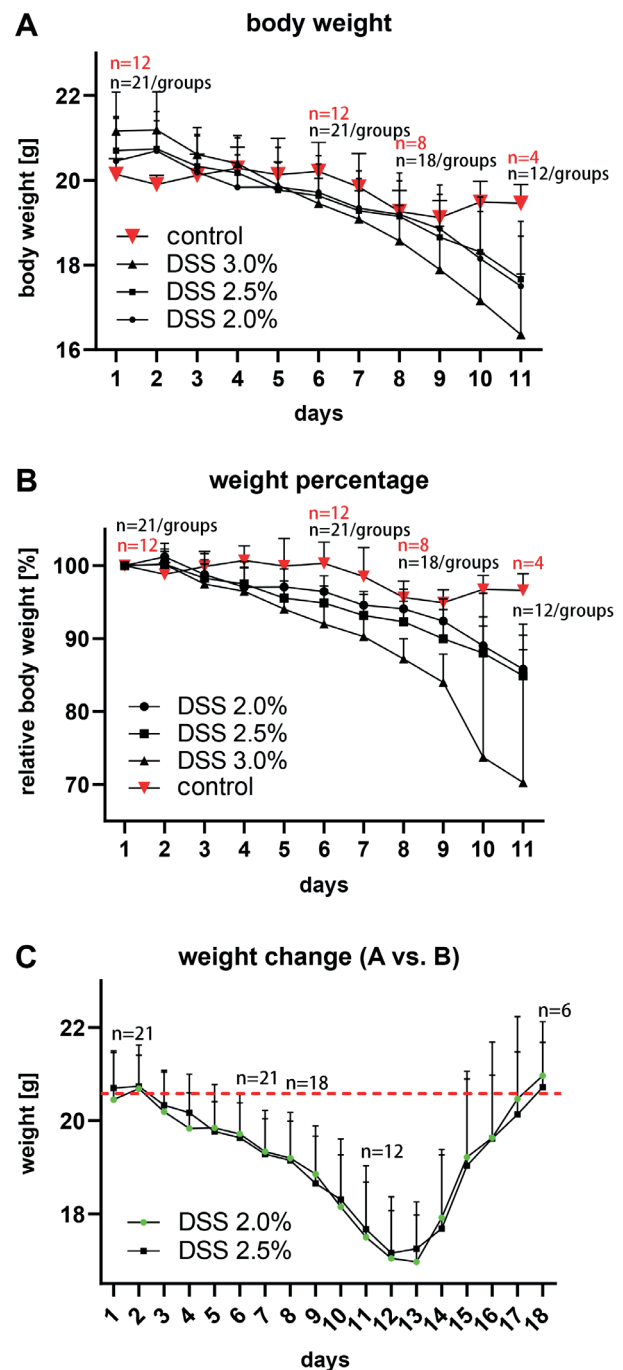


Fig. 2. Changes in body weight during dextran sulfate sodium (DSS) administration

Female C57BL/6J mice (10 weeks old) were administered DSS (2.0%, 2.5% or 3.0%) in drinking water for 5, 7 or 10 days. Samples were taken on the 5th, 7th and 10th day after DSS administration. The red values represent the current number of mice in the control group, and the black values represent the current number of mice in each of the DSS groups. Red points represent the mean value for the control group. The Kruskal–Wallis H rank sum test was used for the analysis. In panels A and B, the results indicate that there were statistical differences between the DSS groups and the control group on the final day ($p = 0.000$). Weight loss rates of mice were different in each group, with the largest rate of decline found in the 3.0% DSS group; repeated measures analysis of variance (rm-ANOVA) was performed and panel C shows that the weight of mice in the 2.0% DSS group and the 2.5% DSS group recovered to the level before exposure 7 days after the DSS administration was discontinued. Moreover, there was no significant difference in body weight between the 2.0% DSS group and the 2.5% DSS group over the full time course of the study ($p = 0.0739$).

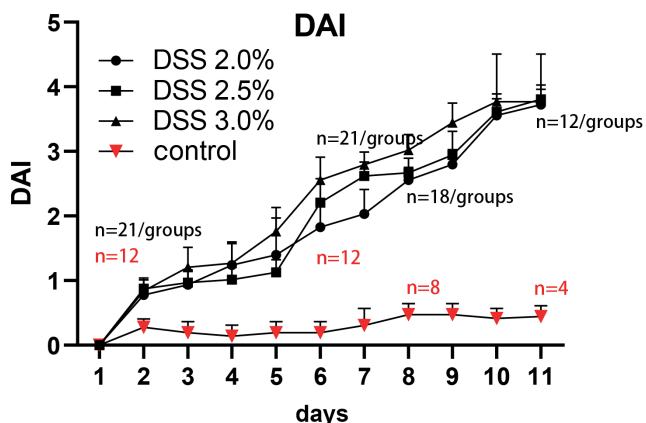


Fig. 3. Changes in disease activity index (DAI) score after exposure to dextran sulfate sodium (DSS). Female C57BL/6J mice (10 weeks old) were administered DSS (2.0%, 2.5% or 3.0%) in drinking water for 5, 7 or 10 days. Samples were taken on the 5th, 7th and 10th day after DSS administration. The red values represent the current number of mice in the control group, and the black values represent the current number of mice in each of the DSS groups. The Kruskal–Wallis H rank sum test was used for the analysis. The final results showed that there were statistical differences between the DSS groups and the control group on the final day ($p = 0.000$). Weight loss rates of mice in each group were different, with the largest rate increase found in the 3.0% DSS group

observed between the 3 DSS groups and the control group. Scores increased most rapidly in the 3.0% DSS group (Fig. 3).

Colon length

A dose-dependent decrease in colon length was found in mice exposed to DSS when compared to the control. However, when the colon shortened to approx. 6 cm, there were no differences found among the 3 groups. Shortened colon length was observed in all 3 treatment groups after 5 days of exposure to DSS. After 7 days of DSS exposure, the change of colon length of mice in each group became

shorter (Fig. 4,5) (Table 4,5). This suggests that 2.5% DSS induces a stable model of IBD.

Pathological and histological score

Significantly increased pathological and histological scores were found in the 3.0% DSS group on day 5. Compared with the control group, the scores for the 2.5% DSS group were significantly higher on the 7th day. On the 10th day, scores had increased in all 3 DSS groups, though there was no difference between them (Fig. 6) (Table 6–9).

Cytokines

Ten serological markers, including interferon- γ (IFN- γ), interleukin (IL)-1 β , IL-2, IL-4, IL-5, IL-6, IL-10, IL-12p70, platelet-derived growth factor-inducible protein KC/growth-regulated oncogene (KC/GRO), and tumor necrosis factor alpha (TNF- α), were determined with MSD (Fig. 7). The IL-4 decreased in the treatment groups to below the detection threshold of MSD, yet it could be detected in the control group (0.15 ± 0.13 pg/mL). The IFN- γ and IL-5 levels increased as the concentration and exposure time to DSS increased in each treatment group. However, there was no statistical difference between the mice exposed to DSS and the control group, which indicated that the activity of IFN- γ and IL-5 had little significance on the model. Similarly, the levels of the anti-inflammatory marker IL-10 were higher in the treatment groups compared to the control group, though the increase was not significant, which suggests that this cytokine was not central to the development of the IBD model. Furthermore, IL-1 β , IL-12p70, KC/GRO, and TNF- α were all significantly elevated after 5 days of exposure to DSS, though there was no

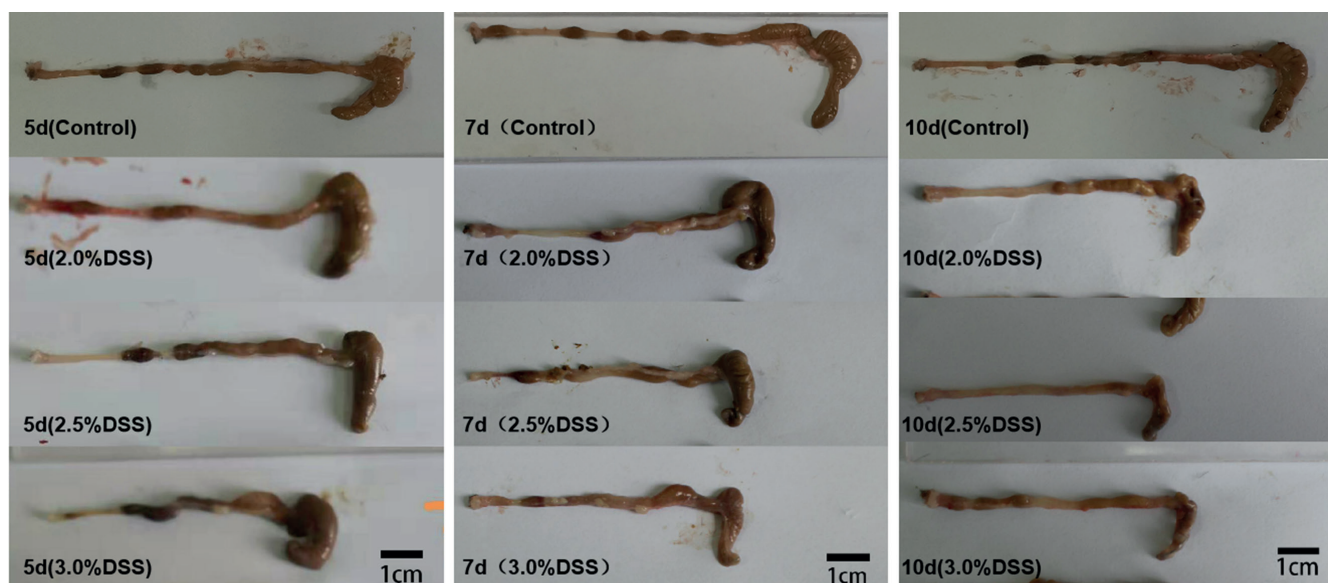


Fig. 4. Colon length of mice observed on different time points of dextran sulfate sodium (DSS) administration

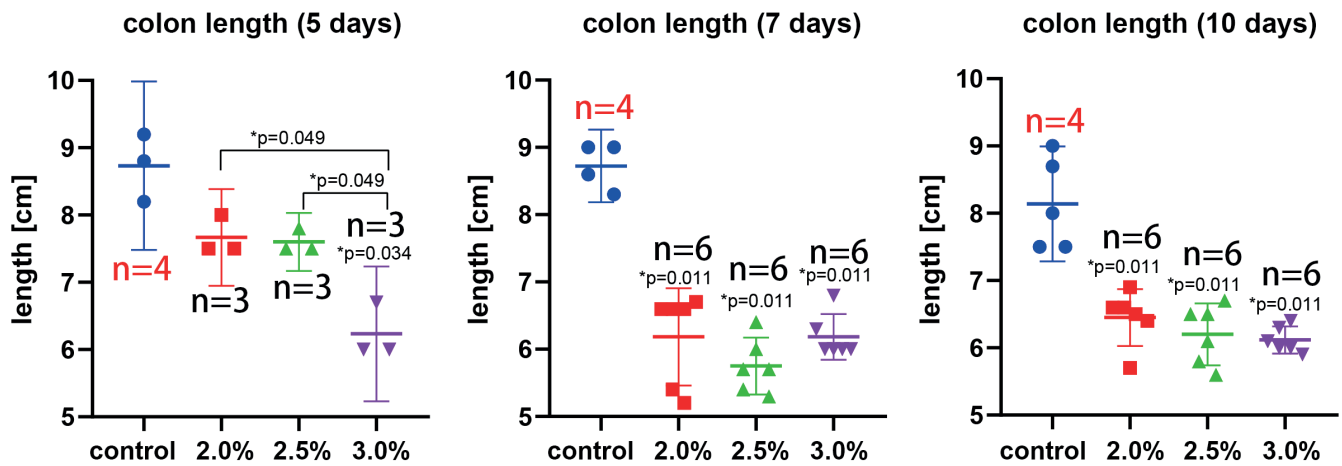


Fig. 5. Changes in colon length during dextran sulfate sodium (DSS) administration. Female C57BL/6J mice (10 weeks old) were administered DSS (2.0%, 2.5% or 3.0%) in drinking water for 5, 7 or 10 days. Intergroup differences were found in colon length. Each value represents the mean \pm 95% confidence interval (95% CI) for 3 or 6 mice. Red values represent the number of mice in the control group currently sampled, and black values represent the number of mice in the DSS groups currently sampled

* $p < 0.05$ (Student's t-test).

Table 4. Colon length (numerical value and overall comparison)

Day	Control [cm]	A	B	C	Overall		
		2.0% [cm]	2.5% [cm]	3.0% [cm]	H	df	p-value
5	8.50 (7.85, 9.00)	7.50 (7.50, 8.00)	7.50 (7.50, 7.80)	6.00 (6.00, 6.70)	8.198	3	0.042
7	8.80 (8.45, 9.00)	6.60 (5.40, 6.00)	5.70 (5.40, 6.00)	6.00 (6.00, 6.30)	11.421	3	0.010
10	8.35 (7.75, 8.85)	6.55 (6.40, 6.00)	6.30 (5.80, 6.50)	6.05 (6.00, 6.30)	11.516	3	0.009

df – degrees of freedom. Data are presented as median (M) and quartiles (Q25, Q75).

Table 5. Colon length (comparison between groups)

Day	A vs. control			B vs. control			C vs. control			A vs B			A vs. c			B vs. c		
	H	df	p-value	H	df	p-value	H	df	p-value	H	df	p-value	H	df	p-value	H	df	p-value
5	2.000	1	0.157	2.000	1	0.157	4.500	1	0.034	0.048	1	0.827	3.857	1	0.050	3.857	1	0.495
7	6.545	1	0.011	6.545	1	0.011	6.545	1	0.011	1.444	1	0.230	0.010	1	0.749	3.103	1	0.078
10	6.545	1	0.011	6.545	1	0.011	6.545	1	0.011	0.923	1	0.337	3.391	1	0.066	0.314	1	0.575

df – degrees of freedom. Data are presented as median (M) and quartiles (Q25, Q75).

Table 6. Pathological scoring (numerical value and overall comparison)

Day	Control [cm]	A	B	C	Overall		
		2.0% [cm]	2.5% [cm]	3.0% [cm]	H	df	p-value
5	0 (0, 0)	1 (0, 1)	1 (0, 2)	1 (1, 3)	5.703	3	0.127
7	0 (0, 0)	1 (0, 3)	3.5 (1, 4)	3.5 (1, 4)	11.028	3	0.012
10	0 (0, 0)	4 (3, 4)	4 (3, 4)	4 (4, 4)	9.605	3	0.022

df – degrees of freedom. Data are presented as median (M) and quartiles (Q25, Q75).

Table 7. Pathological scoring (comparison between groups)

Day	A vs. control			B vs. control			C vs. control			A vs. B			A vs. C			B vs. C		
	H	df	p-value	H	df	p-value	H	df	p-value	H	df	p-value	H	df	p-value	H	df	p-value
5	2.000	1	0.157	2.000	1	0.157	4.500	1	0.034	0.190	1	0.663	1.190	1	0.275	0.429	1	0.513
7	2.909	1	0.088	6.545	1	0.011	6.545	1	0.011	3.103	1	0.078	3.103	1	0.078	0.000	1	1.000
10	6.545	1	0.011	6.545	1	0.011	6.545	1	0.011	0.000	1	1.000	0.231	1	0.631	0.231	1	0.631

df – degrees of freedom.

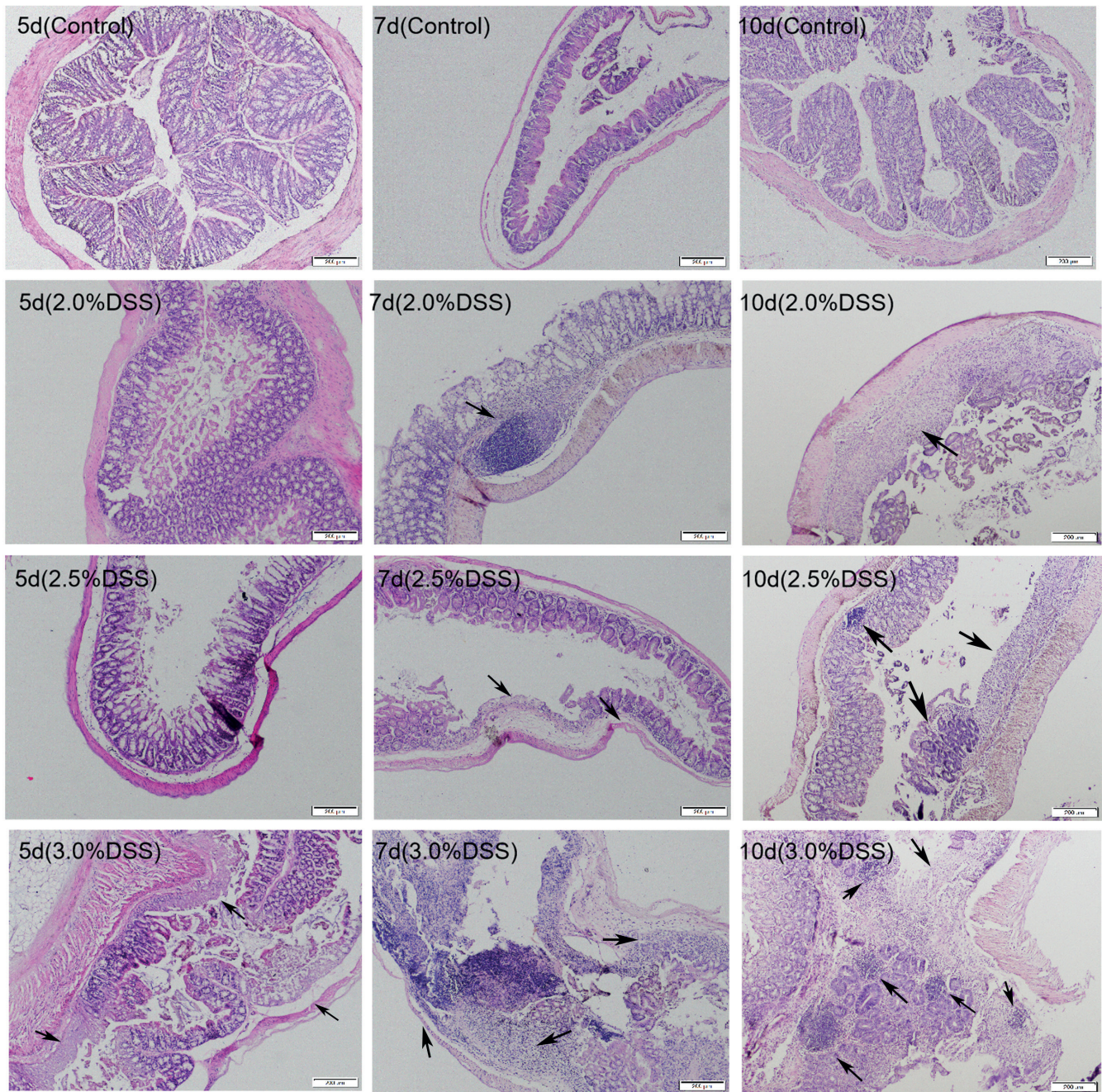


Fig. 6. Changes in colon length following dextran sulfate sodium (DSS) administration ($\times 100$ magnification (200 μm))

difference between the groups after 7 days. Nonetheless, the levels of IL-6 significantly increased, which indicates that it is a useful biomarker of the IBD model.

Mortality

Six mice remained in each of the DSS groups after the 10th day of the experimental protocol, except for the 3% DSS group, in which 1 mouse died on the 9th day. After the DSS-spiked water was removed and the mice were given access to distilled water, all mice in the 3% DSS group died. There was no mortality in the other 2 DSS groups.

Discussion

This study showed differences in a mouse model of IBD induced using 2.0%, 2.5% and 3.0% DSS added to drinking water. After 10 days of exposure to DSS-spiked drinking water, animals from 3 concentration groups displayed an IBD model phenotype. These model-related changes occurred fastest in the mice exposed to 3% DSS, though the differences between the 3% and 2.5% fed mice were subtle before the 7th day. Furthermore, 10 days of exposure to 3% DSS led to a >20% decrease in body weight and an increased mortality rate.

Table 8. Histological scoring (numerical value and overall comparison)

Day	Control [cm]	A	B	C	Overall		
		2.0% [cm]	2.5% [cm]	3.0% [cm]	H	df	p-value
5	0 (0, 0.5)	1 (1, 3)	2 (0, 2)	3 (2, 4)	7.043	3	0.071
7	0.5 (0, 1)	1.5 (1, 3)	2.5 (2, 3)	2.5 (2, 3)	6.506	3	0.089
10	0.5 (0, 1)	3 (2, 3)	3 (3, 3)	3 (3, 4)	9.779	3	0.021

df – degrees of freedom. Data are presented as median (M) and quartiles (Q25, Q75).

Table 9. Histological scoring (comparison between groups)

Day	A vs. control			B vs. control			C vs. control			A vs. B			A vs. C			B vs. C		
	H	df	p-value	H	df	p-value	H	df	p-value	H	df	p-value	H	df	p-value	H	df	p-value
5	3.125	1	0.077	1.531	1	0.126	4.500	1	0.034	0.048	1	0.827	1.714	1	0.190	2.333	1	0.127
7	2.227	1	0.136	3.682	1	0.055	5.500	1	0.020	0.519	1	0.471	1.256	1	0.262	0.103	1	0.749
10	6.545	1	0.011	6.545	1	0.011	6.545	1	0.011	0.160	1	0.689	0.519	1	0.471	0.160	1	0.689

df – degrees of freedom.

Serological testing revealed that the cytokine IL-6 is a good indicator for the development of the IBD model phenotype. The IL-6 is produced by T cells, B cells, monocytes, and polymorphonuclear leukocytes (PMNs), and plays a role in both pro-inflammatory and anti-inflammatory immune responses.¹⁴ Most inflammatory markers were upregulated after 5 days of DSS exposure, though the fact that there were significant differences among the treatment groups indicated that the IBD model had yet to be established. However, the differences in serological markers were similar between the DSS groups after 7 days, and the IBD model was established in the 3.0% group. After a further 3 days of DSS exposure, the model had developed also in the 2.0% and 2.5% groups.

Results regarding colon length could be an important indicator for the development of the IBD mouse model, as colon length decreased in line with increased cytokine levels. Generally, IBD is related to dysregulated mucosal immune responses and barrier function of the intestinal epithelium.¹ Indeed, interleukins are typically used to explore the etiology of IBD and observe the therapeutic effect of drugs. Also, IFN- γ , IL-1 β , IL-12p70, and TNF- α are thought to promote inflammation and injury,^{15,16} while IL-4, IL-5 and IL-10 are related to the inhibition of inflammation.^{17,18} Secreted by T cells, IL-2 is a cytokine that can regulate CD4, CD8, natural killer (NK), and B cells, and increased IL-2 is used as a marker to signal the development of colonic intestinal inflammation.¹⁹ At the same time, IL-5 is related to type 2 immune responses. It can act on eosinophils and basophils during the immune-mediated mechanisms in IBD,²⁰ and has been found in patients after intestinal surgery.¹² The chemokine CXC motif chemokine ligand 1 (CXCL1) participates in the migration of inflammatory cells to the sites of injury, and its levels have been shown to be elevated in Crohn's disease (CD) patients compared to healthy controls. Indeed, the correlation between CXCL1 and disease activity is even stronger than it is for C-reactive protein (CRP).²¹ In summary, a higher

DSS concentration was associated with increased cytokine levels, yet no significant differences were found among the treatment groups as the time of exposure to DSS was prolonged.

Dextran sulfate sodium is widely used to establish IBD models. Many factors, including the molecular weight of DSS, age, sex, the strain of mice, and the administration method, are conventionally considered to exert influence on the model of IBD. Furthermore, microorganisms, especially intestinal flora, have been shown to have an impact on the model. Some microorganisms are thought to be favorable for modeling, and the onset of IBD is understood to result from a combination of microorganisms and innate intestinal immunity.¹² A previous study showed that CD was driven by Th1/Th17 cells (through the production of IFN- γ and IL-12) and ulcerative colitis (UC) by Th2 cells (through the production of IL-4, IL-5, IL-10, and IL-13). Dextran sulfate sodium-induced colitis, though not a typical Th1-like model, more closely matches UC in humans.²² Indeed, the induction of DSS is more likely to cause colorectal damage in the distal regions, which is similar to the intestinal changes found in human UC patients in clinical practice.

In this study, factors that may interfere with the modeling of IBD were selected to create a protocol that would allow for the exploration of the effects of DSS concentration and time. Therefore, all of the investigated factors should be taken into consideration when using the study as a modeling reference resource. Based on the cytokine expression profile of the model, researchers could modify the DSS concentration and exposure time to match their research goals.

Limitations

The limitations of the study include the small number of animals, and the use of a single mouse strain and of female mice only. The addition of more animals, varied

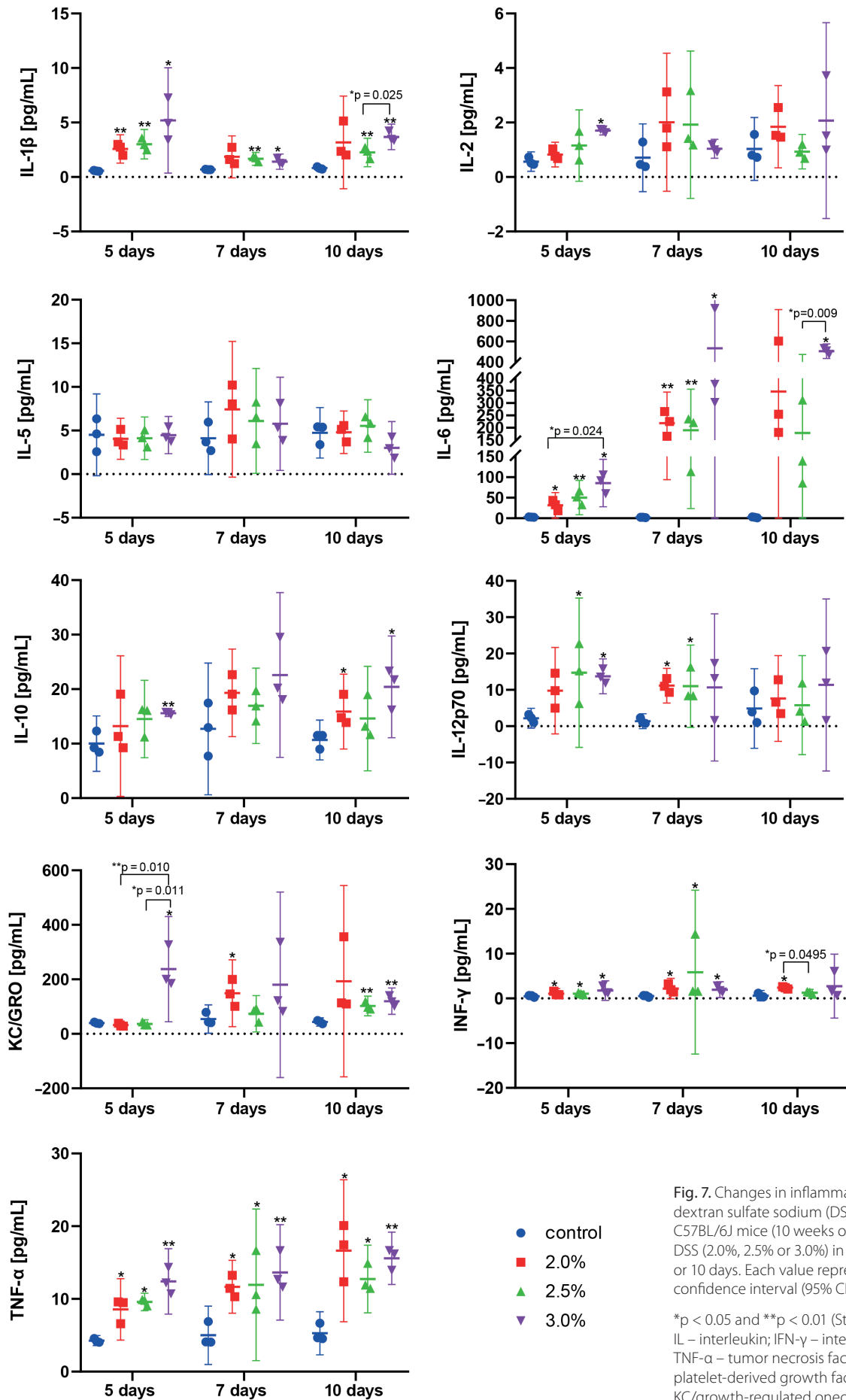


Fig. 7. Changes in inflammatory cytokines following dextran sulfate sodium (DSS) exposure. Female C57BL/6J mice (10 weeks old) were administered DSS (2.0%, 2.5% or 3.0%) in drinking water for 5, 7 or 10 days. Each value represents the mean ± 95% confidence interval (95% CI) for 3 or 6 mice

*p < 0.05 and **p < 0.01 (Student's t-test);
 IL – interleukin; INF-γ – interferon gamma;
 TNF-α – tumor necrosis factor alpha; KC/GRO – platelet-derived growth factor-inducible protein KC/growth-regulated oncogene.

strains and the use of both sexes in future studies would provide more insight and more reliable results. In addition, further research should include mice that have been allowed to recover naturally from DSS-induced intestinal inflammation. Such mice would allow researchers to evaluate the efficacy of drugs for IBD.

Conclusions

The present study investigated the impact of a narrow range of DSS concentrations on the IBD modeling in mice. This provided an accurate and safe modeling concentration, as well as a suitable time period over which to expose the mice to DSS. Exposure to drinking water spiked with 2.5% DSS for 10 days seems to be a compromise that resulted in a higher success rate and lower intragroup differences. After removing DSS, the mice recovered slowly through self-regulation. However, a continuous use of DSS at a high concentration led to a high mortality rate. The periodic use of such DSS doses could be used in the development of the chronic mouse model of inflammatory bowel disease.

The physiological and cytokine profile changes that were observed in the DSS-induced IBD model are useful markers for exploring the etiology of IBD and for observing the effects of putative therapeutics. Furthermore, the results of this study can provide a useful resource for researchers attempting to establish an IBD mouse model that can match their own research needs.

A mouse model of IBD was successfully established using DSS at different concentrations and with different exposure times. It took 10 days for the 2.0% DSS group, 5 days for the 3.0% DSS group and 7 days for the 2.5% DSS group to develop observable changes indicative of IBD. Furthermore, intragroup differences (within 10 days) could be reduced by prolonging the exposure time. However, excessive DSS concentration and longer exposure time (exceeding 7 days) led to increased mortality.

Supplementary files

The supplementary files are available at <https://doi.org/10.5281/zenodo.7305141>. The package contains the following files:

Supplementary File 1. The original data of the study, including the weight change record, DAI score change record, colon length, colon pathological score, and measurement data of cytokines.

Supplementary File 2. The data of the statistical analyses of this study, including the initial statistical analysis (normal distribution, homogeneity of variance, statistical test) and the repeated statistical test during the revision of the text.

Supplementary Table 1. Test methods and test values of each observation index in the study.

ORCID iDs

Xiaoying Jiang  <https://orcid.org/0000-0003-1735-9549>
 Xue Chen  <https://orcid.org/0000-0002-1836-6153>
 RuoXi Dong  <https://orcid.org/0000-0002-8611-3289>
 Jiawen Wang  <https://orcid.org/0000-0003-0979-7127>
 Yibin Pan  <https://orcid.org/0000-0003-3068-854X>
 Yongqing Cao  <https://orcid.org/0000-0002-0052-1784>

References

- Bang B, Lichtenberger LM. Methods of inducing inflammatory bowel disease in mice. *Curr Protoc Pharmacol*. 2016;72:5.58.1–5.58.42. doi:10.1002/0471141755.ph0558s72
- Chassaing B, Aitken JD, Malleshappa M, Vijay-Kumar M. Dextran sulfate sodium (DSS)-induced colitis in mice. *Curr Protoc Immunol*. 2014;104:15.25.1–15.25.14. doi:10.1002/0471142735.im1525s104
- Padua D, Vu JP, Germano PM, Pisegna JR. The role of neuropeptides in mouse models of colitis. *J Mol Neurosci*. 2016;59(2):203–210. doi:10.1007/s12031-015-0688-1
- Yan Y, Kolachala V, Dalmasso G, et al. Temporal and spatial analysis of clinical and molecular parameters in dextran sodium sulfate induced colitis. *PLoS One*. 2009;4(6):e6073. doi:10.1371/journal.pone.0006073
- Mizoguchi E, Nguyen D, Low D. Animal models of ulcerative colitis and their application in drug research. *Drug Des Devel Ther*. 2013;7:1341–1357. doi:10.2147/DDDT.S40107
- Perše M, Cerar A. Dextran sodium sulphate colitis mouse model: Traps and tricks. *J Biomed Biotechnol*. 2012;2012:718617. doi:10.1155/2012/718617
- Stadnicki A, Colman RW. Experimental models of inflammatory bowel disease. *Arch Immunol Ther Exp (Warsz)*. 2003;51(3):149–155. PMID:12894869.
- Melgar S, Karlsson A, Michaëlsson E. Acute colitis induced by dextran sulfate sodium progresses to chronicity in C57BL/6 but not in BALB/c mice: Correlation between symptoms and inflammation. *Am J Physiol Gastrointest Liver Physiol*. 2005;288(6):G1328–G1338. doi:10.1152/ajpgi.00467.2004
- Cooper HS, Murthy SN, Shah RS, Sedergran DJ. Clinicopathologic study of dextran sulfate sodium experimental murine colitis. *Lab Invest*. 1993;69(2):238–249. PMID:8350599.
- Morris GP, Beck PL, Herridge MS, Depew WT, Szewczuk MR, Wallace JL. Hapten-induced model of chronic inflammation and ulceration in the rat colon. *Gastroenterology*. 1989;96(3):795–803. PMID:2914642.
- Scheiffele F, Fuss IJ. Induction of TNBS colitis in mice. *Curr Protoc Immunol*. 2002;49(1):15.19.49. doi:10.1002/0471142735.im1519s49
- Zhou W, Zhang H, Pan Y, Xu Y, Cao Y. circRNA expression profiling of colon tissue from mesalazine-treated mouse of inflammatory bowel disease reveals an important circRNA–miRNA–mRNA pathway. *Aging*. 2021;13(7):10187–10207. doi:10.18632/aging.202780
- Kim JJ, Shajib MdS, Manocha MM, Khan WI. Investigating intestinal inflammation in DSS-induced model of IBD. *J Vis Exp*. 2012;60:3678. doi:10.3791/3678
- Scheller J, Chalaris A, Schmidt-Arras D, Rose-John S. The pro- and anti-inflammatory properties of the cytokine interleukin-6. *Biochim Biophys Acta*. 2011;1813(5):878–888. doi:10.1016/j.bbamcr.2011.01.034
- Maaser C, Housley MP, Imura M, et al. Clearance of *Citrobacter rodentium* requires B cells but not secretory immunoglobulin A (IgA) or IgM antibodies. *Infect Immun*. 2004;72(6):3315–3324. doi:10.1128/IAI.72.6.3315-3324.2004
- Yu D, Zhu H, Liu Y, Cao J, Zhang X. Regulation of proinflammatory cytokine expression in primary mouse astrocytes by coronavirus infection. *J Virol*. 2009;83(23):12204–12214. doi:10.1128/JVI.01103-09
- Moore KW, de Waal Malefyt R, Coffman RL, O'Garra A. Interleukin-10 and the interleukin-10 receptor. *Annu Rev Immunol*. 2001;19(1):683–765. doi:10.1146/annurev.immunol.19.1.683
- Jayme TS, Leung G, Wang A, et al. Human interleukin-4-treated regulatory macrophages promote epithelial wound healing and reduce colitis in a mouse model. *Sci Adv*. 2020;6(23):eaba4376. doi:10.1126/sciadv.aba4376
- Joosse ME, Charbit-Henrion F, Boisgard R, et al. Duplication of the IL2RA locus causes excessive IL-2 signaling and may predispose to very early onset colitis. *Mucosal Immunol*. 2021;14(5):1172–1182. doi:10.1038/s41385-021-00423-5

20. Luo X, Villablanca EJ. Type 2 immunity in intestinal homeostasis and inflammatory bowel disease. *Biochem Soc Trans*. 2021;49(5):2371–2380. doi:10.1042/BST20210535
21. Mello JDC, Gomes LEM, Silva JF, et al. The role of chemokines and adipokines as biomarkers of Crohn's disease activity: A systematic review of the literature. *Am J Transl Res*. 2021;13(8):8561–8574. PMID:34539979.
22. Stevceva L, Pavli P, Husband A, Ramsay A, Doe W. Dextran sulphate sodium-induced colitis is ameliorated in interleukin 4 deficient mice. *Genes Immun*. 2001;2(6):309–316. doi:10.1038/sj.gene.6363782

miR-29a-5p regulates the malignant biological process of liver cancer cells through ARID2 regulation of EMT

Wenke Li^{1,B-D}, Yourang Jiang^{2,B}, Qi Pan^{2,A}, Guang Yang^{3,A}

¹ Department of Hepatological Surgery, The Yongchuan Hospital of Chongqing Medical University, China

² Department of Dermatology, Chongqing Hospital of Traditional Chinese Medicine, China

³ Department of Urology Surgery, The First Affiliated Hospital of Chongqing Medical University, China

A – research concept and design; B – collection and/or assembly of data; C – data analysis and interpretation;

D – writing the article; E – critical revision of the article; F – final approval of the article

Advances in Clinical and Experimental Medicine, ISSN 1899–5276 (print), ISSN 2451–2680 (online)

Adv Clin Exp Med. 2023;32(5):575–582

Address for correspondence

Guang Yang

E-mail: ronalyangguang@sina.com

Funding sources

The study was supported by the National Natural Science Foundation of China (grant No. 81904218 to Q.P.) and Natural Science Foundation of Chongqing, China (grant No. cstc2019jcyj-msxmX0095 to Q.P.).

Conflict of interest

None declared

Received on April 4, 2022

Reviewed on September 13, 2022

Accepted on November 17, 2022

Published online on December 19, 2022

Cite as

Li W, Jiang Y, Pan Q, Yang G. miR-29a-5p regulates the malignant biological process of liver cancer cells through ARID2 regulation of EMT. *Adv Clin Exp Med.* 2023;32(5):575–582. doi:10.17219/acem/156646

DOI

10.17219/acem/156646

Copyright

Copyright by Author(s)

This is an article distributed under the terms of the Creative Commons Attribution 3.0 Unported (CC BY 3.0) (<https://creativecommons.org/licenses/by/3.0/>)

Abstract

Background. Liver cancer, the vast majority of cases being hepatocellular carcinoma (HCC), is now the most malignant tumor in the world. Recurrence and metastasis remain the major obstacles on the way to the successful treatment of HCC. In recent years, the vital function of microRNAs (miRNAs) in human health and disease have been demonstrated. Large amounts of evidence demonstrate that miRNAs play an important role in the occurrence and progression of HCC.

Objectives. To find new targets for improving the early diagnosis, treatment and clinical prognosis of liver cancer.

Materials and methods. We used quantitative reverse transcription-polymerase chain reaction (qRT-PCR) to analyze the expression of miR-29a-5p. A cell counting kit-8 (CCK-8) assay was used to measure the proliferation of liver cancer cells. Wound healing and transwell assays were used to detect migration and invasion in vitro. Western blot was used to detect the expression of the related protein.

Results. The miR-29a-5p was identified as a tumor-related miRNA. It is upregulated in HCC. The overexpression of miR-29a-5p contributes to the proliferation, invasion and metastasis of HCC cells. Furthermore, the downregulation of miR-29a-5p inhibited the growth, migration and invasion of HCC cells in vitro. Subsequently, we used bioinformatics methods to predict that AT-rich interaction domain 2 (*ARID2*) is the downstream target gene of miR-29a-5p. The downregulation of *ARID2* could reverse the tumor suppressive effect caused by the knockdown of miR-29a-5p. Similarly, the epithelial–mesenchymal transition (EMT)-related protein epithelial marker E-cadherin expression increased and the mesenchymal marker Vimentin decreased when we downregulated the expression of miR-29a-5p. Interestingly, the knockdown of *ARID2* could reverse this phenomenon.

Conclusions. Our study demonstrated that miRNA-29a-5p was overexpressed in HCC cells. It promotes the progression of HCC by targeting *ARID2* in an EMT manner.

Key words: liver cancer, metastasis, proliferation, invasion, miR-29a-5p

Background

Hepatocellular carcinoma (HCC) is the 2nd leading cause of cancer-related deaths globally.^{1,2} The 5-year overall survival rate of HCC patients was less than 10%.³ Despite the extensive application of early diagnosis techniques and continuous improvement in treatment strategies such as surgical intervention and targeted chemoradiotherapy,^{4,5} HCC recurrence and metastasis remain the main challenges leading to poor prognosis.⁶ Therefore, more precise targets for diagnosing and treating liver cancer are urgently required to improve the early detection rate and clinical treatment effect of liver cancer.

MicroRNAs (miRNAs) are small noncoding RNAs containing approx. 22 nucleotides. In recent decades, many researchers have focused on the critical role of miRNAs in human health and disease, as miRNA regulation is a common pathway for epigenetic regulation. The miRNAs exert post-transcriptional or translational control on the expression of various genes involved in cancer progression.^{7,8} They can regulate the migration, proliferation, apoptosis, and other malignant biological behaviors of tumor cells in various ways. Several studies have demonstrated that miRNAs are overexpressed in many malignant tumors, including liver cancer. Tumor occurrence and progression often coincide with abnormal miRNA expression. They function as both tumor suppressors and oncogenes, and are critical in tumor development and progression.^{9–13} The miRNAs have also been crucial in cancer development and epithelial–mesenchymal transition (EMT).¹⁴

Epithelial–mesenchymal transition is a unique morphological transformation process; its main mechanism is to transform inactive epithelial cells into active mesenchymal cells, enhancing cancer cell metastasis and invasion.¹⁵ It can also affect the invasive ability, metastasis and chemoresistance of malignant tumors.^{16–18} According to mounting data, miRNAs play an important role in the aggressiveness of cancer cells, including EMT-related cancer metastasis.¹⁹

Previous studies have found that miRNA-29a-5p is closely related to the postoperative recurrence of liver cancer,²⁰ but the precise mechanism remains unknown. In this study, we attempted to delve deeper into this specific mechanism.

Objectives

Due to the significant threat liver cancer poses to human health and the important role of miRNAs in tumors, we conducted this study to find a new mechanism by which miRNAs regulate the progression and development of liver cancer. We explored the miRNA-29a-5p role in liver cancer and its specific mechanism of regulating the biological behavior of liver cancer. It is anticipated that our research will yield new ideas for liver cancer prevention and treatment,

thereby improving the treatment and prognosis of liver cancer patients.

Materials and methods

Cell lines and culture

The human normal liver cell line (LO2) and the liver cancer cell lines (Huh-7, LM-3, MHCC97-H, and HepG2) were purchased from the Institute of Biological Sciences, Chinese Academy of Sciences (Shanghai, China). The cells were cultured in high-glucose complete Dulbecco's modified Eagle's medium (DMEM) (containing 10% fetal bovine serum (FBS)) at 37°C, 5% CO₂.

RNA extraction and polymerase chain reaction

The TRIzol reagent was utilized to separate total RNA (Invitrogen; Thermo Fisher Scientific, Waltham, USA), and miRNA was collected using Biospin miRNA Extraction Kit (GeneCopoeia, Carlsbad, USA). Reverse transcription of the miRNA into cDNA was performed, and quantitative real-time polymerase chain reaction (qRT-PCR) was carried out utilizing All-in-One™ miRNA qRT-PCR Detection System (GeneCopoeia, Carlsbad, USA). Quantitative reverse transcription-polymerase chain reaction was performed using SYBR® Premix Ex Taq™ (Takara, Dalian, China) and PrimeScript™ RT reagent kit (Takara). The miR-29a-5p was normalized to U6, and AT-rich interaction domain 2 (ARID2) was normalized to GAPDH. The quantitative expression levels were measured using the 2^{-ΔΔCt} method.

Cell transfection

Oligonucleotides for hsa-miR-29a-5p mimics and inhibitors were obtained from Genebiogist (Shanghai, China). Small interfering RNA for ARID2 knockdown and blank control siRNA were obtained from GenePharma (Shanghai, China). A day before the transfection, cells were seeded into 6-well plates. When the cell density reached 70–80%, using Lipofectamine 2000 (Invitrogen) at a final dose of 100 nM, cells underwent transfection with oligonucleotides according to the manufacturer's specifications. After 48 h, quantitative reverse transcription-polymerase chain reaction was used to determine the miR-29a-5p transfection effectiveness, and the harvested cells were utilized for subsequent functional and mechanism validation experiments.

Cell proliferation assay

Cell proliferation capacity was assessed using the Cell Counting Kit-8 (CCK-8; Dojindo (FBS), Kumamoto, Japan).

The cells in each treatment group were seeded into 96-well plates, with 4×10^3 cells in each well and 3 replicates in each group. Then, they were cultured at 37°C in 5% CO₂, CCK-8 reagent was added at 0 h, 24 h, 48 h, and 72 h, and the absorbance value was measured at a wavelength of 450 nm.

Wound healing assay

Each treatment group cell was cultured at 37°C in 6-well plates until the density exceeded 95%. Then, we used a 10-microliter pipette tip for cell scratching in the 6-well plate to create an artificial wound. After gently washing each well 3 times with phosphate-buffered saline (PBS), the cells were cultured in serum-free high-glucose DMEM for 24 h. The wound area was visualized and images were captured at 0 h and 24 h.

Cell migration and invasion assays

We tested the ability of cells to invade and migrate with transwell chambers (Corning, Corning, USA). Briefly, cells in each treatment group were trypsin-digested and suspended in serum-free high-glucose DMEM. Before seeding cells from each treatment group into an upper chamber, we added diluted basement Matrigel (BD Biosciences, Franklin Lakes, USA) to each chamber and allowed it to polymerize for 3 h at 37°C. A total of 200 µL of cell suspension (total number of 4×10^4 cells), resuspended in a serum-free medium, was placed in the top section of the chamber, and 600 µL of high-glucose DMEM supplemented with 20% FBS was placed in the lower section of the chamber. Later, cells were cultivated for 24 h and cells were fixed and stained with 4% paraformaldehyde for 15 min at room temperature and 0.1% crystal violet for 20 min at room temperature, respectively. Finally, cells were counted with a microscope in 5 random fields, and images were captured.

Western blotting

Total protein was extracted from each group of cells using phenylmethanesulfonyl fluoride and RIPA lysis buffer (Beyotime, Shanghai, China). Briefly, cells were gently washed twice with cold PBS, scraped and lysed for 30 min on ice with lysis buffer. After lysis completion, centrifugation was performed at 4°C at 12,000 rpm for 15 min, and the supernatant was collected for later use. To determine protein concentration, we employed a BCA protein detection kit (Beyotime). The proteins were separated on a 10% sodium dodecyl-sulfate polyacrylamide gel electrophoresis (SDS-PAGE), transferred to polyvinylidene fluoride (PVDF) membranes (EMD Millipore, St. Louis, USA), and blocked with QuickBlock™ Blocking Buffer (Beyotime) for 30 min at room temperature. Subsequently, the membranes were treated overnight at 4°C with primary antibodies. Then, the membrane was washed 3 times

with Tris-buffered saline with Tween (TBST) before being treated with a secondary antibody for 1 h at room temperature. Next, the membrane was washed 3 times with TBST. Protein bands were visible using enhanced chemiluminescence (ECL; Cell Signaling Technology, Danvers, USA).

Statistical analyses

All observations in this study were made in triplicate. The results were scrutinized using GraphPad Prism v. 8 (GraphPad Software, San Diego, USA) software. For repeated measurements, the general linear model was used to compare the statistical difference among groups. Before conducting one-way analysis of variance (ANOVA) and t-test, the normality and homogeneity of variance of data or variables were tested. If the data conformed to a normal distribution and had homogeneity of variance, the one-way ANOVA and t-test were used to compare the differences between different treatment groups. The value of $p < 0.05$ was considered significantly different.

Results

miR-29a-5p is highly expressed in HCC cells and was successfully knocked down and upregulated

To detect the differential expression of miR-29a-5p in HCC, we examined 4 HCC cell lines, including Huh-7, LM-3, MHCC97-H, HepG2, and the human normal liver cell line (LO2). Figure 1A illustrates that miR-29a-5p was present at lower levels in LO2 cells than in all HCC cell lines. The Huh-7 was selected for the subsequent experiments; hsa-miR-29a-5p mimics and inhibitors were used to upregulate and knock down miR-29a-5p, respectively (Fig. 1B).

miR-29a-5p enhances the proliferation, migration and invasion of HCC cells

The CCK-8, wound healing and transwell assay data confirmed that miR-29a-5p knockdown significantly inhibited cell proliferation (Fig. 2A). Additionally, we discovered that miR-29a-5p knockdown HCC cells had less ability to migrate and invade than control cells (Fig. 2B,C). These results were reversed when miR-29a-5p was upregulated.

ARID2 is a target gene of miR-29a-5p

Subsequently, we utilized an online prediction database (TargetScan, https://www.targetscan.org/vert_80/; starBase, <http://starbase.sysu.edu.cn/>) to predict candidate targets for miR-29a-5p (Fig. 3). As expected, miR-29a-5p silencing significantly upregulated ARID2 expression; similarly, ARID2 was downregulated when miR-29a-5p was overexpressed (Fig. 4).

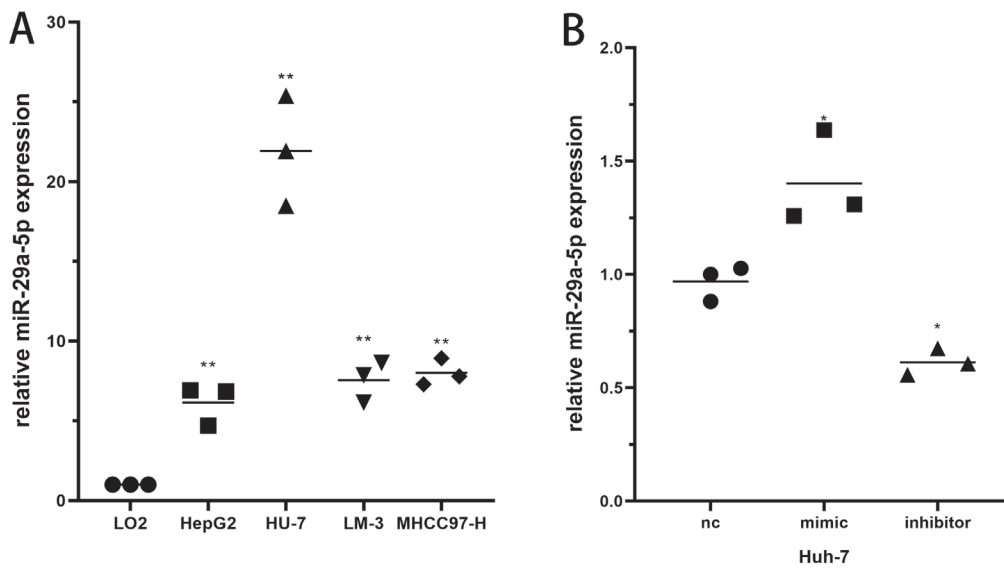


Fig. 1. A. miR-29a-5p expression levels in 4 hepatocellular carcinoma (HCC) cell lines were higher than in the human normal liver cell line (LO2) (3 distinct repetitions, one-way analysis of variance (ANOVA), HepG2: $p = 0.0207$; HU-7: $p < 0.0001$; LM-3: $p = 0.0044$; MHCC97-H: $p = 0.0028$; ** denotes $p < 0.01$); B. miR-29a-5p was knocked down and upregulated in Huh-7 cells (3 distinct repetitions, one-way ANOVA, mimic: $p = 0.0138$; inhibitor: $p = 0.0314$; * denotes $p < 0.05$)

miR-29a-5p regulates EMT through ARID2 and affects HCC cell proliferation, metastasis and invasion

The miR-29a-5p inhibitor and ARID2 siRNA were co-transfected into Huh-7 cells to examine whether ARID2 participated in the changes in the proliferation and migration ability of HCC cells induced by miR-29a-5p (Fig. 5A). As expected, the effects of miR-29a-5p downregulation on cell proliferation and migration were reversed by the treatment with ARID2 siRNA co-transfection (Fig. 5B,C). Simultaneously, after co-transfection with ARID2 siRNA, western blot analysis revealed that E-cadherin expression was lowered, whereas Vimentin expression increased, which suggested that the EMT ability of Huh-7 cell was enhanced (Fig. 5D,E).

Discussion

Primary liver cancer is the 4th most common carcinoma in China, posing a serious threat to the Chinese people's health and life.²¹ Liver cancer metastasis includes 5 typical steps: local invasion of adjacent tissues, intravascular invasion, circulatory system survival, extravasation, and abnormal colonization of the liver or distant organs (extrahepatic colonization). With the increased research into liver cancer and the advancement of medical technology, liver cancer now has a precise multidisciplinary treatment model. Currently, regorafenib, sorafenib and immune checkpoint inhibitors are all molecularly targeted medications that have improved the prognosis of most patients.^{22–25} Despite this, most liver cancer patients have extremely poor prognoses due to the interaction of multiple factors.²⁶ Most patients lose the opportunity for surgery due to the extremely high recurrence rate of liver cancer and the discovery of distant metastases at the initial diagnosis.²⁷ Therefore, finding

a specific molecular marker for early disease prediction and treatment is particularly important.

The abnormal expression of oncogenes often regulates tumorigenesis and cancer progression. Understanding the oncogene function is crucial for preventing and treating carcinoma. Many malignant biological processes, such as cell proliferation and apoptosis, depend on miRNA regulation and autophagy. Mounting evidence suggests that under certain conditions miRNAs act as oncogenes and antioncogenes in HCC cells and regulate malignant biological behaviors such as apoptosis, invasiveness, proliferation, and metastatic abilities.²⁸ Many miRNAs, such as miR-519a and miR-1468 inhibit apoptosis and improve cell proliferation in liver cancer cells.

Interestingly, other miRNAs, including miR-1296 and miR-542-3p, inhibited the EMT, decreasing the HCC cell metastatic capacity. The miR-29a is a conserved miRNA regulating multiple coordinated post-transcriptional programs, thereby participating in diverse biological processes.²⁹ Previous studies have indicated that the overexpression of miR-29a inhibits leukemia cell line growth. However, several other studies have discovered that the increased miR-29a levels in mice promote leukemia progression, suggesting that miRNAs may be a double-edged sword in cancer.³⁰ Similarly, miR-29a regulates glioblastoma disease progression; in glioma patients, low miR-29a expression predicts higher tumor aggressiveness and a worse prognosis.³¹ Numerous studies have examined the link between miRNA-29a-5p and early recurrence of HCC after surgical resection.²⁰ However, the biological function of miRNA-29a-5p in HCC has not been thoroughly described. In this study, miRNA-29a-5p was overexpressed in HCC cells. In vitro functional experiments further indicated that the downregulation of miRNA-29a-5p inhibited HCC cell invasion, migration and proliferation.

The ARID2 is a chromatin-remodeling complex subunit important in biological processes occurring in various

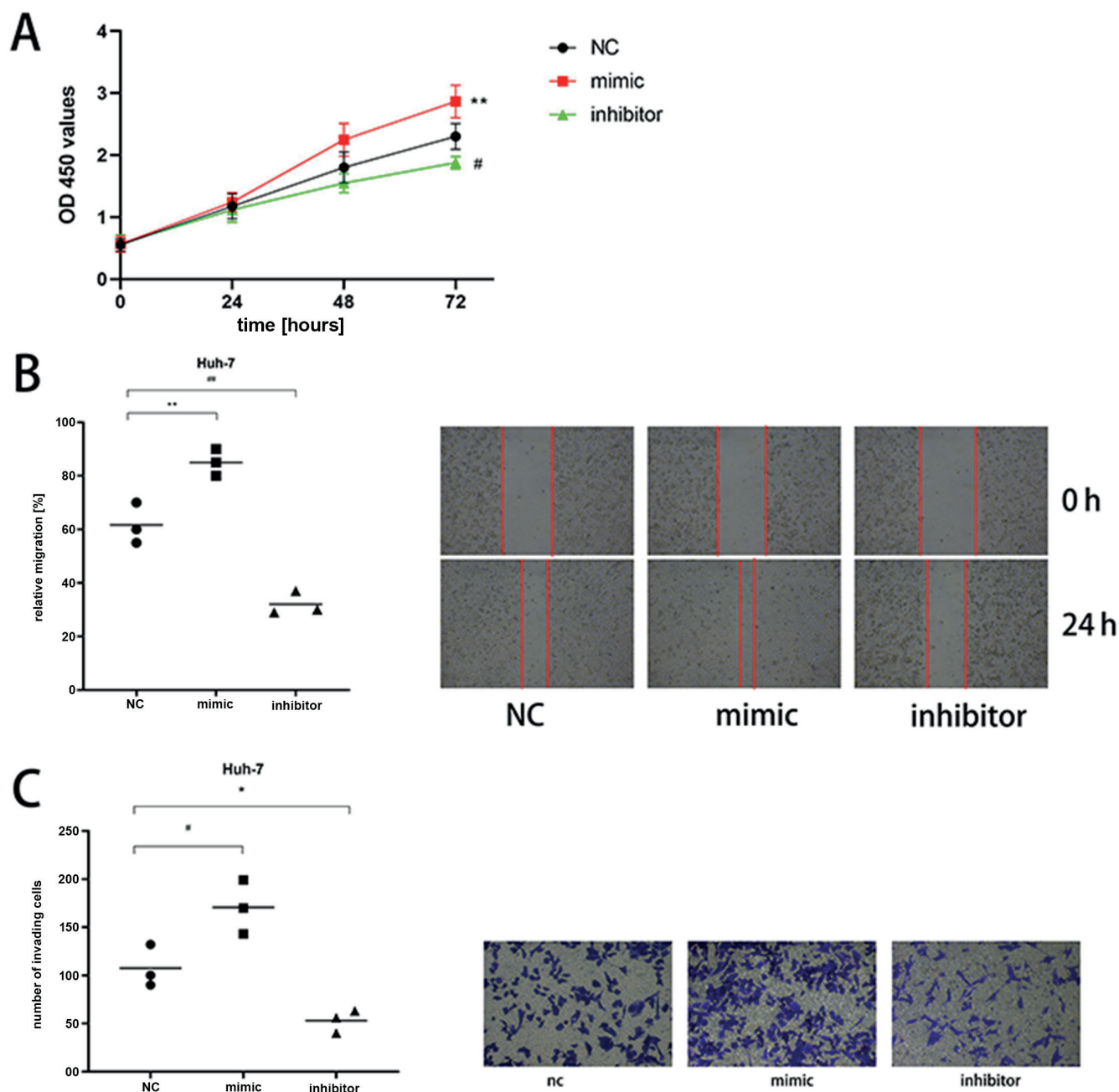


Fig. 2. miR-29a-5p controls the malignant biological behavior of hepatocellular carcinoma (HCC) cells. A. The cell counting kit-8 (CCK-8) detection revealed that HCC cell proliferation could be regulated via miR-29a-5p (Greenhouse–Geisser test, degrees of freedom (df) = 1.608, F = 1115.927, $p < 0.0001$, $\eta^2 = 0.995$, ** denotes $p < 0.01$; B,C. miR-29a-5p was shown to influence the ability of HCC cells to migrate and invade using transwell detection and wound healing assays (3 distinct repetitions, one-way analysis of variance (ANOVA); B. mimic: $p = 0.0055$; inhibitor: $p = 0.0016$; C. mimic: $p = 0.0205$; inhibitor: $p = 0.0460$; * and # denote $p < 0.05$; ** and ## denote $p < 0.01$)

OD – optical density; NC – negative control.

	Predicted consequential pairing of target region (top) and miRNA (bottom)	Site type	Context++ score	Context++ score percentile	Weighted context++ score	Conserved branch length	PCT
Position 2430-2437 of ARID2 3' UTR	5' ... GAUAAUGUCUUCUCAAAAUCAGA...	8mer	-0.12	86	0.00	0	N/A
hsa-miR-29a-5p	3' GACUUGUGUUUCUUUAGUCA						

Fig. 3. The complementary pairing sequences between miR-29a-5p and 3'-UTR of AT-rich interaction domain 2 (ARID2)

types of cells, including transcriptional regulation,³² cell cycle modulation,^{33,34} embryonic development,³⁵ and DNA damage repair.³⁶ The ARID2 mutations occur in most cancers, and this mutation usually results

in partial or complete inactivation of the ARID2 protein.^{37–39} The chromatin-remodeling complex can perform epigenetic regulation.⁴⁰ Similarly, ARID2 sometimes participates in DNA and histone regulation in epigenetic

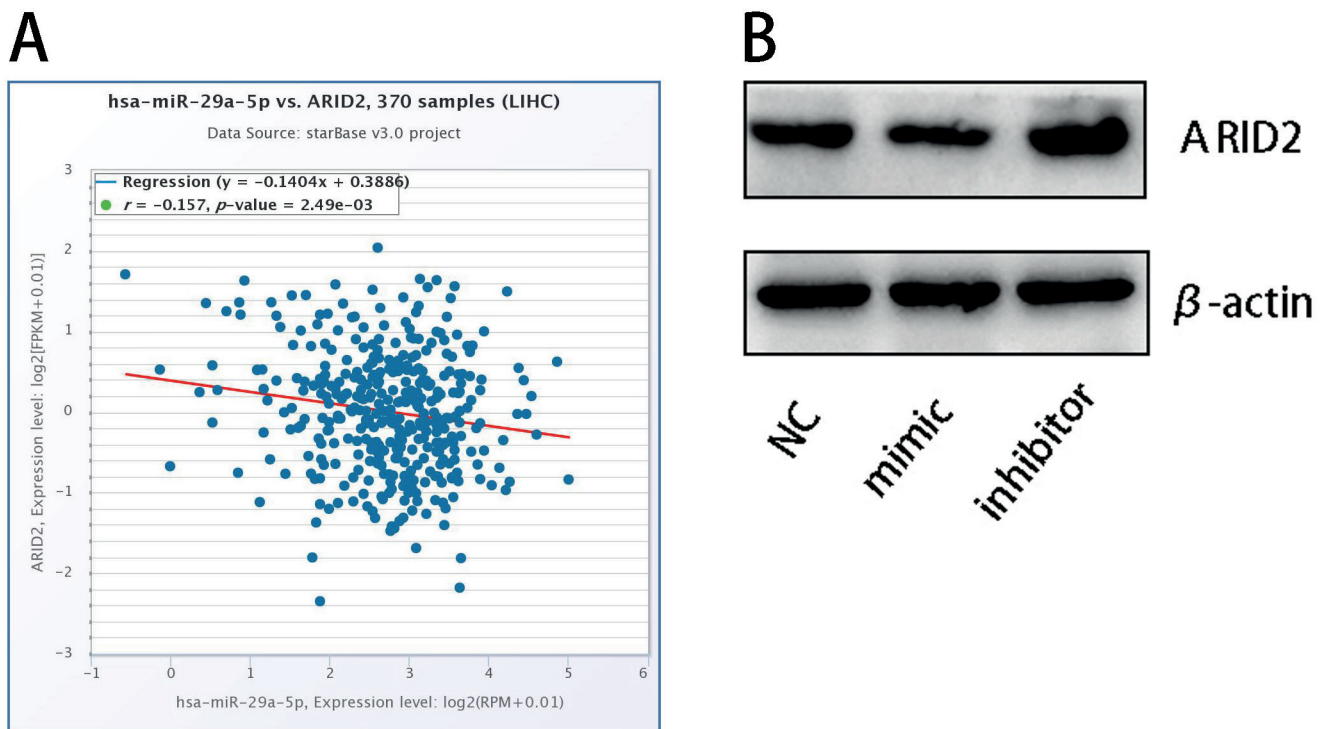


Fig. 4. A. Online prediction of the interaction between miR-29a-5p and AT-rich interaction domain 2 (ARID2); B. miR-29a-5p inhibitors or analogs were transfected into Huh-7 cells; miR-29a-5p negatively regulates ARID2 expression

NC – negative control.

regulation. Numerous studies have reported that ARID2 may become an antioncogene by regulating epigenetics, but its specific regulatory mechanism in tumors remains unknown.

The EMT regulates several malignant tumor behaviors, including proliferation, invasion and metastasis. In many cases, tumor migration and invasion are closely related to EMT, which refers to a specific morphologic transformation process in which an epithelial phenotype transforms into a mesenchymal phenotype, improving the ability of the cells to metastasize and invade. The key features of EMT are the reduced expression of cell adhesion molecules (such as E-cadherin), the transition from a cytokeratin to a Vimentin cytoskeleton, and the morphological properties of mesenchymal cells. Since EMT is a critical biological mechanism that enhances invasion and metastasis, identifying key molecules involved in this phenomenon is critical for studying the mechanism of tumor cell metastasis. Most notably, previous research has established that miRNAs play a critical role in EMT remodeling. Understanding the relationship between EMT-related miRNAs and cancer progression will benefit our clinical and basic research.

Limitations

We investigated the molecular mechanism of miRNA-29a-5p regulating the invasion and metastasis of liver cancer

cells in vitro. However, in vivo functional experiments are required in the future to more comprehensively demonstrate the regulatory role of miRNA-29a-5p in the invasion and metastasis of liver cancer. We should also collect clinical specimens for validation to combine our research with clinical trials. Another point is that the sample size used in our previous work is modest, and we may encounter difficulties in choosing the statistical analysis method. In the future experimental design, we may need to increase the sample size.

Conclusions

Our study demonstrated that miRNA-29a-5p was over-expressed in HCC cells. In vitro experiments further indicated that the downregulation of miRNA-29a-5p attenuated the ability of HCC cells to invade, migrate and proliferate. The miRNA-29a-5p promotes HCC progression by targeting ARID2 through EMT. Our study proved that miRNA-29a-5p could potentially be used as a biomarker and therapeutic target for HCC. Due to the regulatory role of miRNA-29a-5p in HCC, it is expected that miRNA can be used as an early diagnosis and prognostic indicator of HCC. The miRNA-29a-5p-ARID-EMT axis can regulate the metastasis and proliferation of HCC, and it is hoped that a new therapeutic strategy for HCC can be found through this pathway.

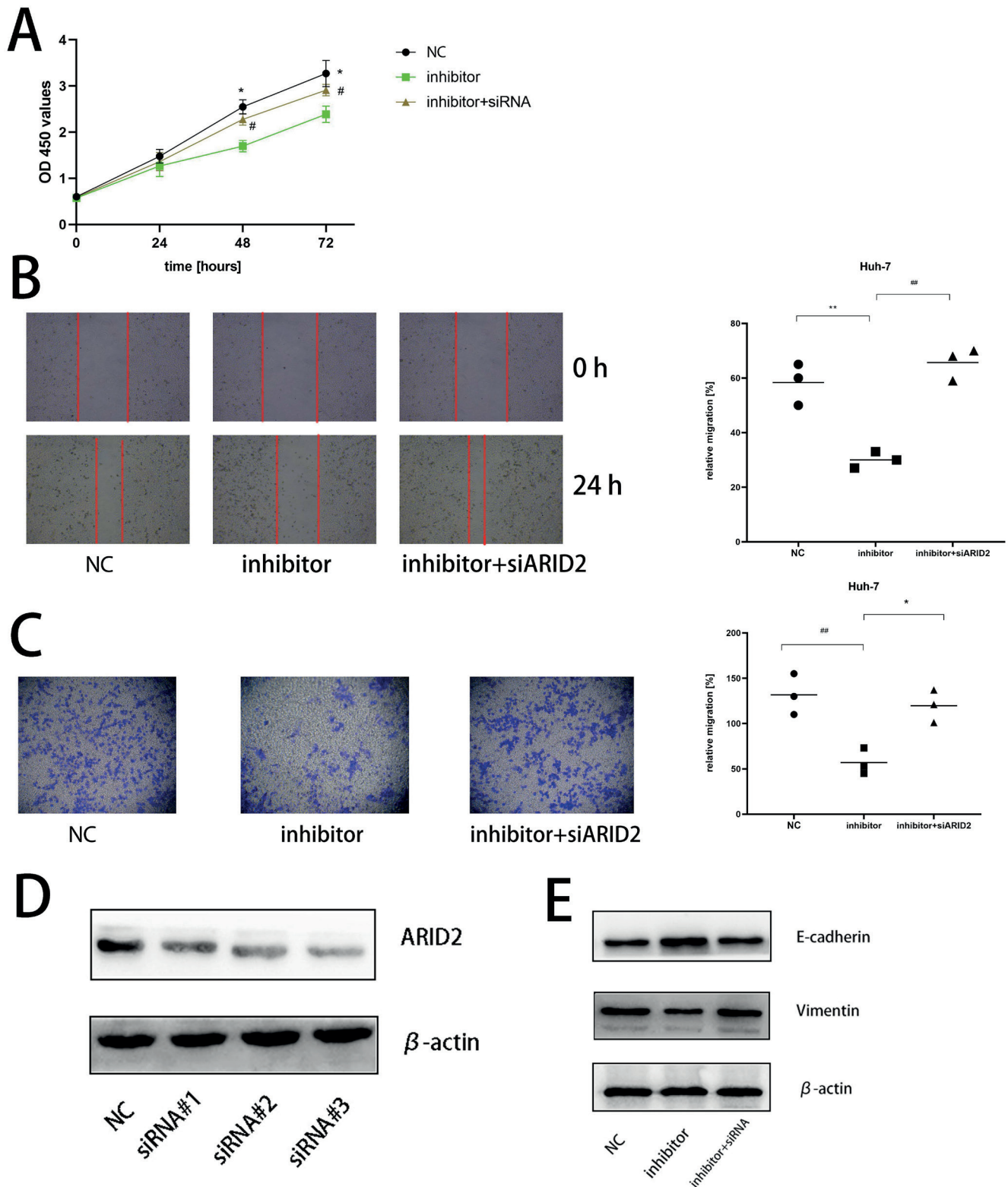






Fig. 5. A. miR-29a-5p knockdown inhibited the Huh-7 cells proliferation, while AT-rich interaction domain 2 (ARID2) silencing reversed its inhibition (Greenhouse–Geisser test, degrees of freedom (df) = 2.157, $F = 555.135$, $p < 0.0001$, $\eta^2 = 0.989$; * and # denote $p < 0.05$); B,C. miR-29a-5p knockdown inhibits the ability to invade and migrate, while *ARID2* gene silencing reverses them (3 distinct repetitions, one-way analysis of variance (ANOVA), B. negative control (NC): $p = 0.0020$; inhibitor+siARID2: $p = 0.0006$; C. NC: $p = 0.0054$; (inhibitor+siARID2) $p = 0.0124$; * denotes $p < 0.05$; ** and ## denote $p < 0.01$). D. Western blot analysis revealed that ARID2 was successfully silenced; E. After co-transfection with ARID2 siRNA, the epithelial–mesenchymal transition (EMT) ability of Huh-7 cells was enhanced

OD – optical density.

ORCID iDs

Wenke Li  <https://orcid.org/0000-0002-3794-4924>
 Yourang Jiang  <https://orcid.org/0000-0001-5350-5019>
 Qi Pan  <https://orcid.org/0000-0002-9498-1270>
 Guang Yang  <https://orcid.org/0000-0002-0096-6599>

References

- Torre LA, Bray F, Siegel RL, Ferlay J, Lortet-Tieulent J, Jemal A. Global cancer statistics, 2012. *CA Cancer J Clin.* 2015;65(2):87–108. doi:10.3322/caac.21262
- Llovet JM, Zucman-Rossi J, Pikarsky E, et al. Hepatocellular carcinoma. *Nat Rev Dis Primers.* 2016;2(1):16018. doi:10.1038/nrdp.2016.18
- Wang H, Lu Z, Zhao X. Tumorigenesis, diagnosis, and therapeutic potential of exosomes in liver cancer. *J Hematol Oncol.* 2019;12(1):133. doi:10.1186/s13045-019-0806-6
- Carr BI. Hepatocellular carcinoma: Current management and future trends. *Gastroenterology.* 2004;127(5):S218–S224. doi:10.1053/j.gastro.2004.09.036
- Llovet JM. Updated treatment approach to hepatocellular carcinoma. *J Gastroenterol.* 2005;40(3):225–235. doi:10.1007/s00535-005-1566-3
- Singal AG, El-Serag HB. Hepatocellular carcinoma from epidemiology to prevention: Translating knowledge into practice. *Clin Gastroenterol Hepatol.* 2015;13(12):2140–2151. doi:10.1016/j.cgh.2015.08.014
- Surgucheva I, Chidambaram K, Willoughby DA, Surguchov A. Matrix metalloproteinase 9 expression: New regulatory elements. *J Ocul Biol Dis Inform.* 2010;3(2):41–52. doi:10.1007/s12177-010-9054-2
- Surgucheva I, Gunewardena S, Rao HS, Surguchov A. Cell-specific post-transcriptional regulation of γ -synuclein gene by micro-RNAs. *PLoS One.* 2013;8(9):e73786. doi:10.1371/journal.pone.0073786
- Chang RM, Xiao S, Lei X, Yang H, Fang F, Yang LY. miRNA-487a promotes proliferation and metastasis in hepatocellular carcinoma. *Clin Cancer Res.* 2017;23(10):2593–2604. doi:10.1158/1078-0432.CCR-16-0851
- Dietrich P, Koch A, Fritz V, Hartmann A, Bosserhoff AK, Hellerbrand C. Wild type Kirsten rat sarcoma is a novel microRNA-622-regulated therapeutic target for hepatocellular carcinoma and contributes to sorafenib resistance. *Gut.* 2018;67(7):1328–1341. doi:10.1136/gutjnl-2017-315402
- Kabir TD, Ganda C, Brown RM, et al. A microRNA-7/growth arrest specific 6/TYRO3 axis regulates the growth and invasiveness of sorafenib-resistant cells in human hepatocellular carcinoma. *Hepatology.* 2018;67(1):216–231. doi:10.1002/hep.29478
- Mizuguchi Y, Takizawa T, Yoshida H, Uchida E. Dysregulated miRNA in progression of hepatocellular carcinoma: A systematic review. *Hepatol Res.* 2016;46(5):391–406. doi:10.1111/hepr.12606
- Morishita A, Masaki T. miRNA in hepatocellular carcinoma. *Hepatol Res.* 2015;45(2):128–141. doi:10.1111/hepr.12386
- Joshi P. MicroRNA in lung cancer. *World J Methodol.* 2014;4(2):59–72. doi:10.5662/wjm.v4.i2.59
- Yang J, Weinberg RA. Epithelial-mesenchymal transition: At the crossroads of development and tumor metastasis. *Dev Cell.* 2008;14(6):818–829. doi:10.1016/j.devcel.2008.05.009
- Serrano-Gomez SJ, Maziveyi M, Alahari SK. Regulation of epithelial-mesenchymal transition through epigenetic and post-translational modifications. *Mol Cancer.* 2016;15(1):18. doi:10.1186/s12943-016-0502-x
- Liao TT, Yang MH. Revisiting epithelial-mesenchymal transition in cancer metastasis: The connection between epithelial plasticity and stemness. *Mol Oncol.* 2017;11(7):792–804. doi:10.1002/1878-0261.12096
- Fischer KR, Durrans A, Lee S, et al. Epithelial-to-mesenchymal transition is not required for lung metastasis but contributes to chemoresistance. *Nature.* 2015;527(7579):472–476. doi:10.1038/nature15748
- Jafri MA, Al-Qahtani MH, Shay JW. Role of miRNAs in human cancer metastasis: Implications for therapeutic intervention. *Semin Cancer Biol.* 2017;44:117–131. doi:10.1016/j.semcancer.2017.02.004
- Zhu HT, Dong QZ, Sheng YY, et al. MicroRNA-29a-5p is a novel predictor for early recurrence of hepatitis B virus-related hepatocellular carcinoma after surgical resection. *PLoS One.* 2012;7(12):e52393. doi:10.1371/journal.pone.0052393
- Zhou J, Sun H, Wang Z, et al. Guidelines for the Diagnosis and Treatment of Hepatocellular Carcinoma (2019 Edition). *Liver Cancer.* 2020;9(6):682–720. doi:10.1159/000509424
- Faivre S, Rimassa L, Finn RS. Molecular therapies for HCC: Looking outside the box. *J Hepatol.* 2020;72(2):342–352. doi:10.1016/j.jhep.2019.09.010
- Jonas S. Vascular invasion and histopathologic grading determine outcome after liver transplantation for hepatocellular carcinoma in cirrhosis. *Hepatology.* 2001;33(5):1080–1086. doi:10.1053/jhep.2001.23561
- Zhou L, Rui JA, Wang SB, Chen SG, Qu Q. Clinicopathological predictors of poor survival and recurrence after curative resection in hepatocellular carcinoma without portal vein tumor thrombosis. *Pathol Oncol Res.* 2015;21(1):131–138. doi:10.1007/s12253-014-9798-2
- Zhang W, Kim R, Quintini C, et al. Prognostic role of plasma vascular endothelial growth factor in patients with hepatocellular carcinoma undergoing liver transplantation. *Liver Transpl.* 2015;21(1):101–111. doi:10.1002/lt.24013
- Raoul JL, Edeline J. Systemic treatment of hepatocellular carcinoma: Standard of care in China and elsewhere. *Lancet Oncol.* 2020;21(4):479–481. doi:10.1016/S1470-2045(20)30082-6
- Song T. Recent advances in surgical treatment of hepatocellular carcinoma. *Drug Discov Ther.* 2015;9(5):319–330. doi:10.5582/ddt.2015.01051
- Cheng CJ, Bahal R, Babar IA, et al. MicroRNA silencing for cancer therapy targeted to the tumour microenvironment. *Nature.* 2015;518(7537):107–110. doi:10.1038/nature13905
- Kriegel AJ, Liu Y, Fang Y, Ding X, Liang M. The miR-29 family: Genomics, cell biology, and relevance to renal and cardiovascular injury. *Physiol Genomics.* 2012;44(4):237–244. doi:10.1152/physiolgenomics.00141.2011
- Oliveira LH, Schiavinato JL, Fráguas MS, et al. Potential roles of micro RNA-29a in the molecular pathophysiology of T-cell acute lymphoblastic leukemia. *Cancer Sci.* 2015;106(10):1264–1277. doi:10.1111/cas.12766
- Ru P, Hu P, Geng F, et al. Feedback loop regulation of SCAP/SREBP-1 by miR-29 modulates EGFR signaling-driven glioblastoma growth. *Cell Rep.* 2017;18(4):1076–1077. doi:10.1016/j.celrep.2017.01.016
- Zhang X, Azhar G, Zhong Y, Wei JY. Zipzap/p200 is a novel zinc finger protein contributing to cardiac gene regulation. *Biochem Biophys Res Commun.* 2006;346(3):794–801. doi:10.1016/j.bbrc.2006.05.211
- Duan Y, Tian L, Gao Q, et al. Chromatin remodeling gene *ARID2* targets cyclin D1 and cyclin E1 to suppress hepatoma cell progression. *Oncotarget.* 2016;7(29):45863–45875. doi:10.18632/oncotarget.10244
- Zhang L, Wang W, Li X, et al. MicroRNA-155 promotes tumor growth of human hepatocellular carcinoma by targeting *ARID2*. *Int J Oncol.* 2016;48(6):2425–2434. doi:10.3892/ijo.2016.3465
- He L, Tian X, Zhang H, et al. BAF200 is required for heart morphogenesis and coronary artery development. *PLoS One.* 2014;9(10):e109493. doi:10.1371/journal.pone.0109493
- Oba A, Shimada S, Akiyama Y, et al. *ARID2* modulates DNA damage response in human hepatocellular carcinoma cells. *J Hepatol.* 2017;66(5):942–951. doi:10.1016/j.jhep.2016.12.026
- Cajuso T, Hänninen UA, Kondelin J, et al. Exome sequencing reveals frequent inactivating mutations in *ARID1A*, *ARID1B*, *ARID2* and *ARID4A* in microsatellite unstable colorectal cancer. *Int J Cancer.* 2014;135(3):611–623. doi:10.1002/ijc.28705
- Li M, Zhao H, Zhang X, et al. Inactivating mutations of the chromatin remodeling gene *ARID2* in hepatocellular carcinoma. *Nat Genet.* 2011;43(9):828–829. doi:10.1038/ng.903
- Hodis E, Watson IR, Kryukov GV, et al. A landscape of driver mutations in melanoma. *Cell.* 2012;150(2):251–263. doi:10.1016/j.cell.2012.06.024
- Hargreaves DC, Crabtree GR. ATP-dependent chromatin remodeling: Genetics, genomics and mechanisms. *Cell Res.* 2011;21(3):396–420. doi:10.1038/cr.2011.32

Hepatitis B virus X protein induces *p16* gene promoter methylation through upregulation of DNA methylation transferases DNMT1 and DNMT3A

*Weiqiang Gan^{1,B–F}, *Yanhong Kang^{2,B–F}, Yingjie Wu^{3,B,F}, Jianyun Zhu^{1,B,F}, Youming Chen^{1,C}, Jianyu Kuang^{1,B}, Jianguo Li^{1,A,F}, Lin Yang^{1,A,F}

¹ Department of Infectious Diseases, Third Affiliated Hospital of Sun Yat-Sen University, Guangzhou, China

² Department of Infectious Diseases, People's Hospital of Zhengzhou University, China

³ Department of Infectious Diseases, Seventh Affiliated Hospital of Sun Yat-Sen University, Shenzhen, China

A – research concept and design; B – collection and/or assembly of data; C – data analysis and interpretation;

D – writing the article; E – critical revision of the article; F – final approval of the article

Advances in Clinical and Experimental Medicine, ISSN 1899–5276 (print), ISSN 2451–2680 (online)

Adv Clin Exp Med. 2023;32(5):583–592

Address for correspondence

Lin Yang

E-mail: linyang1962@163.com

Funding sources

This study was funded by the National Natural Science Foundation of China (grant No. 81071409).

Conflict of interest

None declared

*Weiqiang Gan and Yanhong Kang contributed equally to this work.

Received on December 8, 2021

Reviewed on May 28, 2022

Accepted on November 17, 2022

Published online on December 8, 2022

Cite as

Gan W, Kang Y, Wu Y, et al. Hepatitis B virus X protein induces *p16* gene promoter methylation through upregulation of DNA methylation transferases DNMT1 and DNMT3A [published online as ahead of print on December 8, 2022].

Adv Clin Exp Med. 2023;32(5):583–592.

doi:10.17219/acem/156644

DOI

10.17219/acem/156644

Copyright

Copyright by Author(s)

This is an article distributed under the terms of the Creative Commons Attribution 3.0 Unported (CC BY 3.0) (<https://creativecommons.org/licenses/by/3.0/>)

Abstract

Background. As a tumor suppressor, *p16* can competitively block the cyclin D1-CDK4/6 complex to arrest the cell cycle in the G1 phase. Lack of *p16* gene expression can lead to infinite cell proliferation and malignant transformation.

Objectives. To determine whether the hepatitis B virus X protein (HBx) regulates the methylation and expression of the *p16* gene.

Materials and methods. We constructed a eukaryotic expression vector carrying the *HBx* gene and green fluorescent protein (GFP), and transfected it into HepG2 cells to build cell lines stably expressing GFP and GFP-HBx. The *p16* protein level and *p16* gene methylation were measured in these cell lines. We further detected the mRNA expression of DNA methyltransferases (DNMTs) 1, 3A and 3B. The *DNMT1*, *DNMT3A* and *DNMT3B* gene promoter sequences were inserted into a reporter vector (pGL3-Basic) to build recombinant vectors, which were then transiently transfected into different cell lines. After 48 h, the luciferase activity was measured.

Results. The level of *p16* protein in GFP-HBx/HepG2 cells was significantly lower than in HepG2 and GFP/HepG2 cells. The CpG methylation was present in the *p16* gene promoter region of GFP-HBx/HepG2 cells. The DNMT1 and DNMT3A mRNA levels in GFP-HBx/HepG2 cells were significantly elevated compared to that in the HepG2 cells ($p = 0.0495$). The luciferase activity in GFP-HBx/HepG2 cells transfected with the pGL3-DNMT1/3A pro plasmid was significantly higher than in HepG2 and GFP/HepG2 cells (both $p < 0.05$).

Conclusions. The HBx can induce *p16* gene promoter methylation and inhibit the expression of *p16* in HepG2 cells. This occurs due to HBx activation of DNMT1 and DNMT3A promoters and the induction of *p16* promoter methylation, which downregulates the expression of *p16* protein.

Key words: DNA methylation, *p16*, hepatitis B X protein, DNA methylation transferase

Background

Hepatocellular carcinoma (HCC) is one of the most common malignant tumors in the world. Chronic hepatitis B virus (HBV) infection is the main risk factor for HCC. There are about 296 million HBV-infected persons around the world and approx. 820,000 deaths in this group every year.¹ The risk of HCC is significantly higher in hepatitis B surface antigen (HBsAg)-positive individuals than in uninfected persons. In China, 80% of HCC cases are related to HBV infection.² Hepatitis B virus is the smallest double-stranded DNA virus known to infect humans, and it has been discovered that hepatitis B virus X protein (HBx) plays an important role in the development and progression of HBV-related HCC.^{3–5}

Tumor suppressor gene *p16* is an important cell cycle negative regulatory factor, and lack of *p16* gene expression can lead to infinite cell proliferation and malignant transformation.⁶ Studies have shown that there is a correlation between the regulation of *p16* gene expression and HBx.⁷ There are currently 2 proposed mechanisms how HBx regulates the expression of *p16*. One is that HBx can induce *p16* mutation, which leads to loss of heterozygosity and of expression.⁸ The other is that HBx can activate various transcription factors and signal pathways through transactivation; this process can abnormally activate the enzyme system regulating DNA methylation, induce hypermethylation of the tumor suppressor gene and downregulate its expression.⁹ Recent studies have shown that HBx is a very effective epigenetic modifier that can induce methylation and inactivation of the promoters of tumor suppressor genes, including *p53*, *PTEN* and *E-cadherin*, and this is closely related to the development and progression of HBV-related HCC.^{10,11}

As a transactivator, HBx can combine many factors related to transcription and gene regulation. The DNA methylation is maintained under the action of DNA methyltransferase (DNMT). Currently, 3 DNMTs that exhibit transmethylation activity have been identified: DNMT1, DNMT3A and DNMT3B. The main function of DNMT1 is to maintain methylation. The DNMT3A and DNMT3B interact to cause *de novo* methylation of DNA sequences. At present, the role of HBx transactivation with respect to DNMTs is unclear. Jung et al. reported that HBx can upregulate the expression of DNMT1 and DNMT3A, which induce methylation of the retinoic acid receptor (RAR) β -promoter and thus inhibit its expression.¹² The inhibition of its expression results in a failure of the tumor suppressor protein RA to combine with RAR- β , which results in the malignant transformation of hepatocytes.¹² In our prior work, we reported that HBx upregulates DNMT1 and DNMT3A mRNA and protein expression; however, the underlying molecular mechanism of this effect is unclear.¹³

Objectives

The current study aims to investigate the molecular mechanism underlying HBx regulates the expression of the *p16* gene and if HBx regulates *p16* expressions indirectly through methylation.

Materials and methods

Plasmid construction

The pHBV plasmid containing 1.3 copies of the HBV genome (adr serum type) that can cause the development of HBV virus particles was previously developed by our group and is maintained in our laboratory. Green fluorescent protein (GFP) eukaryotic expression vector pEGFP-C1 was purchased from Biotech Company (Bergisch Gladbach, Germany). The pGL3-Basic and pRL-TK vectors were purchased from Promega (Madison, USA). To construct the pEGFP-HBx recombinant plasmid, the *HBx* gene was amplified using the pHBV plasmid as a template and then cloned into the BglII and KpnI sites of the pEGFP-C1 vector. To construct the pGL3-DNMT1 pro-recombinant plasmid, a human DNMT1 promoter sequence (ENST00000340748)¹⁴ was amplified from normal human genomic DNA (BioChain, Newark, USA), and then cloned into the XhoI and HindIII sites of the pGL3-Basic vector. To construct pGL3-DNMT3A/B pro-recombinant plasmids, human DNMT3A and DNMT3B promoter sequences (ENST00000264709, ENST00000328111)^{15,16} were amplified and cloned into the KpnI and BglII sites of the pGL3-Basic vector.

Primers used for all of the constructs are shown in Table 1. All constructs were confirmed using 1.2% agarose gel electrophoresis (Biowest, Nuaille, France) and DNA sequencing (Takara, Kusatsu, Japan).

Cell cultures and transfections

The human hepatoma cell line HepG2 was maintained in our laboratory. The HepG2 cell line was propagated and maintained in Dulbecco's modified Eagle's medium (DMEM) (Gibco, Waltham, USA) supplemented with 10% fetal bovine serum (FBS) (HyClone, Logan, USA). Cultures were incubated in a humidified atmosphere at 37°C with 5% CO₂.

All transfections were performed with Lipofectamine™ 2000 Reagent (Invitrogen, Carlsbad, USA), according to the manufacturer's recommendations. Transfected cells were observed with an inverted fluorescence microscope (Nikon Eclipse TS100/100F; Nikon Corp., Tokyo, Japan) 6 h after transfection.

Table 1. Primers used in the construction of plasmids and RT-PCR

Use	Primer name	Sequence (5'–3')
Construction of pGFP-HBx	pHBx forward	GGAAGATCTATGGCTGCTAGGGTGTGCTG
	pHBx reverse	CGGGGTACCTTAGGCAGAGGTGAAAAAGT
RT-PCR for HBx	HBx forward	ATGGCTGCTAGGGTGTGCTG
	HBx reverse	TTAGGCAGAGGTGAAAAAGT
RT-PCR for GAPDH	GAPDH forward	CATCACCATCTTCCAGGAGCGAG
	GAPDH reverse	GTGCTCAGTGTAGCCAGGATGC
Methylation-specific PCR	p16-m forward	AGAGGGTGGGGCGGATCG
	p16-m reverse	CTACCCGACCCCGAACCCG
Non-methylation-specific PCR	p16-nm forward	GTTATTAGAGGGTGGGGTGGATTG
	p16-nm reverse	CCTCTACCCAACCCCAACCA
RT-qPCR for DNMT1	DNMT1 forward	GCCAACGAGTCTGGCTTTGAG
	DNMT1 reverse	GTGTCGATGGGACACAGGTGA
RT-qPCR for DNMT3A	DNMT3A forward	GCATCCACTGTGAATGATAAGC
	DNMT3A reverse	GGTCTTTGCCCTGCTTTATG
RT-qPCR for DNMT3B	DNMT3B forward	CCAACAACACGCAACCAG
	DNMT3B reverse	GCTCTGATCTTCATCCCTC
RT-qPCR for GAPDH	qGAPDH forward	GCACCGTCAAGGCTGAGAAC
	qGAPDH reverse	TGGTGAAGACGCCAGTGA
Construction of pGL3-DNMT1 pro	DNMT1pro forward	CCGCTCGAGGCATGGGCCTTATACACTGTG
	DNMT1pro reverse	CCCAAGCTTCCAGGGAGCTACGGGGAAAT
Construction of pGL3-DNMT3A pro	DNMT3Apro forward	CACGGTACCCTACTTGGACACCTCAAGGTA
	DNMT3Apro reverse	GAAGATCTCGCTCATTACCGTATGGCCG
Construction of pGL3-DNMT3B pro	DNMT3Bpro forward	CACGGTACCGGCTGGAACCCAGGTAGCCA
	DNMT3Bpro reverse	AGAAGATCTCACCTGCCGAGGGCTGGCT

GFP – green fluorescent protein; HBx – hepatitis B virus X protein; DNMT – DNA methylation transferases; RT-qPCR – reverse transcription quantitative polymerase chain reaction; GAPDH – glyceraldehyde 3-phosphate dehydrogenase.

Screening of stably transfected cell lines – G418 (geneticin) screening experiment

The HepG2 cells (2000 cells/mL) were placed in 96-well plates. The G418 was added on days 1, 2, 3, and 4, respectively, at concentrations of 0, 200, 400, 600, 800, and 1000 µg/mL. At 20 days of culture, the lowest concentration that resulted in the death of all cells was 600 µg/mL. Therefore, 800 µg/mL was selected for day 2 screening. The HepG2 cells were transfected with pEGFP-HBx, and after 24 h of transfection the culture medium was removed, the cells were washed with phosphate-buffered saline (PBS) 3 times, treated with trypsin, and centrifuged at 1500 rpm for 5 min. The G418 (800 µg/mL) was added to 5 mL of complete DMEM culture medium and placed in a 25-mL ventilated culture bottle; the solution was changed daily. The HepG2 cells transfected with empty vector pEGFP-C1 were used as a control. The 800 µg/mL concentration of G418 was screened for 20 days.

An inverted fluorescence microscope (Nikon Eclipse TS100/100F) was used to visualize monoclonal cells expressing GFP. The cells were washed 3 times with PBS and treated with trypsin. Under microscopic visualization, the monoclonal cells were carefully aspirated with a pointed pipette and placed into a 25-mL ventilated

culture bottle. Complete DMEM with a G418 concentration of 800 µg/mL was added, and after the culture bottle was full of cell clones, it was amplified in vitro. The cells were named GFP/HepG2 (transfected with pEGFP-C1) and GFP-HBx/HepG2 (transfected with pEGFP-HBx).

Reverse transcription polymerase chain reaction (RT-PCR)

The RNA was isolated from harvested cells using an RNA Isolation Kit (TianGen, Beijing, China), according to the manufacturer's instructions. The cDNA was then synthesized from the RNA using a PrimeScript® RT Reagent Kit with gDNA Eraser (Takara). Polymerase chain reaction was performed at 95°C for 5 min, followed by 35 cycles of 98°C for 10 s, 68°C for 10 s, and 72°C for 5 min. The subsequent PCR products were visualized with 1.2% agarose gel electrophoresis.

An SYBR® Premix ExTaq™ II Kit (Takara) was used to perform quantitative PCR (qPCR) of human DNMT1, DNMT3A and DNMT3B. Glyceraldehyde 3-phosphate dehydrogenase (GAPDH) was used for normalization. The primers are shown in Table 1. The PCR conditions were 95°C for 30 s, followed by 40 cycles of 95°C for 5 s and then 60°C for 20 s.

Methylation-specific PCR (MSP)

The promoter sequence of the human *p16* gene (ENST000004494) was obtained University of California Santa Cruz Genome Browser (<http://genome.ucsc.edu>). The CpG islands were predicted using MetaPrime (Supplementary Figure 1). Methylation and non-methylation primers were designed using the Methyl Primer Express v. 1.0 software (Applied Biosystems Inc., Carlsbad, USA), MethPrimer (<http://www.urogene.org/methprimer/>), Primer Premier 5.0 (PREMIER Biosoft, San Francisco, USA), and Oligo 7.0 (Molecular Biology Insights, Inc., Cascade, USA) (Table 1). Methylation-specific PCR was conducted using an EpiTect MSP Kit (Qiagen, Hilden, Germany), according to the manufacturer's instructions. The PCR conditions were 95°C for 10 min, followed by 40 cycles of 94°C for 15 s, 55°C for 30 s, 72°C for 30 s, and 72°C for 10 min. The subsequent PCR products were visualized using 1.2% agarose gel electrophoresis.

Western blotting

The M-PER™ Mammalian Protein Extraction Reagent (Pierce, Rockford, USA) was used to extract the total protein from the transfected cells, and protein concentration was determined using BCA Protein Assay Reagent A (Pierce) according to the manufacturer's instruction. Proteins were separated with 10% sodium dodecyl-sulfate polyacrylamide gel electrophoresis (SDS-PAGE), transferred to nitrocellulose membranes, and then detected using the appropriate antibodies, with 12 h incubation time for primary antibody and 2 h for secondary antibody. Rabbit anti-GAPDH was purchased from Xianzhi Company (Guangzhou, China), anti-HBx was purchased from Santa Cruz Biotechnology (Dallas, USA) and anti-p16 was purchased from Cell Signaling Technology (Danvers, USA).

Determination of DNMT1, DNMT3A and DNMT3B gene promoter activity

The stably transfected cells GFP/HepG2, GFP-HBx/HepG2 and HepG2 were transiently transfected with pGL3-DNMT1

pro, pGL3-DNMT3A pro, pGL3-DNMT3B pro, and pGL3-Basic (control) together with the Renilla luciferase plasmid phRL-tk. The double-luciferase reporter assay system (Promega) was used to detect the activity of luciferase.

Statistical analyses

With a limited sample size (3–9), the assumption of normality was not adopted to the continuous variables in this study, and only nonparametric statistical tests were used. For all comparisons among HepG2, GFP/HepG2 and GFP-HBx/HepG2 groups, the results were indicated using a dot-plot with medians, and the significance was tested using the Kruskal–Wallis test and Dunn's test with Bonferroni adjustment as post hoc test. The Mann–Whitney U test was used in the comparison between the 2 groups. The detailed statistics, p-value, sample size, and testing method were reported in Supplementary Tables. All analyses were done using IBM SPSS v. 25 software (IBM Corp., Armonk, USA). The statistical significance level for all the tests was set at a p 0.05 (two-tailed).

Results

Construction and identification of the pEGFP-HBx eukaryotic expression vector

Based on the designed target gene primers, the *HBx* gene fragment was approx. 470 bp long and this finding was consistent with the prediction (Fig. 1A). The recombinant plasmid pEGFP-HBx was treated with rapid restriction endonucleases BglI and KpnI. The products were subjected to 1% agarose gel electrophoresis, and the empty plasmid (pEGFP-C1) was used as a control. The DNA bands of 4700 bp were observed for both, while a DNA band of 470 bp was only observed for the recombinant vector (Fig. 1B). Sequencing results of the recombinant plasmid confirmed that HBx was inserted between the BglII and KpnI digestion sites of the pEGFP-C1 empty vector. Blast homology comparison using the National Center for Biotechnology Information (NCBI) database showed that

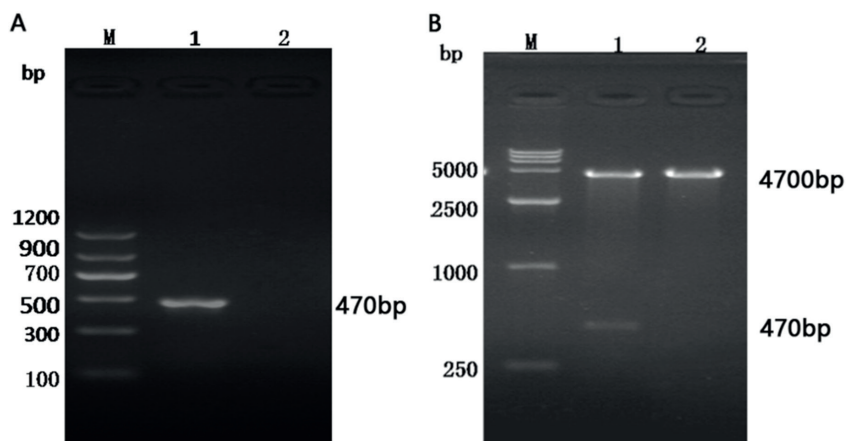


Fig. 1. Gel electrophoresis. A. Polymerase chain reaction (PCR) product of hepatitis B virus X protein (*HBx*) gene (470 bp). M – marker, 1 – *HBx* gene cDNA, 2 – negative control; B. Plasmids treated with BglII and KpnI. M – marker, 1 – pEGFP-HBx, 2 – pEGFP-C1

the *HBx* gene was forwardly connected to the pEGFP-C1 eukaryotic vector, and was named pEGFP-HBx for this study.

Construction of pGL3-DNMTs pro-recombinant plasmids

The electrophoresis showed a band of approx. 850 bp for DNMT1, 1000 bp for DNMT3A and 900 bp for DNMT3B, which implied that the amplification was successful (Fig. 2A,B). The digestion of the pGL3-DNMT pro-recombinant plasmids by relative restriction endonucleases showed a size of 850 bp for DNMT1, 1000 bp for DNMT3A and 900 bp for DNMT3B, indicating that the connections were successful (Fig. 2C,D). The sequence analysis of the recombinant plasmids confirmed that the DNMT1, DNMT3A and DNMT3B promoters were positively inserted into the pGL3-Basic vector, and were respectively named pGL3-DNMT1 pro, pGL3-DNMT3A pro and pGL3-DNMT3B pro.

Establishment of HepG2 cell lines stably expressing GFP and GFP-HBx protein

The HepG2 cells were transfected with pEGFP-C1 or pEGFP-HBx and screened for about 20 days with

G418. All HepG2 cells in the blank control died. Resistant cell clones were observed in the pEGFP-C1 and pEGFP-HBx plasmid transfection groups. Cell clones expressing GFP were carefully selected under the inverted fluorescence microscope. Cells stably expressing GFP were screened out under white light and fluorescence, and named GFP/HepG2 and GFP-HBx/HepG2, respectively (Fig. 3).

Detection of *HBx* gene expression using RT-PCR and western blotting

Reverse transcription polymerase chain reaction was used to detect the expression of *HBx* based on the mRNA isolated from the different stable cell lines. The results showed that the gene fragments of GFP-HBx/HepG2 cells were the expected size, while the RT-PCR products of HepG2 and GFP/HepG2 cells exhibited no bands on electrophoresis, indicating that *HBx* gene transcription was present in GFP-HBx/HepG2 cells (Fig. 4A). The detection of *HBx* protein expression in stably transfected cells using western blotting showed that *HBx* could be detected in GFP-HBx/HepG2 cells but not GFP/HepG2 or HepG2 cells (Fig. 4B).

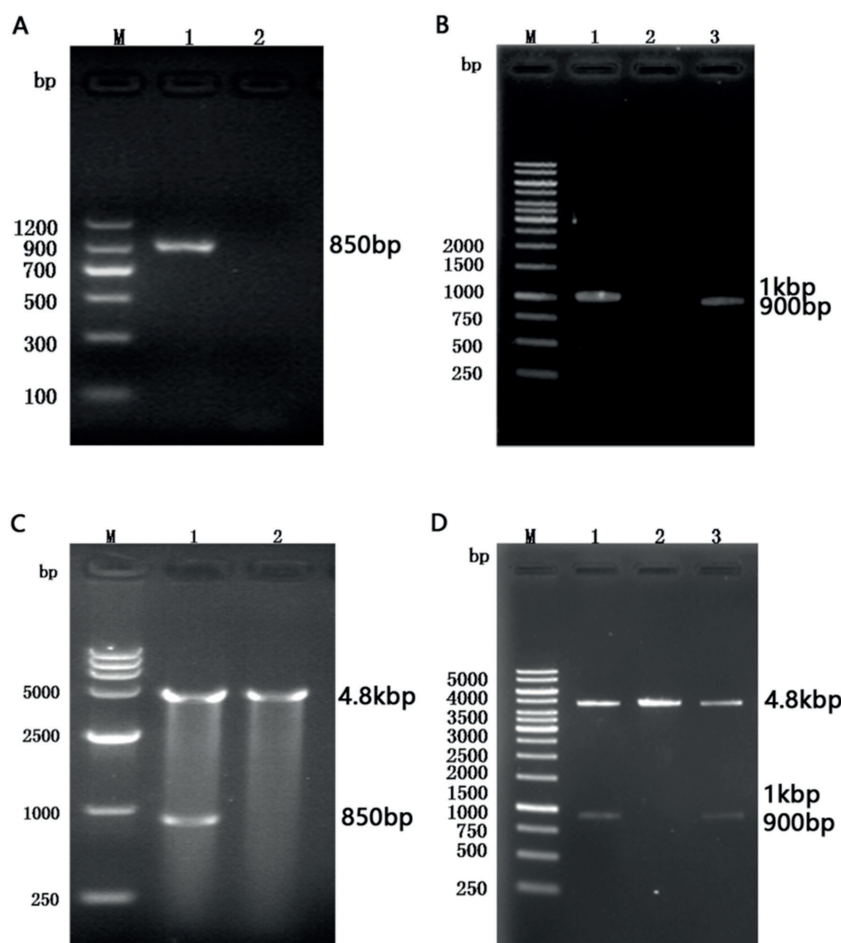


Fig. 2. Gel electrophoresis. A. Polymerase chain reaction (PCR) product of DNMT1 promoter. M – marker, 1 – DNMT1 promoter cDNA, 2 – negative control; B. PCR product of DNMT3A and DNMT3B promoters. M – marker, 1 – DNMT3A promoter cDNA, 2 – negative control, 3 – DNMT3B promoter cDNA; C. Plasmids treated using western XhoI and HindIII. M – marker, 1 – pGL3-DNMT1 pro, 2 – pGL3-Basic; D. Plasmids treated using western KpnI and BglII. M – marker, 1 – pGL3-DNMT3A pro, 2 – pGL3-Basic, 3 – pGL3-DNMT3B-pro

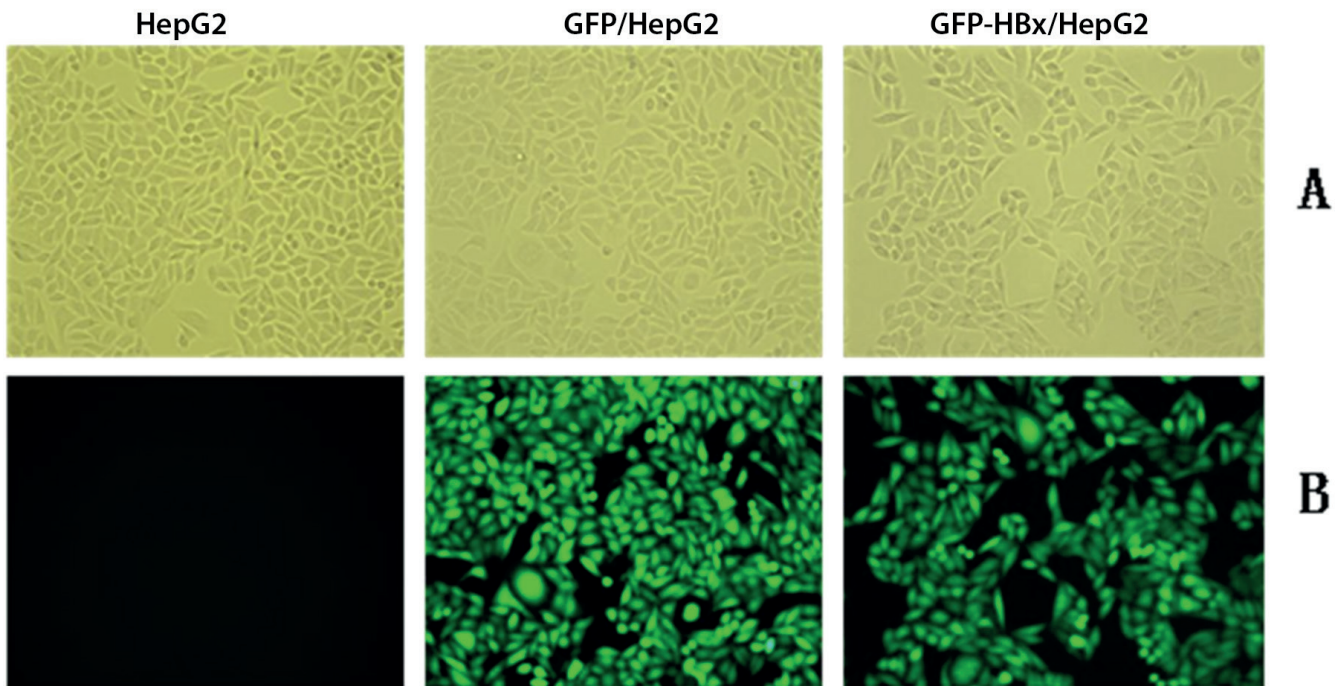


Fig. 3. HepG2 cells stably expressing green fluorescent protein (GFP) and GFP-hepatitis B virus X protein (HBx) fusion protein. A. Light microscopy ($\times 200$ magnification); B. Fluorescence microscopy ($\times 200$ magnification)

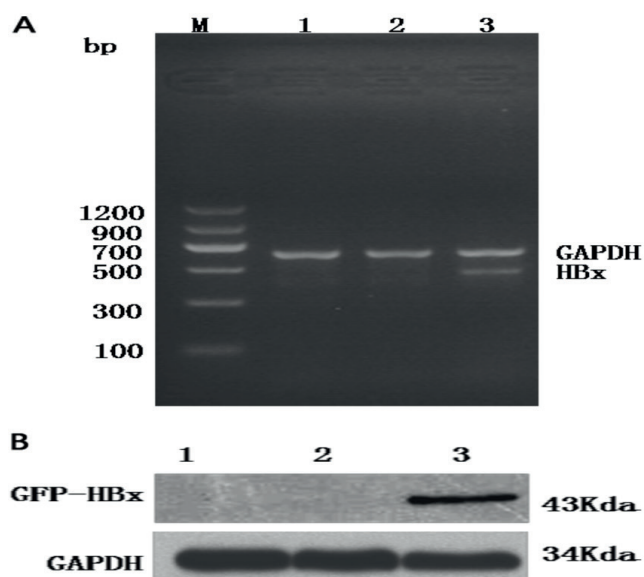


Fig. 4. A. Detection of hepatitis B virus X protein (HBx) gene mRNA with gel electrophoresis. M – marker, 1 – HepG2, 2 – green fluorescent protein (GFP)/HepG2, 3 – GFP-HBx/HepG2; B. Detection of HBx with western blotting. 1 – HepG2, 2 – GFP/HepG2, 3 – GFP-HBx/HepG2

GAPDH – glyceraldehyde 3-phosphate dehydrogenase; HBx – hepatitis B virus X protein.

p16 protein levels in different cell types

After the Kruskal–Wallis test, no significant difference of p16 relative gray value was found among HepG2, GFP/HepG2 and GFP-HBx/HepG2 groups (as indicated in Supplementary Table 1,2). However, the level of p16 protein in GFP-HBx/HepG2 cells was significantly lower than in GFP/HepG2 cells and HepG2 cells ($p = 0.049$, $p = 0.049$)

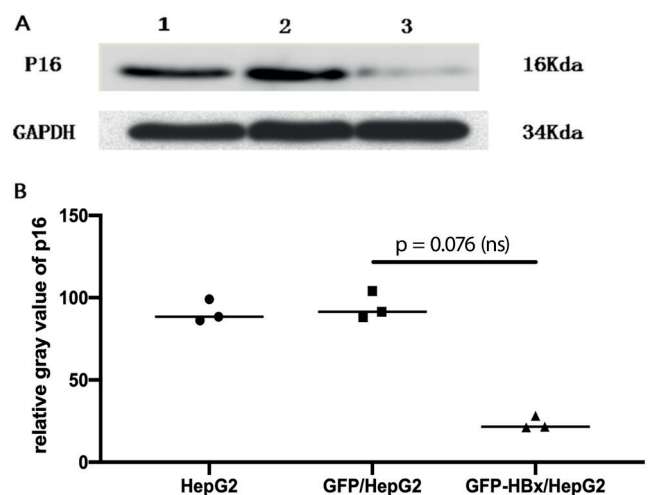


Fig. 5. A. Detection of p16 protein with western blotting. 1 – HepG2; 2 – green fluorescent protein (GFP)/HepG2; 3 – GFP-HBx/HepG2; B. Relative gray value of p16; * $p < 0.05$

GAPDH – glyceraldehyde 3-phosphate dehydrogenase; HBx – hepatitis B virus X protein.

in separate Mann–Whitney U tests, while there was no significant difference in the p16 protein level between GFP/HepG2 and HepG2 cells (Fig. 5A,B). Since the authors believe that the differences in p16 protein levels were worthy of interpretation, both the Kruskal–Wallis test and the Mann–Whitney U test results were reported.

The methylation products and demethylation products in the promoter region of the *p16* gene were detected with MSP. Only the demethylation products were amplified in HepG2 cells and GFP/HepG2 cells, while both the demethylation and methylation products were amplified

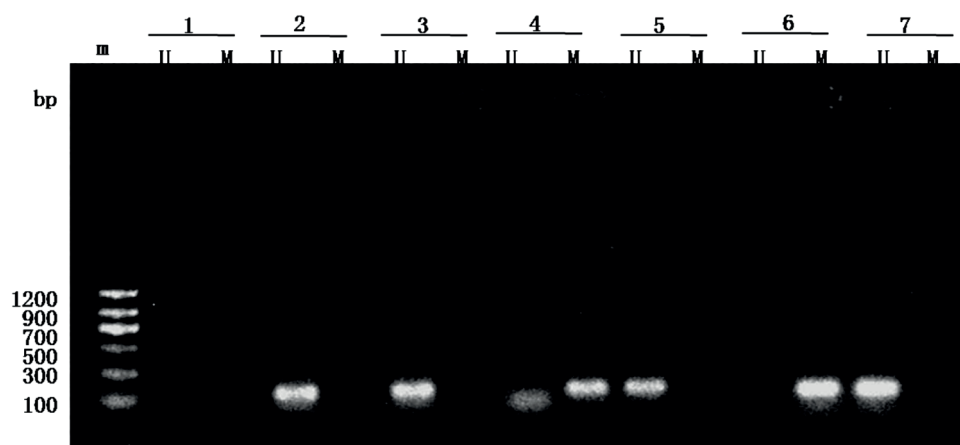


Fig. 6. Gel electrophoresis. Detection of p16 promoter methylation using methylation-specific polymerase chain reaction (MSP). m – marker; M – methylation polymerase chain reaction (PCR), U – demethylation polymerase chain reaction (PCR); 1 – negative control; 2 – HepG2; 3 – green fluorescent protein (GFP)/HepG2; 4 – GFP-HBx/HepG2; 5 – GFP-HBx/HepG2 plus 5-Aza-2'-DC (20 μmol/L for 3 days); 6 – methylation positive control; 7 – demethylation positive control

in GFP-HBx/HepG2 cells (Fig. 6). Methylation products were not detected in GFP-HBx/HepG2 cells 3 days after the addition of 5-Aza-2'-deoxycytidine (20 μmol/L) (Fig. 6).

The impact of HBx on the transcription of DNMTs

The expression level of DNMT mRNA in HepG2 cells was set at 1.00. The expressions of DNMT1 and DNMT3A mRNA in GFP-HBx/HepG2 cells were significantly higher than in the GFP/HepG2 cells ($p = 0.0495$), while there was no difference in DNMT3B mRNA ($p > 0.05$) (Fig. 7). Detailed statistics and p-values were reported in Supplementary Table 3.

Impact of HBx on DNMT promoter activity

The relative activity of luciferase in each group was compared among the different cell lines transfected with different plasmids. The activity of luciferase in HepG2 cells transfected with pGL3-Basic was set at 1.0. There was no statistical difference in luciferase activity among the 3 blank groups transfected with the pGL3-Basic vector. The relative luciferase activity in GFP-HBx/HepG2 cells transfected with the pGL3-DNMT1 pro and pGL3-DNMT3A pro plasmids was significantly higher than in the GFP/HepG2 and HepG2 cells ($p < 0.05$). There was no difference in activity among the 3 groups when transfected with pGL3-Basic or pGL3-DNMT3B plasmids (the relative activity was transformed using log10 to level down the disparity of scale) (Fig. 8 and Supplementary Table 1,2).

Discussion

In this study, we found that HBx can induce *p16* gene promoter methylation and inhibit the expression of the *p16* gene. Importantly, the results showed that the mechanism by which HBx regulates the expression of the *p16* gene is through the upregulation of DNMT1 and DNMT3A

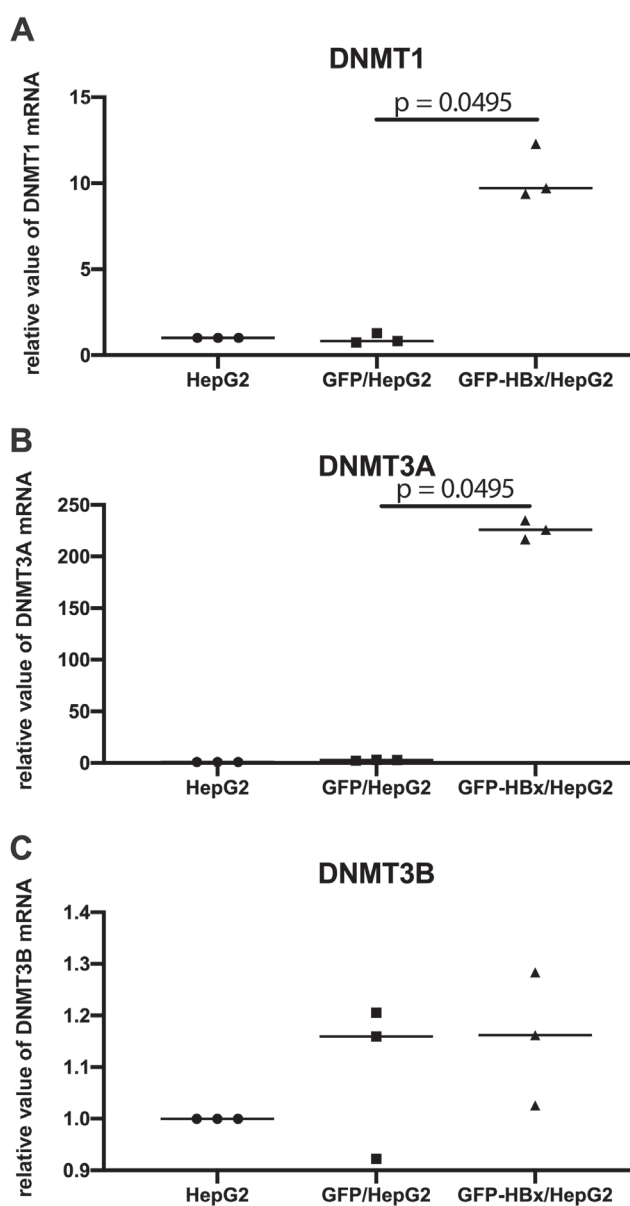


Fig. 7. A. Detection of DNMT1 mRNA using real-time polymerase chain reaction (PCR); B. Detection of DNMT3A mRNA using real-time PCR; C. Detection of DNMT3B mRNA using real-time PCR; * $p < 0.05$ compared with the other 2 groups

GFP – green fluorescent protein; HBx – hepatitis B virus X protein.

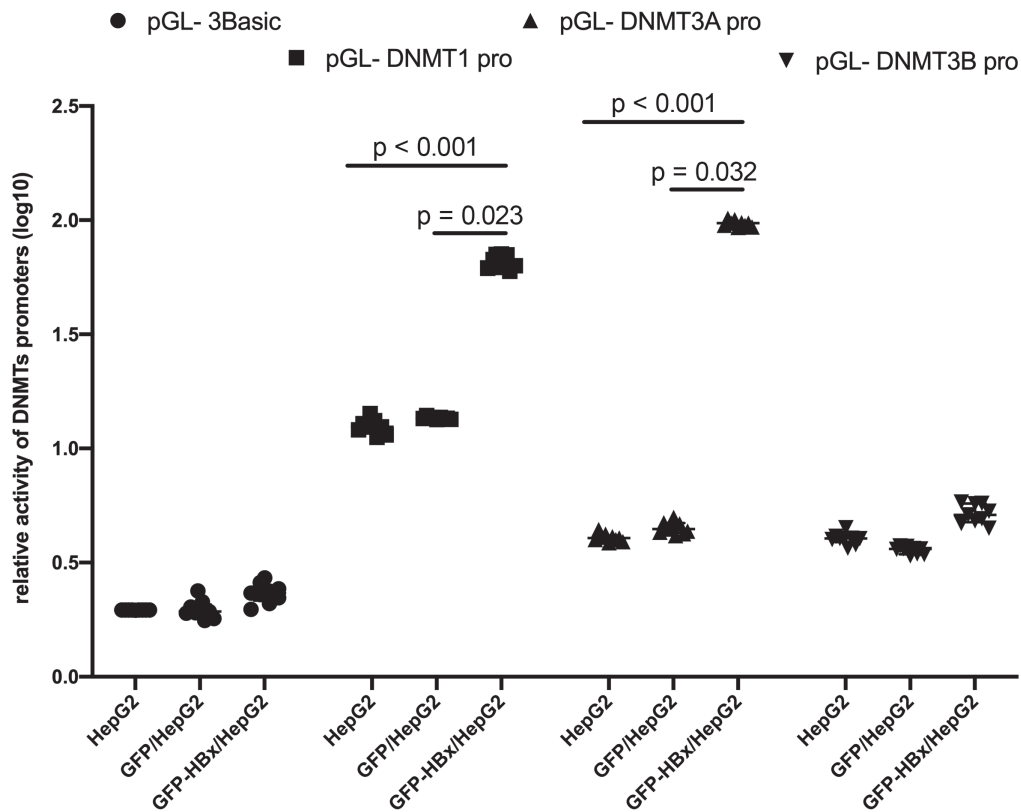


Fig. 8. Detection of luciferase activity among different cell lines transfected with different plasmids. The relative activity was transformed using log₁₀ to level down the disparity of scale; *p < 0.05

DNMTs – DNA methylation transferases.

gene promoter activity, which enhances their transcription and expression. The DNMT1 and DNMT3A belong to a family of DNA methyltransferase enzymes that catalyze the transfer of methyl groups to specific CpG structures in DNA, alter chromatin structure and regulate gene expression.¹⁷ This subsequently results in methylation of the *p16* gene promoter and the downregulation of gene expression.

The *HBx* gene is the smallest and most conservative gene among the 4 open reading frames of the HBV genome.¹⁸ The *HBx* can activate a variety of oncogenes and transcription factors, including C-myc, AP-1, NF- κ B, and AP-2.¹⁸ The *HBx* is involved in tumor cell metabolism, proliferation, apoptosis, invasion, and metastasis.^{19,20} Current research has also suggested that HBx is an effective epigenetic modifier, which may activate various transcription factors via transactivation, and downregulate the expression of tumor suppressor genes by hypermethylation.

The fusion expression of an exogenous target protein and GFP can facilitate real-time monitoring and intracellular localization of a target gene²¹; hence, GFP expression of the pEGFP-C1 vector was used in this study. The *HBx* gene was inserted into pEGFP-C1 to construct the recombinant plasmid pEGFP-HBx. The pEGFP-C1 empty vector and pEGFP-HBx were transfected into the human hepatic carcinoma cell line HepG2. The results showed that both transfected cells effectively expressed GFP. After G418 screening, HepG2 cells with stable expression of GFP and GFP-HBx were obtained, and after 40 generations of culture, the cells still expressed strong fluorescence.

The RT-PCR and western blotting showed that HepG2 cells transfected with pEGFP-HBx expressed the *HBx* gene. These results showed that HepG2 cell lines stably expressing GFP and GFP-HBx fusion protein were successfully established, and provided a platform for subsequent studies.

As the most important negative regulator of the cell cycle, tumor suppressor gene *p16* regulates cell growth and differentiation by binding and inhibiting cell cycle-dependent protein kinases CDK4 and CDK6, and reduces retinoblastoma protein phosphorylation. The loss of *p16* gene expression can cause infinite cell proliferation and induce malignant transformation of cells. Our results showed that there was a significant negative correlation between *p16* and HBx expression in GFP-HBx/HepG2 cells. Therefore, we speculated that there might be a mechanism by which HBx downregulates *p16* expression. Many viruses, including HBV, can induce methylation of tumor suppressor genes, and thus downregulate their expression.²² It has been reported that *p16* promoter methylation in HCC is significantly related to HBV infection.^{23,24} There are several causes of *p16* gene inactivation, such as gene loss, gene mutation, promoter hypermethylation, and homozygous deletion. Prior studies have focused on tumor suppressor gene mutations, while recent studies have shown that epigenetic abnormalities of tumor suppressor gene methylation are common causes for the development and progression of malignant tumors.²⁵ Importantly, HBx is a multi-functional viral protein closely related to the development of HCC, and recent studies have

suggested that HBx is an effective epigenetic modifier that can inactivate tumor suppressor genes by inducing methylation. Our results showed that the exogenous transfection of the *HBx* gene resulted in the methylation of some CpG sites in the *p16* gene promoter sequence in HepG2 cells. The treatment of GFP-HBx/HepG2 cells with 5-Aza-2'-deoxycytidine resulted in the recovery of the demethylated state of the *p16* gene promoter, indicating that DNA methylation was one of the reasons for the downregulation of the *p16* gene by HBx.

The upregulation of the expression of DNMTs has been found in many malignant tumors, including HCC.²⁶ Abnormally high expression of DNMT1 is closely related to the occurrence of ovarian cancer, cervical cancer, lung cancer, gastric cancer, and liver cancer.²⁶ The DNMT1 participates in characteristics of tumor cells such as unlimited proliferation, migration and invasion, and plays an important role in the maintenance of a continuous methylation state of tumor-related genes.^{27,28} However, the specific mechanisms by which DNMTs promote liver cancer have not been elucidated. Recent studies have shown that many viruses, including HBV, can upregulate the expression of DNMTs, thus causing the methylation of tumor suppressor genes and downregulation of their expression.^{29,30} Jung et al. reported that HBx can induce the methylation of the RAR- β promoter by upregulating the expression of DNMT1 and DNMT3A.¹² This results in the failure of tumor suppressor RA to combine with RAR- β , which leads to the failure of tumor suppressor activity and the subsequent malignant transformation of hepatocytes.¹² At present, the role of DNMTs in the process of HBx-induced p16 methylation is not clear. Therefore, we designed specific primers to amplify DNA fragments, including DNMT1, DNMT3A and DNMT3B promoter regions, and constructed corresponding promoter reporter vectors, in order to study the effect of HBx on DNMTs at the promoter level.

Limitations

We found that HBx significantly upregulated the promoter transcription activity of DNMT1 and DNMT3A. In addition, the mRNA expression of the *DNMT1* and *DNMT3A* genes was also increased, while HBx had no significant effect on DNMT3B at the promoter level and the mRNA level. Therefore, we speculate that DNMT1 and DNMT3A may play a catalytic role in the methylation of the *p16* gene promoter induced by HBx, probably via the mechanism of extensive transactivation. Previous studies have shown that HBx is a powerful transactivator.³¹ Although HBx in the nucleus cannot directly bind to DNA, it can interact with a variety of transfer factor proteins, resulting in the increase of transcription activity of specific genes. However, how HBx regulates the expression of DNMTs is still unclear, and further research is needed.

Conclusions

In conclusion, we successfully constructed the eukaryotic expression vector pEGFP-HBx carrying the *HBx* gene, and stably transfected it into HepG2 cells. We found that HBx can induce *p16* gene promoter methylation and inhibit the expression of the *p16* gene. The mechanism by which HBx regulates the expression of the *p16* gene is the upregulation of *DNMT1* and *DNMT3A* gene promoter activity, which enhances their transcription and expression. This subsequently results in the methylation of the *p16* gene promoter and the downregulation of gene expression.

Supplementary data

The supplementary files are available at <https://doi.org/10.5281/zenodo.7332522>. The package consists of the following files:








Supplementary Figure 1. p16 CpG island prediction through Metaprime.

Supplementary Table 1. Kruskal–Wallis test results for Fig. 5 and Fig. 8.

Supplementary Table 2. Dunn's test with Bonferroni adjustment as post hoc comparison results for Fig. 5 and Fig. 8.

Supplementary Table 3. Mann–Whitney U test results for Fig. 7.

ORCID iDs

Weiqiang Gan  <https://orcid.org/0000-0002-8934-2829>
 Yanhong Kang  <https://orcid.org/0000-0003-1030-0552>
 Yingjie Wu  <https://orcid.org/0000-0001-5244-9940>
 Jianyun Zhu  <https://orcid.org/0000-0002-2875-7932>
 Youming Chen  <https://orcid.org/0000-0003-1360-6936>
 Jianyu Kuang  <https://orcid.org/0000-0002-7134-923X>
 Jianguo Li  <https://orcid.org/0000-0002-9406-7921>
 Lin Yang  <https://orcid.org/0000-0002-3282-7091>

References

- World Health Organization. *Fact Sheets: Hepatitis B*. Geneva, Switzerland: World Health Organization; 2019. <https://www.who.int/news-room/fact-sheets/detail/hepatitis-b>. Accessed June 24, 2022.
- Wang F, Fan J, Zhang Z, Gao B, Wang H. The global burden of liver disease: The major impact of China. *Hepatology*. 2014;60(6):2099–2108. doi:10.1002/hep.27406
- Zheng B, Gao W, Huang X, et al. HBx promotes the proliferative ability of HL-7702 cells via the COX-2/Wnt/ β -catenin pathway. *Mol Med Rep*. 2018;17(6):8432–8438. doi:10.3892/mmr.2018.8906
- Wu CC, Wu DW, Lin YY, Lin PL, Lee H. Hepatitis B virus X protein represses LKB1 expression to promote tumor progression and poor postoperative outcome in hepatocellular carcinoma. *Surgery*. 2018;163(5):1040–1046. doi:10.1016/j.surg.2017.11.030
- Li C, Lin C, Cong X, Jiang Y. PDK1-WNK1 signaling is affected by HBx and involved in the viability and metastasis of hepatic cells. *Oncol Lett*. 2018;15(4):5940–5946. doi:10.3892/ol.2018.8001
- Serra S, Chetty R. p16. *J Clin Pathol*. 2018;71(10):853–858. doi:10.1136/jclinpath-2018-205216
- Cha S, Jang KL. Hepatitis B virus X protein stimulates cell growth by downregulating p16 levels via PA28y-mediated proteasomal degradation. *J Gen Virol*. 2020;101(9):963–971. doi:10.1099/jgv.0.001461
- Arzumanyan A, Friedman T, Kotei E, Ng IOL, Lian Z, Feitelson MA. Epigenetic repression of E-cadherin expression by hepatitis B virus x antigen in liver cancer. *Oncogene*. 2012;31(5):563–572. doi:10.1038/onc.2011.255

9. Ehrlich M. DNA hypermethylation in disease: Mechanisms and clinical relevance. *Epigenetics*. 2019;14(12):1141–1163. doi:10.1080/15592294.2019.1638701
10. Dandri M. Epigenetic modulation in chronic hepatitis B virus infection. *Semin Immunopathol*. 2020;42(2):173–185. doi:10.1007/s00281-020-00780-6
11. Dewantoro O, Gani RA, Akbar N. Hepatocarcinogenesis in viral hepatitis B infection: The role of HBx and p53. *Acta Med Indones*. 2006;38(3):154–159. PMID:16953033.
12. Jung JK, Park SH, Jang KL. Hepatitis B virus X protein overcomes the growth-inhibitory potential of retinoic acid by downregulating retinoic acid receptor-2 expression via DNA methylation. *J Gen Virol*. 2010;91(2):493–500. doi:10.1099/vir.0.015149-0
13. Zhu YZ, Zhu R, Shi LG, et al. Hepatitis B virus X protein promotes hypermethylation of p16INK4A promoter through upregulation of DNA methyltransferases in hepatocarcinogenesis. *Exp Mol Pathol*. 2010;89(3):268–275. doi:10.1016/j.yexmp.2010.06.013
14. Yanagisawa Y, Ito E, Yuasa Y, Maruyama K. The human DNA methyltransferases DNMT3A and DNMT3B have two types of promoters with different CpG contents. *Biochim Biophys Acta*. 2002;1577(3):457–465. doi:10.1016/S0167-4781(02)00482-7
15. Park IY, Sohn BH, Yu E, et al. Aberrant epigenetic modifications in hepatocarcinogenesis induced by hepatitis B virus X protein. *Gastroenterology*. 2007;132(4):1476–1494. doi:10.1053/j.gastro.2007.01.034
16. Song J, Rechkoblit O, Bestor TH, Patel DJ. Structure of DNMT1-DNA complex reveals a role for autoinhibition in maintenance DNA methylation. *Science*. 2011;331(6020):1036–1040. doi:10.1126/science.1195380
17. Surguchov A, Bernal L, Surguchev AA. Phytochemicals as regulators of genes involved in synucleinopathies. *Biomolecules*. 2021;11(5):624. doi:10.3390/biom11050624
18. Chen W, Huang L, Liu H, Li XM, Xu CM. Expressions of HBV X gene regulated by different promoters and their effects on cell apoptosis. *Eur Rev Med Pharmacol Sci*. 2018;22(18):5906–5913. doi:10.26355/eurrev_201809_15919
19. Torresi J, Tran BM, Christiansen D, Earnest-Silveira L, Schwab RHM, Vincan E. HBV-related hepatocarcinogenesis: The role of signalling pathways and innovative ex vivo research models. *BMC Cancer*. 2019;19(1):707. doi:10.1186/s12885-019-5916-6
20. Wei Y, Neuveut C, Tiollais P, Buendia MA. Molecular biology of the hepatitis B virus and role of the X gene. *Pathol Biol*. 2010;58(4):267–272. doi:10.1016/j.patbio.2010.03.005
21. Shaner NC, Patterson GH, Davidson MW. Advances in fluorescent protein technology. *J Cell Sci*. 2007;120(24):4247–4260. doi:10.1242/jcs.005801
22. Fernandez AF, Esteller M. Viral epigenomes in human tumorigenesis. *Oncogene*. 2010;29(10):1405–1420. doi:10.1038/onc.2009.517
23. Kaur P, Paliwal A, Durantel D, et al. DNA methylation of hepatitis B virus (HBV) genome associated with the development of hepatocellular carcinoma and occult HBV infection. *J Infect Dis*. 2010;202(5):700–704. doi:10.1086/655398
24. Csepregi A, Ebert MP, Röcken C, et al. Promoter methylation of CDKN2A and lack of p16 expression characterize patients with hepatocellular carcinoma. *BMC Cancer*. 2010;10(1):317. doi:10.1186/1471-2407-10-317
25. Anzola M, Cuevas N, Lopez-Martinez M, De Pancorbo MM, Burgos JJ. p16INK4A gene alterations are not a prognostic indicator for survival in patients with hepatocellular carcinoma undergoing curative hepatectomy. *J Gastroenterol Hepatol*. 2004;19(4):397–405. doi:10.1111/j.1440-1746.2003.03305.x
26. Lyko F. The DNA methyltransferase family: A versatile toolkit for epigenetic regulation. *Nat Rev Genet*. 2018;19(2):81–92. doi:10.1038/nrg.2017.80
27. Robert MF, Morin S, Beaulieu N, et al. DNMT1 is required to maintain CpG methylation and aberrant gene silencing in human cancer cells. *Nat Genet*. 2003;33(1):61–65. doi:10.1038/ng1068
28. Song J, Teplova M, Ishibe-Murakami S, Patel DJ. Structure-based mechanistic insights into DNMT1-mediated maintenance DNA methylation. *Science*. 2012;335(6069):709–712. doi:10.1126/science.1214453
29. Oh BK, Kim H, Park HJ, et al. DNA methyltransferase expression and DNA methylation in human hepatocellular carcinoma and their clinicopathological correlation. *Int J Mol Med*. 2007;20(1):65–73. doi:10.3892/ijmm.20.1.65
30. Burgers WA, Blanchon L, Pradhan S, de Launoit Y, Kouzarides T, Fuks F. Viral oncoproteins target the DNA methyltransferases. *Oncogene*. 2007;26(11):1650–1655. doi:10.1038/sj.onc.1209950
31. Slagle BL, Bouchard MJ. Hepatitis B virus X and regulation of viral gene expression. *Cold Spring Harb Perspect Med*. 2016;6(3):a021402. doi:10.1101/cshperspect.a021402

hsa_circ_0038382 upregulates T-box transcription factor 5 to inhibit keloid formation by interacting with miR-940

*Meihong Cai^{1,A,C,D}, *Zhen Hu^{2,C-E}, Lin Liu^{3,B,D,E}, Jiangwei Su^{3,E,F}

¹ Department of Dermatology, Wuhan Wuchang Hospital, Wuchang Hospital Affiliated to Wuhan University of Science and Technology, China

² Department of Dermatology, Wuhan Third Hospital, China

³ Department of Dermatology, Ezhou Central Hospital, China

A – research concept and design; B – collection and/or assembly of data; C – data analysis and interpretation;

D – writing the article; E – critical revision of the article; F – final approval of the article

Advances in Clinical and Experimental Medicine, ISSN 1899–5276 (print), ISSN 2451–2680 (online)

Adv Clin Exp Med. 2023;32(5):593–601

Address for correspondence

Jiangwei Su

E-mail: SuJiangwei3@163.com

Funding sources

None declared

Conflict of interest

None declared

* Meihong Cai and Zhen Hu contributed equally to this work.

Received on April 15, 2022

Reviewed on September 30, 2022

Accepted on October 21, 2022

Published online on November 22, 2022

Abstract

Background. A keloid is a benign fibroproliferative skin tumor whose formation is regulated by circular RNAs (circRNAs). However, the effect and regulatory mechanism of hsa_circ_0038382 on keloid formation have not been investigated.

Objectives. This study aimed to identify the function and mechanism of hsa_circ_0038382 in keloid formation.

Materials and methods. The expression levels of hsa_circ_0038382, microRNA-940 (miR-940) and T-box transcription factor 5 (*TBX5*) were measured using real-time quantitative reverse transcription polymerase chain reaction (qRT-PCR). After cell transfection of keloid fibroblasts, the effect of the hsa_circ_0038382/miR-940/*TBX5* axis on keloid formation was assessed using cell function tools such as the cell counting kit-8 (CCK-8) assay, transwell migration assay and transwell invasion assay. The binding sites among hsa_circ_0038382, miR-940 and *TBX5* were predicted with CircInteractome and TargetScan, and further identified using luciferase assays.

Results. The levels of hsa_circ_0038382 and *TBX5* were reduced, whereas the level of miR-940 was elevated in keloid samples. Cell function experiments confirmed that hsa_circ_0038382 can inhibit keloid formation by suppressing proliferation, migration and invasion of keloid fibroblasts. Luciferase assays proved that hsa_circ_0038382 can absorb miR-940 to regulate *TBX5* expression in keloids. Additionally, the overexpression of *TBX5* restored the effect of hsa_circ_0038382 knockdown on keloid fibroblasts.

Conclusions. This study suggests that hsa_circ_0038382 attenuates keloid formation by regulating the miR-940/*TBX5* axis, which might provide a potential therapeutic target in the treatment of keloid formation.

Key words: keloid, hsa_circ_0038382, miR-940, *TBX5*

Cite as

Cai M, Hu Z, Liu L, Su J. hsa_circ_0038382 upregulates T-box transcription factor 5 to inhibit keloid formation by interacting with miR-940. *Adv Clin Exp Med.* 2023;32(5):593–601. doi:10.17219/acem/155949

DOI

10.17219/acem/155949

Copyright

Copyright by Author(s)

This is an article distributed under the terms of the Creative Commons Attribution 3.0 Unported (CC BY 3.0) (<https://creativecommons.org/licenses/by/3.0/>)

Background

A keloid, characterized by the hyperproliferation of fibroblasts and abnormal deposition of collagen fibers, is a benign fibroproliferative skin tumor.^{1,2} Keloid formation is caused by cutaneous injuries, including trauma, burns and surgery,³ and involves multiple regulators, including cytokines, gene regulators and inflammatory factors.⁴ The overproliferation of fibroblast, overproduction of collagen and abnormal extracellular matrix remodeling are key factors in keloid formation.⁵ For keloid therapy, the mainstay of treatment is conservative therapy, such as surgery alone or in combination with depot steroids. However, a high recurrence rate often leads to unsatisfactory outcomes.^{6,7} Hence, an in-depth investigation of the mechanisms behind keloid formation is urgently required for keloid treatment.

Circular RNAs (circRNAs), which are non-coding RNAs, are more stable than linear RNAs because they form a continuous circle.⁸ Accumulating evidence reveals that aberrantly expressed circRNAs in keloids play key roles in regulating keloid formation.^{9–11} For example, circRNA nuclear receptor-interacting protein 1 (circNRIP1) is overexpressed in keloid tissues, and the downregulation of circNRIP1 expression inhibited the proliferation of keloid-derived fibroblasts.¹⁰ The overexpression of another circRNA, circ_101238, has been shown to promote the proliferation and inhibit the apoptosis of keloid fibroblasts.⁹ We identified a novel circRNA, hsa_circ_0038382, by analyzing a keloid circRNA microarray from the Gene Expression Omnibus (GEO) database. Because of the lack of knowledge regarding the effects of hsa_circ_0038382 on keloids, this study is the first to investigate the function of hsa_circ_0038382 in keloids.

The circRNAs that interact with microRNAs (miRNAs) to regulate downstream target genes have been confirmed in multiple human diseases, such as cancer, osteoporosis and cardiac hypertrophy.^{12–14} In keloids, circRNA protein tyrosine phosphatase non-receptor type 12 (PTPN12) has been reported to target the miR-21-5p/*SMAD7* axis, thereby inhibiting keloid fibroblast growth.¹⁵ Our study predicted that miR-940 might be the downstream miRNA of hsa_circ_0038382 using CircInteractome (<https://circinteractome.nia.nih.gov/>) analysis. The miR-940 has been reported as a tumor promoter in breast cancer¹⁶ and endometrial carcinoma,¹⁷ and as an antitumor factor in non-small cell lung carcinoma¹⁸ and esophageal squamous cell carcinoma.¹⁹ However, the effects of miR-940 on keloids remain unknown. Here, we explored the influence of miR-940 and the interaction between hsa_circ_0038382 and miR-940 on keloids.

T-box transcription factor 5 (*TBX5*), containing a DNA-binding domain T-box sequence, can induce cell apoptosis.²⁰ Previous studies have confirmed the antitumor function of *TBX5* in colon cancer,²¹ non-small cell lung carcinoma²² and cutaneous melanoma.²³ Nevertheless, the mechanism of action of *TBX5* in keloids remains unclear. Using TargetScan (<https://www.targetscan.org>), *TBX5* was predicted

to be the target gene of miR-940; however, the relationship between *TBX5* and miR-940 has not been reported. Therefore, we explored the function and mechanism of action of *TBX5* in keloids.

Objectives

Based on a bioinformatic analysis and a literature review, we speculated that hsa_circ_0038382 might affect keloid formation through the miR-940/*TBX5* axis. Therefore, the present study aimed to identify the function of the hsa_circ_0038382/miR-940/*TBX5* axis on keloids, and assess whether it could be a novel therapeutic target for keloid treatment.

Materials and methods

Microarray analysis

The GSE184097 from the GEO database is a circRNA expression microarray containing keloid and normal skin samples. The ASCRP3013082 is the ID of hsa_circ_0038382 in GSE184097. The GEO2R was used to identify hsa_circ_0038382 expression in keloids and normal skin samples. The binding sites of hsa_circ_0038382, miR-940 and *TBX5* were predicted using CircInteractome and TargetScan.

Clinical sample collection

Keloids and paired normal skin tissues (>5 cm from the keloid) were collected from 28 patients in our hospital. None of the patients had received radiotherapy, chemotherapy or laser treatment before surgery. Our study was approved by the Ethics Committee of Wuhan Wuchang Hospital, China (approval No. 2022006). All patients signed an informed consent form. The clinical characteristics of the patients are presented in Table 1.

Real-time quantitative reverse transcription polymerase chain reaction (qRT-PCR)

Total RNA was isolated using RNAiso Plus (TaKaRa, Tokyo, Japan), and miRNA was isolated using the miRNeasy FFPE Kit (BioTeke, Wuxi, China). Reverse transcription was performed using a PrimeScript RT kit (TaKaRa). Real-time quantitative reverse transcription polymerase chain reaction was performed using SYBR™ Green PCR Master Mix (TaKaRa) with the following primer sequences: hsa_circ_0038382: forward, 5'-CGGGCCTATATGGAGAA-CAA-3' and reverse, 5'-TCTCTCCTCACTGCCCAACT-3'; miR-940: forward, 5'-GTATAAAGGGCCCCCGCT-3' and reverse, 5'-AGGGTCCGAGGTATTCGCACT-3'; and *TBX5*: forward, 5'-CTCAAGCTCACCAACAACCA-3' and

Table 1. Clinical characteristics of 28 patients with keloid

Variable	Number (total = 28)
Age, median (range) [years]	36 (26–48)
Sex	
Male, n	13
Female, n	15
Number of keloid nodules	
1	11
2–4	9
≥5	8
Location	
Face, neck	5
Trunk, shoulder	17
Extremities	6
Symptom	
Itching	10
Pain	1
Itching & pain	17

reverse, 5'-CAGGAAAGACGTGAGTGCAG-3'. The relative expression was calculated using the $2^{-\Delta\Delta CT}$ method²⁴ with glyceraldehyde 3-phosphate dehydrogenase (*GAPDH*) and U6 as internal references.

Cell culture and transfection

Human keloid fibroblasts (HKFs; CP-H235) were purchased from Procell Life Science and Technology Co., Ltd. (Wuhan, China), whereas normal human dermal fibroblasts (HDFs; BNCC358600) were purchased from the BeNa Culture Collection (Beijing, China). All cells were cultured in Dulbecco's modified Eagle's medium (DMEM) containing 10% fetal bovine serum (FBS), 1% penicillin and 1% streptomycin under 5% CO₂ and at 37°C.

Silencing RNAs (siRNAs) targeting *hsa_circ_0038382* (si-*hsa_circ_0038382*), negative control (NC) of siRNAs, miR-940 mimic, and mimic-NC were constructed by RiboBio (Guangzhou, China). The *hsa_circ_0038382* and *TBX5* overexpression vectors were also constructed by RiboBio using pcDNA3.1-circRNA or pcDNA3.1 vectors. The corresponding empty vector (pcDNA3.1-circRNA or pcDNA3.1) was used as the NC of the overexpression vector. For cell transfection, the 50 nM vectors mentioned above were transfected into HKFs at 50% confluence. After transfection for 48 h, qRT-PCR was performed to assess the transfection efficiency.

CCK-8 assay

Human dermal fibroblasts were seeded in a 96-well cell culture plate (3000/well). After transfection for 0, 24, 48, and 72 h, 10 µL of cell counting kit-8 (CCK-8) solution (Dojindo, Kumamoto, Japan) was pipetted into each well

and incubated for another 2 h at 37°C. Finally, the optical density (OD) value was recorded at 450 nm using a microplate reader (YK-SY96A; Yunke, Beijing, China).

EdU assay

The 5-ethynyl-2'-deoxyuridine (EdU) assays were performed to assess cell proliferation using an EdU cell proliferation kit (Solarbio Science & Technology Co., Ltd., Beijing, China). Transfected HKFs (1×10^4 cells/well) were seeded in 96-well plates and incubated overnight. The next day, 100 µL of 50 µM EdU solution was added to the HKFs and incubated for 2 h. After washing the HKFs with phosphate-buffered saline (PBS), the cells were fixed with fixative, treated with 0.1% Triton X-100, washed with PBS, and incubated with 100 µL of Apollo staining reaction solution. Then, the cells were incubated with 100 µL of $1 \times$ Hoechst 33342. Finally, they were observed and photographed using a fluorescence microscope (Olympus BX51; Olympus Corp., Tokyo, Japan).

Transwell migration and invasion assays

Matrigel diluted with a serum-free medium at a ratio of 1:8 was added to the polycarbonate film and incubated overnight for the invasion assay, but not for the migration assay. After transfection, 1×10^5 HKFs were added to the upper chamber with 200 µL of serum-free medium. Simultaneously, 600 µL of medium containing 10% FBS was added to the lower chamber. After incubation for 24 h, migratory and invasive HKFs were fixed using 4% paraformaldehyde and stained with 0.05% crystal violet. The cells were observed under an optical microscope (Olympus CX21; Olympus Corp., Tokyo, Japan). The number of cells was calculated in 5 random fields in each transwell chamber using ImageJ software (National Institutes of Health, Bethesda, USA).

Luciferase assay

Wild-type vectors of *hsa_circ_0038382/TBX5* (*hsa_circ_0038382*-WT/*TBX5*-WT) and mutant vectors of *hsa_circ_0038382/TBX5* (*hsa_circ_0038382*-MUT/*TBX5*-MUT) were constructed by RiboBio using pMIR-REPORT™ (Ambion, Austin, USA) vectors. Subsequently, each of the constructed luciferase reporter vectors was transfected into HKFs at 70% confluence along with miR-940 mimic or mimic-NC. After transfection for 48 h, luciferase activity was evaluated using a dual-luciferase reporter assay kit (Promega, Madison, USA).

Western blotting

Total protein was obtained from HKFs using a Total Protein Extraction Kit (PI250; Applygen Technologies Inc., Beijing, China). After determining the protein concentration with the aid of a BCA kit (Pierce, Rockford, USA), sodium

dodecyl-sulfate polyacrylamide gel electrophoresis (SDS-PAGE) gels (10%) were used to separate 20 μ g of protein. The separated proteins were transferred onto polyvinylidene fluoride (PVDF) membranes. The membranes were blocked with 5% skim milk and incubated with TBX4 antibody (ab137833; Abcam, Cambridge, USA) or GAPDH antibody (ab9485; Abcam) at 4°C overnight, followed by the incubation with a fluorescent rabbit antibody (LI-COR Biosciences, Bad Homburg vor der Höhe, Germany) for 3 h at 37°C. The protein blots were acquired using Odyssey 3.2 (LI-COR Biosciences).

Statistical analyses

All experiments were performed in triplicate, and the data were analyzed using GraphPad Prism v. 8 (GraphPad Software, San Diego, USA) with a paired or unpaired Student's t-test (between the 2 groups) or analysis of variance (ANOVA) test (>2 groups), followed by the Tukey's multiple comparisons test. All data were identified as normally distributed using the Shapiro–Wilk test. Data are presented as a mean \pm standard deviation ($M \pm SD$). The value of $p < 0.05$ was considered statistically significant.

Results

hsa_circ_0038382 was downregulated in keloid

The GSE184097, a circRNA microarray, was downloaded from GEO DataSets, and differentially expressed

circRNAs were compared in keloid samples ($n = 4$) to normal skin samples ($n = 4$) with an adjusted p -value < 0.05 (Fig. 1A). In the GSE184097 microarray, GSM5577905, GSM5577906, GSM5577907, and GSM5577908 were the keloid samples, whereas GSM5577909, GSM5577910, GSM5577911, and GSM5577912 were the adjacent normal skin samples. The hsa_circ_0038382 expression was reduced in the 4 keloid samples compared to the 4 adjacent normal skin samples (Fig. 1B and Table 2). We collected keloid and adjacent normal tissues from 28 patients to identify the expression of hsa_circ_0038382 in our clinical samples. Our qRT-PCR data further showed that hsa_circ_0038382 levels were reduced by 50% in keloid tissues compared with paired normal skin tissues (Fig. 1C). Similarly, the expression of hsa_circ_0038382 in HKFs was downregulated by more than 50% compared to that in normal HDFs (Fig. 1D). The bioinformatics analysis and qRT-PCR experiments confirmed the downregulation of hsa_circ_0038382 in keloids.

Table 2. Sample values for hsa_circ_0038382 in GSE184097

Source	Sample	Value
Keloid dermal fibroblasts	GSM5577905	5.18
	GSM5577906	5.42
	GSM5577907	5.46
	GSM5577908	5.40
Normal dermal fibroblasts	GSM5577909	6.81
	GSM5577910	6.82
	GSM5577911	5.94
	GSM5577912	6.03

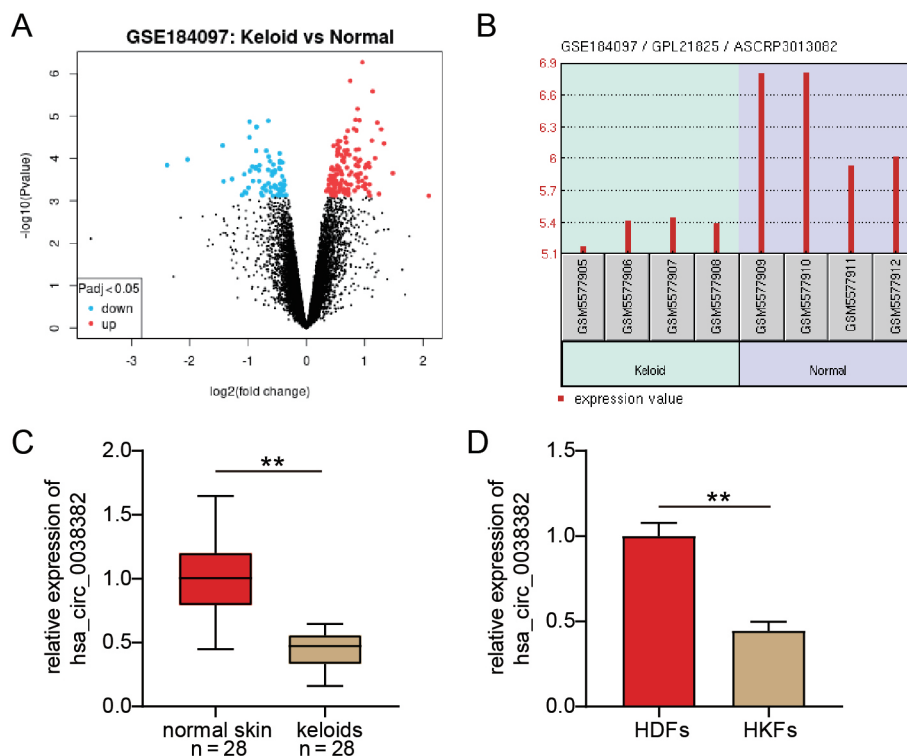


Fig. 1. The hsa_circ_0038382 was downregulated in keloid. A. Differentially expressed circular RNAs (circRNAs) in GSE184097; B. Downregulation of hsa_circ_0038382 in keloid samples; C. hsa_circ_0038382 expression was reduced in keloid tissues as identified using real-time quantitative reverse transcription polymerase chain reaction (qRT-PCR), $n = 28$; D. hsa_circ_0038382 expression was reduced in HKFs as identified using qRT-PCR

GSE184097 – circRNA microarray for keloid samples and normal skin samples; HDFs – normal human dermal fibroblasts; HKFs – human keloid fibroblasts; ** $p < 0.01$.

hsa_circ_0038382 attenuates keloid formation in vitro

To verify the function of hsa_circ_0038382 in keloids, we transfected HKFs with hsa_circ_0038382 overexpression or knockdown vectors. The qRT-PCR was used to determine the transfection efficiency, which showed that the hsa_circ_0038382 overexpression vector induced > 6-fold increase in hsa_circ_0038382 expression in HKFs, and si-hsa_circ_0038382 caused a 70% decrease in its expression in HKFs (Fig. 2A). The CCK-8 assay demonstrated that the proliferation of HKFs was impaired in the hsa_circ_0038382 overexpression group, whereas it was enhanced in the si-hsa_circ_0038382 group (Fig. 2B). The EdU assay was used to confirm the change in the proliferation of transfected HKFs. The results revealed that the hsa_circ_0038382 overexpression vector led to >60% decrease in the EdU-positive rate, whereas hsa_circ_0038382 knockdown resulted in a 1.8-fold increase in the EdU-positive rate (Fig. 2C). Transwell migration and invasion assays revealed that the overexpression of hsa_circ_0038382 promoted migration and invasion of HKFs, whereas hsa_circ_0038382 knockdown inhibited the migration and invasion of HKFs (Fig. 2D). These data indicate that hsa_circ_0038382 attenuates keloid formation in vitro.

miR-940 targeted by hsa_circ_0038382 promotes HKF proliferation

To identify the key miRNA binding to hsa_circ_0038382, an online tool, CircInteractome, was used to predict miRNA binding to hsa_circ_0038382. Based on the CircInteractome prediction, 2 binding sites were found between hsa_circ_0038382 and miR-940 (Fig. 3A). After performing a luciferase assay to identify the binding sites, the miR-940 mimic induced a 50% decrease in luciferase activity in the hsa_circ_0038382-WT group, a 40% decrease in the hsa_circ_0038382-MUT1 group, and a 25% decrease in the hsa_circ_0038382-MUT2 group (Fig. 3B). However, the luciferase activity in the co-hsa_circ_0038382-MUT group was affected by the miR-940 mimic. Compared to normal skin tissues, the expression of miR-940 in keloid tissues showed a 5-fold elevation (Fig. 3C). The Pearson's correlation analysis showed that the expression of hsa_circ_0038382 was negatively correlated with miR-940 expression in keloid tissues ($R = -0.6620$, Fig. 3D). After the transfection of HKFs with the miR-940 mimic, the proliferation of HKFs was enhanced (Fig. 3E). These results prove that miR-940 could be targeted by hsa_circ_0038382 and contribute to the proliferation of HKFs.

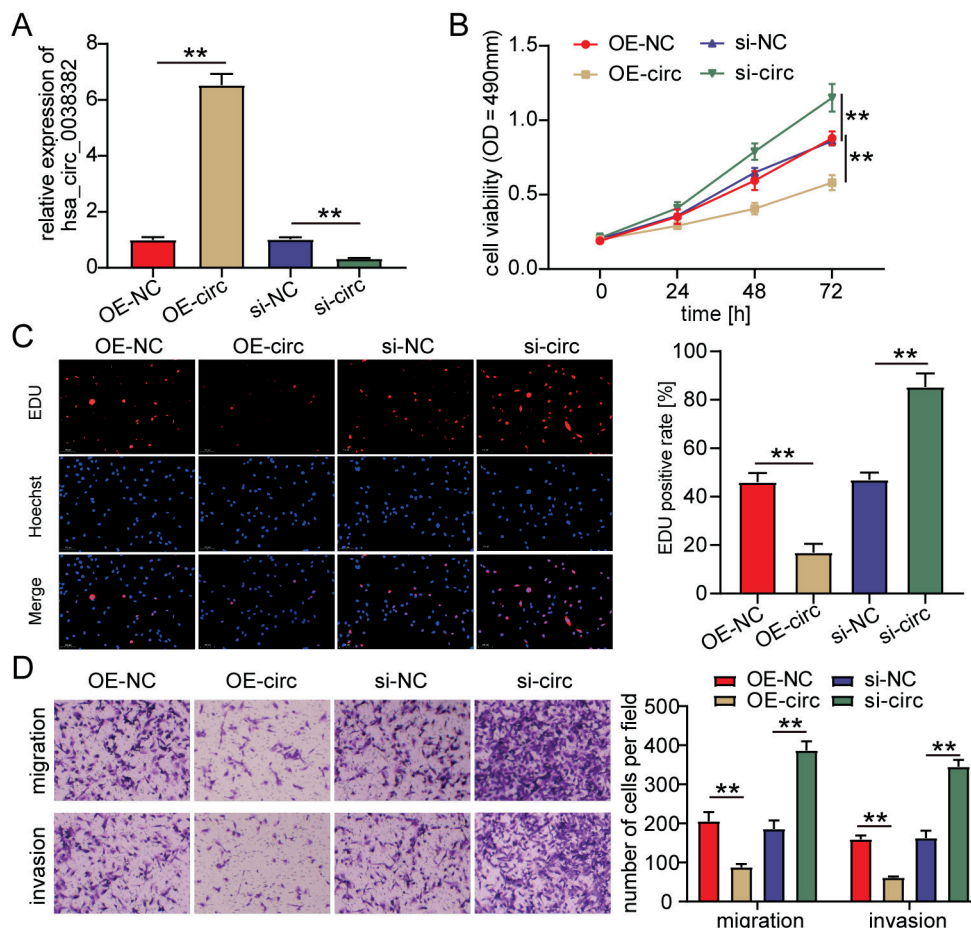


Fig. 2. The hsa_circ_0038382 attenuates keloid formation in vitro. A. Real-time quantitative reverse transcription polymerase chain reaction (qRT-PCR) identified the high transfection efficiency of hsa_circ_0038382 overexpression vectors and si-hsa_circ_0038382 vectors in human keloid fibroblasts (HKFs); B. Cell counting kit-8 (CCK-8) assays detected the effect of hsa_circ_0038382 on the proliferation of HKFs; C. The 5-ethynyl-2'-deoxyuridine (EdU) assays further detected the effect of hsa_circ_0038382 on the proliferation of HKFs; D. Transwell migration and invasion assays measured the effect of hsa_circ_0038382 on the migration and invasion of HKFs with the quantification of cell number at $\times 200$ magnification

OE-NC – negative control of hsa_circ_0038382 overexpression vector; OE-circ – hsa_circ_0038382 overexpression vector; si-NC – negative control of si-hsa_circ_0038382; si-circ – si-hsa_circ_0038382; OD – optical density; ** $p < 0.01$.

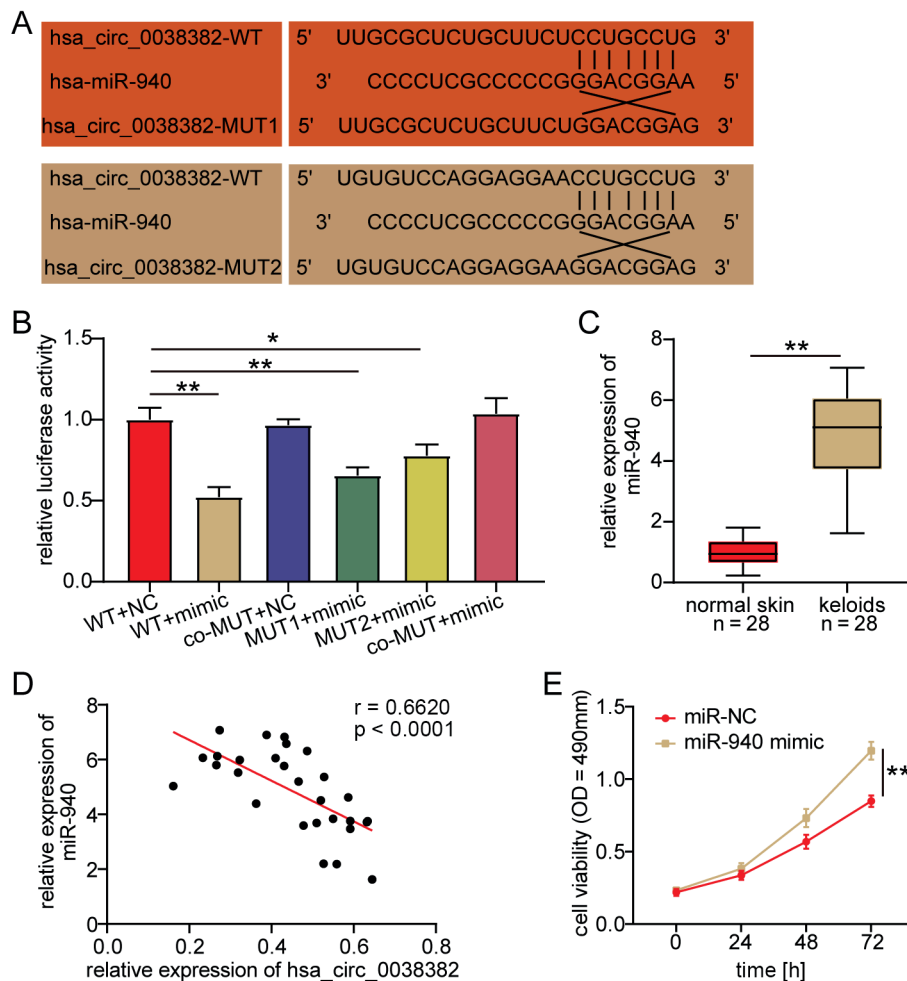


Fig. 3. The miR-940 targeted by hsa_circ_0038382 promotes human keloid fibroblast (HKF) proliferation. **A.** CircInteractome predicted the binding sites between hsa_circ_0038382 and miR-940; **B.** Luciferase assay confirmed the binding sites between hsa_circ_0038382 and miR-940 in HKFs; **C.** Real-time quantitative reverse transcription polymerase chain reaction (qRT-PCR) confirmed the upregulation of miR-940 in keloid tissues, $n = 28$; **D.** Pearson's correlation analysis confirmed the negative correlation between hsa_circ_0038382 and miR-940 in keloid tissues; **E.** Cell counting kit-8 (CCK-8) assays revealed the positive effect of miR-940 on the proliferation of HKFs

WT – wild-type hsa_circ_0038382; MUT1 – mutant at site 1 of hsa_circ_0038382; MUT2 – mutant at site 2 of hsa_circ_0038382; co-MUT – mutant at site 1 and 2 of hsa_circ_0038382; NC – negative control of miR-940 mimic; + – co-transfection; miR-NC – negative control of miR-940 mimic; OD – optical density; * $p < 0.05$; ** $p < 0.01$.

TBX5, a target gene of miR-940, inhibits HKF proliferation

To explore the downstream regulators of miR-940, TargetScan, an online tool, was used to predict the target genes of miR-940. According to TargetScan predictions, there is a binding site between *TBX5* and miR-940 (Fig. 4A). The luciferase assay further confirmed the binding site between *TBX5* and miR-940, because the miR-940 mimic reduced the luciferase activity in the *TBX5*-WT group but did not affect the luciferase activity in the *TBX5*-MUT group (Fig. 4B). Compared with normal skin tissues, *TBX5* expression was significantly reduced in keloid tissues ($p < 0.01$, Fig. 4C). The Pearson's correlation analysis revealed a negative correlation between *TBX5* and miR-940 expression in keloid tissues ($R = -0.7279$, Fig. 4D), and a positive correlation between *TBX5* and hsa_circ_0038382 expression in keloid tissues ($R = 0.7335$, Fig. 4E). After the transfection with the *TBX5* overexpression vectors, the proliferation of HKFs declined (Fig. 4F). These data confirm that *TBX5* targeted by miR-940 promotes the proliferation of HKFs.

TBX5 overexpression reversed the effect of hsa_circ_0038382 knockdown on HKFs

Since *TBX5* acts downstream of the hsa_circ_0038382/miR-940 axis, we transfected HKFs with hsa_circ_0038382 knockdown with or without the *TBX5* overexpression vectors. Western blotting showed that the *TBX5* protein expression was inhibited by 50% in HKFs with hsa_circ_0038382 knockdown. However, *TBX5* overexpression vectors recovered the effects of hsa_circ_0038382 knockdown on *TBX5* protein expression (Fig. 5A). We performed cell functional experiments to explore whether *TBX5* could recover the effect of hsa_circ_0038382 on the proliferation, migration and invasion of HKFs. As shown in Fig. 5B, the increase in proliferation induced by si-hsa_circ_0038382 was reversed by the co-transfection with *TBX5* overexpression vectors in HKFs. The EdU assay further confirmed that the overexpression of *TBX5* recovered the increase in the EdU-positive rate caused by si-hsa_circ_0038382 (Fig. 5C). Similarly, the enhanced migration and invasion abilities of HKFs caused by hsa_circ_0038382 knockdown were impaired by the co-transfection with *TBX5* overexpression vectors (Fig. 5D). Cell function experiments identified that the positive effect of hsa_circ_0038382 downregulation on HKFs was reversed by the overexpression of *TBX5*.

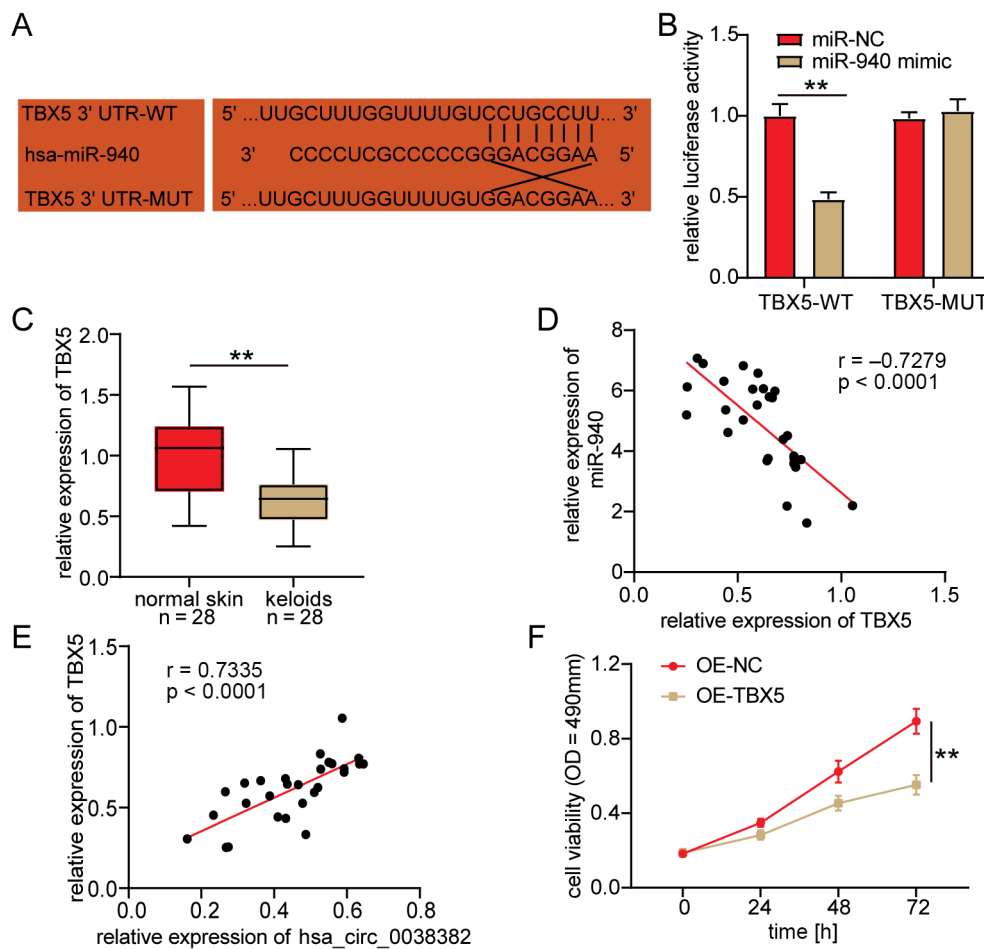


Fig. 4. T-box transcription factor 5 (*TBX5*), a target gene of miR-940, inhibits human keloid fibroblast (HKF) proliferation. **A.** TargetScan predicted the binding site between *TBX5* and miR-940; **B.** Luciferase assay confirmed the binding site between *TBX5* and miR-940 in HKFs; **C.** Real-time quantitative reverse transcription polymerase chain reaction (qRT-PCR) confirmed the downregulation of *TBX5* in keloid tissues, n = 28; **D.** Pearson's correlation analysis revealed the negative correlation between *TBX5* and miR-940 in keloid tissues; **E.** Pearson's correlation analysis revealed the positive correlation between *TBX5* and hsa_circ_0038382 in keloid tissues; **F.** Cell counting kit-8 (CCK-8) assays proved the negative effect of miR-940 on the proliferation of HKFs

TBX5-WT – wild-type *TBX5* 3'UTR; *TBX5*-MUT – mutant *TBX5* 3'UTR; miR-NC – negative control of miR-940 mimic; OE-NC – negative control of *TBX5* overexpression vectors; OE-*TBX5* – *TBX5* overexpression vectors; OD – optical density; **p < 0.01.

Discussion

Recently, the circRNAs have been reported to participate in keloid formation.^{10,11,25} This study revealed that the novel circRNA, hsa_circ_0038382, was downregulated in keloid tissues and fibroblasts, and it enhanced the proliferation, migration and invasion abilities of keloid fibroblasts. Moreover, we showed that hsa_circ_0038382, miR-940 and *TBX5* form a circRNA-miRNA-mRNA regulatory network to regulate keloid formation.

The circRNAs play key roles in multiple human diseases, although they do not code protein.^{26–28} Due to the rapid development of RNA sequencing technology, microarray analysis has been a good method for identifying key circRNAs in human diseases.²⁹ Zhang et al. applied high-throughput RNA sequencing technology and bioinformatic analysis and confirmed that the key circRNAs in keloids were hsa_circRNA_0008259, hsa_circRNA_0005480 and hsa_circRNA_0002198.³⁰ In this study, we achieved a circRNA microarray of keloids (GSE184097) from the GEO database and confirmed that hsa_circ_0038382 was downregulated in keloid samples. After transfecting hsa_circ_0038382 overexpression vectors or si-hsa_circ_0038382 into keloid fibroblasts, hsa_circ_0038382 was found to inhibit keloid formation, which uncovered the function of hsa_circ_0038382 in keloids for the first

time. Currently, the treatment of keloids includes surgical excision combined with radiotherapy, corticosteroids, pressure therapy, and other treatments.³¹ However, because of the high recurrence rate, no single treatment has been proven to be the most effective.⁶ We identified the abnormal expression of hsa_circ_0038382 in keloids. Its overexpression inhibited keloid formation. Our results suggested that hsa_circ_0038382 may be a biomarker for keloid prognosis, and emerging drugs targeting hsa_circ_0038382 may effectively inhibit keloid formation.

An increasing number of studies have reported that the regulatory network formed by circRNAs, miRNAs and mRNAs participates in biological processes such as cell proliferation,²⁷ cell apoptosis³² and cell differentiation.³³ Liu et al. confirmed the regulatory network formed by circPTPN12, miR-21-5p and *SMAD7* in keloid fibroblasts, showing that circPTPN12 inhibits the growth of keloid fibroblasts by targeting miR-21-5p/*AMAD7* axis.¹⁵ The circ_101238 targets the miR-138-5p/*CDK6* axis, promoting the proliferation and inhibiting the apoptosis of keloid fibroblasts.⁹ In this study, we used keloid fibroblasts to confirm that hsa_circ_0038382 could bind miR-940 to upregulate the target gene (*TBX5*) of miR-940. In other words, hsa_circ_0038382, miR-940 and *TBX5* formed the regulatory network to regulate keloid formation.

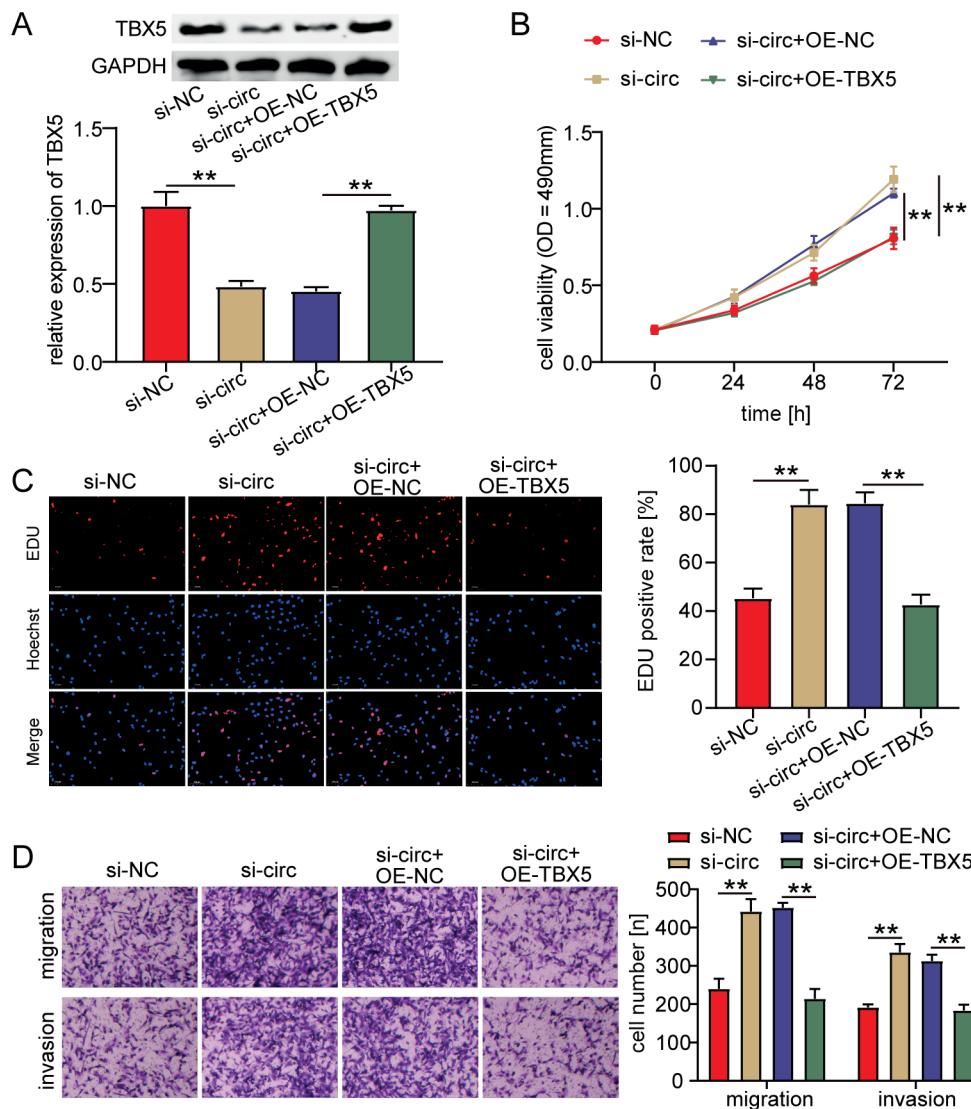


Fig. 5. Overexpression of T-box transcription factor 5 (TBX5) reversed the effect of hsa_circ_0038382 knockdown on human keloid fibroblasts (HKFs). **A.** Western blotting detected the expression of TBX5 protein in transfected HKFs; **B,C.** Cell counting kit-8 (CCK-8) assay (**B**) and 5-ethynyl-2'-deoxyuridine (EdU) assay (**C**) detected the proliferation of transfected HKFs; **D.** Transwell migration and invasion assays measured the abilities of migration and invasion of transfected HKFs with the quantification of cell number at $\times 200$ magnification

si-NC – negative control of si-hsa_circ_0038382; si-circ – si-hsa_circ_0038382; OE-NC – negative control of TBX5 overexpression vector; OE-TBX5 – TBX5 overexpression vector; GAPDH – glyceraldehyde 3-phosphate dehydrogenase; OD – optical density; ** $p < 0.01$.

The role of miR-940 has been reported in multiple diseases, such as sepsis,³⁴ spinal cord injury³⁵ and cancer.³⁶ The overexpression of miR-940 has been shown to induce the progression of cervical cancer. However, its overexpression inhibits the malignancy of lung cancer.³⁷ These previous studies suggest different roles of miR-940 in various cancers. The effect of miR-940 on keloids as benign skin fibroproliferative tumors should be explored. Here, we confirmed that miR-940, downstream of hsa_circ_0038382, contributes to the proliferation of keloid fibroblasts. In addition, our study identified *TBX5* as the target gene of miR-940 in keloid fibroblasts.

The overexpression of *TBX5* inhibits colony formation but induces cell apoptosis, thereby attenuating cell proliferation and invasion in tumor cells.^{20,21} In non-small cell lung carcinoma cells, low levels of *TBX5* indicated poor tumor-node-metastasis (TNM) stages, histopathologic type and lymph node status. Additionally, the overexpression of *TBX5* suppressed tumor growth in vivo.²² In cutaneous melanoma, *TBX5* knockdown

promotes cutaneous melanoma cell proliferation, migration and invasion, suggesting an antitumor role of *TBX5* in cutaneous melanoma. Similar to a previous study on *TBX5* in other cancers, our study confirmed that the overexpression of *TBX5* inhibits the proliferation of keloid fibroblasts. In addition, in hsa_circ_0038382 knockdown experiments, the overexpression of *TBX5* restored the promotive effect of hsa_circ_0038382 in keloid fibroblasts.

Limitations

There are some limitations to our study. The study used the microarray analysis and cell function experiments to evaluate the effects of keloid formation, but the effect of the hsa_circ_0038382/miR-940/*TBX5* axis on keloid formation in vivo needs to be further investigated. Moreover, the clinical value of the hsa_circ_0038382/miR-940/*TBX5* axis needs to be explored by collecting more clinical samples.

Conclusions

This study, for the first time, demonstrated the inhibitory effect of hsa_circ_0038382 on keloids by suppressing the proliferation, migration and invasion of keloid fibroblasts. The miR-940/TBX5 was identified as the downstream regulator of hsa_circ_0038382 in keloid formation. Our results provide novel therapeutic targets in keloid prevention.

ORCID iDs

Meihong Cai  <https://orcid.org/0000-0002-4229-4399>

Zhen Hu  <https://orcid.org/0000-0002-0313-9513>

Lin Liu  <https://orcid.org/0000-0002-7945-9337>

Jiangwei Su  <https://orcid.org/0000-0001-9442-1399>

References

- Liu T, Ma X, Ouyang T, et al. Efficacy of 5-aminolevulinic acid–based photodynamic therapy against keloid compromised by downregulation of SIRT1-SIRT3-SOD2-mROS dependent autophagy pathway. *Redox Biol.* 2019;20:195–203. doi:10.1016/j.redox.2018.10.011
- Shi K, Qiu X, Zheng W, Yan D, Peng W. MiR-203 regulates keloid fibroblast proliferation, invasion, and extracellular matrix expression by targeting EGR1 and FGF2. *Biomed Pharmacother.* 2018;108:1282–1288. doi:10.1016/j.biopha.2018.09.152
- Jfri A, O'Brien E, Alavi A, Goldberg SR. Association of hidradenitis suppurativa and keloid formation: A therapeutic challenge. *JAAD Case Rep.* 2019;5(8):675–678. doi:10.1016/j.jcdr.2019.06.001
- Lee S, Kim SK, Park H, et al. Contribution of autophagy-Notch1-mediated NLRP3 inflammasome activation to chronic inflammation and fibrosis in keloid fibroblasts. *Int J Mol Sci.* 2020;21(21):8050. doi:10.3390/ijms21218050
- Lee H, Jang Y. Recent understandings of biology, prophylaxis and treatment strategies for hypertrophic scars and keloids. *Int J Mol Sci.* 2018;19(3):711. doi:10.3390/ijms19030711
- Bojanic C, To K, Hatoum A, et al. Mesenchymal stem cell therapy in hypertrophic and keloid scars. *Cell Tissue Res.* 2021;383(3):915–930. doi:10.1007/s00441-020-03361-z
- Shin JY, Yun SK, Roh SG, Lee NH, Yang KM. Efficacy of 2 representative topical agents to prevent keloid recurrence after surgical excision. *J Oral Maxillofac Surg.* 2017;75(2):401.e1–401.e6. doi:10.1016/j.joms.2016.10.009
- Kristensen LS, Andersen MS, Stagsted LVW, Ebbesen KK, Hansen TB, Kjems J. The biogenesis, biology and characterization of circular RNAs. *Nat Rev Genet.* 2019;20(11):675–691. doi:10.1038/s41576-019-0158-7
- Yang D, Li M, Du N. Effects of the circ_101238/miR-138-5p/CDK6 axis on proliferation and apoptosis keloid fibroblasts. *Exp Ther Med.* 2020;20(3):1995–2002. doi:10.3892/etm.2020.8917
- Wang B, Yin H, Zhang H, Wang T. CircNRP1 facilitates keloid progression via FXR1-mediated upregulation of miR-503-3p and miR-503-5p. *Int J Mol Med.* 2021;47(5):70. doi:10.3892/ijmm.2021.4903
- Shi J, Yao S, Chen P, et al. The integrative regulatory network of circRNA and microRNA in keloid scarring. *Mol Biol Rep.* 2020;47(1):201–209. doi:10.1007/s11033-019-05120-y
- Liu J, Xue N, Guo Y, et al. CircRNA_100367 regulated the radiation sensitivity of esophageal squamous cell carcinomas through miR-217/Wnt3 pathway. *Aging.* 2019;11(24):12412–12427. doi:10.18632/aging.102580
- Yu L, Liu Y. CircRNA_0016624 could sponge miR-98 to regulate BMP2 expression in postmenopausal osteoporosis. *Biochem Biophys Res Commun.* 2019;516(2):546–550. doi:10.1016/j.bbrc.2019.06.087
- Li H, Xu JD, Fang XH, et al. Circular RNA circRNA_000203 aggravates cardiac hypertrophy via suppressing miR-26b-5p and miR-140-3p binding to Gata4. *Cardiovasc Res.* 2020;116(7):1323–1334. doi:10.1093/cvr/cvz215
- Liu F, Li T, Zhan X. Silencing circular RNAPTNP12 promoted the growth of keloid fibroblasts by activating Wnt signaling pathway via targeting microRNA-21-5p. *Bioengineered.* 2022;13(2):3503–3515. doi:10.1080/21655979.2022.2029108
- Zhang H, Peng J, Lai J, et al. MiR-940 promotes malignant progression of breast cancer by regulating FOXO3. *Biosci Rep.* 2020;40(9):BSR20201337. doi:10.1042/BSR20201337
- Zhou Z, Xu YP, Wang LJ, Kong Y. MiR-940 potentially promotes proliferation and metastasis of endometrial carcinoma through regulation of MRV11. *Biosci Rep.* 2019;39(6):BSR20190077. doi:10.1042/BSR20190077
- Gu GM, Zhan YY, Abuduwaili K, et al. MiR-940 inhibits the progression of NSCLC by targeting FAM83F. *Eur Rev Med Pharmacol Sci.* 2018;22(18):5964–5971. doi:10.26355/eurrev_201809_15927
- Wang H, Song T, Qiao Y, Sun J. MiR-940 inhibits cell proliferation and promotes apoptosis in esophageal squamous cell carcinoma cells and is associated with post-operative prognosis. *Exp Ther Med.* 2019;19(2):833–840. doi:10.3892/etm.2019.8279
- He ML, Chen Y, Peng Y, et al. Induction of apoptosis and inhibition of cell growth by developmental regulator hTBX5. *Biochem Biophys Res Commun.* 2002;297(2):185–192. doi:10.1016/S0006-291X(02)02142-3
- Yu J, Ma X, Cheung KF, et al. Epigenetic inactivation of T-box transcription factor 5, a novel tumor suppressor gene, is associated with colon cancer. *Oncogene.* 2010;29(49):6464–6474. doi:10.1038/onc.2010.370
- Ma R, Yang Y, Tu Q, Hu K. Overexpression of T-box transcription factor 5 (TBX5) inhibits proliferation and invasion in non-small cell lung carcinoma cells. *Oncol Res.* 2017;25(9):1495–1504. doi:10.37277/096504017X14883287513729
- Dong X, Wang Y, Qu Y, Liu J, Feng X, Xu X. MicroRNA-603 promotes progression of cutaneous melanoma by regulating TBX5. *Comput Math Methods Med.* 2021;2021:1888501. doi:10.1155/2021/1888501
- Livak KJ, Schmittgen TD. Analysis of relative gene expression data using real-time quantitative PCR and the $2^{-\Delta\Delta CT}$ method. *Methods.* 2001;25(4):402–408. doi:10.1006/meth.2001.1262
- Wang J, Wu H, Xiao Z, Dong X. Expression profiles of lncRNAs and circRNAs in keloid. *Plast Reconstr Surg Glob Open.* 2019;7(6):e2265. doi:10.1097/GOX.0000000000002265
- Li X, Ding J, Wang X, Cheng Z, Zhu Q. NUDT21 regulates circRNA cyclization and ceRNA crosstalk in hepatocellular carcinoma. *Oncogene.* 2020;39(4):891–904. doi:10.1038/s41388-019-1030-0
- Huang Z, Ma W, Xiao J, Dai X, Ling W. CircRNA_0092516 regulates chondrocyte proliferation and apoptosis in osteoarthritis through the miR-337-3p/PTEN axis. *J Biochem.* 2021;169(4):467–475. doi:10.1093/jb/mvaa119
- Chang X, Zhu G, Cai Z, et al. MiRNA, lncRNA and circRNA: Targeted molecules full of therapeutic prospects in the development of diabetic retinopathy. *Front Endocrinol.* 2021;12:771552. doi:10.3389/fendo.2021.771552
- Li S, Teng S, Xu J, et al. Microarray is an efficient tool for circRNA profiling. *Brief Bioinform.* 2019;20(4):1420–1433. doi:10.1093/bib/bby006
- Zhang Z, Yu K, Liu O, et al. Expression profile and bioinformatics analyses of circular RNAs in keloid and normal dermal fibroblasts. *Exp Cell Res.* 2020;388(1):111799. doi:10.1016/j.yexcr.2019.111799
- Ojeh N, Bharatha A, Gaur U, Forde AL. Keloids: Current and emerging therapies. *Scars Burns Heal.* 2020;6:205951312094049. doi:10.1177/2059513120940499
- Lv YS, Wang C, Li LX, Han S, Li Y. Effects of circRNA_103993 on the proliferation and apoptosis of NSCLC cells through miR-1271/ERG signaling pathway. *Eur Rev Med Pharmacol Sci.* 2020;24(16):8384–8393. doi:10.26355/eurrev_202008_22635
- Chen X, Ouyang Z, Shen Y, et al. CircRNA_28313/miR-195a/CSF1 axis modulates osteoclast differentiation to affect OVX-induced bone absorption in mice. *RNA Biol.* 2019;16(9):1249–1262. doi:10.1080/15476286.2019.1624470
- Zhang S, Wei Y, Liu J, Zhuang Y. MiR-940 serves as a diagnostic biomarker in patients with sepsis and regulates sepsis-induced inflammation and myocardial dysfunction. *J Inflamm Res.* 2021;14:4567–4574. doi:10.2147/JIR.S316169
- Wang B, Shen PF, Qu YX, et al. MiR-940 promotes spinal cord injury recovery by inhibiting TLR4/NF- κ B pathway-mediated inflammation. *Eur Rev Med Pharmacol Sci.* 2019;23(8):3190–3197. doi:10.26355/eurrev_201904_17677
- Hou L, Chen M, Yang H, et al. MiR-940 inhibited cell growth and migration in triple-negative breast cancer. *Med Sci Monit.* 2016;22:3666–3672. doi:10.12659/MSM.897731
- Jiang K, Zhao T, Shen M, et al. MiR-940 inhibits TGF- β -induced epithelial-mesenchymal transition and cell invasion by targeting Snail in non-small cell lung cancer. *J Cancer.* 2019;10(12):2735–2744. doi:10.7150/jca.31800

